Physical-Layer Cooperation in Coded OFDM Relaying Systems

Dissertation

zur Erlangung des akademischen Grades

Doktor der Ingenieurwissenschaften (Dr.-Ing.)

vorgelegt dem Fachbereich 1 (Physik/Elektrotechnik)

der Universität Bremen

von

M.Sc. Meng Wu

Tag des öffentlichen Kolloquiums:	05. Oktober 2017
Gutachter der Dissertation:	Prof. Dr.-Ing. A. Dekorsy
	Prof. Dr.-Ing. A. Klein
Weitere Prüfer:	Prof. Dr.-Ing. K.-D. Kammeyer
	Prof. Dr.-Ing. habil. V. Kühn

Ulm, Oktober 2017

Preface

Die vorliegende Arbeit entstand im Rahmen meiner Tätigkeit als wissenschaftlicher Mitarbeiter am Arbeitsbereich Nachrichtentechnik des Instituts für Telekommunikation und Hochfrequenztechnik der Universität Bremen.

Erstens möchte ich Herrn Prof. Dr.-Ing. A. Dekorsy meine allerherzlichste Dankbarkeit für seine Betreuung aussprechen, die zum Erfolg dieser Promotion durch hilfreiche Begleitung und Anregungen sowie endlose Ermutigung führt. Frau Prof. Dr.-Ing. A. Klein von der technische Universität Darmstadt gilt mein großer Dank für die Übernahme des Zweitgutachtens und ihr Interesse an dieser Arbeit. Den Herren Prof. Dr.-Ing. K.-D. Kammeyer und Prof. Dr.-Ing. habil. V. Kühn aus der Universität Rostock bin ich für ihre Tätigkeit als Prüfer verbunden.

Neben den Gutachtern trägt Herr Dr.-Ing. D. Wübben hohen Anteil am Gelingen dieser Arbeit, deshalb gilt ihm meine tiefe Dankbarkeit für die fachliche Beratungen und wertvolle Anregungen bei der Durchführung der zwei "Communications in Interference Limited Networks (COIN)" Projekten. Ich bedanke mich auch bei Herren Dr.-Ing. C. Bockelmann, Dipl.-Ing. M. Woltering und Dr.-Ing. F. Lenkeit für die reichhaltigen Diskussionen. Weiterer Dank geht an Herren Dr.-Ing. D. Wübben, Dipl.-Ing. M. Woltering, M.Sc. Y. Ji, M.Sc. G. Xu und Dipl.-Ing B.-S. Shin für die sorgfältige Durchsicht dieses Manuskripts und die hilfreichen Ratschläge. Gleichfalls gilt mein Dank der Deutschen Forschungsgemeinschaft (DFG) für die Finanzierung meiner Stelle während der Projektlaufzeit.

Meinen besonderen Dank verdienen Herren M.Sc. F. Monsees, Dipl.-Ing. M. Woltering und Dr.-Ing. F. Lenkeit für die Unterstützung bei der deutschen kulturellen Integration, die aus meiner Sicht ebenso wichtig wie die fachliche Vertiefung ist.

Ohne den Rückhalt meiner Familie hätte ich die Promotion bestimmt nicht geschafft, und so gilt mein aufrichtiger Dank meinen Eltern für die unendliche geistige Aufmunterung. Zu guter Letzt möchte ich mich bei

meiner geliebten Ehefrau Dr. rer. pol. F. Li für ihr konstantes Verständnis und ihre bedingungslose Unterstützung bedanken.

Ulm, Oktober 2017

Meng Wu

Contents

Chapter 1

Introduction

1.1 Motivation

One of the major challenges in the field of mobile communications is to reliably support transmissions with high data rate over wide areas. To achieve this goal, the concept of cooperative communication has attracted increasing interests over the last decade as a promising candidate in combating path-loss and enhancing coverage. In addition to cooperation between multiple sources and destinations, intermediate relaying nodes can be deployed to assist the end-to-end transmission, e.g., between base stations and mobile terminals in cellular networks. By processing and forwarding the received message at these relays, the effective path-loss is reduced significantly using the exploited cooperative diversity.

On the other hand, another dominating research topic lies in multiple-antenna systems. Enabled by equipping multiple antennas at the transceivers, these multiple-input multiple-output (MIMO) systems provide increased data rate with boosted transmission reliability. However, in many practical applications, implementing several antennas at one device may not be possible, e.g., at wireless sensor nodes due to the limitation of physical size and node complexity. Inspired by cooperative communications to overcome this restriction, the relays that are distributed in space are treated as a virtual node, where MIMO techniques at both transmitter side and receiver side can be applied in a distributed fashion.

Since a relaying node can not transmit and receive at the same time and frequency, a half-duplex constraint is commonly assumed that causes a tremendous loss in spectral efficiency. Therefore, to preserve the performance improvements achieved by relay assisted cooperative communications, this

limit factor has to be loosed or compensated by exploiting other degrees of freedom in the relaying networks. One possible approach is to extend the one-way relaying communication from the source to the destination via a relay to a two-way sense, where both sources intend to exchange information with each other supported by the relay. For example, if both sources transmit to the relay simultaneously while the relay broadcasts a joint message back to the sources in succession, the halved spectral efficiency in one-way relaying can be compensated completely.

1.2 Thesis Origin and Focus

The contents and Achievements of this thesis are based on the work of two successive DFG projects within the priority program "Communications in Interference Limited Networks (COIN)"

- Physical layer cooperation in distributed relaying systems
- Physical layer network coding in two-way relaying systems with multiple-antenna relays or distributed single-antenna relays.

The aim of both projects is to develop efficient physical-layer cooperation schemes in the context of one-way relaying and two-way relaying, respectively. Of special interest is that orthogonal frequency division multiplexing (OFDM) transmissions are assumed to combat multi-path fading with channel coding applied to exploit the corresponding frequency selectivity. In case of a single relay scenario, the key investigation point is on the operation at the relay, i.e., how to generate the relay message to be forwarded to the destination based on its receive signal. This is especially challenging in two-way relaying communication as the relay needs to estimate a joint message based on network coding. When multiple relays are available, it should be determined how the relays cooperate with each other to estimate the source message and to transmit jointly to the destination. Different schemes are studied and compared with each other based on both analytical and numerical results. The hardware impact as well as cooperation overhead is also considered for practical system designs. This thesis includes these above mentioned aspects and gives insights into designing relaying networks with physical-layer cooperation under a variety of circumstances.

1.3 Main Contributions

Within the focus on designing physical-layer cooperation schemes in coded OFDM based one-way and two-way relaying systems, the main contributions

of this thesis are found in own previous publications, as listed below [1]

- In [WW11, WLW+16a], several OFDM-based relaying schemes are investigated and compared in a triplet relay network based on the conventional relaying schemes.
- In [WXW+11, WXW+12, WLW+16a], multiple relays are introduced to support the end-to-end transmission. In this context, adaptive inter-relay cooperation (IRC) schemes are designed that allow information exchange among the relays for joint reception and transmission.
- In [WWD13a, WLW+16b], mutual information based analysis is initiated for physical-layer network coding (PLNC) schemes in two-way relaying networks with coded OFDM. An optimal phase control strategy is also proposed that improves the PLNC schemes.
- In [WLW+14, WLW+16b], carrier frequency offset (CFO) mismatch is analyzed and the impact is mitigated by interference cancellation tailored to PLNC schemes.
- In [WWD13b, WWD14b, WLW+16b], the two-way relaying network is extended to a MIMO relay scenario, and the increased spatial degrees of freedom is exploited for PLNC.
- In [WWD14a, WLW+16b], a distributed two-way relaying network is considered, where a modified adaptive broadcast scheme with minor signaling overhead is proposed that outperform the traditional scheme.

Besides the above contributions covered in this thesis, there are some issues relating to the relaying topic that have been investigated in own previous publications but not discussed here. These aspects include

- In [WWWK10], coded cooperation using bi-layer and punctured LDPC codes is implemented in a triplet relay network, where the relay forwards only redundancy information to the destination instead of the whole codeword.
- In [WWD11a, WWD11b], error rate based power allocation schemes are proposed in the triplet relay network.
- In [WXW+11, WXW+12, WLW+16a], baseband and RF energies are modeled and embedded into the system performance for the distributed relaying network with IRC.

[1] These contributions are emphasized once again with more detail in each chapter's Overview and Summary respectively with related own publications cited therein.

- In [WLW+14, WLW+16b], the two-way relaying network with CFO mismatch is implemented on a real-time hardware platform using LTE-near parametrization to justify the feasibility of the PLNC schemes.

1.4 Thesis Structure

This thesis is organized in 7 chapters. In the sequel, an overview for each of the remaining chapters is presented capturing the structure of the thesis.

In Chapter 2, the fundamentals and preliminaries required to understand the presented physical-layer cooperation schemes for relaying systems in later chapters are given. Starting with the basic baseband structure of a digital communication system, the OFDM transmission and reception model in the frequency domain is derived. Subsequently, the principle of channel coding is explicated with two commonly used codes specified as examples. Digital modulation schemes are then introduced and the role of soft-output demodulation is addressed. Furthermore, two specific MIMO techniques are demonstrated that exploit spatial diversity in multiple-antenna systems. Relevant information theory basics are discussed at last.

Chapter 3 focuses on one-way relaying networks with a single relay. After introducing the basic concepts for relay assisted communications, several conventional relaying schemes are shortly reviewed. Since the application of OFDM is assumed, a selection of these relaying schemes are adapted and modified correspondingly with their performances compared subsequently.

The one-way relaying communication is supported with multiple relays in Chapter 4. Beginning with system description of such a distributed relaying network, cooperation methodologies at both the receiver and transmitter sides of the relay nodes forming a virtual cluster are discussed to implement MIMO techniques in a distributed manner. To this end, concrete cooperation approaches between the relays are proposed in the sequel by allowing message exchange within the relay cluster. The cooperation overhead is incorporated by resorting to a throughput analysis.

To compensate the loss of spectral efficiency due to the half-duplex constraint, two-way relaying is discussed in Chapter 5 employing a single relay. An overview of two-way relaying schemes requiring different number of phases is firstly given. Focusing on the two-phase scheme, several detection and decoding strategies are presented that estimate a network coded message from the superimposed receive signal at the single-antenna relay. Since the performance of these schemes strongly depends on the phase information of the channel, an optimal phase control strategy is developed with reduced overhead in OFDM systems. Subsequently, asynchrony issues are discussed, which are of significant importance in two-phase two-way relaying

communications. Efficient approaches are also proposed to mitigate the impairments caused by asynchronous transmissions. Finally, a multi-antenna relay is employed that facilitates common MIMO detection schemes with low complexity while satisfactory performance is achieved in certain cases.

In Chapter 6, the two-way relaying network is extended to a distributed scenario with multiple relays. After depicting the system model, a traditional adaptive broadcast transmission scheme is introduced, which is improved by a modified scheme making use of the event that a relay only decodes one source message correctly. Outage behaviors of both schemes are semi-analytically studied to visualize the superior performance of the proposed scheme. Moreover, based on a simple scheduling approach, only minor overhead is required for the modified scheme.

Finally, a summary is given in Chapter 7 that provides concluding remarks and emphasizes on the main contributions of this thesis. An outlook about open questions and future research topics are also discussed.

1.5 Notation

In the following, a short list of the notations to be used is exhibited. If not otherwise stated, these definitions hold for all parts throughout the thesis. At the end of this work, all employed symbols are listed in detail in the extended symbol list.

- Lower-case italic letters x denote scalars or the scalar elements in a vector or matrix.
- Lower-case and upper-case bold letters $\mathbf{x}$ and $\mathbf{X}$ denote vectors and matrices, respectively.
- Elements of a vector are indicated by subscripts, e.g., the ℓth element of $\mathbf{x}$ is denoted by x_ℓ.
- The element wise conjugate, the transpose and the conjugate transpose of a matrix $\mathbf{X}$ are given by $\mathbf{X}^*$, $\mathbf{X}^T$ and $\mathbf{X}^H$, respectively.
- The natural logarithm is denoted as log, whereas $\log_2$ and $\log_{10}$ denote the logarithm to base 2 and 10, respectively.

Chapter 2

Fundamentals and Preliminaries

2.1 Overview

In the course of this chapter, the rudimentary structure of digital communication systems as well as the fundamental transmitter and receiver components are discussed to serve as basics for the following chapters. Firstly, the general system setup and channel model are elaborated in Section 2.2. To combat multi-path fading, as assumed for the channel throughout this work, OFDM is employed as air interface and reviewed in Section 2.3. Subsequently, two core aspects in digital communications, namely, channel coding and digital modulation, are examined in Section 2.4 and Section 2.5, respectively. Therein, some commonly used channel codes and modulation schemes are shortly presented schematically. Furthermore, considering multiple-antenna systems, two basic diversity-exploiting schemes are studied in Section 2.6 at the receiver side and transmitter side, which are widely applied in the upcoming chapters. In succession, basics of information theory used to derive channel capacity by mutual information are illustrated in Section 2.7 to get insights into system performance upper bound. Finally, this chapter is summarized in Section 2.8.

2.2 Basics of Digital Communications

In this section, the basic structure of a wireless digital communication system is demonstrated [Kam11]. As shown in Fig. 2.1 for the block diagram of the

baseband processing chain, the system consists of a transmitter, a wireless channel and a receiver, where the transmitter sends messages to the receiver via the channel. In the following subsections, each part of these entities is to be explicated in general. Specific components within the transmitter and the receiver for this baseband model are to be discussed in the next sections.

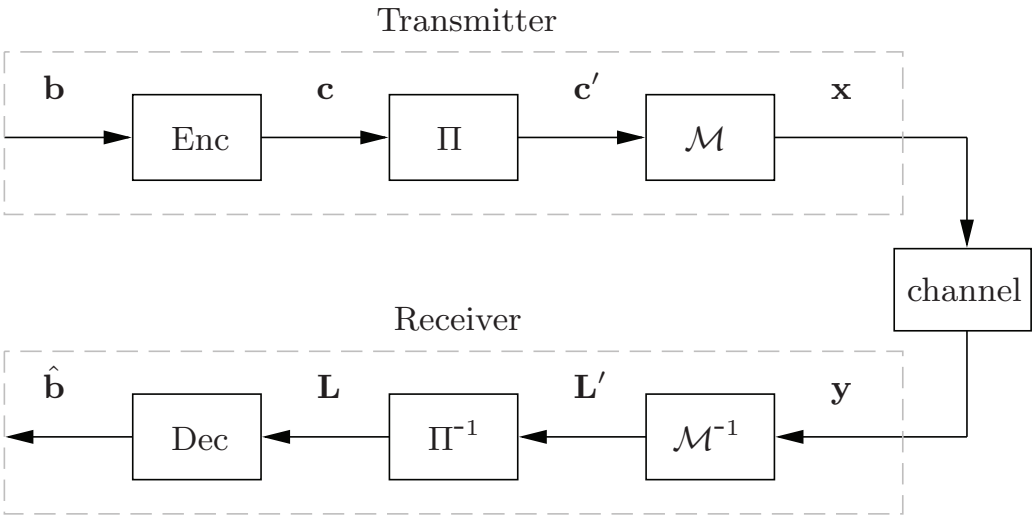

Figure 2.1: Block diagram of the baseband processing chain for a digital communication system.

2.2.1 Transmitter

At the transmitter, the information bit sequence $\mathbf{b}$ is firstly channel coded, which results in a codeword $\mathbf{c}$ that carriers either explicitly or implicitly the original information as well as some redundant information dependent on $\mathbf{b}$. Subsequently, $\mathbf{c}$ is interleaved to $\mathbf{c}'$, which basically permutates the orders of the bits in the codeword to avoid the occurrence of burst errors from the channel. The interleaved bits are then modulated to the symbol vector $\mathbf{x}$ by a modulator $\mathcal{M}$ to be transmitted over the channel. The channel coding and modulation processes are to be introduced in Section 2.4 and Section 2.5, respectively.

2.2.2 Channel

For mobil radio communications, the radio waves propagated in the free space are generally disturbed by shadowing, scattering and reflections. As a result, multiple replicas of the same signal arrive at the receiver with different time delays, attenuations and phases, constituting a multi-path channel that

has to be considered adequately in practical systems with proper design of techniques to combat or even make use of this characteristic. Moreover, if the channel varies with time due to movements of the transmitter or the receiver, this channel becomes time-variant with the equivalent baseband channel impulse response represented as

$$h(t,\tau) = \sum_{n_\mathrm{H}=0}^{N_\mathrm{H}-1} h(t, n_\mathrm{H}) \cdot \delta(\tau - \tau_{n_\mathrm{H}}) \; . \tag{2.1}$$

Here, the observation time is denoted as t. The complex valued channel coefficient $h(t, n_\mathrm{H})$ corresponds to the n_H-th path with delay τ_{n_H}, where there are N_H effective channel taps in total and $n_\mathrm{H} = 0, 1, \cdots, N_\mathrm{H} - 1$. On the other hand, the time variation of the channel causes Doppler frequency shift [Kam11]. In this work, this effect is not considered, i.e., the mobile radio channel is assumed to be time-invariant, such that the channel representation (2.1) is simplified to

$$h(\tau) = \sum_{n_\mathrm{H}=0}^{N_\mathrm{H}-1} h_{n_\mathrm{H}} \cdot \delta(\tau - \tau_{n_\mathrm{H}}) \; . \tag{2.2}$$

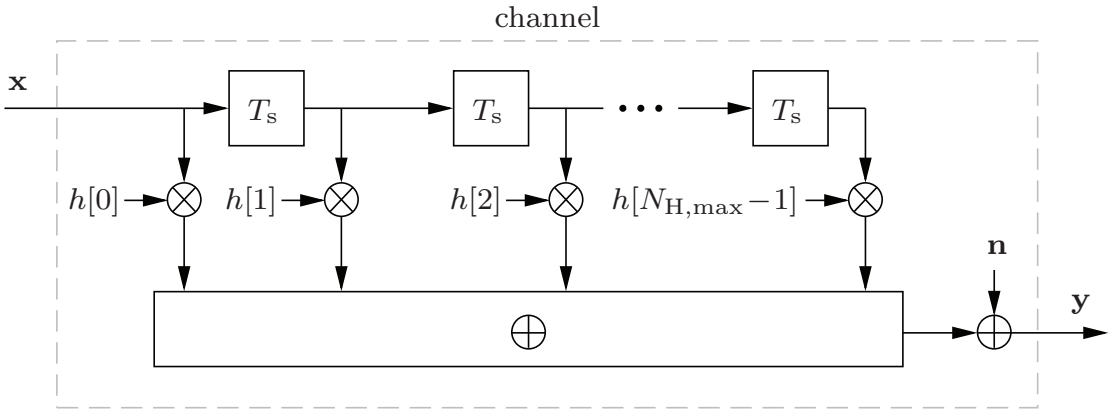

Figure 2.2: Symbol rate tapped delay model of a multi-path mobile radio channel.

Typically, the multi-path channel is modeled by a time discrete finite impulse response (FIR) filter with the tapped delay line shown in Fig. 2.2 at symbol rate. Therein, the transmit signal is passed through the channel and weighted at each tap with the complex channel coefficients $h[0], h[1], \cdots, h[N_{\mathrm{H,max}} - 1]$. Note that the total length of the channel filter $N_{\mathrm{H,max}} = \lceil \tau_{\max} / T_\mathrm{s} \rceil$ has to be an integer, which depends on the ratio of the maximum channel delay $\tau_{\max} = \max\{\tau_{n_\mathrm{H}}\}$ and the symbol duration T_s. Furthermore, the N_H channel taps correspond to the non-zero components

$h\left[\lceil \tau_{n_\mathrm{H}}/T_\mathrm{s} \rceil\right] = h_{n_\mathrm{H}}$ whereas the other filter coefficients are zeros. To this end, the channel impulse response discretized at rate $1/T_\mathrm{s}$ with index κ can be presented as

$$h(\kappa) = \sum_{n_\mathrm{H}=0}^{N_\mathrm{H}-1} h_{n_\mathrm{H}} \cdot \delta(\kappa - \lceil \tau_{n_\mathrm{H}}/T_\mathrm{s} \rceil) \; . \tag{2.3}$$

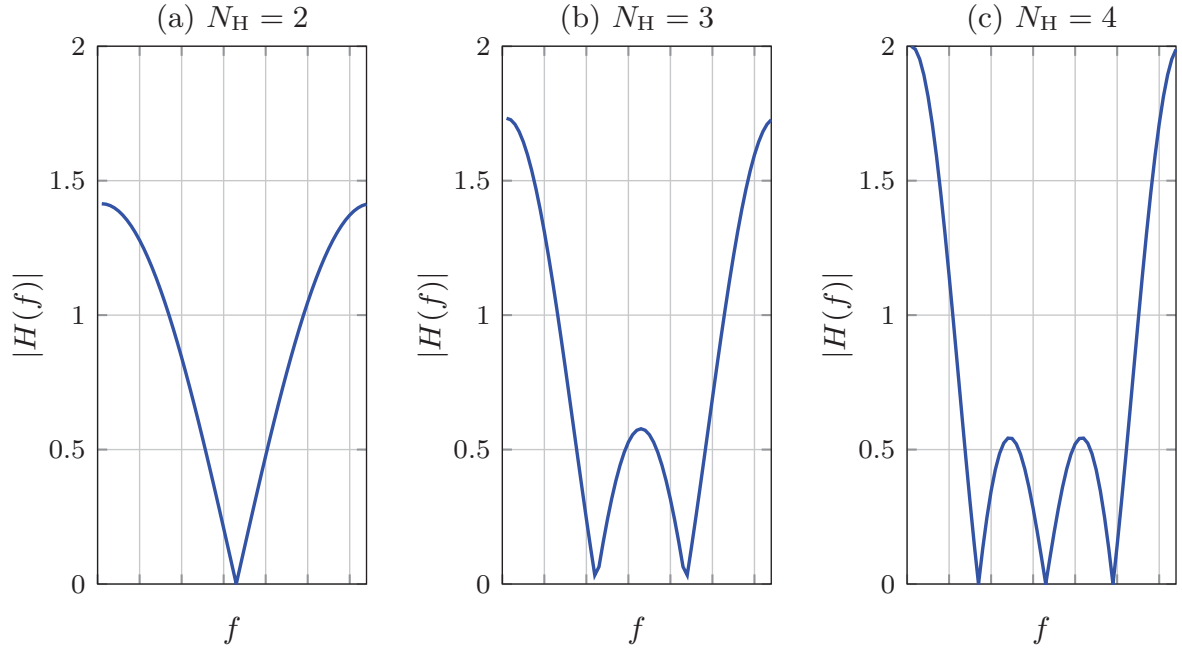

Figure 2.3: Amplitude of the frequency representation for a $\mathbf{1}_{N_\mathrm{H}\times 1}$ multi-path channel. (a) for $N_\mathrm{H} = 2$, (b) for $N_\mathrm{H} = 3$ and (c) for $N_\mathrm{H} = 4$.

To achieve the receive signal vector $\mathbf{y}$, the transmit signal vector $\mathbf{x}$ is convolved with the FIR channel filter plus some additive white Gaussian noise (AWGN) vector $\mathbf{n}$, where $\mathbf{n}$ has zero mean and variance σ_n^2. Therefore, the system equation can be written as

$$\mathbf{y} = \mathbf{h} * \mathbf{x} + \mathbf{n} \tag{2.4}$$

with the operator $*$ denoting the linear convolution between two vectors. Due to the impact of the multi-path channel, the signals transmitted previously 'slide' into the current transmit signal, causing inter-symbol interference (ISI) in the time domain. This time dispersion results in fluctuations in the frequency domain and therefore the multi-path channel is known to be frequency selective. Obviously, more effective channel taps lead to increased frequency selectivity. For example, this is observed in Fig. 2.3 by the amplitude of the frequency representation $H(f)$ for a multi-path channel with N_H taps defined as $\mathbf{1}_{N_\mathrm{H}\times 1}$ of symbol rate $1/T_\mathrm{s}$, $N_\mathrm{H} = 2, 3, 4$.

2.2.3 Receiver

At the receiver, the receive signal vector after equalization and denoted as $\mathbf{y}$ is fed to a demodulator $\mathcal{M}^{-1}$. Assuming that the receiver has perfect channel knowledge achieved from channel estimation, the demodulator produces soft information in the form of a log-likelihood ratio (LLR) vector $\mathbf{L}'$ corresponding to the code bits $\mathbf{c}'$. Details of such a soft-output demodulator are presented in Subsection 2.5.2. Since the receiver is also aware of the permutation order of the code bits, $\mathbf{L}'$ can be de-interleaved to $\mathbf{L}$ that corresponds to the un-interleaved codeword $\mathbf{c}$. Consequently, the soft values $\mathbf{L}$ are forwarded to the decoder, where the information bits are estimated and denoted as $\hat{\mathbf{b}}$.

To combat the ISI introduced by the multi-path channel and elaborated in the previous subsection, equalization is usually required at the receiver before demodulating the receive signal. Designing sophisticated time-domain equalizers excludes the scope of this work but can be found in [Kam11]. Instead, orthogonal frequency division multiplexing (OFDM) is applied, which facilitates simple one-tap equalization in the frequency domain as discussed in the next section.

2.3 Orthogonal Frequency Division Multiplexing

As illustrated in Subsection 2.2.2, the multi-path channel leads to ISI in the time domain and fading in the frequency domain. To save the effort of designing time domain equalizers with high complexity, multi-carrier schemes such as OFDM can be employed [Kam11]. To this end, the frequency band is divided into L multiple subcarriers such that each subchannel can be treated to be flat. Correspondingly, simple one-tap equalization is possible for each individual subcarrier. This concept is illustrated in Fig. 2.4 for the frequency domain representation of a multi-path channel.

The block diagram of the baseband processing chain for a digital communication system using OFDM is shown in Fig. 2.5. Therein, the coded and interleaved bit vector $\mathbf{c}'$ is converted from serial to parallel (S/P), where each m bit tuple is mapped to a symbol level signal in the frequency domain. The collected symbol vector $\mathbf{x}$ is then transformed to time domain by inverse fast Fourier transformation (IFFT), yielding $\mathbf{x}_t$ as one OFDM symbol after parallel to serial (P/S) conversion. After adding a guard interval (GI) $\mathbf{x}_{t,\mathrm{CP}}$ known as cyclic prefix (CP), the signal vector $[\mathbf{x}_t^T \ \mathbf{x}_{t,\mathrm{CP}}^T]^T$ is transmitted over the frequency selective channel.

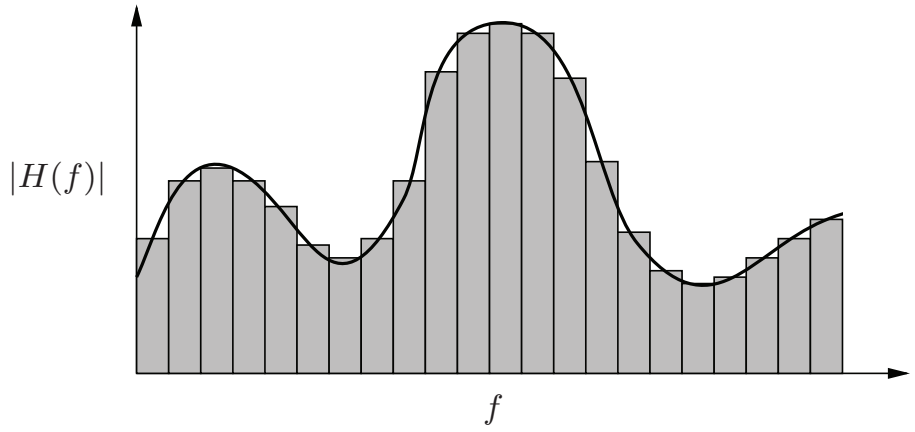

Figure 2.4: Frequency domain representation of a frequency selective channel, where each subcarrier is assumed to experience a flat channel.

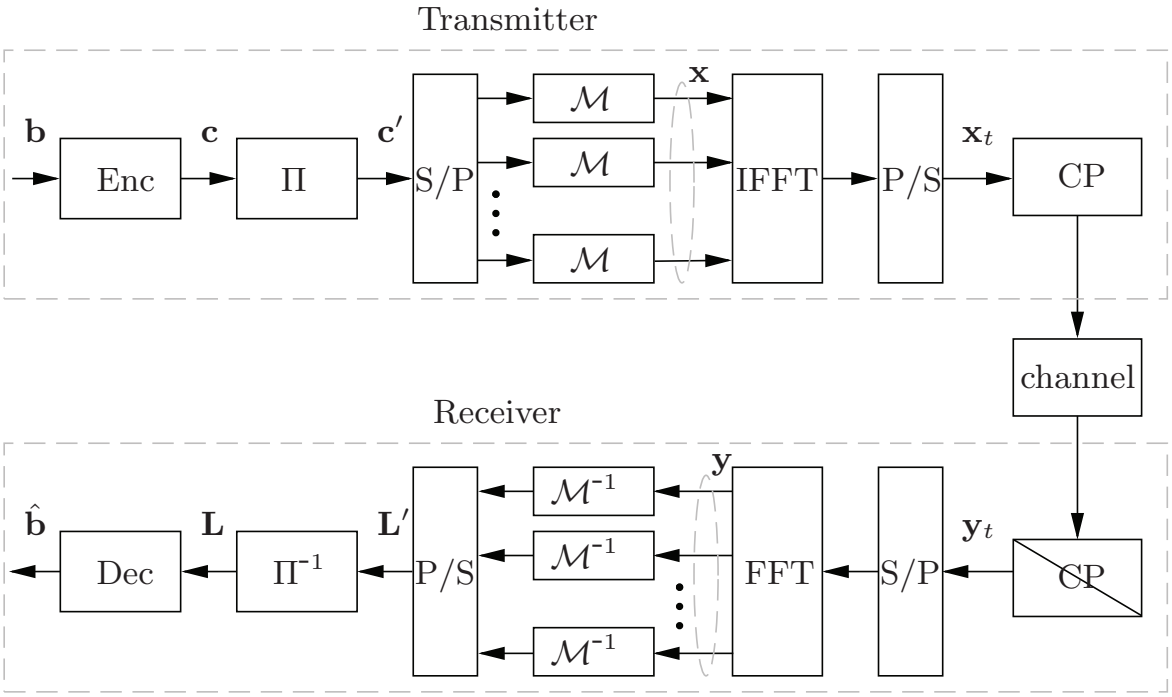

Figure 2.5: Block diagram of the baseband processing chain for a digital communication system using OFDM.

Cyclic Prefix

In Fig. 2.6, the time line for OFDM transmission with the application of CP is demonstrated. Denoting T_{OFDM} and T_{CP} the length of an OFDM symbol without CP and the CP, respectively, the last $T_{\mathrm{CP}}/T_{\mathrm{OFDM}}$ part of each OFDM symbol is copied and inserted in front of this symbol. Therefore, if the CP length is chosen to be longer than the maximum channel time

delay, i.e., $T_{\mathrm{CP}} > \tau_{\max}$ as shown in the figure, ISI between OFDM symbols can be completely avoided. For example, the signal leakage caused by multi-path effect from the ith OFDM symbol only falls in the CP of the $(i+1)$th OFDM symbol, and thus the desired symbol itself is not interfered. Another functionality of inserting CP is to transfer the linear convolution between the channel impulse response and the transmit data sequence into circular convolution, such that efficient implementation like fast Fourier transformation (FFT) and IFFT can be used to transform the signal between time and frequency domains. On the flip side, CP leads to performance degradation as overhead. Typically, a CP insertion with $T_{\mathrm{CP}}/T_{\mathrm{OFDM}} = 1/4$ yields approximately 1dB signal to noise ratio (SNR) loss [Kam11].

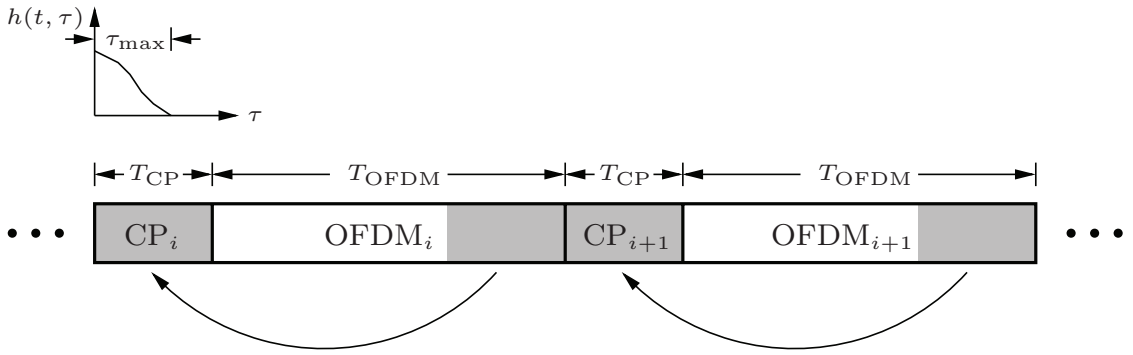

Figure 2.6: Time line for OFDM transmissions with CP. The influence of the channel impulse response in the time domain is also presented.

At the receiver side as shown in Fig. 2.5, the CP is firstly removed for each OFDM symbol to yield the ISI-free signal vector $\mathbf{y}_t$ in the time domain, which is subsequently transformed to the frequency domain by FFT after S/P conversion. Correspondingly, the system equation for each subcarrier $\ell = 1, 2, \cdots, L$ after FFT can be written as

$$y_\ell = h_\ell x_\ell + n_\ell \ , \tag{2.5}$$

which is ISI free. The collected signal vector $\mathbf{y}$ is demodulated and converted by P/S. The LLRs $\mathbf{L}'$ achieved from the demodulators are de-interleaved and decoded to get the detected $\hat{\mathbf{b}}$.

2.4 Channel Coding

Channel coding plays a vital role in modern wireless communication systems, which protects the information against transmission errors by adopting an appropriate encoder/decoder set at the transceiver to detect or even correct

these errors. The reduced errors mainly come at the expense of adding redundancy to the information, such that the effective data rate is decreased.

Since the majority of digital communication systems transmit binary data with bits taken from the finite Galois field (GF) $\mathrm{GF}(2) = \{0, 1\}$, binary channel codes are considered in this work. Specifically, the encoding process at the transmitter maps a vector $\mathbf{b}$ of N_b binary information bits to the code vector $\mathbf{c}$ containing $N_c > N_b$ binary bits by an encoder Γ as

$$\mathbf{c} = \Gamma(\mathbf{b}) \; . \tag{2.6}$$

This can be interpreted as that $N_c - N_b$ redundancy bits are added to the information word $\mathbf{b}$ to form the codeword $\mathbf{c}$, resulting in a systematic code when the information bits are explicitly presented in the code bits. Otherwise, non-systematic codes are defined with $\mathbf{b}$ implicitly contained in $\mathbf{c}$. Furthermore, the code rate $0 < R_\mathrm{C} < 1$ is defined as

$$R_\mathrm{C} = \frac{N_b}{N_c} \; . \tag{2.7}$$

At the receiver, the decoder makes use of the redundant information to estimate the information bits sent from the transmitter. The decoding rule should be designed properly that corresponds to the encoding process. Therefore, the transmission errors can be either detected or corrected using different channel codes, yielding improved error rate performance.

Basically, channel coding can be classified into error detection codes and error correction codes. The former class is able to detect whether there exist erroneous bits in the codeword, e.g., by using cyclic redundancy check (CRC) codes. The latter class corrects the transmission errors depending on the correction capability of the chosen codes. In the sequel, two examples of error correction codes are reviewed, namely, rate compatible punctured convolutional (RCPC) codes and low-density parity-check (LDPC) codes, as they are employed in the following chapters.

2.4.1 Rate Compatible Punctured Convolutional Codes

A well known class of channel codes is convolutional codes, as firstly introduced by Elias [Eli55]. Prominent features of this code family are its simple structure, ease of encoding and convenient decoding either by the Viterbi algorithm [Vit67] or the Bahl, Cocke, Jelinek and Raviv (BCJR) algorithm [BCJR74]. Furthermore, this code class offers the elementary blocks for a bunch of concatenated coding schemes such as Turbo codes [BGT93]. In the sequel, the basics of convolutional codes are firstly elaborated.

Defined by the generator polynomials, the structure of a convolutional code is described in terms of a succession of bits that are delayed using memory elements and influence each other for one output. As a simple example for illustration, a half-rate code with two polynomials $[7, 5]_8$ in octal base is considered. For this code, the non-systematic encoder structure is depicted in Fig. 2.7, where D represents a memory element that delays the input. The upper output code bit c_1 corresponds to the binary representation of the polynomial 7 and the lower one c_2 to 5 with an input information bit b. More specifically, using the mod-2 sum (XOR) operation $\oplus$, c_1 is calculated by the currently input bit XORed with the previous two input bits. On the other hand, only XORing the current input bit and the input bit before the previous one yields c_2. Since one input bit leads to two output bits using two polynomials, a code rate of $R_\mathrm{C} = 0.5$ is obtained for this code. Moreover, another important parameter besides R_C for convolutional codes is the constraint length L_c, which is the number of memories plus 1 and characterizes the number of input bits that influence each other. For instance, $L_c = 3$ for the code in Fig. 2.7.

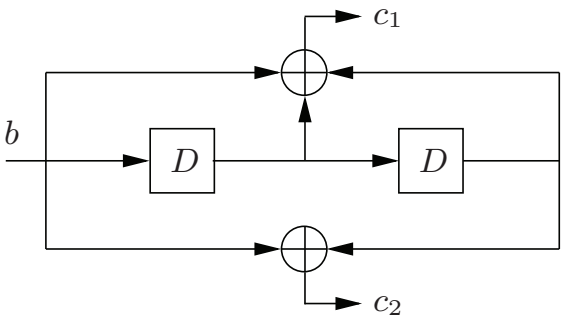

Figure 2.7: A non-systematic convolutional encoder with the polynomials $[7, 5]_8$, where one input bit b results in two output bits c_1 and c_2.

In order to provide rate compatible property for a code whose rate can be adapted in a large range without much change on the code structure as well as the encoding and decoding processes, RCPC codes are introduced by Hagenauer [Hag88]. For this punctured code family, well defined periodic puncturing schemes are applied to raise the initial rate $R_{\mathrm{C,mom}}$ of a mother code to a desired rate R_C. Note that random puncturing may destroy the properties of the code, leading to severe performance degradation. Therefore, the puncturing pattern has to be designed appropriately to avoid catastrophic codes. By numerical search to find good codes with such valid periodic patterns, the mother code with rate $R_{\mathrm{C,mom}} = 1/3$ and constraint length $L_c = 4$ is taken as an example, which uses the generator polynomials $[13, 17, 11]_8$. Resorting to a puncturing period of $N_\mathrm{P} = 8$ that denotes after

$$\mathbf{P}_{\mathrm{C}} = \begin{cases} \begin{bmatrix} 1 & 1 & 1 & 1 & 1 & 1 & 1 & 1 \\ 1 & 1 & 1 & 1 & 1 & 1 & 1 & 1 \\ 1 & 1 & 1 & 1 & 1 & 1 & 1 & 1 \end{bmatrix} & R_{\mathrm{C}} = 1/3 \\ \begin{bmatrix} 1 & 1 & 1 & 1 & 1 & 1 & 1 & 1 \\ 1 & 1 & 1 & 1 & 1 & 1 & 1 & 1 \\ 1 & 1 & 1 & 0 & 1 & 1 & 1 & 0 \end{bmatrix} & R_{\mathrm{C}} = 4/11 \\ \begin{bmatrix} 1 & 1 & 1 & 1 & 1 & 1 & 1 & 1 \\ 1 & 1 & 1 & 1 & 1 & 1 & 1 & 1 \\ 1 & 0 & 1 & 0 & 1 & 0 & 1 & 0 \end{bmatrix} & R_{\mathrm{C}} = 2/5 \\ \begin{bmatrix} 1 & 1 & 1 & 1 & 1 & 1 & 1 & 1 \\ 1 & 1 & 1 & 1 & 1 & 1 & 1 & 1 \\ 1 & 0 & 0 & 0 & 1 & 0 & 0 & 0 \end{bmatrix} & R_{\mathrm{C}} = 4/9 \\ \begin{bmatrix} 1 & 1 & 1 & 1 & 1 & 1 & 1 & 1 \\ 1 & 1 & 1 & 1 & 1 & 1 & 1 & 1 \\ 0 & 0 & 0 & 0 & 0 & 0 & 0 & 0 \end{bmatrix} & R_{\mathrm{C}} = 1/2 \\ \begin{bmatrix} 1 & 1 & 1 & 1 & 1 & 1 & 1 & 1 \\ 1 & 1 & 0 & 1 & 1 & 1 & 0 & 1 \\ 0 & 0 & 0 & 0 & 0 & 0 & 0 & 0 \end{bmatrix} & R_{\mathrm{C}} = 4/7 \\ \begin{bmatrix} 1 & 1 & 1 & 0 & 1 & 1 & 1 & 0 \\ 1 & 1 & 0 & 1 & 1 & 1 & 0 & 1 \\ 0 & 0 & 0 & 0 & 0 & 0 & 0 & 0 \end{bmatrix} & R_{\mathrm{C}} = 2/3 \\ \begin{bmatrix} 1 & 1 & 1 & 0 & 1 & 1 & 1 & 0 \\ 1 & 0 & 0 & 1 & 1 & 0 & 0 & 1 \\ 0 & 0 & 0 & 0 & 0 & 0 & 0 & 0 \end{bmatrix} & R_{\mathrm{C}} = 4/5 \\ \begin{bmatrix} 1 & 1 & 1 & 0 & 1 & 1 & 1 & 0 \\ 1 & 0 & 0 & 1 & 0 & 0 & 0 & 1 \\ 0 & 0 & 0 & 0 & 0 & 0 & 0 & 0 \end{bmatrix} & R_{\mathrm{C}} = 8/9 \end{cases} \tag{2.8}$$

how many information bits the puncturing pattern is repeated, the following code rates can be achieved as

$$R_{\mathrm{C}} = \{1/3, 4/11, 2/5, 4/9, 1/2, 4/7, 2/3, 4/5, 8/9\} \ , \tag{2.9}$$

which are ordered from the lowest to the highest [Hag88]. The encoder structure of the mother code is shown in Fig. 2.8. The corresponding output bits $[c_1\ c_2\ c_3]^T$ are punctured out according to the patterns defined by the puncturing matrices, as presented in (2.8) for different code rates in (2.9), respectively. Taking the matrix

$$\mathbf{P}_{\mathrm{C}} = \begin{bmatrix} 1 & 1 & 1 & 0 & 1 & 1 & 1 & 0 \\ 1 & 0 & 0 & 1 & 0 & 0 & 0 & 1 \\ 0 & 0 & 0 & 0 & 0 & 0 & 0 & 0 \end{bmatrix} \tag{2.10}$$

for $R_{\mathrm{C}} = 8/9$ as an illustrative example, the (i, j)th entry indicates whether c_i generated by the jth input bit is punctured out (0) or not (1), $i = 1, 2, 3$ and $j = 1, 2, \cdots, 8$. For instance, the third output bit is omitted whereas the first and the second output bits are preserved when inputting the first bit. As a result, 9 output bits are maintained after puncturing during one puncturing period of $N_{\mathrm{P}} = 8$ input bits, which yields a code rate $R_{\mathrm{C}} = 8/9$. At the decoder, zero values are forced to the puncturing positions since no information is transmitted at those positions.

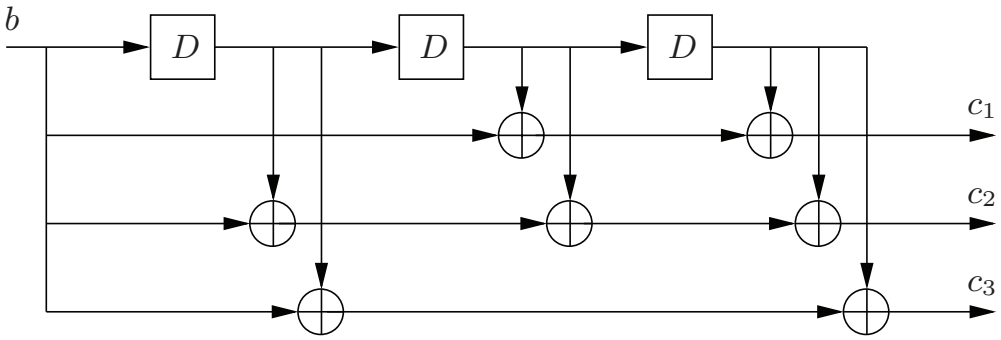

Figure 2.8: Encoder structure of the mother code for RCPC code construction using polynomials $[11, 15, 13]_8$ with one input bit b and three output bits c_1, c_2 and c_3.

2.4.2 Low-Density Parity-Check Codes

LDPC codes were firstly proposed by Gallager in 1962 [Gal62]. However, no importance was attached to this special type of coding scheme due to its

high computational complexity in the decoding process. Therefore, it was forgotten for nearly three decades until its rediscovery by MacKay and Neal in 1996 [MN96], and remained as a hot topic sine then. LDPC codes are nothing more than a class of linear block codes with the parity-check matrix being sparse, which claim capacity-approaching property based on iterative decoding. For example, the best known LDPC code of rate $R_{\mathrm{C}} = 0.5$ is able to approach the Shannon limit by 0.0045 dB [CFRU01].

In the sequel, the construction of linear block codes is firstly elaborated. Specifically, the information word $\mathbf{b}$ is multiplied with the transpose of a $N_b \times N_c$ generator matrix $\mathbf{G}_c = \begin{bmatrix} \mathbf{I} & \mathbf{P} \end{bmatrix}$, yielding the codeword $\mathbf{c}$ as

$$\mathbf{c} = \mathbf{G}_c^T \mathbf{b} = \begin{bmatrix} \mathbf{b} \\ \mathbf{P}^T \mathbf{b} \end{bmatrix} . \tag{2.11}$$

Note that this results in a systematic code since the information bits $\mathbf{b}$ are explicitly represented in the code bits $\mathbf{c}$ due to the identity matrix $\mathbf{I}$ in $\mathbf{G}_c$. On the other hand, the matrix $\mathbf{P}$ is used to generate the redundancy bits that protect the information bits from erroneous transmissions. After reception and detection, the parity-check matrix $\mathbf{H}_c$ is used to check and correct and bit-level errors, as discussed in [Moo05], with $\mathbf{H}_c = \begin{bmatrix} \mathbf{P}^T & \mathbf{I} \end{bmatrix}$ fulfilling the following condition

$$\mathbf{G}_c \mathbf{H}_c^T = \begin{bmatrix} \mathbf{I} & \mathbf{P} \end{bmatrix} \begin{bmatrix} \mathbf{P}^T & \mathbf{I} \end{bmatrix}^T = \mathbf{0} . \tag{2.12}$$

As an example for illustration, a simple linear block code, namely, $(7, 4)$ Hamming code [Moo05] is considered. To encode the $N_b = 4$ information bits into $N_c = 7$ code bits with 3 redundancy bits, the 4×7 generator matrix $\mathbf{G}_c$ given by

$$\mathbf{G}_c = \begin{bmatrix} 1 & 0 & 0 & 0 & 0 & 1 & 1 \\ 0 & 1 & 0 & 0 & 1 & 0 & 1 \\ 0 & 0 & 1 & 0 & 1 & 1 & 0 \\ 0 & 0 & 0 & 1 & 1 & 1 & 1 \end{bmatrix} \tag{2.13}$$

is multiplied with the information word $\mathbf{b}$, as shown in (2.11). The corresponding parity-check matrix is defined as

$$\mathbf{H}_c = \begin{bmatrix} 0 & 1 & 1 & 1 & 1 & 0 & 0 \\ 1 & 0 & 1 & 1 & 0 & 1 & 0 \\ 1 & 1 & 0 & 1 & 0 & 0 & 1 \end{bmatrix} . \tag{2.14}$$

Gallager [Gal62] has pointed out, both theoretically and practically, that by delicately designing $\mathbf{H}_c$, followed by inversely constructing $\mathbf{G}_c$, tremendous performance gains can be achieved when $\mathbf{H}_c$ is a sparse matrix, resulting in the LDPC code family. The sparsity of a matrix implies that only a minor amount of entries 1 in $\mathbf{H}_c$ are present compared to the entries 0. By defining each code bit as a variable node (column of $\mathbf{H}_c$), and abstractly, each equation constraint (row of $\mathbf{H}_c$) as a check node, there is an edge between a pair of variable node and check node if and only if the corresponding cross position in $\mathbf{H}_c$ is 1. Furthermore, a cycle is defined as a path starting from a certain variable node and returning back to this node with no edges come across twice or more, whereas the total number of the experienced edges represents the size of the cycle. When applying iterative decoding for LDPC codes [Bri01, RU07] based on belief propagation in the sum-product algorithm [KFL01], information is exchanged iteratively between the variable nodes and the check nodes. Therefore, the decoding performance is deteriorated with the presence of small-size cycles since the information may get trapped in those cycles without updates from the whole $\mathbf{H}_c$. To conquer this problem, the progressive edge growth (PEG) algorithm [HEA05, Wu08] can be adopted, which tries to maximize the size of cycles when constructing $\mathbf{H}_c$.

Besides intelligently allocating the edges in $\mathbf{H}_c$ to yield superior performance, the statistical distribution of the edges should also be chosen carefully to construct LDPC codes with good property. To this end, two classifications of LDPC codes are distinguished, i.e., regular and irregular codes. In case of regular codes, as considered by Gallager [Gal62], the number of edges is fixed in each column and row, respectively. Although this code class is easy to handle due to its fixed parametrization, no competency in capacity-approaching characteristic is observed compared to irregular LDPC codes with unequal weights of edges in the columns and rows. Based on density evolution [Urb01], the optimal variable node and check node distributions specifying their respective weights of edges can be calculated.

Similar to that for convolutional codes extended by RCPC codes, optimal design of rate compatible LDPC codes based on puncturing also exists in the literature. Basically, the puncturing patterns are chosen delicately such that the properties of the mother LDPC code are preserved to the largest extent in the punctured code. Details of this aspect is omitted here but can be found in [HKM04, HKKM06].

2.5 Digital Modulation

In this section, some commonly used digital modulation schemes are firstly introduced to map the codeword to transmit symbols in the complex constella-

tion plane. Subsequently, the principle of soft demodulation is demonstrated to demap the detected receive signal for soft-input soft-output channel decoding.

2.5.1 Alphabet Constrained Mapping

For digital communications, the bit level message is mapped to symbols according to a given mapping rule specified by the modulator $\mathcal{M}$, i.e.,

$$\mathbf{x} = \mathcal{M}(\mathbf{c}') = \mathcal{M}(\Pi(\mathbf{c})) \; . \tag{2.15}$$

Here, m code bits result in one symbol differentiated by either amplitude or phase or both of them in the complex plane. In other words, each modulated symbol contains m-bit information, leading to 2^m possible constellation points in total. In the sequel, some most commonly used modulation techniques are demonstrated.

- **Binary phase shift keying** (**BPSK**) is a digital phase modulation scheme that maps each bit to one symbol. For example, considering the mapping rule $\mathbf{x} = 1 - 2 \cdot \mathbf{c}'$ as shown in Fig. 2.9(a), this yields $0 \rightarrow 1$ and $1 \rightarrow -1$, which indicates that transmitting one symbol delivers $m = 1$ bit information.

- **Quaternary phase shift keying** (**QPSK**) also makes use of the phase information to differ the constellation points but exploits both real and imaginary dimensions in the complex plain whereas BPSK is defined only in the real domain. In this case, each pair of adjacent constellation points has an equal phase difference of $\pi/2$ and each transmitting symbol contains $m = 2$ bit information. An exemplary mapping rule is shown in Fig. 2.9(b).

- **M-ary phase shift keying** (**M-PSK**) is a generalization of PSK depending on the phase of the $M = 2^m$ different constellation points, where the phase is equivalently distributed with the phase difference equal to $2\pi/M$ between adjacent constellation points. For BPSK and QPSK, M is equal to 2 and 4, respectively. One possible mapping rule is shown in Fig. 2.9(c) for 8-PSK with each transmitting symbol containing $m = 3$ bit information.

- **M-ary quadrature amplitude modulation** (**M-QAM**) includes the information in both phase and amplitude of the M constellation points in the complex plane. Commonly used QAM schemes are 4-QAM, 16-QAM and 64-QAM, where 4-QAM is identical to QPSK. In

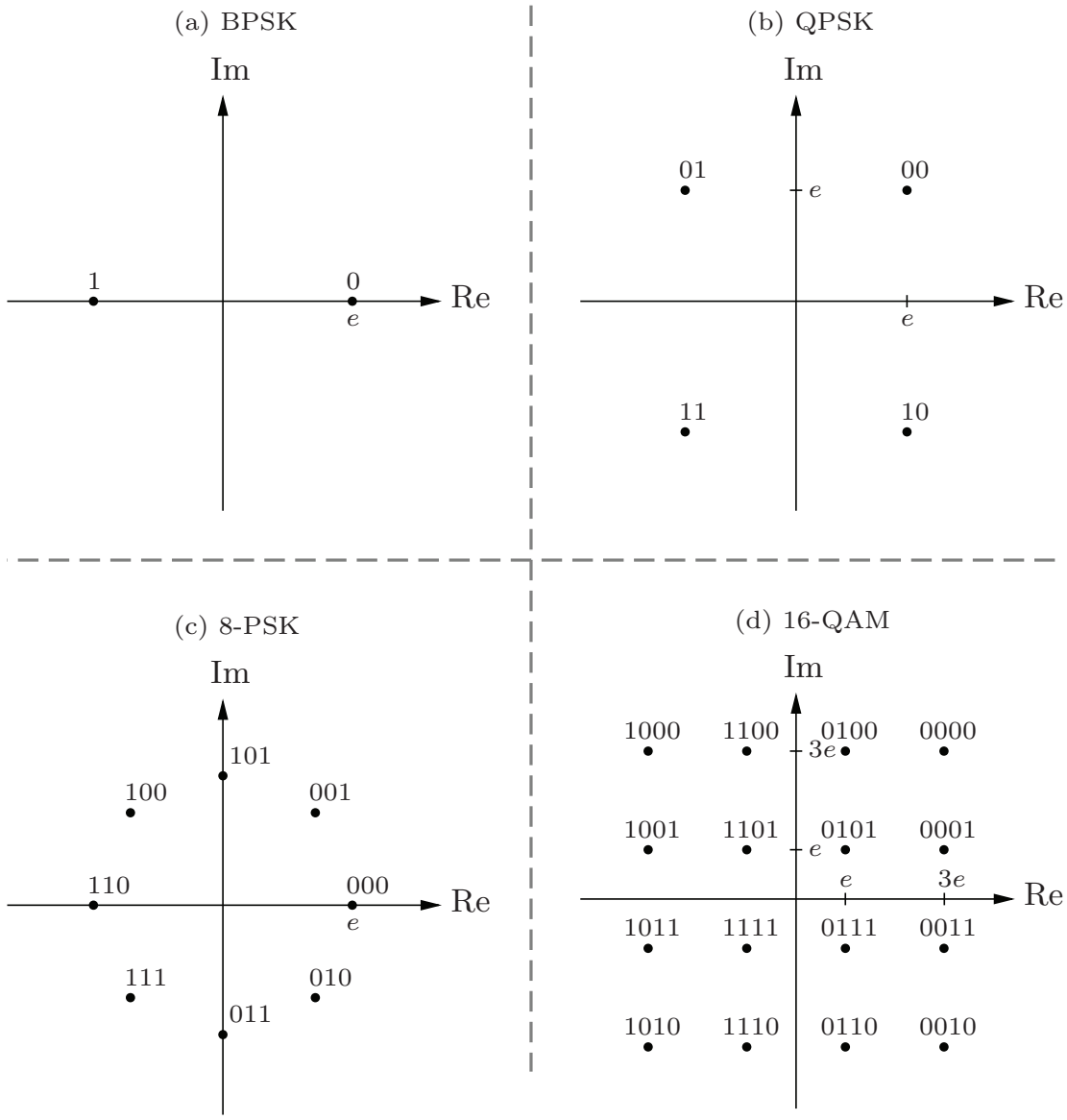

Figure 2.9: Graphical illustration for the constellation of alphabet constrained modulation with gray mapping. (a) for BPSK, (b) for QPSK, (c) for 8-PSK and (d) for 16-QAM.

Fig. 2.9(d) an exemplary mapping rule for 16-QAM is presented with each transmitting symbol containing $m = 4$ bit information.

In Fig. 2.9 gray mapping is applied, which ensures that every pair of adjacent constellation points in the complex plane has only one bit difference. In this context, if one symbol is misjudged to one of its adjacent symbols, only one bit error occurs with respect to this symbol, resulting in improved bit error rate (BER) performance compared to non Gray mapping schemes.

Furthermore, the averaged transmit power $\mathcal{P} = \mathrm{E}\left\{|x|^2\right\}$ should be irrespective of the mapping rules. Assuming all symbols occur with equal

probability, the unit distance e defined in Fig. 2.9 for the exemplary modulation schemes leading to the same $\mathcal{P}$ is given by

$$e = \begin{cases} \sqrt{\mathcal{P}} & \text{for BPSK} \\ \sqrt{\mathcal{P}}/\sqrt{2} & \text{for QPSK} \\ \sqrt{\mathcal{P}} & \text{for 8-PSK} \\ \sqrt{\mathcal{P}}/\sqrt{10} & \text{for 16-QAM} , \end{cases} \tag{2.16}$$

which is achieved by representing the power components by e and forcing the averaged value over all constellation points to $\mathcal{P}$.

2.5.2 Soft-Output Demapping

According to the mapping strategy applied at the transmitter, the receiver demaps the receive signal at symbol-level to bit-level message in the form of LLR (or L-value) as mentioned in Subsection 2.2.3. The LLR is a sort of soft information that measures the reliability of the estimated hard information. The L-value of a code bit c_ν is defined as the natural logarithm of the quotient between the probabilities that $c_\nu = 0$ and $c_\nu = 1$, which is given by [HOP96]

$$L(c_\nu) = \log \frac{\Pr\{c_\nu = 0\}}{\Pr\{c_\nu = 1\}} . \tag{2.17}$$

The L-value spreads in the range $(-\infty, \infty)$. When the occurrence of bit 0 and bit 1 are equally probable, i.e., $\Pr\{c_\nu = 0\} = \Pr\{c_\nu = 1\} = 0.5$, it results in an L-value equal to 0. In practice, this is commonly assumed for the transmitted bit sequence, indicating zero a-priori information.

Considering a flat fading channel or one subcarrier for a multi-path channel using OFDM, the system equation reads $y = hx+n$. Furthermore, c_ν denotes the νth code bit in the bit tuple that is modulated to the transmit symbol x with the index $\nu = 1, 2, \cdots, m$. By some simple probability manipulations, the L-value of c_ν conditioned on the receive signal y is calculated as

$$\begin{aligned} L(\hat{c}_\nu|y) &= \log \frac{\Pr\{c_\nu = 0|y\}}{\Pr\{c_\nu = 1|y\}} \\ &= \log \frac{\sum_{x \in \mathcal{A}_\nu^0} p\{y|x\}}{\sum_{x \in \mathcal{A}_\nu^1} p\{y|x\}} \\ &= \log \frac{\sum_{x \in \mathcal{A}_\nu^0} \exp\left\{\frac{|y-hx|^2}{\sigma_n^2}\right\}}{\sum_{x \in \mathcal{A}_\nu^1} \exp\left\{\frac{|y-hx|^2}{\sigma_n^2}\right\}} . \end{aligned} \tag{2.18}$$

Here, $\mathcal{A}_\nu^\xi$ denotes the set containing the symbols with the νth code bit equal to ξ, i.e., $c_\nu = \xi$, $\xi = 0, 1$. Note that the cardinality of $\mathcal{A}_\nu^\xi$ is equal to $|\mathcal{A}_\nu^\xi| = M/2$. In Fig. 2.10, the classification of the M constellation points into the sets $\mathcal{A}_1^0$ and $\mathcal{A}_1^1$ is shown for the first code bit c_1 in the bit tuple modulated to x. For graphical illustration, the exemplary mapping rules, namely, BPSK, QPSK, 8-PSK and 16-QAM shown in Fig. 2.9 are considered. With respect to a receive signal y on the complex plane, the solid lines and dashed lines correspond to the entries of x with c_1 equal to 0 and 1, respectively.

The a-posteriori probability (APP) involved in (2.18) that c_ν is transmitted conditioned on receiving y is given by

$$\Pr\{c_\nu = \xi | y\} = \sum_{x \in \mathcal{A}_\nu^\xi} \Pr\{x|y\} = \frac{\Pr\{x\}}{\Pr\{y\}} \sum_{x \in \mathcal{A}_\nu^\xi} p\{y|x\} \tag{2.19}$$

applying the Baye's rule. The scaling factor $\frac{\Pr\{x\}}{\Pr\{y\}}$ can be calculated using the completeness condition $\Pr\{c_\nu = 0|y\} + \Pr\{c_\nu = 1|y\} = 1$. With the channel knowledge h yielding a deterministic channel condition, the probability density $p\{y|x\}$ in the equations above can be deduced from AWGN channels as [Kam11]

$$p\{y|x\} = \frac{1}{\pi\sigma_n^2} \exp\left\{\frac{|y - hx|^2}{\sigma_n^2}\right\} . \tag{2.20}$$

2.6 Spatial Diversity

Compared to single-input single-output (SISO) systems, MIMO system setup in the sense of multiple transmit and receive antennas achieves either multiplexing or diversity gain or the combination of both [ZT03]. In this section, the focus is on exploiting the diversity gain at both the receiver and the transmitter by employing two commonly used MIMO schemes as illustrated in the following.

2.6.1 Maximum Ratio Combining

A single-input multiple-output (SIMO) system is considered in Fig. 2.11, where a transmitter is equipped with a single antenna and a receiver is equipped with $K > 1$ antennas. It is assumed that the links between the transmit antenna and the kth receive antenna are uncorrelated, with $k = 1, 2, \cdots, K$, and the fading channels are flat. To this end, the receive signal y_k at different antennas are weighted by the conjugate of the corresponding

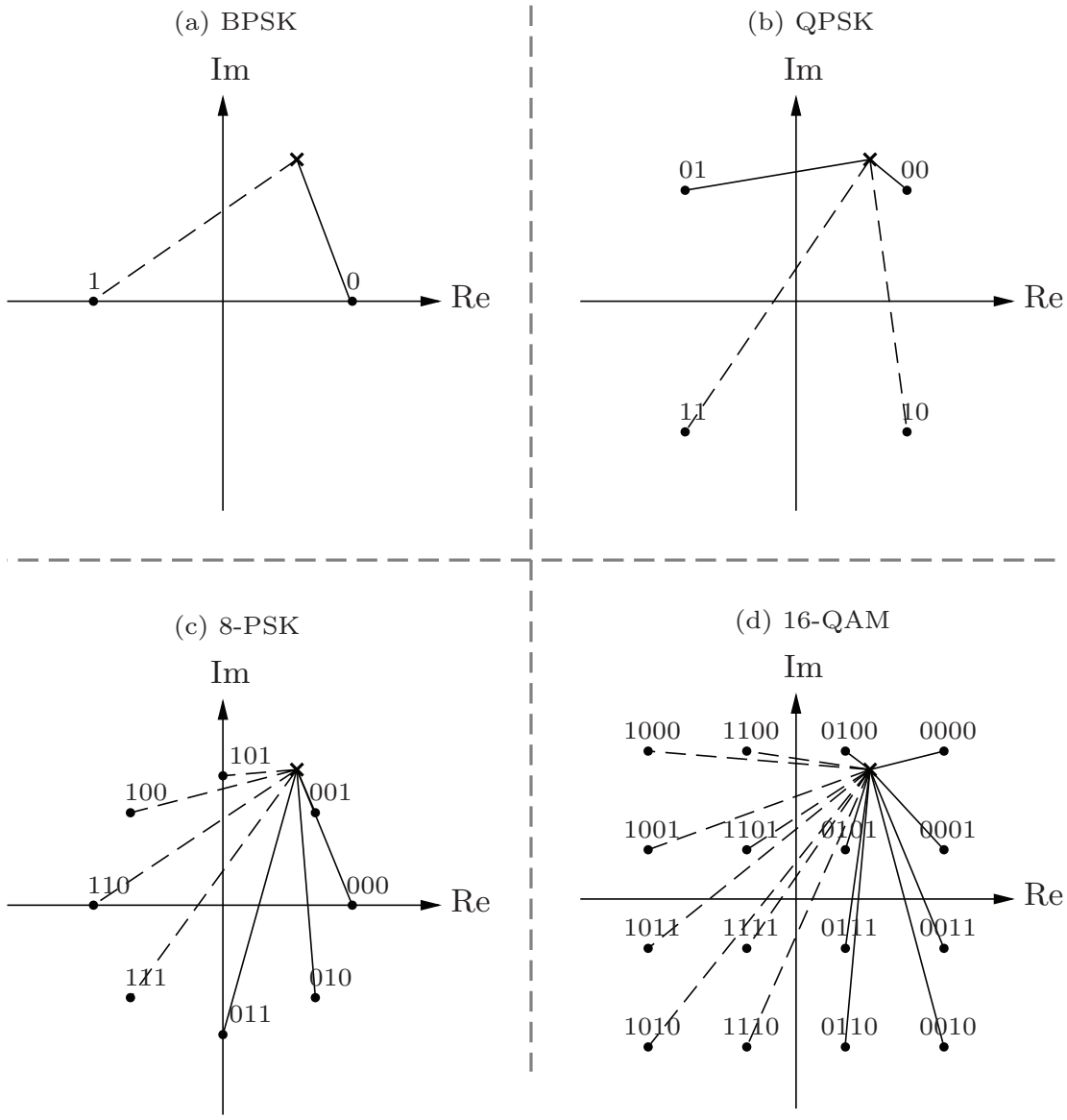

Figure 2.10: Graphical illustration for the constellation of alphabet constrained modulation with gray mapping. (a) for BPSK, (b) for QPSK, (c) for 8-PSK and (d) for 16-QAM. The receive signal y is marked as 'x'. Solid lines and dashed lines correspond to the entries of x with the first code bit c_1 equal to 0 and 1, respectively.

channel coefficient h_k^* and summed up, yielding the combined signal as

$$y_{\mathrm{MRC}} = \sum_{k=1}^{K} h_k^* y_k = \sum_{k=1}^{K} h_k^* (h_k x + n_k) = \sum_{k=1}^{K} |h_k|^2 x + \sum_{k=1}^{K} h_k^* n_k \; . \qquad (2.21)$$

Such a combining scheme is termed maximum ratio combining (MRC) since the receive SNR is maximized [Küh06]. Assuming normalized transmit

power, i.e., $\mathrm{E}\left\{|x|^2\right\} = 1$, the SNR of the combined signal is derived as

$$\mathrm{SNR} = \frac{\left(\sum_{k=1}^{K} |h_k|^2\right)^2}{\sum_{k=1}^{K} |h_k|^2 \sigma_n^2} = \sum_{k=1}^{K} \frac{|h_k|^2}{\sigma_n^2} = \sum_{k=1}^{K} \mathrm{SNR}_k \,, \tag{2.22}$$

which indicates that the effective SNR is equivalent to the sum of the SNRs from all links. Note that when using OFDM transmission in a frequency selective environment, the above analysis can be regarded as a subcarrier wise representation in the frequency domain. In other words, MRC is applied on each subcarrier respectively, where the assumption of a flat channel with different channel coefficients on the subcarriers is valid.

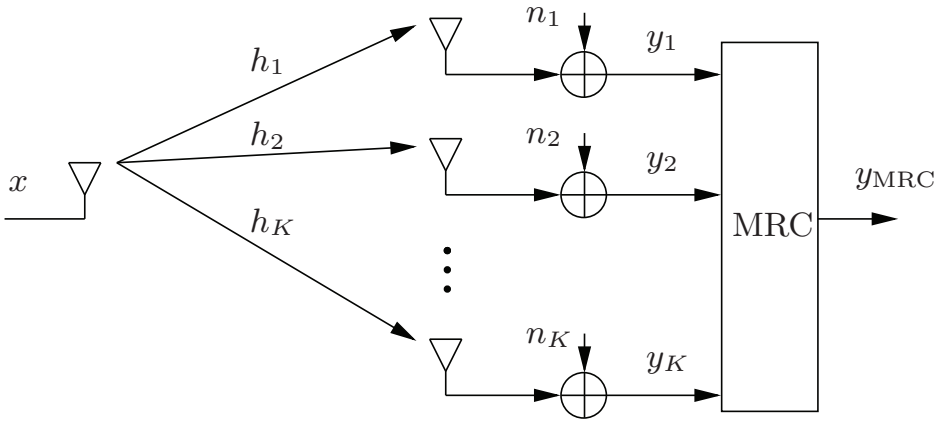

Figure 2.11: SIMO system with K receive antennas applying MRC to exploit receive diversity.

2.6.2 Orthogonal Space-Time Block Codes

For a multiple-input single-output (MISO) system, e.g., the transmitter is equipped with K antennas whereas only a single antenna is available at the receiver, space-time codes (STCs) can be applied to exploit transmit diversity without channel state information (CSI) at the transmitter [Küh06]. As shown in Fig. 2.12, the transmit signal is firstly pre-coded in both space and time dimensions before transmission. To be specific, N_s symbols are space-time coded among the K antennas in N_t time slots, resulting in a data rate

$$R_{\mathrm{ST}} = \frac{N_s}{N_t} \leq 1 \,. \tag{2.23}$$

In general, the following categories of STCs are commonly used in practice to exploit the spatial diversity at the transmitter side, including orthogonal

space-time block codes (OSTBCs) in [Ala98, TJC98], quasi-orthogonal space-time block codes (QOSTBCs) in [Jaf01], space-time Trellis codes (STTCs) in [TSC98, TNSC99], linear dispersion codes (LDCs) in [HH02], and so on. In this work, OSTBC is considered, which is employed in the upcoming chapters due to the facts that

- It can be easily adapted in systems with distributed transmit antennas. Furthermore, deletion of one or more layers of the code doesn't destroy the orthogonal code structure.
- Only linear detection with low computational efforts is required. This facilitates ease of implementation in practical systems.

In the sequel, the design of OSTBC for different number of transmit antennas and the corresponding detection process are illustrated.

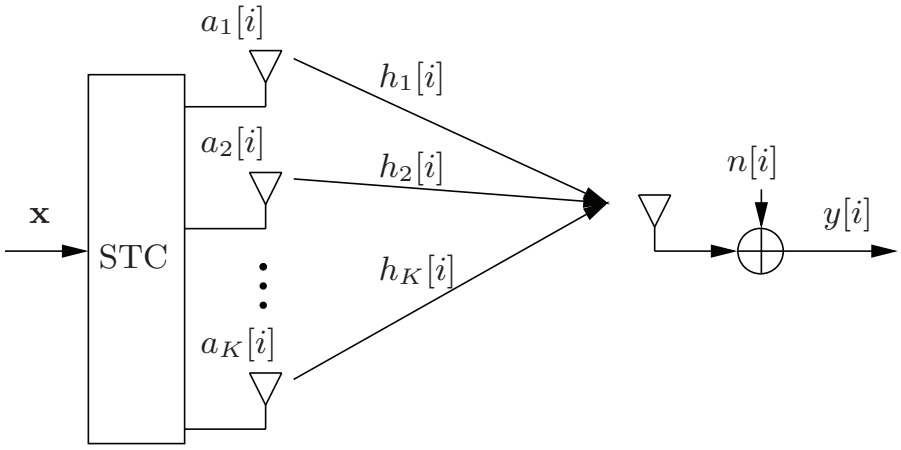

Figure 2.12: MISO system with K transmit antennas applying STC to exploit transmit diversity at time instant i.

Alamouti Code

For ease of illustration how an OSTBC is constructed and how it works, the most simple example known as Alamouti code [Ala98] is used. In this scheme, $K = 2$ transmit antennas are employed, on which the space-time code is distributed. Each pair of $N_s = 2$ symbols x_1 and x_2 are space-time coded and transmitted over $N_t = 2$ time slots, resulting in a data rate R_{ST} for OSTBC as $R_{\mathrm{OSTBC}} = N_s/N_t = 1$. The corresponding space-time code matrix $\mathbf{T}_2 = [\mathbf{a}[i]\ \mathbf{a}[i+1]]$ is defined as

$$\mathbf{T}_2 = \frac{1}{\sqrt{2}} \begin{bmatrix} x_1 & -x_2^* \\ x_2 & x_1^* \end{bmatrix} . \tag{2.24}$$

Here, the factor $\frac{1}{\sqrt{2}}$ ensures normalized transmit power when employing two transmit antennas. The columns $\mathbf{a}[i]$ and $\mathbf{a}[i+1]$ in $\mathbf{T}_2$ denote the transmit vectors in two successive time slots. Specifically, x_1 and x_2 are transmitted over the two antennas in the ith time slot while $-x_2^*$ and x_1^* are transmitted in the $(i+1)$th time slot subsequently. It is noted that $\mathbf{T}_2$ has the property that

$$\mathbf{T}_2^H \mathbf{T}_2 = \frac{1}{2}\left(|x_1|^2 + |x_2|^2\right)\mathbf{I}_2 \,, \tag{2.25}$$

indicating that the two layers of the space-code matrix are orthogonal to each other. The orthogonality condition is also fulfilled for the codes designed for more than two transmit antennas as shown later on. Therefore, this orthogonal code family applied block wise is termed OSTBC.

Implementing the Alamouti scheme, the receive signal vector $\mathbf{y} = [y[i]\ y[i+1]]^T$ collected in both the ith and the $(i+1)$th time slots is given by

$$\mathbf{y} = \begin{bmatrix} y[i] \\ y[i+1] \end{bmatrix} = \frac{1}{\sqrt{2}} \begin{bmatrix} x_1 & x_2 \\ -x_2^* & x_1^* \end{bmatrix} \begin{bmatrix} h_1 \\ h_2 \end{bmatrix} + \begin{bmatrix} n[i] \\ n[i+1] \end{bmatrix} = \mathbf{T}_2^T \mathbf{h} + \mathbf{n} \,, \tag{2.26}$$

where $\mathbf{n} = [n[i]\ n[i+1]]^T$ denotes the corresponding noise vector. The channel coefficients included in $\mathbf{h} = [h_1\ h_2]^T$ for the 2×1 MISO channel are assumed to be invariant during the two successive time slots. After receiving and taking the conjugate of the receive signal $y[i+1]$, the modified signal vector $\tilde{\mathbf{y}} = [y[i]\ y^*[i+1]]^T$ can be written as

$$\tilde{\mathbf{y}} = \begin{bmatrix} y[i] \\ y^*[i+1] \end{bmatrix} = \frac{1}{\sqrt{2}} \begin{bmatrix} h_1 & h_2 \\ h_2^* & -h_1^* \end{bmatrix} \begin{bmatrix} x_1 \\ x_2 \end{bmatrix} + \begin{bmatrix} n[i] \\ n^*[i+1] \end{bmatrix} = \frac{1}{\sqrt{2}} \mathbf{H}_2 \tilde{\mathbf{x}} + \tilde{\mathbf{n}} \tag{2.27}$$

by re-ordering the two linear equations. Herein, the equivalent channel matrix $\mathbf{H}_2$ has an orthogonal structure with the property that

$$\mathbf{H}_2^H \mathbf{H}_2 = \left(|h_1|^2 + |h_2|^2\right)\mathbf{I}_2 \,. \tag{2.28}$$

To this end, the vector $\tilde{\mathbf{y}}$ is filtered by $\mathbf{H}_2^H$. Note that this linear detection approach essentially corresponds to matched filtering. Therefore, the filter output $\mathbf{H}_2^H \tilde{\mathbf{y}}$ contains the transmit symbols x_1 and x_2 in each layer without cross-layer interference. Furthermore, the noise term is also filtered as $\mathbf{H}_2^H \tilde{\mathbf{n}}$, yielding the SNR equivalent in both layers as

$$\mathrm{SNR} = \frac{1}{2} \frac{\left(|h_1|^2 + |h_2|^2\right)^2}{\left(|h_1|^2 + |h_2|^2\right)\sigma_n^2} = \frac{1}{2}\left(\frac{|h_1|^2}{\sigma_n^2} + \frac{|h_2|^2}{\sigma_n^2}\right) = \frac{1}{2}\left(\mathrm{SNR}_1 + \mathrm{SNR}_2\right) \,. \tag{2.29}$$

Compared to (2.22) for the effective SNR in a SIMO system with $K = 2$ receive antennas employing MRC, the effective SNR of the Alamouti scheme in a MISO system looks similar except for a penalty factor $\frac{1}{2}$. This is because the channel knowledge at the receiver side in the SIMO system provides a $10 \log_{10} K \approx 3\text{dB}$ antenna gain, which is not achievable without CSI at the transmitter side in the MISO system. However, the diversity gain of order 2 is identical in both cases.

Extension to More than Two Transmit Antennas

The Alamouti scheme presented above works exclusively for two transmit antennas. When more than two antennas are available, other OSTBCs exist with lower rate R_{OSTBC}. In general, OSTBC with rate $R_{\text{OSTBC}} = 1/2$ can be designed for arbitrary number of transmit antennas, whereas rate-$R_{\text{OSTBC}} = 3/4$ OSTBC only exists for $K = 3$ and $K = 4$ antennas. These OSTBCs are introduced in [TJC98]. For example, the space-time code matrices $\mathbf{T}_3$ for $K = 3$ and $\mathbf{T}_4$ for $K = 4$ are given by

$$\mathbf{T}_3 = \frac{1}{\sqrt{3}} \begin{bmatrix} x_1 & -x_2 & -x_3 & -x_4 & x_1^* & -x_2^* & -x_3^* & -x_4^* \\ x_2 & x_1 & x_4 & -x_3 & x_2^* & x_1^* & x_4^* & -x_3^* \\ x_3 & -x_4 & x_1 & x_2 & x_3^* & -x_4^* & x_1^* & x_2^* \end{bmatrix} \tag{2.30}$$

and

$$\mathbf{T}_4 = \frac{1}{\sqrt{4}} \begin{bmatrix} x_1 & -x_2 & -x_3 & -x_4 & x_1^* & -x_2^* & -x_3^* & -x_4^* \\ x_2 & x_1 & x_4 & -x_3 & x_2^* & x_1^* & x_4^* & -x_3^* \\ x_3 & -x_4 & x_1 & x_2 & x_3^* & -x_4^* & x_1^* & x_2^* \\ x_4 & x_3 & -x_2 & x_1 & x_4^* & x_3^* & -x_2^* & x_1^* \end{bmatrix}, \tag{2.31}$$

respectively. Both matrices indicate that $N_s = 4$ symbols are transmitted over $N_t = 8$ time slots, resulting in a data rate $R_{\text{OSTBC}} = N_s/N_t = 1/2$ and thus the spectral efficiency is reduced. Moreover, the transmit power is normalized among all transmit antennas by the factor $\frac{1}{\sqrt{K}}$. It is also noted that the channel coefficients have to be constant during the $N_t = 8$ time slots for successful linear detection at the receiver.

Using the OSTBCs with the code matrices $\mathbf{T}_3$ and $\mathbf{T}_4$, the data rate loss due to $R_{\text{OSTBC}} = 1/2$ leads to halved spectral efficiency. As alternatives,

$\mathbf{T}'_3$ and $\mathbf{T}'_4$ defined as

$$\mathbf{T}'_3 = \frac{1}{\sqrt{3}} \begin{bmatrix} 2x_1 & -2x_2^* & \sqrt{2}x_3^* & \sqrt{2}x_3^* \\ 2x_2 & 2x_1^* & \sqrt{2}x_3^* & -\sqrt{2}x_3^* \\ \sqrt{2}x_3 & \sqrt{2}x_3 & -x_1 - x_1^* + x_2 - x_2^* & x_1 - x_1^* + x_2 + x_2^* \end{bmatrix} \tag{2.32}$$

and

$$\mathbf{T}'_4 = \frac{1}{\sqrt{4}} \begin{bmatrix} 2x_1 & -2x_2^* & \sqrt{2}x_3^* & \sqrt{2}x_3^* \\ 2x_2 & 2x_1^* & \sqrt{2}x_3^* & -\sqrt{2}x_3^* \\ \sqrt{2}x_3 & \sqrt{2}x_3 & -x_1 - x_1^* + x_2 - x_2^* & x_1 - x_1^* + x_2 + x_2^* \\ \sqrt{2}x_3 & -\sqrt{2}x_3 & -x_1 - x_1^* - x_2 - x_2^* & -x_1 - x_1^* - x_2 - x_2^* \end{bmatrix} \tag{2.33}$$

can be applied for $K = 3$ and $K = 4$ transmit antennas, respectively. Since $N_s = 3$ symbols are transmitted over $N_t = 4$ time slots, the data rate by using $\mathbf{T}'_3$ and $\mathbf{T}'_4$ is $R_{\text{OSTBC}} = N_s/N_t = 3/4$, which is improved compared to that for $\mathbf{T}_3$ and $\mathbf{T}_4$. Additionally, the channel coefficients need only to be invariant during $N_t = 4$ time slots. The detection mechanism of the above mentioned exemplary OSTBCs for $K = 3$ and $K = 4$ transmit antennas is similar to that described for the Alamouti code, and thus is omitted here. More details are referred to [TJC98, Küh06].

The analysis for OSTBC presented above is based on the assumption of flat fading channels, where the channel coefficients have to be invariant during N_t time slots such that the orthogonality of the code is preserved. However, when OFDM transmissions are applied in multi-path fading channels, performance loss is incurred by operating OSTBC in the adjacent N_t subcarriers in the frequency domain as the channel varies gradually in these subcarriers[1]. As an alternative, it can be interpreted that OSTBC is performed on OFDM frame base still in the time domain [LW00, MP00], with the assumption that the channel is block fading and remains constant during N_t OFDM frames. In this case, the signal entries of the space-time code matrices in (2.24), (2.30), (2.31), (2.32) and (2.33) are all regarded as OFDM symbols. Due to the avoidance of orthogonality loss, the second approach is adopted when OSTBC is applied in the following chapters.

[1] To be precise, this is called space-frequency code as coding takes place over subcarriers instead of time.

2.7 Information Theory

To understand the fundamental limits that are theoretically achievable in communication systems, one needs to track back to the mathematical field of information theory founded by Shannon [Sha48]. In this context, the basic concepts of information, entropy, mutual information and capacity are shortly reviewed in this section, which provide support to the analysis in the later chapters.

2.7.1 Information and Entropy

The information I contained in a transmit symbol x, which corresponds to a random process, is dependent on its probability $\Pr\{x\}$ and is defined as

$$I(x) = \log_2 \frac{1}{\Pr\{x\}} = -\log_2 \Pr\{x\} \ . \tag{2.34}$$

Here the logarithm of base 2 is used since digital communication systems are regarded to binary representation of data, therefore, $I(x)$ is measured in bits. The average information of a random process is called entropy and can be written as

$$H(x) = -\mathrm{E}\{\log_2 \Pr\{x\}\} = \begin{cases} -\sum_x \Pr\{x\} \log_2 \Pr\{x\} & \text{discrete} \\ -\int_x \Pr\{x\} \log_2 \Pr\{x\}\, dx & \text{continuous} \end{cases} \tag{2.35}$$

in case of discrete and continuous x, respectively. For example, assuming that M-QAM modulation is applied, one transmit symbol x contains $m = \log_2 M$ bits and each M-QAM symbol occurs with equal probability $\Pr\{x\} = 2^{-m}$. Thus, the entropy $H(x)$ can be calculated as

$$H(x) = -\sum_x \Pr\{x\} \log_2 \Pr\{x\} = -\sum_x 2^{-m} \log_2 2^{-m} = m \ , \tag{2.36}$$

which indicates that the average amount of information carried by x is m bits. This is in accordance with the fact that m bits are modulated to one M-QAM symbol.

2.7.2 Mutual Information

In the previous subsection, the information of the source is depicted. In communication systems, it is of interest how much information can be transmitted from the source to the sink, in other words, what influence does the physical channel impose on the information transfer. To this

end, the information available at the source that is conveyed to the sink is defined as mutual information (MI) $I(x;y)$. For elaboration on MI, the joint information of two random variables with respect to the transmit and receive symbols is firstly introduced, as given by

$$I(x,y) = \log_2 \frac{1}{\Pr\{x,y\}} = -\log_2 \Pr\{x,y\} \ , \tag{2.37}$$

where $\Pr\{x,y\}$ denotes the probability that both x and y occur. Correspondingly, the joint entropy is achieved by averaging $I(x,y)$ as

$$H(x,y) = -\mathrm{E}\{\log_2 \Pr\{x,y\}\} = -\sum_x \sum_y \Pr\{x,y\} \log_2 \Pr\{x,y\} \tag{2.38}$$

assuming discrete representation of x and y exemplarily here and in the sequel. $H(x,y)$ contains the total amount of information available in the communication system and can be decomposed into

$$H(x,y) = H(x) + H(y|x) = H(y) + H(x|y) \ . \tag{2.39}$$

Here $H(x|y)$, termed equivocation, denotes the conditional entropy that corresponds to the information of x being not part of y. Since y is completely known at the sink, $H(x|y)$ is essentially the information that got lost during the transmission. With the help of (2.38) and (2.39), $H(x|y)$ can be easily derived as

$$H(x|y) = -\mathrm{E}\{\log_2 \Pr\{x|y\}\} = -\sum_x \sum_y \Pr\{x,y\} \log_2 \Pr\{x|y\} \ . \tag{2.40}$$

On the other hand, the conditional entropy $H(y|x)$ corresponds to the information not originated from the source but received at the sink. In other words, $H(y|x)$ is the information that y contains if x is known, which stems from the distortion and noise in the channel. In case of assuming reliable communication, this amount of information is infinitely small and useless, thus named irrelevance.

Graphical illustration of the information transfer process described above in a communication system is shown in Fig. 2.13. It can be observed that MI, i.e., the information sent correctly from the source to the sink, can be calculated by

$$I(x;y) = H(x) - H(x|y) = H(y) - H(y|x) = H(x) + H(y) - H(x,y) \ . \tag{2.41}$$

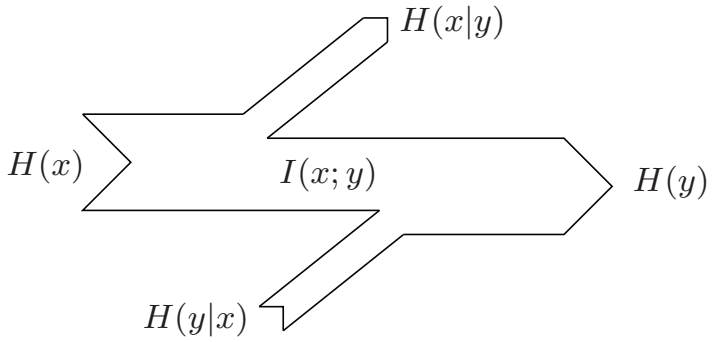

Figure 2.13: Graphical illustration of information transfer in a communication system. The mutual information $I(x;y)$ is transmitted from the source to the sink.

Inserting (2.35) and (2.40) into (2.41), yields

$$I(x;y) = \sum_x \sum_y \Pr\{x,y\} \log_2 \frac{\Pr\{x,y\}}{\Pr\{x\}\Pr\{y\}} \tag{2.42a}$$

$$= \sum_x \Pr\{x\} \sum_y \Pr\{y|x\} \log_2 \frac{\Pr\{y|x\}}{\sum_x \Pr\{y|x\}\Pr\{x\}} \,. \tag{2.42b}$$

This indicates that MI depends on the conditional probability $\Pr\{y|x\}$ determined by the channel and the a-priori probability $\Pr\{x\}$ of the transmit symbol. Therefore, for a given channel condition, the mutual information can be maximized by optimizing the statistics of the input alphabet, resulting in the capacity of this channel as

$$C = \max_{\Pr\{x\}} I(x;y) \,. \tag{2.43}$$

Shannon's channel coding theorem states that there must exist a code of rate $R_\mathrm{C} \leq C$ designed in such a way to guarantee error-free transmission [Sha48]. Since the codeword length is assumed to be arbitrary long, no specific methodology about how to design the code is given by the theorem. However, this motivates and provides milestone for practical channel code designs, e.g., the capacity-approaching Turbo codes [BGT93] and LDPC codes [MN96].

2.7.3 Capacity in AWGN Channels

In this subsection, the capacity of AWGN channels is derived with Gaussian input signal. Note that Gaussian is the optimal signal distribution considering continuous input x [Sha48], where x is of zero-mean and variance σ_x^2.

Furthermore, the entropy of a Gaussian distributed random variable x is given by

$$H(x) = \log_2\left(\pi e \sigma_x^2\right) \ . \tag{2.44}$$

Following the MI definition in (2.41), the capacity of AWGN channels can be deduced as

$$\begin{aligned} C &= H(y) - H(y|x) = H(y) - H(n) \\ &= \log_2\left(\pi e \sigma_y^2\right) - \log_2\left(\pi e \sigma_n^2\right) \\ &= \log_2\left(\pi e (\sigma_x^2 + \sigma_n^2)\right) - \log_2\left(\pi e \sigma_n^2\right) \\ &= \log_2\left(\frac{\sigma_x^2 + \sigma_n^2}{\sigma_n^2}\right) = \log_2\left(1 + \mathrm{SNR}\right) \ . \end{aligned} \tag{2.45}$$

Here, $H(y|x) = H(n)$ since the transmit symbol x is only subject to the Gaussian noise n, which remains uncertain at the receiver. Additionally, the variance of the receive signal y is calculated as $\sigma_y^2 = \sigma_x^2 + \sigma_n^2$ due to statistically independent x and n. (2.45) demonstrates the amount of information that can be conveyed in AWGN channels by a Gaussian distributed input signal for a given SNR, which grows unboundedly with increasing SNR.

2.7.4 Capacity with Discrete Alphabet

In digital communication systems, discrete alphabets introduced in Subsection 2.5.1 are applied to map the codeword to symbols. e.g., M-QAM. In this case, the MI with discrete transmit signal x and continuous receive signal y is required and can be formulated as

$$I(x;y) = \int_y \sum_x \Pr\{y|x\} \Pr\{x\} \log_2 \frac{\Pr\{y|x\}}{\sum_x \Pr\{y|x\} \Pr\{x\}} dy \ . \tag{2.46}$$

Assuming equiprobable transmit symbols in practice, the MI (2.46) corresponds to the channel capacity using M-QAM modulation. Since no closed form solution exits, this MI expression has to be evaluated numerically.

The capacity for continuous Gaussian input signal and discrete M-QAM alphabet in AWGN channels are shown in Fig. 2.14. As can be observed in the figure, Gaussian input acts as the upper-bound with the capacity expanding logarithmically as the SNR increases. The capacity of the M-QAM schemes are bounded by that of Gaussian and saturate at finite levels. Specifically, the maximum capacity for BPSK, 4-QAM and 16-QAM are 1, 2 and 4 bits/s/Hz, respectively, which correspond to the number of bits $m = \log_2 M$ that are carried in each M-QAM symbol.

Note that the capacity is averaged over different channel realizations in fading channels, resulting in the ergodic capacity. In case of multi-path

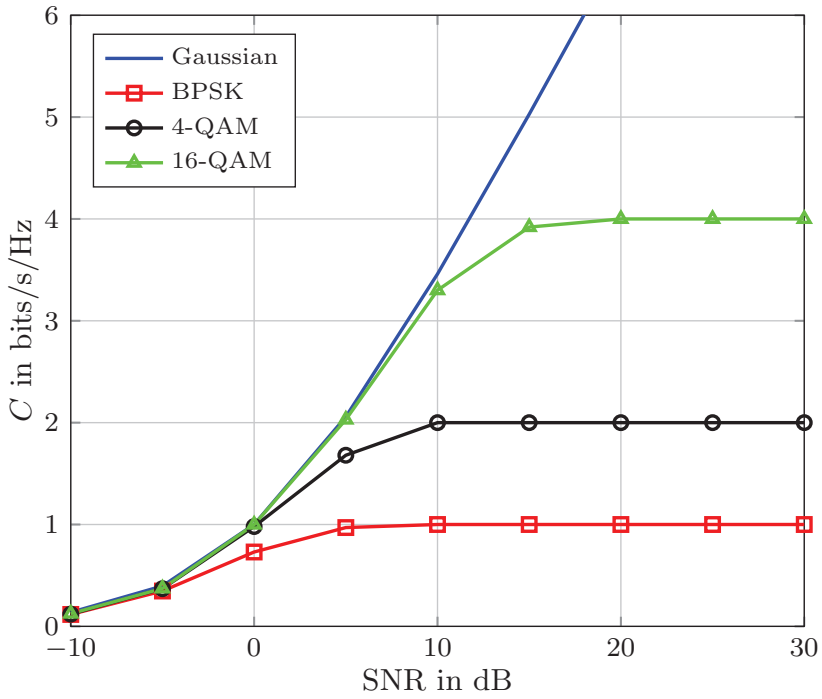

Figure 2.14: Capacity of AWGN channels with Gaussian input signal as well as different discrete alphabets, namely, BPSK, 4-QAM and 16-QAM.

fading using OFDM transmissions, the ergodic capacity is achieved by also averaging over the subcarriers in the frequency domain.

2.8 Chapter Summary

In this chapter, the fundamentals of digital communication systems only considering baseband processing are presented to serve as basics for the following chapters. In Section 2.2, the system setup involving the transmitter and receiver structure as well as the channel model are discussed in general. The application of OFDM efficiently combats frequency selectivity from the multi-path fading channel with simple one-tap equalization, which is presented in Section 2.3. Channel coding and digital modulation are elaborated in Section 2.4 and Section 2.5, respectively, with exemplary coding and modulation schemes introduced therein. In Section 2.6, two diversity-exploiting schemes are examined in the context of multiple-antenna systems. Both schemes serve as benchmarks in distributed relaying networks specified in the later chapters. In the final analysis, information theory related issues are shortly reviewed in Section 2.7, which provide insights into the theoretical limits of system performance in terms of mutual information for specific scenarios under consideration in this work.

Chapter 3

One-Way SISO Relaying

3.1 Overview

Cooperative communications enjoy increasing research interests in wireless networks by offering multi-folded advantages such as higher system throughput and coverage extension. For example, the link from the source to the destination can be expanded by an additional relaying node to assist the direct transmission. This intermediate relay node between both terminals is intended to reduce the effective path-loss magnificently and provides cooperative diversity. To this end, the functionality of the relaying node needs to be carefully defined to enhance the end-to-end system performance, which heavily depends on the topology of the relaying network. In terms of the operation method at the relay, different relaying schemes are distinguished that should be studied and compared under practical circumstances.

In this chapter, the basics of cooperative communication supported by relays are elaborated first in Section 3.2 with recapture of a selection of the most commonly used traditional relaying schemes in the literature. Note that this relay assisted transmission is defined in a one-way sense from the source to the destination. Moreover, the spatial diversity is constrained to single-antenna nodes and only one relay is present to assist the transmission. Such a 'one-way SISO relaying' setup will be extended to more complex configurations in later chapters. One contribution of this work is to adapt the classical relaying schemes to coded OFDM transmissions since each subcarrier has a varying link quality in this case [WW11, WLW$^+$16a], which are presented in Section 3.3. Their performances are examined and compared in Section 3.4 considering different channel codes and network topologies. Section 3.5 summarizes the main topics and achievements of this chapter.

3.2 Basics of Relaying Communications

The basic concepts for relay assisted cooperative communication are presented in this section. For the sake of illustration, a simple triplet relaying network is considered. The principles of several classical relaying schemes are shortly reviewed as well.

3.2.1 System Model

In wireless communications, the performance of the transmission from a source node to a destination node may be severely degraded due to large path-loss and shadowing effects. As a solution, the application of cooperative strategies attracts increasing interests, which offers several advantages such as improved error rate performance, boosted system throughput and coverage extension. To this end, the source-destination link is expanded by additional transceivers in the link, e.g., relaying nodes.

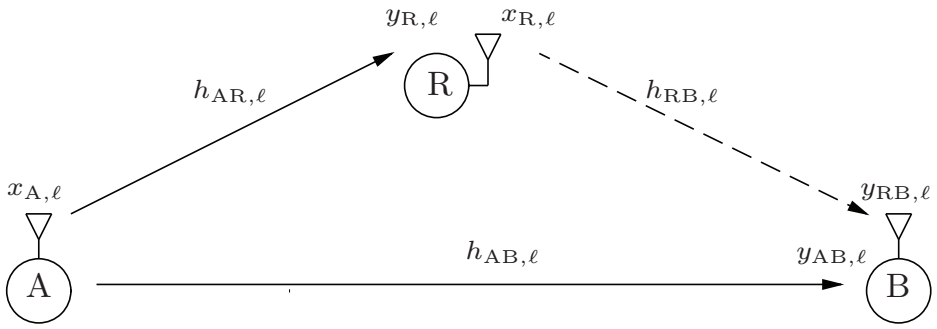

Figure 3.1: A single-relay system operating in a half-duplex mode, where the relay R supports the transmission from the source A to the destination B in two phases.

The system model of a relaying network is shown in Fig. 3.1, where the transmission from the source A to the destination B is supported by an intermediate relay R. Due to the half-duplex constraint, i.e., one node is not able to transmit and receive at the same time and frequency, the overall communication is divided into two phases. In the first phase, as indicated by the solid line in the figure, the source message is transmitted from source A to relay R. After reception, R forwards a processed message to the destination B in the second phase, as indicated by the dashed line in the figure. Finally, B estimates the source message from its receive signal. Due to the broadcast nature of the wireless channels, the destination B also receives a replica of the source message in the first phase, which can be utilized jointly with the relay message. Note that R can also only forward an auxiliary message to

B in this case since the desired message is entirely contained in the receive signal directly from A. Examples of such a coded cooperation approach are found in [Wu09, WWWK10] but not included in this work.

3.2.2 Conventional Relaying Schemes

Distinguished by the operation at the relay, a selection of conventional relaying schemes are shortly reviewed focusing on their basic relaying principles in the sequel. Some of these are extended and modified in case of OFDM transmissions in the next section.

Amplify-Forward

A simple approach to perform the relay functionality is linearly amplifying the receive signal constrained by the available power budget at the relay, as referred to amplify-forward (AF) [LTW04]. In this way, not only the desired signal but also the noise from the source-relay link is amplified, which is forwarded to the destination and degrades the overall system performance. However, no decoding module is required at the relay, and thus the computational complexity is relatively low.

Quantize-Forward

In modern digital communication systems, pure AF relaying poses practical challenges since the receive signal at the relay has to be quantized and stored with finite resolution by analog-to-digital conversion (ADC). In this context, the quantize-forward (QF) relaying scheme proposed in [SY08] is a more practically implementable alternative, which quantizes the receive signal with a finite number of bits per sample at the relay and forwards this quantized version to the destination.

Decode-Forward

To avoid noise amplification in AF, the source message is estimated by decoding the receive signal at the relay. Correspondingly, the noise from the source-relay link can be totally removed in case of correct decoding and the estimated source message is re-encoded and relayed to the destination. Since decoding is performed at the relay, this scheme is termed decode-forward (DF) [LTW04], which achieves coding gain at the relay compared to AF. However, when decoding errors occur, the estimated message containing erroneous information will be forwarded, causing error propagation that jeopardizes the performance at the destination.

Decode-Estimate-Forward

Since the erroneous hard decisions from decoding the source message will propagate to the destination, one alternative to mitigate this impairment is to exploit the varying reliability of the bits at the relay by the application of soft relaying techniques, for example, decode-estimate-forward (DEF). In this case, soft information in the form of the expectation values of the estimated code bits known as soft bits are transmitted from the relay to the destination [WWK08, WWK09, Wei13, Len16]. However, the distribution of the transmit signal at the relay is continuous, which has to be determined such that the corresponding LLRs at the destination can be calcuated correctly. As a result, this leads to increased computational effort as the trade-off for improved error rate performance.

Hybrid Decode-Amplify-Forward

The above mentioned relaying schemes operate in a non-adaptive mode, i.e., the relay always transmits to the destination using AF, QF, DF or DEF irrespective of the channel condition or decoding status. On the other hand, adaptive relaying allows the relay to exploit the status information and adjust the applied relaying strategy correspondingly. For instance, in the hybrid decode-amplify-forward (HDAF) [DZ09a, DZ09b] relaying scheme, the source message is firstly decoded at the relay. Assuming the application of a perfect CRC code, the relay is aware of the decoding status. If error-free decoding is achieved, this correctly decoded source message is forwarded to the destination, corresponding to DF without error propagation. Otherwise, AF is employed. In this way, the advantages of both AF and DF are jointly exploited at the expense of adapting the relaying strategies. This adaptive relaying scheme is beyond the scope of this work.

3.3 OFDM-based Relaying Schemes

In order to investigate different relaying schemes, the cooperative network shown in Fig. 3.1 with a single half-duplex relay R supporting the transmission from the source A to the destination B is considered, where all the three nodes are equipped with a single antenna. As the application of OFDM is assumed to combat multi-path fading for practical considerations, this results in a varying link quality per subcarrier. Correspondingly, the most commonly used conventional relaying schemes presented in the previous section, namely, AF and DF, should be adjusted to OFDM transmissions and may be modified to yield improved performance, as presented in [Ste10, WW11].

In the first phase, the binary information word $\mathbf{b}_\mathrm{A}$ of length N_b is encoded by a linear channel code Γ into the binary source codeword $\mathbf{c}_\mathrm{A} = \Gamma(\mathbf{b}_\mathrm{A})$ of length N_c, yielding the code rate $R_\mathrm{C} = N_b/N_c$. Subsequently, this codeword is interleaved and mapped to the OFDM symbol vector $\mathbf{x}_\mathrm{A} = \mathcal{M}(\mathbf{c}_\mathrm{A})$ of length $L = N_c/m$ employing a mapper $\mathcal{M}$ with an M-ary modulation alphabet. Here, $m = \log_2 M$ represents the number of bits contained in each subcarrier. Note that unless otherwise mentioned, each OFDM symbol vector is individually encoded with L denoting the number of subcarriers. Furthermore, the source symbol vector $\mathbf{x}_\mathrm{A} = [x_{\mathrm{A},1}\ x_{\mathrm{A},2}\ \cdots\ x_{\mathrm{A},L}]^T$ consists of L symbols $x_{\mathrm{A},\ell}$, $\ell = 1, 2, \cdots, L$, where the symbol $x_{\mathrm{A},\ell} = \mathcal{M}(c_{\mathrm{A},\ell})$ is dependent on m code bits that are collected in the code bit tuple $c_{\mathrm{A},\ell} = [c_{\mathrm{A},1,\ell}\ c_{\mathrm{A},2,\ell}\ \cdots\ c_{\mathrm{A},m,\ell}]^T$. Assuming the availability of the direct link between A and B, the source symbol vector $\mathbf{x}_\mathrm{A}$ is then broadcast through the wireless channels, which yields the receive signal on the ℓth subcarrier at relay R and destination B as

$$y_{\mathrm{R},\ell} = h_{\mathrm{AR},\ell} x_{\mathrm{A},\ell} + n_{\mathrm{R},\ell} \tag{3.1a}$$

$$y_{\mathrm{AB},\ell} = h_{\mathrm{AB},\ell} x_{\mathrm{A},\ell} + n_{\mathrm{AB},\ell}\ , \tag{3.1b}$$

respectively. Using the receive signal vector $\mathbf{y}_\mathrm{R} = [y_{\mathrm{R},1}\ y_{\mathrm{R},2}\ \cdots\ y_{\mathrm{R},L}]^T$, the relay generates the transmit symbol vector $\mathbf{x}_\mathrm{R} = [x_{\mathrm{R},1}\ x_{\mathrm{R},2}\ \cdots\ x_{\mathrm{R},L}]^T = f(\mathbf{y}_\mathrm{R})$ for the transmission in the second phase based on the selected relaying function $f(\cdot)$. Therefore, the receive signal vector at the destination B on the ℓth subcarrier is given by

$$y_{\mathrm{RB},\ell} = h_{\mathrm{RB},\ell} x_{\mathrm{R},\ell} + n_{\mathrm{RB},\ell}\ . \tag{3.2}$$

Consequently, the receive vectors $\mathbf{y}_\mathrm{AB}$ in the first phase from source A and $\mathbf{y}_\mathrm{RB}$ in the second phase from relay R are jointly considered to estimate the source message by, e.g., MRC, as shown in Fig. 3.2 for the block diagram of the whole relaying system.

The average transmit power of the source A on subcarrier ℓ is normalized and denoted as $\mathcal{P}_{\mathrm{A},\ell} = \mathrm{E}\{|x_{\mathrm{A},\ell}|^2\} = 1$. Assuming perfect CSI at the receiver, but no CSI is available at the transmitter, equal power is allocated on all subcarriers and thus the total transmit power at the source is given by $\mathcal{P}_\mathrm{A} = L \cdot \mathcal{P}_{\mathrm{A},\ell}$. Similarly, $\mathcal{P}_{\mathrm{R},\ell} = \mathrm{E}\{|x_{\mathrm{R},\ell}|^2\}$ and $\mathcal{P}_\mathrm{R}$ denote the average transmit power on subcarrier ℓ and the total transmit power at the relay, respectively. It is noted that the power is not necessarily equal on all subcarriers, see e.g., in Subsection 3.3.2 later on. However, normalized transmit power is still assumed, yielding $\sum_{\ell=1}^{L} \mathcal{P}_{\mathrm{R},\ell}/L = 1$.

Assuming multi-path fading channels with N_H channel taps in the time domain, the corresponding channel coefficients $h_{\mathrm{AR},\ell}$, $h_{\mathrm{AB},\ell}$ and $h_{\mathrm{RB},\ell}$ in (3.1)

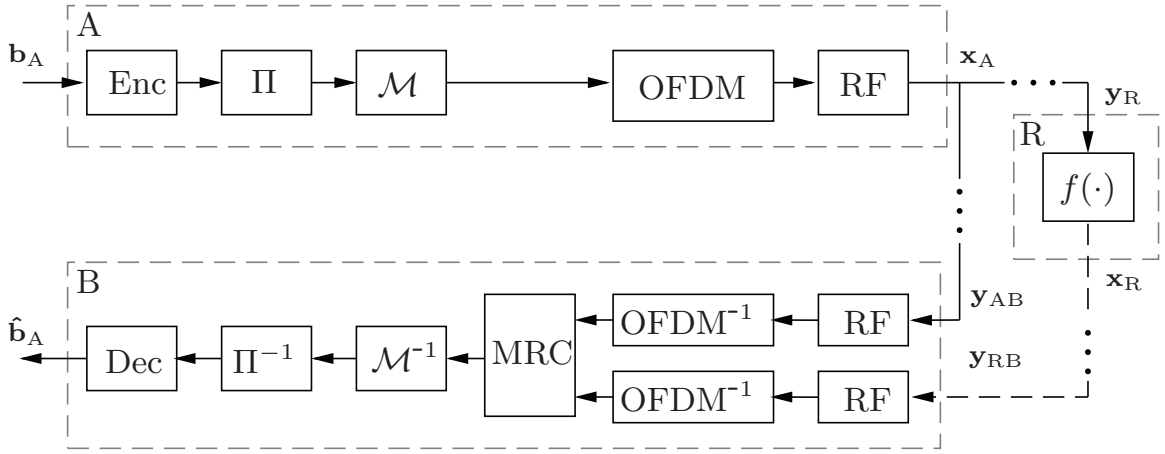

Figure 3.2: Block diagram of a relaying system with coded OFDM to combat multi-path fading channels ($\cdots$). After reception from source A, relay R forwards the message $\mathbf{x}_\mathrm{R} = f(\mathbf{y}_\mathrm{R})$ to destination B.

and (3.2) are defined in the frequency domain with variance $\sigma_\mathrm{H}^2 = 1/(N_\mathrm{H} d^\alpha)$ for the AR, AB and RB links, respectively. Therein, the path-loss exponent is denoted as α and $d \in \{d_\mathrm{AR}, d_\mathrm{AB}, d_\mathrm{RB}\}$ represent the distance components for these links. Moreover, the AWGN terms $n_{\mathrm{R},\ell}$, $n_{\mathrm{AB},\ell}$ and $n_{\mathrm{RB},\ell}$ are i.i.d. zero-mean complex random variables with variance σ_n^2.

3.3.1 Amplify-Forward with Constant Power

In the context of AF, the relay simply forwards an amplified version of the receive signal $\mathbf{y}_\mathrm{R}$ constrained by its power budget. Regarding to OFDM systems, the amplification can be performed either in the frequency domain or in the time domain. For the former case, the same transmit power $\mathcal{P}_{\mathrm{R},\ell}$ is achieved on each subcarrier. To meet such a subcarrier wise equal power constraint [WW11], the amplification factor on the ℓth subcarrier is given by

$$\beta_\ell = \sqrt{\frac{1}{|h_{\mathrm{AR},\ell}|^2 + \sigma_n^2}} \tag{3.3}$$

with the corresponding block diagram at the relay shown in Fig. 3.3. The receive signal in the time domain is firstly transformed to the frequency domain. Afterwards, the amplification is performed subcarrier wise as $x_{\mathrm{R},\ell} = \beta_\ell y_{\mathrm{R},\ell}$. Each element in the resulting signal vector $\mathbf{x}_\mathrm{R}$ is of equal power, which is transformed to the time domain again for transmission. Therefore, this OFDM-based relaying scheme is termed AF with constant power (AF-CP). Note that besides the subcarrier wise multiplication, two FFT/IFFT opera-

tions are required as extra overhead for baseband processing, contributing to computational complexity.

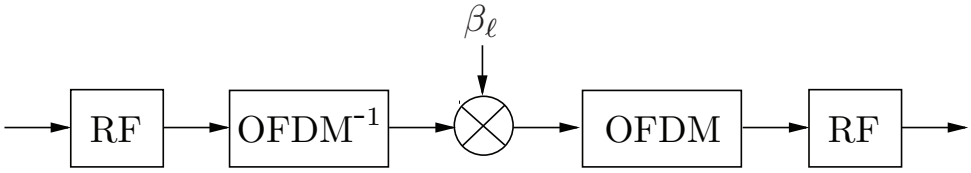

Figure 3.3: Block diagram at the relay for AF-CP, where the amplification is performed in frequency domain with different β_ℓ per subcarrier.

Substituting $x_{\mathrm{R},\ell} = \beta_\ell y_{\mathrm{R},\ell}$ into (3.2), the receive signal at the destination B can be rewritten as

$$\begin{aligned} y_{\mathrm{RB},\ell} &= h_{\mathrm{RB},\ell}\beta_\ell(h_{\mathrm{AR},\ell}x_{\mathrm{A},\ell} + n_{\mathrm{R},\ell}) + n_{\mathrm{RB},\ell} \\ &= h_{\mathrm{RB},\ell}\beta_\ell h_{\mathrm{AR},\ell}x_{\mathrm{A},\ell} + h_{\mathrm{RB},\ell}\beta_\ell n_{\mathrm{R},\ell} + n_{\mathrm{RB},\ell} \\ &= h_{\mathrm{ARB},\ell}x_{\mathrm{A},\ell} + n_{\mathrm{ARB},\ell} \end{aligned} \tag{3.4}$$

with the equivalent channel coefficient $h_{\mathrm{ARB},\ell} = h_{\mathrm{RB},\ell}\beta_\ell h_{\mathrm{AR},\ell}$ and the equivalent noise term $n_{\mathrm{ARB},\ell} = h_{\mathrm{RB},\ell}\beta_\ell n_{\mathrm{R},\ell} + n_{\mathrm{RB},\ell}$ of variance $\sigma^2_{n,\mathrm{ARB},\ell} = (\beta_\ell^2|h_{\mathrm{RB}}|^2 + 1)\sigma_n^2$. Subsequently, both receive signal vectors $\mathbf{y}_{\mathrm{AB}}$ from the source A and $\mathbf{y}_{\mathrm{RB}}$ from the relay R are combined using subcarrier wise MRC. The maximum SNR on each subcarrier is achieved by considering the varying noise variances of both links in the combiner as

$$\begin{aligned} \tilde{x}_{\mathrm{MRC},\ell} &= \frac{h^*_{\mathrm{AB},\ell}}{\sigma_n^2}y_{\mathrm{AB},\ell} + \frac{h^*_{\mathrm{ARB},\ell}}{\sigma^2_{n,\mathrm{ARB},\ell}}y_{\mathrm{RB},\ell} \\ &= h_{\mathrm{MRC},\ell}x_{\mathrm{A},\ell} + n_{\mathrm{MRC},\ell} \end{aligned} \tag{3.5}$$

with the equivalent parameters

$$h_{\mathrm{MRC},\ell} = \frac{|h_{\mathrm{AB},\ell}|^2}{\sigma_n^2} + \frac{|h_{\mathrm{ARB},\ell}|^2}{\sigma^2_{n,\mathrm{ARB},\ell}} \triangleq \mathrm{SNR}_\ell \tag{3.6a}$$

$$\sigma^2_{n,\mathrm{MRC},\ell} = h_{\mathrm{MRC},\ell} \tag{3.6b}$$

used for soft demapping at the destination B. It is noticed that the equivalent SNR on the ℓth subcarrier is identical to the equivalent channel coefficient after MRC, as shown in (3.6a), which corresponds to the sum of the SNRs for both the AB link and the ARB link. After demapping, the resulting LLRs from the demodulator are de-interleaved and fed to the binary channel decoder to estimate the source message.

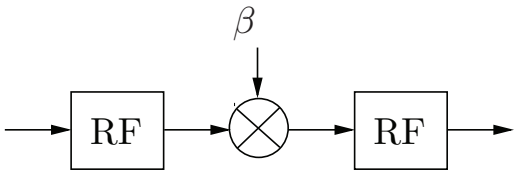

Figure 3.4: Block diagram at the relay for AF-CG, where the amplification is performed in time domain with a common β over all subcarriers.

3.3.2 Amplify-Forward with Constant Gain

In contrast to AF-CP, the amplification can be also carried out in the time domain. To this end, an equal gain is achieved on all subcarriers by a common amplification factor β defined as

$$\beta = \sqrt{\frac{1}{||\mathbf{h}_{\mathrm{AR}}||^2/L + \sigma_n^2}} \tag{3.7}$$

with the block diagram at the relay shown in Fig. 3.4. Using this common factor, the transmit signal on the ℓth subcarrier yields $x_{\mathrm{R},\ell} = \beta y_{\mathrm{R},\ell}$. Since the receive signal on each subcarrier is subject to the same amplification gain, this scheme is referred to AF with constant gain (AF-CG). Note that in comparison to AF-CP with equal power allocation, AF-CG allocates more power to subcarriers with receive signals of larger amplitude $|y_{\mathrm{R},\ell}|$ at the relay, i.e., to subcarriers with higher SNR on the AR link, which can be observed in Fig. 3.5. For MRC at the destination B, (3.5) and (3.6) are employed with the constant β.

The advantage of AF-CG over AF-CP is that the signal processing at the relay remains in the time domain, and thus no FFT/IFFT operations are required. To this end, computational efforts can be reduced, which is a crucial point in practical implementation aspects.

3.3.3 Decode-Forward

The AF scheme ignores the applied channel code and amplifies the noise besides the desired signal at the relay R. In order to exploit the coding gain, the DF scheme is employed. As shown in Fig. 3.6 for the corresponding block diagram at R, the receive signal vector $\mathbf{y}_{\mathrm{R}}$ is demodulated and decoded to estimate the source information word $\mathbf{b}_{\mathrm{A}}$. Specifically, the LLRs $\mathbf{L}_{\mathrm{A},b}$ for the information bits from the decoder output are quantized, resulting in $\hat{\mathbf{b}}_{\mathrm{A,DF}}$. Subsequently, these estimates are re-encoded by channel coding, yielding the estimated codeword $\hat{\mathbf{c}}_{\mathrm{A,DF}}$ at the relay. The interleaved code bits are again

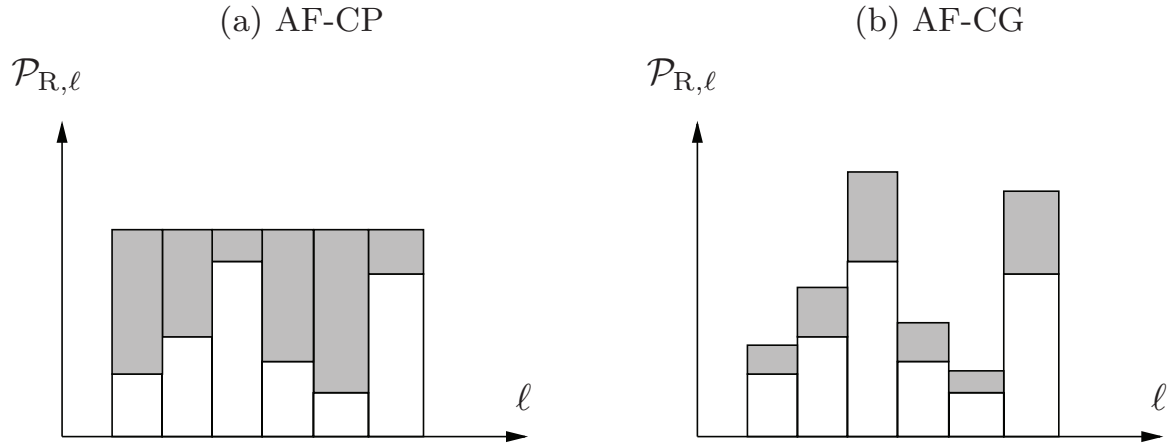

Figure 3.5: Power allocation for AF-CP in (a) and AF-CG in (b) with the blank bars and gray bars representing the subcarrier wise channel gain and the amplification gain, respectively. Equal power $\mathcal{P}_{\mathrm{R},\ell}$ is achieved for AF-CP, whereas more power is allocated to subcarriers with larger channel gain for AF-CG.

mapped to the OFDM symbol vector $\mathbf{x}_{\mathrm{R}}$ using $\mathcal{M}$, which is forwarded to the destination. For simplicity the same coding and modulation schemes at the relay are employed as the source. Furthermore, when decoding is performed at the relay, the relay power $\mathcal{P}_{\mathrm{R}}$ is normalized and equally assigned over all subcarriers, i.e., $\mathcal{P}_{\mathrm{R},\ell} = \mathrm{E}\{|x_{\mathrm{R},\ell}|^2\} = 1$ and $\mathcal{P}_{\mathrm{R}} = L \cdot \mathcal{P}_{\mathrm{R},\ell}$.

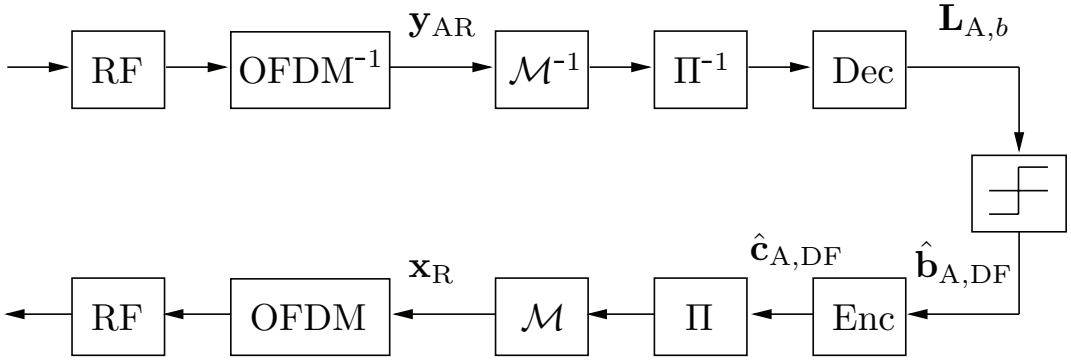

Figure 3.6: Block diagram at the relay for DF, where the estimated information bits $\hat{\mathbf{b}}_{\mathrm{DF}}$ are re-encoded to yield the estimated code bits $\hat{\mathbf{c}}_{\mathrm{DF}}$.

Supposing that the relay performs error-free decoding, i.e., $\hat{\mathbf{b}}_{\mathrm{A,DF}} = \mathbf{b}_{\mathrm{A}}$, the MRC at destination B is presented as

$$\begin{aligned} \tilde{x}_{\mathrm{MRC},\ell} &= \frac{h^*_{\mathrm{AB},\ell}}{\sigma_n^2} y_{\mathrm{AB},\ell} + \frac{h^*_{\mathrm{RB},\ell}}{\sigma_n^2} y_{\mathrm{RB},\ell} \\ &= h_{\mathrm{MRC},\ell} x_{\mathrm{A},\ell} + n_{\mathrm{MRC},\ell} \end{aligned} \tag{3.8}$$

with the equivalent channel and noise variance

$$h_{\mathrm{MRC},\ell} = \frac{|h_{\mathrm{AB},\ell}|^2}{\sigma_n^2} + \frac{|h_{\mathrm{RB},\ell}|^2}{\sigma_n^2} \triangleq \mathrm{SNR}_\ell \tag{3.9a}$$

$$\sigma_{n,\mathrm{MRC},\ell}^2 = h_{\mathrm{MRC},\ell} \, . \tag{3.9b}$$

However, if decoding errors occur at the relay, these erroneous decisions will be propagated to the destination, and thus jeopardize the performance of MRC significantly. Such an impact will be even more dominating if the RB link is much stronger than the AR link, which happens, e.g., when the relay is located closer to the destination compared to the source. Therefore, it would be beneficial to exploit reliability information of the relay at the destination. For instance, the knowledge about the SNR of the AR link implying the decoding reliability at the relay can be used, as to be discussed in the next subsection.

3.3.4 Decode-Quantize-Forward

As error propagation jeopardizes the performance of DF, this can be mitigated using reliability information of the decoding results at the relay. To this end, the correspondence of the code bit error (CBE) at the relay with the amplitude of the channel coefficient $|h_{\mathrm{AR},\ell}|$ is investigated firstly, which is shown in Fig. 3.7 [WW11]. Note that $|h_{\mathrm{AR},\ell}|^2$ is proportional to the SNR of the AR link. For one fixed arbitrary channel realization, the CBE for the estimated codeword $\hat{\mathbf{c}}_{\mathrm{A,DF}}$ is achieved by transmitting a large number of OFDM symbols over this channel using BPSK and an optimized LDPC code. It can be observed in the figure, that the subcarrier wise CBEs normalized to the largest value among all CBEs are uniformly distributed over the subcarriers, indicating no direct relationship between $|h_{\mathrm{AR},\ell}|$ and the CBE. This is because in case of a decoding failure at the relay, i.e., $\hat{\mathbf{b}}_{\mathrm{A,DF}} \neq \mathbf{b}_{\mathrm{A}}$, the erroneous information word $\hat{\mathbf{b}}_{\mathrm{A,DF}}$ is used for re-encoding, which results in an erroneous codeword $\hat{\mathbf{c}}_{\mathrm{A,DF}}$. Due to the LDPC encoder structure, the information bit errors are spread over the whole codeword $\mathbf{c}_{\mathrm{R}}$, and furthermore, the whole OFDM symbol $\mathbf{x}_{\mathrm{R}}$. Therefore, the uniformly distributed CBEs are irrespective of the reliability information about the AR link and can not be exploited at the destination B.

In order to make use of the reliability information $|h_{\mathrm{AR},\ell}|$ at B to mitigate error propagation, the decode-quantize-forward (DQF) approach is developed [WW11], which estimates the code bits directly from the channel decoder without re-encoding at the relay. As shown in Fig. 3.8 for the block diagram, the LLRs of the code bits $\mathbf{L}_{\mathrm{A},c}$ are quantized, leading to the estimated codeword $\hat{\mathbf{c}}_{\mathrm{A,DQF}}$ for DQF. Note that in contrast to DF, this estimate

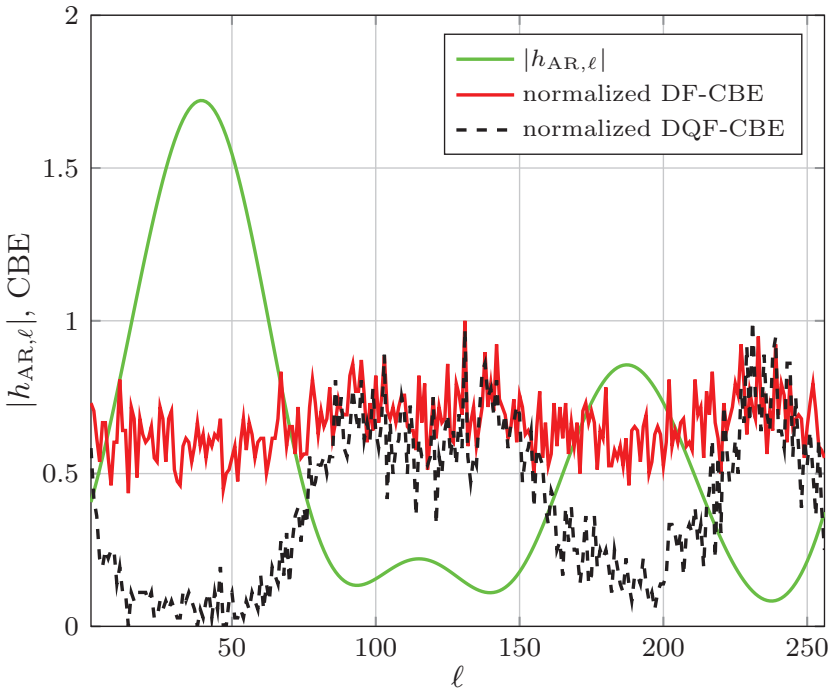

Figure 3.7: Amplitude of the channel coefficient $|h_{\mathrm{AR},\ell}|$ versus normalized CBEs of DF and DQF at the relay for one fixed arbitrary channel realization with $N_{\mathrm{H}} = 5$ channel taps in time domain and $L = 256$ subcarriers.

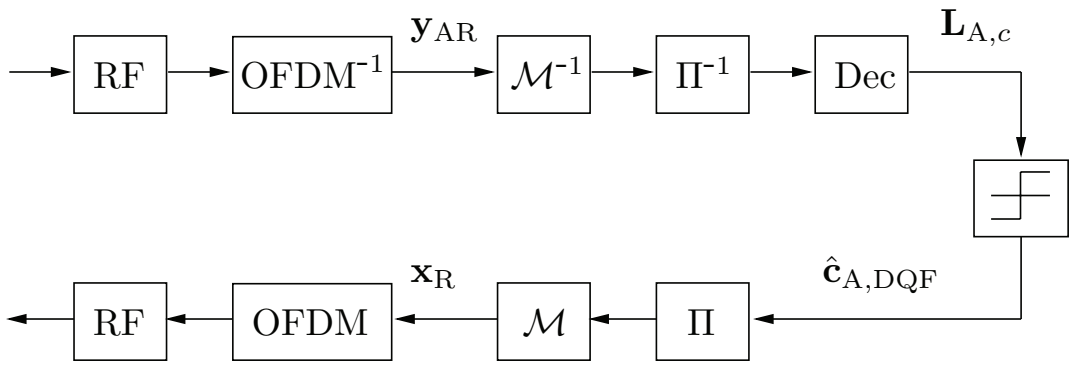

Figure 3.8: Block diagram at the relay for DQF, where the estimated code bits $\hat{\mathbf{c}}_{\mathrm{DQF}}$ are directly generated from the decoder without re-encoding.

$\hat{\mathbf{c}}_{\mathrm{A,DQF}}$ is not necessarily a valid codeword. However, as can be observed in Fig. 3.7, for DQF less CBEs occur with larger $|h_{\mathrm{AR},\ell}|$, or equivalently, higher SNR of the AR link. On the other hand, erroneous estimates for the code bits are more likely for smaller $|h_{\mathrm{AR},\ell}|$. This indicates an explicit correspondence of the CBE with the SNR of the AR link. In order to exploit this correspondence in DQF, a modified MRC (mMRC) at the destination B is proposed, which reduces the impact of decoding errors at the relay R.

To this end, a virtual model is constructed for R based on a zero-forcing (ZF) equalizer. Furthermore, the mMRC is derived according to this DQF model, which follows a heuristic approach and therefore the maximum SNR at B is not guaranteed.

For the derivation of the mMRC, the hypothetical ZF equalizer at the relay yields the output

$$\begin{aligned}\tilde{x}_{\mathrm{R,ZF},\ell} &= \frac{y_{\mathrm{R},\ell}}{h_{\mathrm{AR},\ell}} = x_{\mathrm{A},\ell} + \frac{n_{\mathrm{R},\ell}}{h_{\mathrm{AR},\ell}} \\ &= x_{\mathrm{A},\ell} + n_{\mathrm{ZF},\ell}\ ,\end{aligned} \tag{3.10}$$

which can be treated as an equivalent noise disturbance $n_{\mathrm{ZF},\ell}$ with variance $\sigma^2_{n,\mathrm{ZF},\ell} = \sigma^2_n/|h_{\mathrm{AR},\ell}|^2$ added to the transmit signal $x_{\mathrm{A},\ell}$. The above equation indicates that subcarriers with lower SNR of the AR link suffer from greater noise amplification, resulting in more decision errors. Assuming for the derivation of the DQF model that the ZF equalizer output (3.10) is directly relayed to the destination, the corresponding receive signal at the destination then reads

$$y_{\mathrm{RB,ZF},\ell} = h_{\mathrm{RB},\ell}\tilde{x}_{\mathrm{R,ZF},\ell} + n_{\mathrm{RB},\ell} \tag{3.11a}$$

$$= h_{\mathrm{RB},\ell}x_{\mathrm{A},\ell} + \frac{h_{\mathrm{RB},\ell}}{h_{\mathrm{AR},\ell}}n_{\mathrm{R},\ell} + n_{\mathrm{RB},\ell} \tag{3.11b}$$

$$= h_{\mathrm{RB},\ell}x_{\mathrm{A},\ell} + n_{\mathrm{RB,ZF},\ell} \tag{3.11c}$$

that involves an equivalent noise term $n_{\mathrm{RB,ZF},\ell}$ with variance

$$\sigma^2_{n,\mathrm{RB,ZF},\ell} = \left(1 + \frac{|h_{\mathrm{RB},\ell}|^2}{|h_{\mathrm{AR},\ell}|^2}\right)\sigma^2_n\ . \tag{3.12}$$

Applying this ZF-based model, MRC used at the destination in the DQF scheme to combine the receive signal vectors $\mathbf{y}_{\mathrm{AB}}$ and $\mathbf{y}_{\mathrm{RB}}$ subcarrier wise can be formulated as

$$\tilde{x}_{\mathrm{mMRC},\ell} = \frac{h^*_{\mathrm{AB},\ell}}{\sigma^2_n}y_{\mathrm{AB},\ell} + \frac{h^*_{\mathrm{RB},\ell}}{\sigma^2_{n,\mathrm{RB,ZF},\ell}}y_{\mathrm{RB},\ell} \tag{3.13a}$$

$$= \frac{h^*_{\mathrm{AB},\ell}}{\sigma^2_n}y_{\mathrm{AB},\ell} + \frac{1}{\sigma^2_n}\frac{h^*_{\mathrm{RB},\ell}}{1 + \frac{|h_{\mathrm{RB},\ell}|^2}{|h_{\mathrm{AR},\ell}|^2}}y_{\mathrm{RB},\ell} \tag{3.13b}$$

$$= h_{\mathrm{mMRC},\ell}x_{\mathrm{A},\ell} + n_{\mathrm{mMRC},\ell} \tag{3.13c}$$

with equivalent parameters

$$h_{\mathrm{mMRC},\ell} = \frac{|h_{\mathrm{AB},\ell}|^2}{\sigma^2_n} + \frac{1}{\sigma^2_n}\frac{|h_{\mathrm{RB},\ell}|^2}{1 + \frac{|h_{\mathrm{RB},\ell}|^2}{|h_{\mathrm{AR},\ell}|^2}} \triangleq \mathrm{SNR}_\ell \tag{3.14a}$$

$$\sigma^2_{n,\mathrm{mMRC},\ell} = h_{\mathrm{mMRC},\ell}\ . \tag{3.14b}$$

It is noted that this approach essentially carries out a weighting using the SNR of the AR link, or in other words, using the reliability information of the decoder output at the relay. Generally, the subcarrier with a lower SNR of the AR link from the relay experiences a greater suppression at the destination. In case of $|h_{\mathrm{AR}}|^2 \gg |h_{\mathrm{RB}}|^2$, this mMRC approaches the common MRC (cMRC) that assumes error-free decoding at the relay. On the other hand, i.e., $|h_{\mathrm{AR}}|^2 \ll |h_{\mathrm{RB}}|^2$, the signal $y_{\mathrm{RB},\ell}$ from the relay is 'almost' abandoned at the destination. Therefore, adaptive exploitation of the varying decoding reliability at the relay is achieved.almost

3.4 Performance Evaluation

In this section, the end-to-end system performance of relaying networks is evaluated in the sense of BER and frame error rate (FER), where an OFDM frame is in error when at least one bit is erroneously decoded. In the link-level simulations, either convolutional codes or LDPC codes are used and compared since the characteristics of the relaying schemes may differ from the strength of the applied channel codes. Furthermore, different network topologies are also considered as this plays a key role when comparing the relaying schemes.

Parameter Settings

For performance evaluation of different relaying schemes, the triplet relaying network in Fig. 3.1 is considered with the three nodes on a line. Adopting a topology model with relative distance definition, i.e., the distance between the source and the destination is set to $d_{\mathrm{AB}} = 1$, the distance between the source and the relay is denoted as $0 < d_{\mathrm{AR}} < 1$, resulting in the distance between the relay and the destination to be $d_{\mathrm{RB}} = 1 - d_{\mathrm{AR}}$. The path-loss exponent is set to $\alpha = 4$ and the multi-path channel contains $N_{\mathrm{H}} = 5$ equal power taps. Moreover, equal power is assumed at the source and at the relay in this work, in other words, $\mathcal{P}_{\mathrm{A}} = \mathcal{P}_{\mathrm{R}}$. Power allocation issues in this context are discussed, e.g., in [WWD11a, WWD11b], but are beyond the scope of this work. The SNR is defined as $\mathrm{SNR} = 1/\sigma_n^2$.

For OFDM transmissions, $L = 256$ subcarriers are used with 16-QAM modulation for the relaying network. As a reference, the direct transmission (DT) is also considered but with 4-QAM such that a fair comparison to the relaying communication subject to the half-duplex constraint is obtained with respect to the spectral efficiency. In view of channel coding, either non-recursive non-systematic convolution codes or optimized irregular LDPC codes of the same rate $R_{\mathrm{C}} = 0.5$ are applied. In case of convolutional codes,

the constraint length is set to $L_c = 4$ with the polynomials $[13, 17, 11]_8$ and BCJR decoder is used for decoding. For LDPC codes, the optimal degree distributions are achieved from [Urb01] by density evolution and the PEG algorithm [HEA05] is applied to generate the parity-check matrix. A maximum number of 100 iterations are employed for LDPC decoding. In addition, each OFDM symbol is encoded individually to exploit frequency selectivity from the $N_{\mathrm{H}} = 5$ channel taps.

Relaying using Convolutional Codes

The BER and FER performance of different OFDM-based relaying schemes as well as the DT applying convolutional codes are shown in Fig. 3.9, Fig. 3.10 and Fig. 3.11 with $d_{\mathrm{AR}} = 0.1$, $d_{\mathrm{AR}} = 0.5$ and $d_{\mathrm{AR}} = 0.9$, respectively. The involved relaying schemes are AF-CP, AF-CG, DF, DQF with cMRC and DQF with mMRC. It can be observed in Fig. 3.9, that when the relay is close to the source, AF-CP, DF and DQF with both cMRC and mMRC perform almost identically. This is because the reliable AR link rarely leads to decoding errors at the relay, irrespective of DF or DQF. On the other hand, AF yields minor noise amplification in this case. Furthermore, it is noted that AF-CP outperforms AF-CG by approximately 1 dB since when no CSI at the transmitter side is available, equal power allocation among the subcarriers performs optimally, as is the case for AF-CP. Additionally, most relaying schemes are superior to the DT, especially with respect to the BER performance as the SNR increases.

When the relay is located in the middle of the terminal nodes, i.e., $d_{\mathrm{AR}} = 0.5$, all relaying schemes achieve tremendous performance gains over the DT, as shown in Fig. 3.10. As observed in this figure, AF-CP still outperforms AF-CG slightly. DF achieves similar performance as DQF with cMRC, which is superior to AF in the low SNR region but loses diversity gain as the SNR increases due to error propagation. The diversity gain is preserved by the DQF relaying scheme with mMRC, which outperforms the other schemes almost over the whole investigated SNR region, although being slightly worse than DF in the low SNR region.

Fig. 3.11 indicates that, except AF, the other relaying schemes achieve even worse performance compared to the DT when the relay approaches the destination. Thus, AF is preferred to DF and DQF in this case. DQF with mMRC leads to enhanced performance gain over DF and DQF with cMRC due to dramatic suppression of the signals on subcarriers with less reliability. Moreover, both AF-CP and AF-CG perform similarly. This is attributed to the fact that the severe noise amplification in AF is the dominating factor whereas the influence of unequally allocating the transmit power over the subcarriers in AF-CG at the relay becomes much less significant.

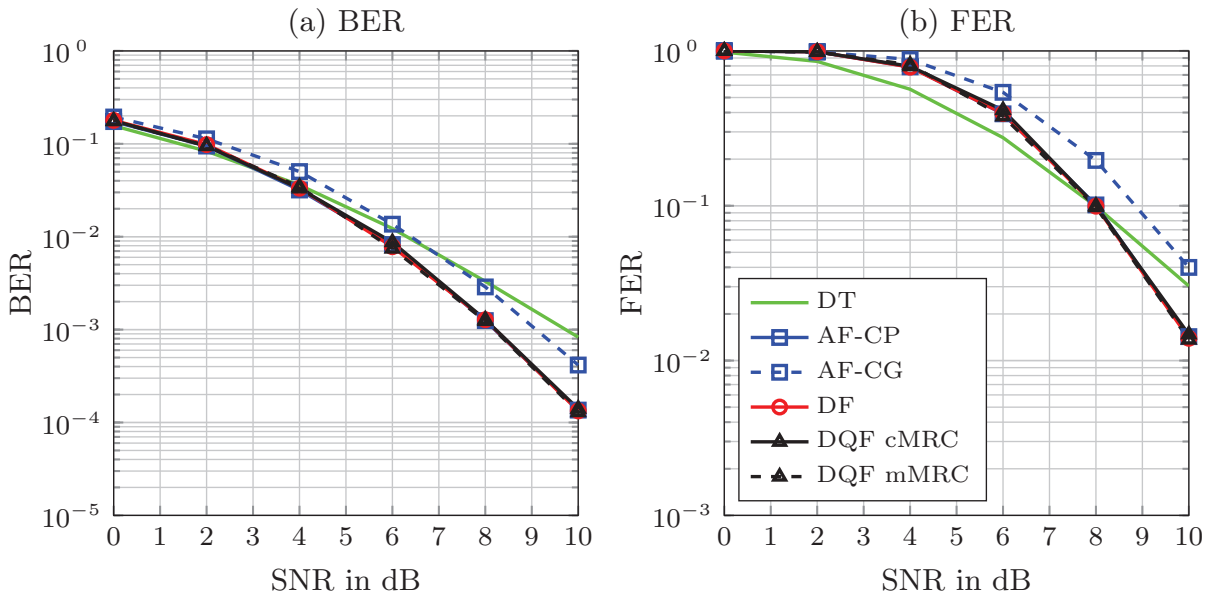

Figure 3.9: Error rate performance at destination B for different OFDM-based relaying schemes with $d_{\mathrm{AR}} = 0.1$, convolutional code is applied, (a) for BER and (b) for FER.

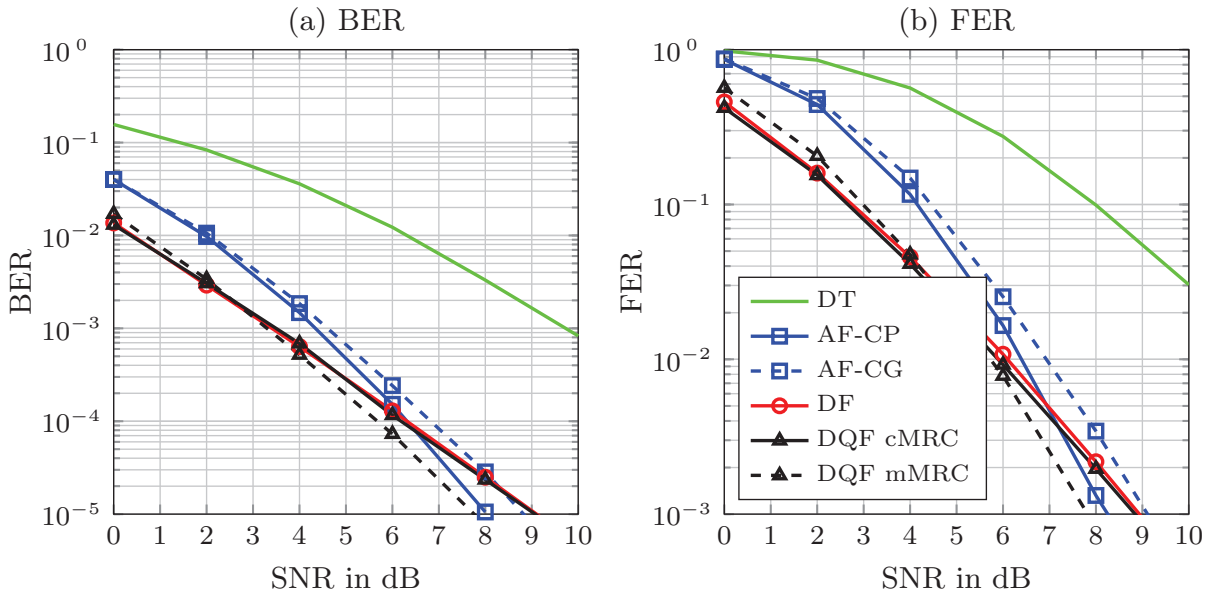

Figure 3.10: Error rate performance at destination B for different OFDM-based relaying schemes with $d_{\mathrm{AR}} = 0.5$, convolutional code is applied, (a) for BER and (b) for FER.

To further visualize the dependency of the relaying system performance on the network topology, both BER and FER are plotted in Fig. 3.12 with d_{AR} altering from 0.1 to 0.9 and a fixed SNR = 4dB. It is shown in the

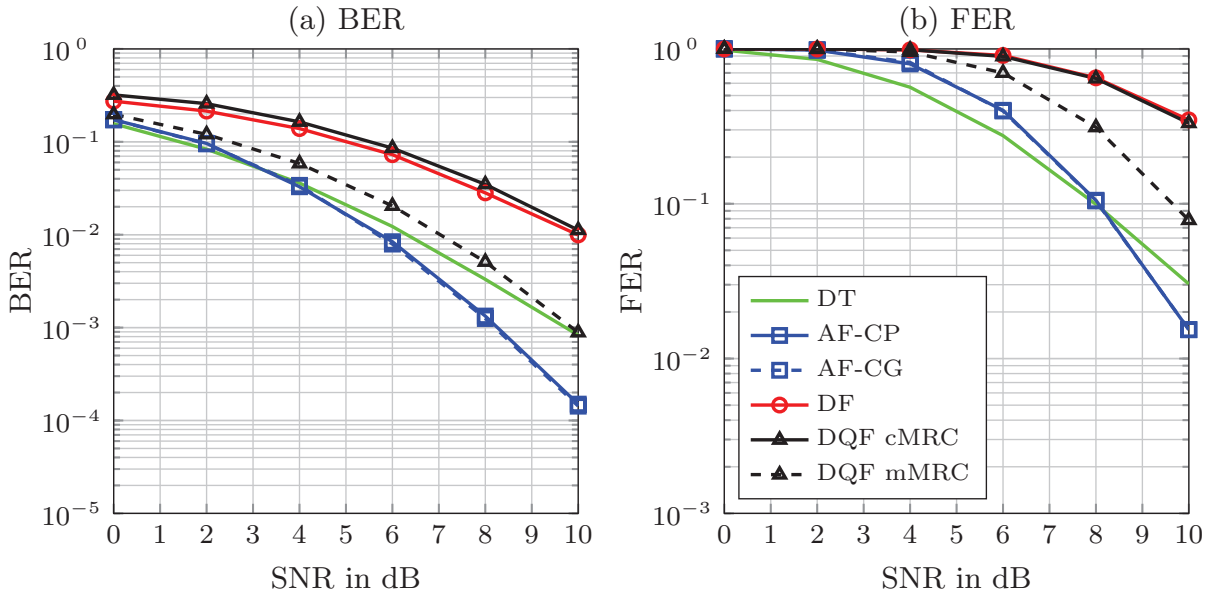

Figure 3.11: Error rate performance at destination B for different OFDM-based relaying schemes with $d_{\mathrm{AR}} = 0.9$, convolutional code is applied, (a) for BER and (b) for FER.

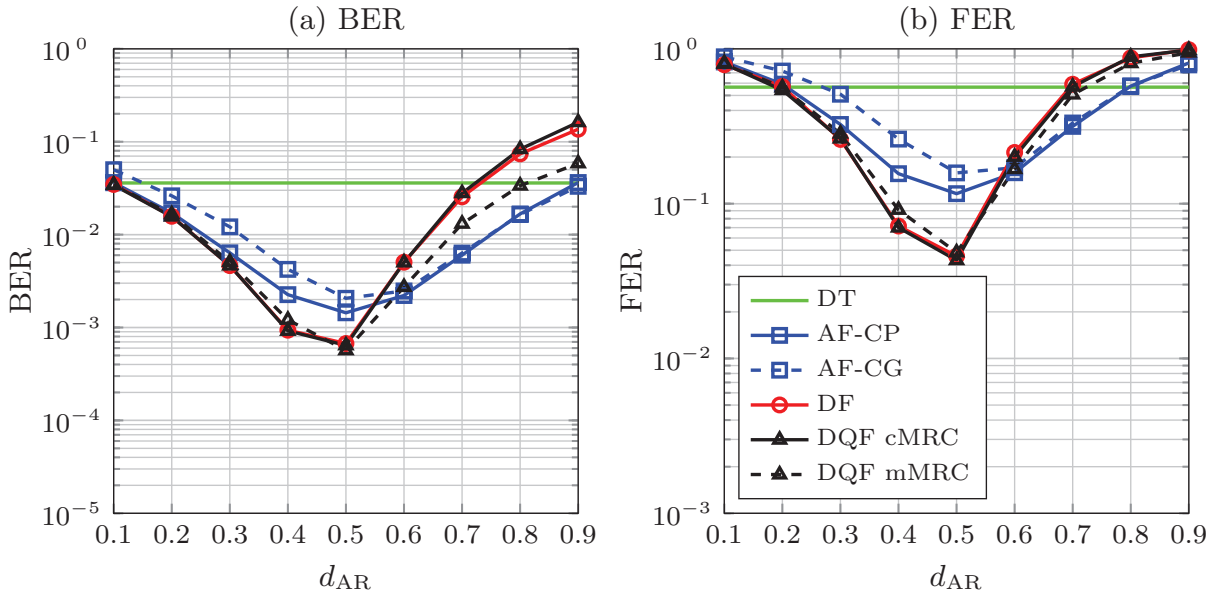

Figure 3.12: Error rate performance at destination B for different OFDM-based relaying schemes with SNR = 4dB, convolutional code is applied, (a) for BER and (b) for FER.

figure that the best performance is achieved in a symmetrical network, i.e., $d_{\mathrm{AR}} = 0.5$ for all relaying schemes. AF-CG is inferior compared to AF-CP when the relay is not in the vicinity of the destination. DF and DQF with

cMRC perform almost identically no matter where the relay is positioned. Most importantly, DQF with mMRC achieves enhanced performance gain over DF as the relay moves to the destination, even though it is still worse than AF in this case.

Relaying using LDPC Codes

The link-level simulations in Fig. 3.9, Fig. 3.10 and Fig. 3.11 applying convolutional codes are re-considered in Fig. 3.13, Fig. 3.14 and Fig. 3.15 when LDPC codes are employed, respectively. Obviously, the error rate performance is improved in all system scenarios by using stronger channel codes, especially for FER. On the other hand, the relaying schemes that perform decoding at the relay obtain greater benefits from using LDPC codes as this results in more reliable relay estimates and correspondingly less performance degradation from error propagation. Specifically, comparing Fig.3.9(b) and Fig.3.13(b) when $d_{\mathrm{AR}} = 0.1$, even AF-CG outperforms the DT significantly in LDPC coded systems at high SNR whereas AF-CG only achieves comparable performance as the DT in case of convolutional codes. When $d_{\mathrm{AR}} = 0.5$, the comparison between Fig.3.10(b) and Fig.3.14(b) shows that, due to more robust decoding results at the relay, LDPC-based DF becomes worse than AF-CP until FER $= 10^{-3}$ while this cross-point occurs earlier at FER $= 4 \times 10^{-3}$ for convolutional codes. In addition, LDPC

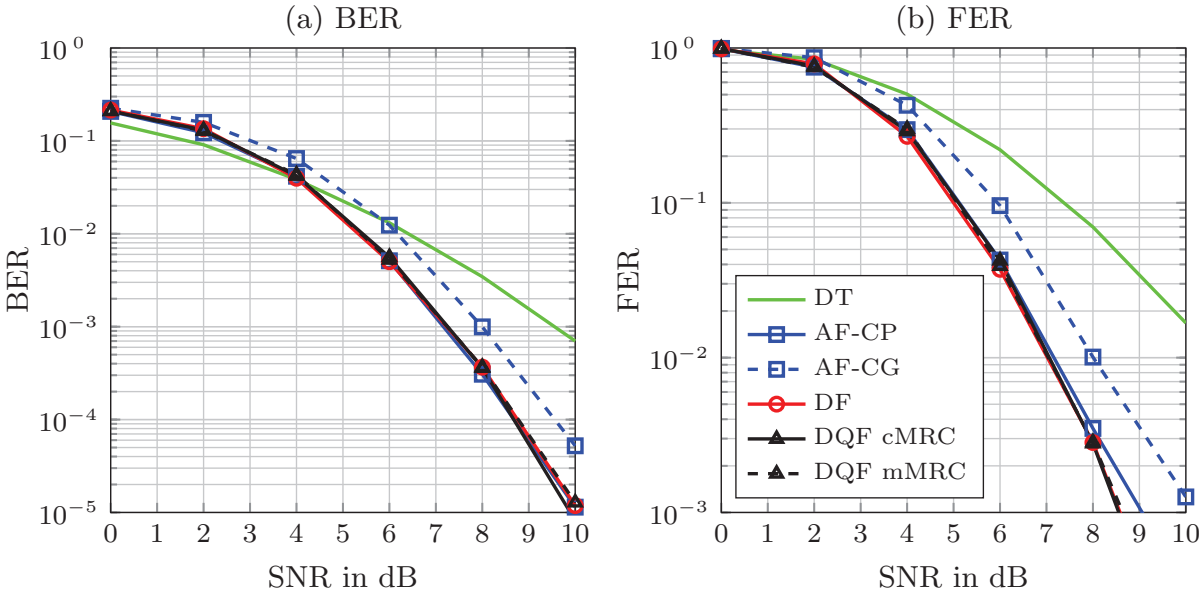

Figure 3.13: Error rate performance at destination B for different OFDM-based relaying schemes with $d_{\mathrm{AR}} = 0.1$, LDPC code is applied, (a) for BER and (b) for FER.

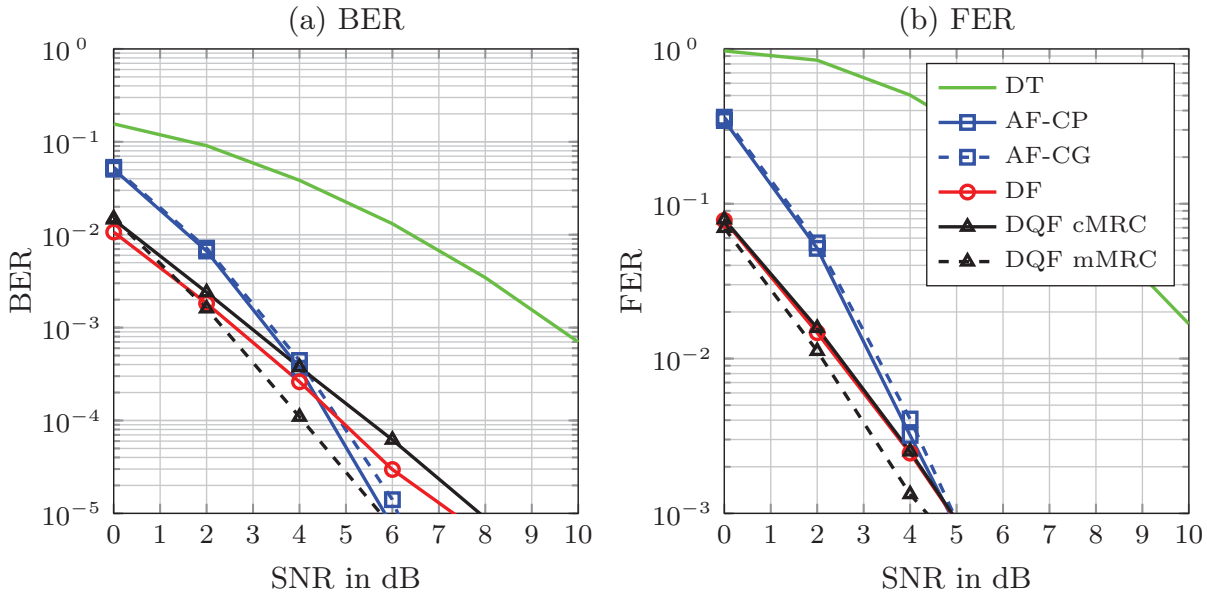

Figure 3.14: Error rate performance at destination B for different OFDM-based relaying schemes with $d_{\mathrm{AR}} = 0.5$, LDPC code is applied, (a) for BER and (b) for FER.

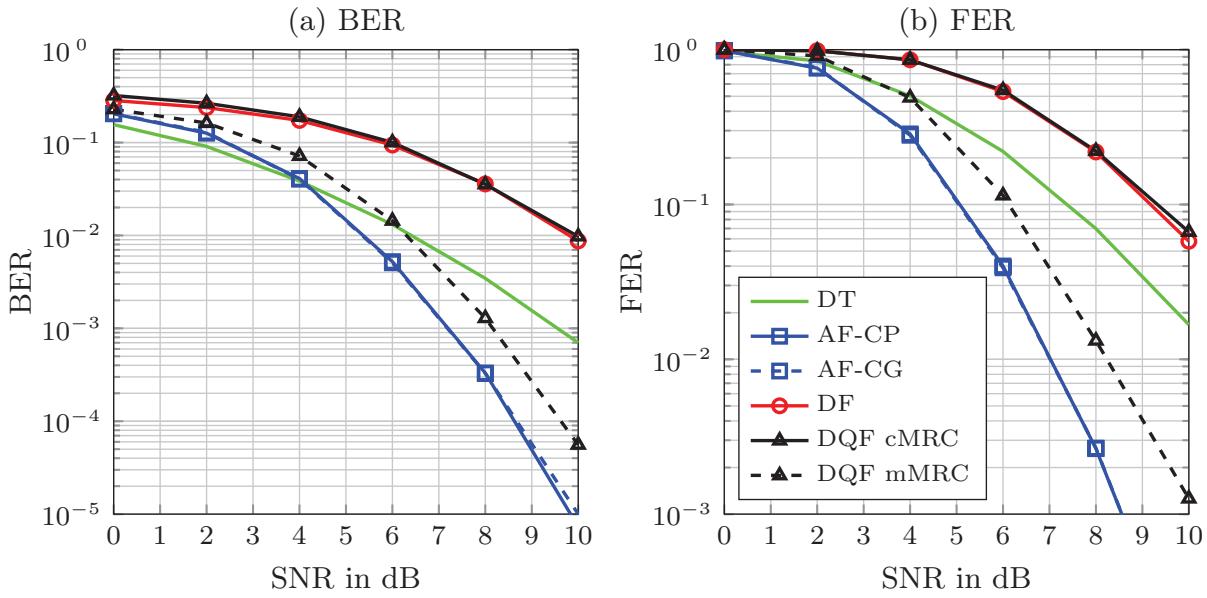

Figure 3.15: Error rate performance at destination B for different OFDM-based relaying schemes with $d_{\mathrm{AR}} = 0.9$, LDPC code is applied, (a) for BER and (b) for FER.

codes enable great performance gains for DQF with mMRC over the DT in case of $d_{\mathrm{AR}} = 0.9$, which is oppositely true when using convolutional codes, as compared in Fig.3.11(b) and Fig.3.15(b).

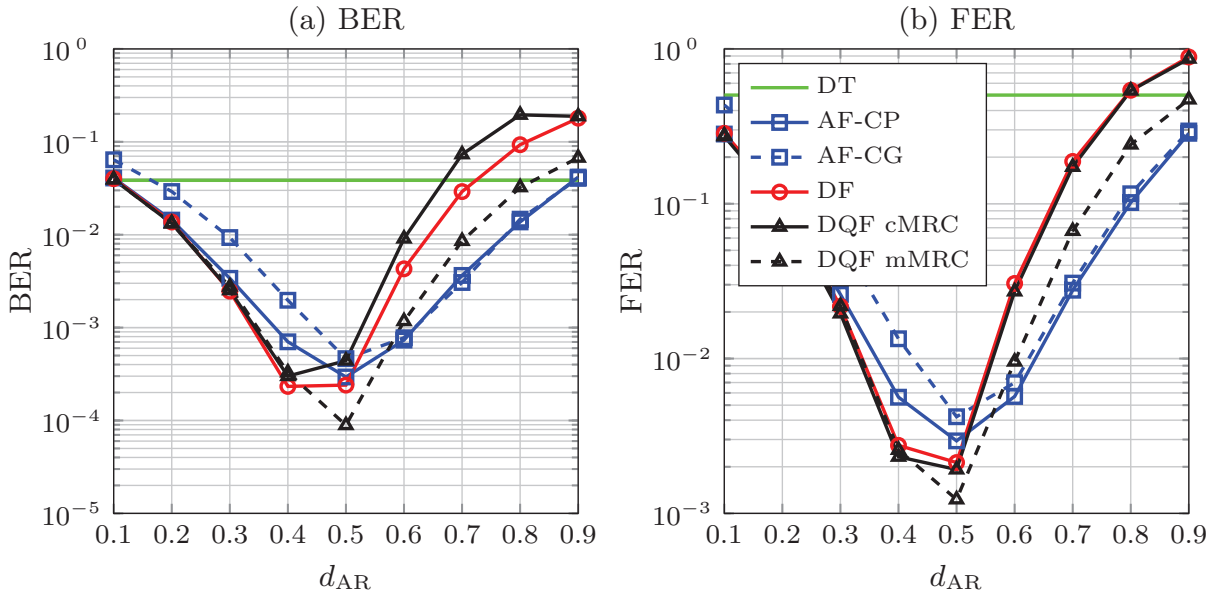

Figure 3.16: Error rate performance at destination B for different OFDM-based relaying schemes with SNR = 4dB, LDPC code is applied, (a) for BER and (b) for FER.

In the final analysis, the dependency of the error rate performance on the distance d_{AR} with fixed SNR = 4dB for convolutional codes shown in Fig. 3.12 is re-simulated using LDPC codes in Fig. 3.16 for completeness. The observations here are similar to those in Fig. 3.12 with convolutional codes. For example, the performance gain of AF-CP over AF-CG is present when the relay is closer to the source. The relaying schemes that perform decoding at the relay lose the gain and become worse than AF as the relay moves to the destination due to error propagation. It is also noticeable that the benefit of the DQF relaying scheme with mMRC is more visible in the case when the relay is in the middle.

3.5 Chapter Summary

This chapter deals with one-way SISO relaying networks, i.e., only one relay is present to support the transmission from the source to the destination whereas all three involved nodes are equipped with a single antenna. The basic concepts for this relay-assisted cooperative communication system with a selection of traditional relaying schemes are firstly discussed in Section 3.2.1. In case of applying OFDM transmission, modifications to these schemes are required due to different link qualities over the subcarriers. To this end, the following OFDM-based relaying schemes are presented

and compared, namely, amplify-forward with constant power (AF-CP), amplify-forward with constant gain (AF-CG), decode-forward (DF), decode-quantize-forward (DQF) either with common MRC (cMRC) or modified MRC (mMRC) [WW11, WLW+16a] in Section 3.3. It has been shown in Section 3.4 by performance evaluations that AF-CP outperforms AF-CG slightly, but AF-CG saves a pair of FFT/IFFT operation compared to AF-CP as the amplification is carried out in the time domain. Most importantly, the novel DQF relaying scheme with mMRC achieves the most superior performance compared to the other schemes when the relay is in the middle of the source and the destination. As the relay moves to the destination, AF becomes beneficial over the other relaying schemes, whereas DQF with mMRC still outperforms DF significantly due to efficient suppression of error propagation.

Chapter 4

One-Way Distributed Relaying

4.1 Overview

Cooperative communications supported by a relay node improve the end-to-end performance of the direct transmission from the source to the destination, as presented in Chapter 3. In practical scenarios, for example, wireless sensor networks, multiple intermediate nodes may be available to assist the transmission. In this context, these relaying nodes can be clustered to form a virtual antenna array (VAA) and the signal processing and coding approaches known from multiple-antenna systems can be implemented at the VAA in a distributed manner. For this purpose, cooperation between the relaying nodes is required by allowing dedicated information exchange within the VAA. Correspondingly, the type and amount of exchanged information have to be defined carefully depending on the specific conditions. Since such message exchange also consumes physical resources, the resulting overhead needs to be considered adequately to achieve fair comparisons between cooperative strategies with different levels of cooperation.

In Section 4.2, the system model is depicted for a one-way distributed relaying network, where multiple relays are available to support the transmission from the source to the destination. Since all nodes are equipped with a single antenna, only spatial diversity defined in a cooperative manner is available by treating the relays as a virtual cluster with multiple distributed antennas. Based on this system setup, distributed MIMO technologies can be applied at both the receiver side and transmitter side of the VAA by cooperation within the relay cluster. General explication of cooperation levels in this respect

is given in Section 4.3. As the main contribution of this chapter, specific cooperation approaches requiring information exchange within the VAA are presented in Section 4.4, which are adapted to different scenarios depending on the relay status after decoding [WXW+11, WXW+12, WLW+16a]. To take into account the extra physical resources in terms of time, a throughput analysis is initiated for performance evaluation. Numerical results exhibiting the performance at both the VAA for the cooperation between the relays and the destination for the overall system are shown in Section 4.5. Finally, the contents of this chapter are summarized in Section 4.6.

4.2 System Model

A one-way distributed relaying network is considered, where the source A communicates with the destination B supported by K relays R_k, $1 \leq k \leq K$, as shown in Fig. 4.1. For simplicity, the source-destination link is assumed to be not available due to severe path-loss between the two end nodes. The relays constitute a VAA [Doh03, LW03] and operate in half-duplex mode. All involved nodes are equipped with a single antenna. Furthermore, assuming that the network has a fixed topology, each relay R_k is aware of its own index k. In this chapter, the relays are assumed to be close to each other as in [LW03]. Therefore, the distance between source A and each relay R_k is set to be identical as d_{AR}, while all source-relay links are still uncorrelated with each other. Similarly, d_{RB} is defined as the distance between R_k and destination B. When the VAA is located in the middle between A and B, normalized distance is assumed as $d_{\mathrm{AB}} = 1$ and $d_{\mathrm{AR}} = d_{\mathrm{RB}} = 0.5 \gg d_{\mathrm{R}}$ with d_{R} denoting the distance between the relays.

To combat multi-path fading, coded OFDM is employed for both AR and RB transmissions. Similar to that described in Section 3.3 for the signal processing at source A, the information word $\mathbf{b}_{\mathrm{A}}$ is encoded by a linear channel code of rate R_{C}, yielding the codeword $\mathbf{c}_{\mathrm{A}} = \Gamma(\mathbf{b}_{\mathrm{A}})$. Subsequently, $\mathbf{c}_{\mathrm{A}}$ is mapped to an OFDM vector $\mathbf{x}_{\mathrm{A}}$ with L symbols using modulator $\mathcal{M}$, i.e., $\mathbf{x}_{\mathrm{A}} = \mathcal{M}(\mathbf{c}_{\mathrm{A}})$, which is transmitted to the VAA in the first phase as shown by the solid lines in Fig. 4.1. Denoting the transmit symbol on the ℓth subcarrier as $x_{\mathrm{A},\ell}$, $1 \leq \ell \leq L$, the ℓth receive signal $y_{\mathrm{R},k,\ell}$ at relay R_k is given by

$$y_{\mathrm{R},k,\ell} = h_{\mathrm{AR},k,\ell} x_{\mathrm{A},\ell} + n_{\mathrm{R},k,\ell} \; . \tag{4.1}$$

Assuming DF relaying in Subsection 3.3.3, relay R_k estimates the source message by decoding the receive signal vector $\mathbf{y}_{\mathrm{R},k} = [y_{\mathrm{R},k,1} \; y_{\mathrm{R},k,2} \; \cdots \; y_{\mathrm{R},k,L}]^T$. After re-encoding and mapping, this yields the transmit symbol vector $\mathbf{x}_{\mathrm{R},k} = [x_{\mathrm{R},k,1} \; x_{\mathrm{R},k,2} \; \cdots \; x_{\mathrm{R},k,L}]^T$ at R_k to be relayed to destination B in

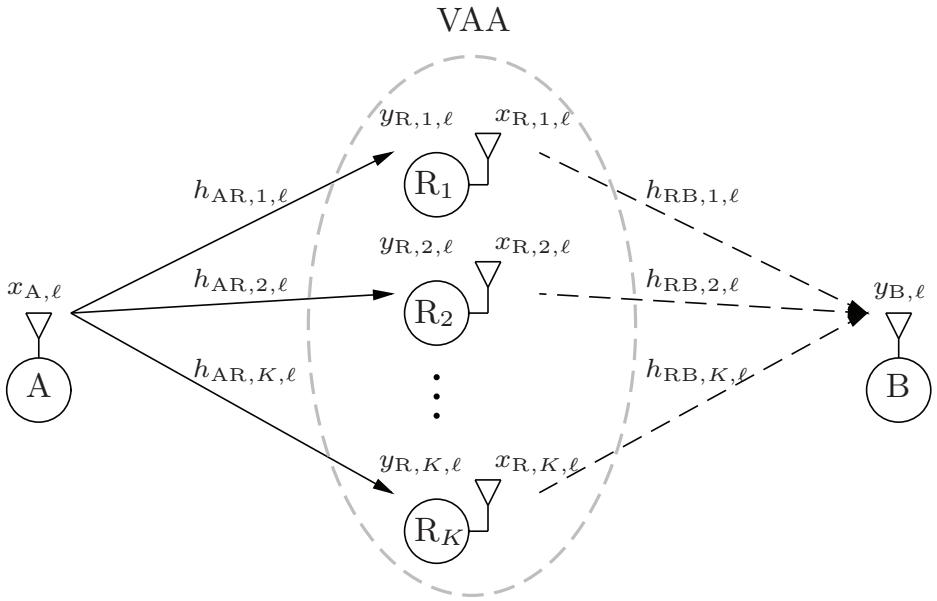

Figure 4.1: A one-way distributed relaying system operating in a half-duplex mode, where K relays constituting a VAA support the transmission from source A to destination B in two phases.

the second phase as shown by the dashed lines in Fig. 4.1. Consequently, B estimates the source message from its receive signal $\mathbf{y}_{\mathrm{B}}$.

The transmit power at source A and the VAA is denoted as $\mathcal{P}_{\mathrm{A}}$ and $\mathcal{P}_{\mathrm{R}}$ with both equal to each other, i.e., $\mathcal{P}_{\mathrm{A}} = \mathcal{P}_{\mathrm{R}}$. $\mathcal{P}_{\mathrm{R}}$ is equally assigned to all transmitting relays. Similar as before, the available power is normalized and equally allocated over the subcarriers in each OFDM symbol without CSI at the transmitter side. The frequency selective channels are assumed to be Rayleigh block fading containing N_{H} equal power taps in the time domain. Correspondingly, the ℓth channel coefficients $h_{\mathrm{AR},k,\ell}$ and $h_{\mathrm{RB},k,\ell}$ for the links between A and R_k in (4.1) and between R_k and B, respectively, are defined in the frequency domain, both of which have a variance $\sigma_h^2 = 1/(N_{\mathrm{H}} d^{\alpha})$. Here, $d \in \{d_{\mathrm{AR}}, d_{\mathrm{RB}}\}$ denotes the distance of an arbitrary source-relay link or relay-destination link since all relays are assumed to be close to each other. The Gaussian noise term $n_{\mathrm{R},k,\ell}$ is an i.i.d. zero-mean complex random variable with variance σ_n^2.

4.3 Introduction to Distributed MIMO Technologies

In multiple-anntenna system, many MIMO technologies have been proposed to exploit either the diversity gain or multiplexing gain or both of them

due to spatially separated transmit and receive antennas. For example, the diversity gain can be exploited by STC at the transmitter and MRC at the receiver as discussed in Subsection 2.6.

However, the application of these MIMO schemes has to be re-considered if the antennas are geographically distributed, e.g., considering multiple single-antenna relays that constitute a VAA shown in Fig. 4.1. In this case, the transmission from source A to the VAA forms a virtual SIMO system whereas the transmission from the VAA to destination B forms a virtual MISO system. In this chapter, it is assumed that the transceivers in the VAA can cooperate with each other to approach a MIMO relay system with one relay equipped with multiple antennas, but extra overhead such as information exchange among the relays is required for both cooperatively transmitting and receiving at the VAA. In the sequel, the cooperation at both the receiver side and transmitter side of the VAA is illustrated separately.

4.3.1 Cooperation at Receiver Side of VAA

The cooperation at the receiver side of the VAA is dependent on the type and amount of exchanged information among the relays after receiving and decoding the source message at each relay individually. In contrast to the case without cooperation, where relay R_k only relies on its local receive message $\mathbf{y}_{\mathrm{R},k}$ to estimate $\mathbf{c}_{\mathrm{A}}$, possible cooperation approaches at the VAA receiver side to improve the local decoding performance include

- Exchanged information among the relays can be in the form of hard bits from relays that decode the source message correctly, which serve as side information for the relays that fail to perfectly decode the source message. In this manner, the relays try to help each other for correct decoding with reasonable amount of exchanged information.

- When no relay is able to achieve error-free decoding of the source message, the hard bits may not be generated correctly. In this case, the receive signals can be exchanged among the relays. Note that if the whole frame of receive signal at each relay is exchanged with each other, this equivalently corresponds to a MIMO relay system, where spatial diversity can be fully exploited due to multiple replica of receive signals. However, the required overhead to exchange all receive signals among the relays becomes extremely large, and thus the system throughput considering the message exchange overhead among the relays is decreased tremendously.

  As an alternative, only part of the receive signals are exchanged among the relays. To this end, it needs to be determined which part of the

receive signals should be selected for exchange, implying that the trade-off between the improved error rate performance and the amount of required overhead has to be investigated.

4.3.2 Cooperation at Transmitter Side of VAA

For the transmission from the VAA to the destination B, the relays transmit cooperatively using distributed antennas either with cooperation at the VAA receiver side or not. To this end, possible approaches for cooperation at the transmitter side of the VAA are

- Orthogonal transmission from the VAA to the destination, which means that the transmission from each relay to the destination occupies different physical resources. For example, the relays transmit in successive time slots. Therefore, the ℓth receive signal at B from R_k is given by

$$y_{\mathrm{B},k,\ell} = h_{\mathrm{RB},k,\ell} x_{\mathrm{R},k,\ell} + n_{\mathrm{B},k,\ell} \; . \tag{4.2}$$

  As a result, destination B collects K independent replicas of the source message and can apply, e.g., MRC, to combine $y_{\mathrm{B},k,\ell}$, $1 \leq k \leq K$. As denoted previously that T_{OFDM} is the time duration of each transmission including one OFDM symbol, the total time consumption amounts to $K \cdot T_{\mathrm{OFDM}}$ for the relays transmitting to the destination. Due to tremendous expansion of required physical resources, this scheme is not considered in the sequel.

- Without the availability of CSI at the transmitter side, STC can be applied that allows the relays to transmit simultaneously at the same frequency in a distributed manner [SB05]. In this case, denoting $x_{\mathrm{R},k,\ell}$ the space-time coded signal, the corresponding superimposed receive signal at destination B can be written as

$$y_{\mathrm{B},\ell} = \sum_{k=1}^{K} h_{\mathrm{RB},k,\ell} x_{\mathrm{R},k,\ell} + n_{\mathrm{B},\ell} \; . \tag{4.3}$$

  The receive signal vector $\mathbf{y}_{\mathrm{B}} = [y_{\mathrm{B},1} \; y_{\mathrm{B},2} \; \cdots \; y_{\mathrm{B},L}]^T$ is linearly filtered for STC detection, followed by channel decoding to estimate the source message. One of the key issues is that extra effort is required to synchronize the relays so that they transmit at the same time due to the distributed nature of the transmit antennas in the VAA, as discussed in [HGWC09, AJ15] but not included here.

  In this work, the application of distributed orthogonal space-time block codes (D-OSTBC) is assumed for the transmission from the

VAA to destination B as in [DLA02, LW03]. Such an orthogonal STC family is advantageous in that each column of the code matrix $\mathbf{T}$ defined in Subsection corresponding to each transmitting antenna is orthogonal. Therefore, absence of an antenna in the distributed VAA results in deletion of a column in $\mathbf{T}$, which is equivalent to that antenna experiencing a deep fading, but the rest columns still remain orthogonal. To this end, the residual diversity benefit of the code is maintained. Ignoring the data rate loss due to orthogonal code design, the equivalent system equation for (4.3) can be formulated as

$$y_{\mathrm{B},\ell} = \sqrt{\frac{1}{K}\sum_{k=1}^{K}|h_{\mathrm{RB},k,\ell}|^2}\, x_{\mathrm{R},\ell} + n_{\mathrm{B},\ell}\ . \tag{4.4}$$

For practical system designs, more than two transmit antennas lead to a rate loss R_{OSTBC} for OSTBC, as discussed in Subsection 2.6.2. In order to achieve the same data rate when different number of transmit antennas is employed, rate matching can be applied by adapting the channel code rate in the RB link to $R_{\mathrm{C,RB}} > R_{\mathrm{C}}$, such that $R_{\mathrm{OSTBC}} R_{\mathrm{C,RB}} = R_{\mathrm{C}}$ holds.

- One of the alternatives to ease the synchronization requirement while preserving the spatial diversity gain is relay selection. To this end, only one relay is selected based on some given criteria, e.g., SNR and decoding status. The selected relay R_κ transmits to destination B with the system equation represented as

$$y_{\mathrm{B},\ell} = h_{\mathrm{RB},\kappa,\ell} x_{\mathrm{R},\kappa,\ell} + n_{\mathrm{B},\ell}\ , \tag{4.5}$$

whereas the other relays keep silent. For example, considering DF relaying, the relay with the highest SNR on the relay-destination link is selected out of the relay set that contains the relays decoding the source message correctly, which transmits to the destination exclusively [TN07, TN08]. However, a feedback channel from the destination to the VAA is required to feedback this CSI indicating which relay should transmit. In this chapter, no CSI at the transmitter side is assumed, therefore, relay selection is not considered here.

4.4 Adaptive Inter-Relay Cooperation

In this section, adaptive inter-relay cooperation (IRC) schemes are presented that allow information exchange between the relays. The goal is to achieve

improved decoding performance at the VAA such that the transmission to the destination is more reliable. After a general description about the system setup for adaptive IRC, two specific IRC approaches depending on the decoding status at the VAA are demonstrated. In succession, a throughput analysis is given that incorporates the IRC overhead.

4.4.1 General Description

The application of distributed MIMO technologies within the VAA requires information exchange among the relays. To this end, IRC is enabled that allows dedicated transmissions within the VAA. Assuming a time division mode, the time duration for both transmissions from source A to the VAA and from the VAA to destination B is equal and denoted by T_{OFDM}. The IRC phase occupies an independent time slot with duration T_{IRC}, as shown in Fig. 4.2. Note that the source-destination link is not considered in this distributed relaying scenario for simplicity.

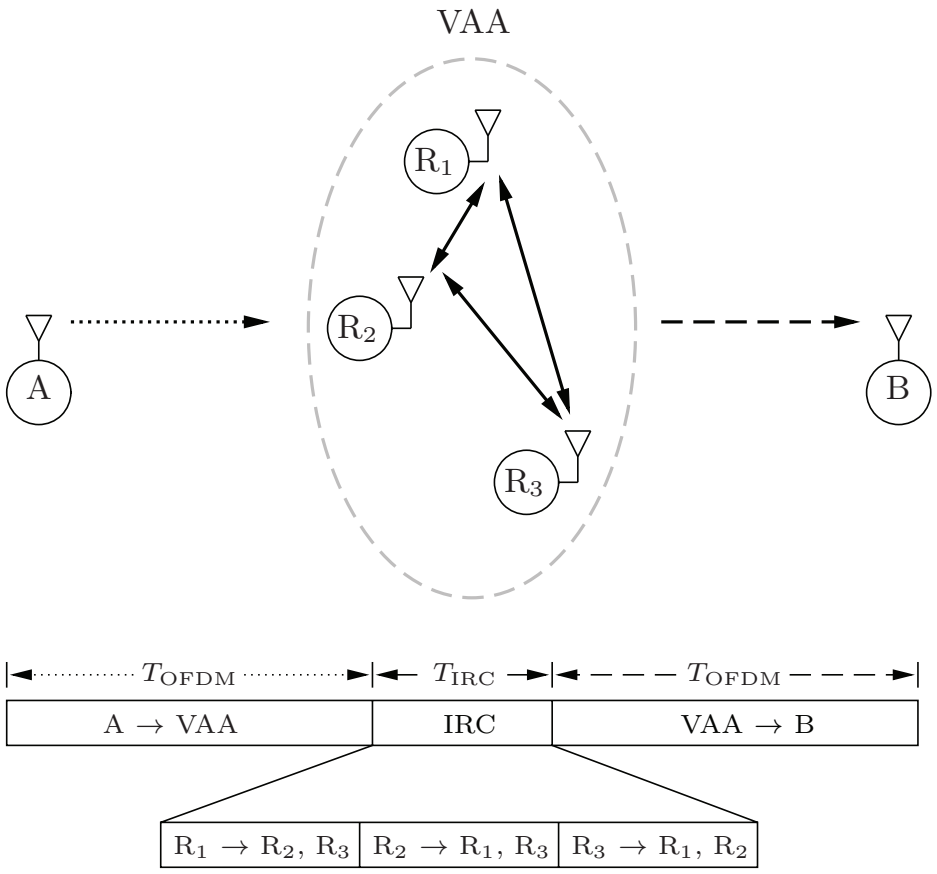

Figure 4.2: A distributed relaying system with $K = 3$ relays and IRC operating in a time division mode. Both transmissions from A to VAA ($\cdots$) and from VAA to B (- -) consume time T_{OFDM}, whereas the time duration dedicated to IRC (-) is T_{IRC}.

In this chapter, DF is employed as the relaying scheme and the relays transmit to the destination using D-OSTBC. Upon receiving from the source, the relays decode the source message individually. Assuming that a CRC code is applied at the source, which is capable of detecting errors perfectly with negligible overhead, each relay R_k is aware of its own decoding status. The relays now inform each other about their decoding status by broadcasting a one-bit acknowledgement (ACK) or negative acknowledgement (NAK) denoted as a CRC bit. Since a fixed network structure is assumed, each relay R_k knows its own index k. This facilitates the relays to send the CRC bits in a pre-fixed order without extra overhead, e.g., R_1 sends first and after receiving the CRC bit from R_k, R_{k+1} sends its CRC bit. Consequently, all relays are aware of the set $\mathcal{D}$ containing all correct relays[1]. Depending on the cardinality $|\mathcal{D}|$, three events can be distinguished, in which different IRC strategies are specified adaptively, as described in the sequel.

- **Event E_1: $|\mathcal{D}| = K \rightarrow$ all relays correct**
  The exchange of auxiliary information among the relays is not necessary since all relays have already decoded the source message correctly. Therefore, K relays participate in the transmission to destination B using D-OSTBC.

- **Event E_2: $1 \leq |\mathcal{D}| < K \rightarrow$ some relays correct**
  In this case, hard decided bits can be exchanged from one of the the correct relays, e.g., from $\mathrm{R}_\kappa \in \mathcal{D}$, to the $(K - |\mathcal{D}|)$ erroneous relays. Based on the auxiliary information achieved in the IRC phase together with the own message received from source A, each erroneous relay not in $\mathcal{D}$ performs re-decoding and exchanges the new CRC bit again within the VAA.

- **Event E_3: $|\mathcal{D}| = 0 \rightarrow$ no relay correct**
  When no relay is able to decode the source message, still exchanging hard decided bits as in the previous case leads to error propagation within the VAA since they may not be generated correctly. Therefore, the whole received frame or part of the frame is exchanged among the relays in the IRC phase. Subsequently, re-decoding is performed at all relays, followed by the exchange the new CRC bits again to ascertain which event the VAA is in after this stage of IRC.

The state diagram for IRC with respect to different events is shown in Fig. 4.3. Let p_i and p_i' denote the event probability that E_i occurs before

[1] A correct relay is defined as the relay that can decode the source message perfectly, i.e., without decoding errors. An erroneous relay is that fails to decode the source message perfectly, i.e., with decoding errors.

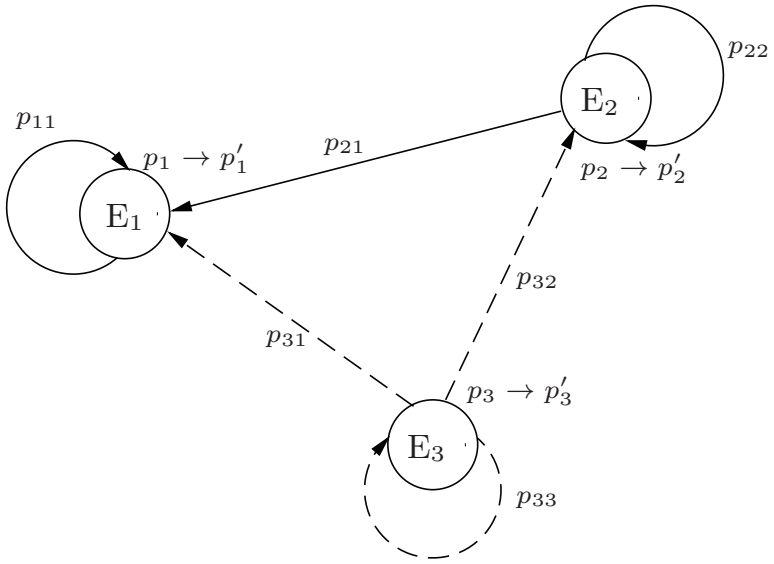

Figure 4.3: State diagram of IRC with respect to different events. The transfer process is divided into two successive phases. If E_3 occurs, IRC based on exchanging the receive signals is applied, as shown by the dashed lines. If E_2 occurs afterwards, IRC based on exchanging compressed hard bits is applied, as shown by the solid lines.

and after IRC, respectively. The transfer probability that E_i turns to E_j is denoted as p_{ij}, where $1 \leq i, j \leq 3$. Since the presented IRC scheme aims at letting the relays help each other and thus increasing the number of correct relays, the corresponding transfer matrix $\mathbf{A}_{\text{IRC}}$ can be simplified to a lower triangle matrix as

$$\mathbf{A}_{\text{IRC}} = \begin{pmatrix} p_{11} & p_{12} & p_{13} \\ p_{21} & p_{22} & p_{23} \\ p_{31} & p_{32} & p_{33} \end{pmatrix} = \begin{pmatrix} 1 & 0 & 0 \\ p_{21} & p_{22} & 0 \\ p_{31} & p_{32} & p_{33} \end{pmatrix} \tag{4.6}$$

due to the fact that $p_{ij} = 0$ if $i < j$. The event probabilities p_i are dependent on the SNR of the source-relay links and the transfer probabilities p_{ij} are related to the type and amount of exchanged information for IRC. Letting $\mathbf{p}_{\text{IRC}} = [p_1 \ p_2 \ p_3]^T$ and $\mathbf{p}'_{\text{IRC}} = [p'_1 \ p'_2 \ p'_3]^T$, the state transfer process depicted in Fig. 4.3 due to IRC can be expressed mathematically as

$$\mathbf{p}'_{\text{IRC}} = \mathbf{A}_{\text{IRC}} \mathbf{p}_{\text{IRC}} \ , \tag{4.7}$$

which can be decomposed into the following equations

$$p_1' = p_1 + (p_2 + p_3 p_{32})\, p_{21} + p_3 p_{31} \tag{4.8a}$$
$$p_2' = (p_2 + p_3 p_{32})\, p_{22} \tag{4.8b}$$
$$p_3' = p_3 p_{33} \tag{4.8c}$$

using (4.6). Note that the completeness condition has to be fulfilled for $\mathbf{p}_{\mathrm{IRC}}$ and $\mathbf{p}'_{\mathrm{IRC}}$, i.e., $p_1 + p_2 + p_3 = 1$ leads to $p_1' + p_2' + p_3' = 1$. Furthermore, the transfer process is divided into two successive phases presented in Fig. 4.3. Specifically, if E_3 occurs, IRC based on exchanging the receive signals is applied, as shown by the dashed lines. If E_2 occurs afterwards, IRC based on exchanging compressed hard bits is applied, as shown by the solid lines. In the upcoming sections, specific IRC strategies for E_2 and E_3 are demonstrated, respectively.

4.4.2 Inter-Relay Cooperation with Correct Relays

If event E_2 occurs, i.e., some but not all relays achieve correct decoding, the IRC scheme based on punctured channel codes is applied [WXW+11]. Basically, this scheme is motivated from incremental redundancy in hybrid automatic repeat request (HARQ), which makes use of auxiliary information for re-decoding if the initial decoding fails [Che06]. As shown in Fig. 4.4 for the block diagram at source A, the information bits $\mathbf{b}_{\mathrm{A}}$ are encoded to a codeword $\mathbf{c}_{\mathrm{A,mom}}$ of length N using a channel code with mother rate $R_{\mathrm{C,mom}}$. Afterwards, N_{pun} bits are punctured, resulting in a shortened codeword $\mathbf{c}_{\mathrm{A}}$ of length $N_c = N - N_{\mathrm{pun}}$ and code rate $R_{\mathrm{C}} > R_{\mathrm{C,mom}}$. The punctured codeword is further interleaved and modulated for transmission to the relays. It is noted that the interleaver is omitted here and in the sequel for simplicity.

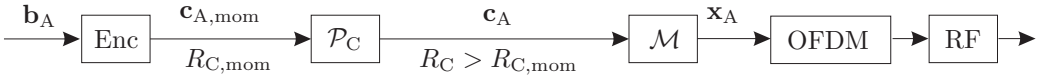

Figure 4.4: Processing chain at source A by using a punctured channel code with mother code rate $R_{\mathrm{C,mom}}$. N_{pun} bits are punctured resulting in a code for transmission with rate R_{C}.

After local decoding and exchanging the CRC bits, one of the relays with correct decoding result $\mathrm{R}_\kappa \in \mathcal{D}$, e.g., the one with the smallest index $\kappa = \min_{\mathrm{R}_k \in \mathcal{D}} k$, re-generates and broadcasts $N_{\mathrm{IRC}} \leq N_{\mathrm{pun}}$ punctured bits to the other relays. As shown in Fig. 4.5, the upper dashed block depicts the processing chain at relay R_κ. After error-free decoding, all or part of

the punctured bits from the mother codeword are generated. Note that less exchanged punctured bits lead to smaller amount of overhead but less performance gain. This trade-off is to be observed in the simulation results later on by resorting to a throughput analysis. The punctured bits are then modulated using a high modulation alphabet $\mathcal{M}_{\mathrm{IRC}}$ and transmitted over a single-carrier inter-relay (IR) channel. Since the relays within the VAA are assumed to be close to each other, this results in a robust IR transmission. Subsequently, as shown in the lower dashed block in Fig. 4.5, each relay R_j that has decoding errors re-decodes the source message with the help of the punctured bits received from the IR channel. Specifically, instead of feeding zeros to the punctured positions of the codeword as for initial decoding in the de-puncturing module $\mathcal{P}_{\mathrm{C}}^{-1}$, the soft punctured bits obtained from IRC are used. Also note that $\overline{\mathcal{P}}_{\mathrm{C}}$ and $\mathcal{P}_{\mathrm{C}}$ in Fig. 4.5 represent the puncturing modules producing the punctured bits and the punctured codeword, respectively. In order to inform the other relays about the re-decoding status, these relays broadcast the CRC bits again to determine the new set $\mathcal{D}'$, where $\mathcal{D}' \supseteq \mathcal{D}$ holds. This indicates that this IRC scheme may increase the number of relays with correctly decoded source message. Finally, only the relays in set $\mathcal{D}'$ transmit to the destination B using D-OSTBC.

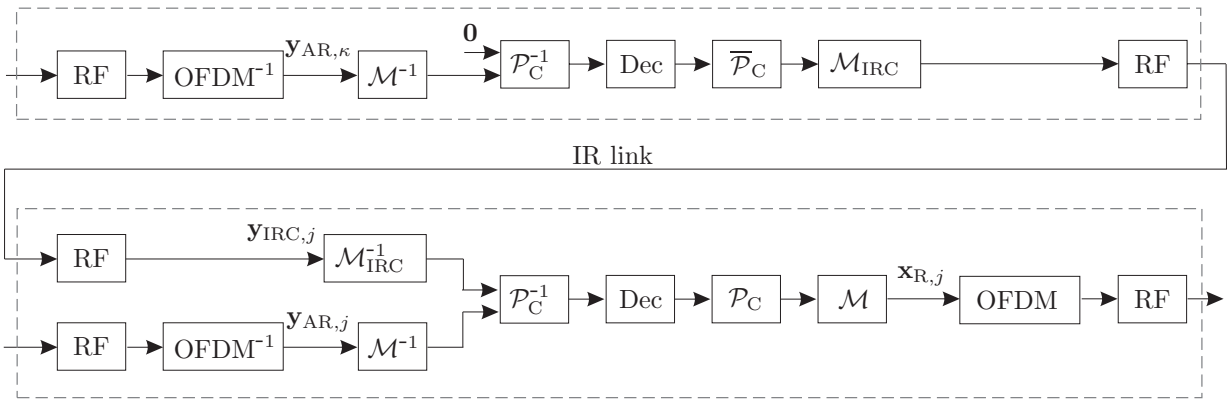

Figure 4.5: Processing chain at the selected correct relay R_κ (upper dashed block) and one of the relays R_j that fails correct decoding (lower dashed block).

4.4.3 Inter-Relay Cooperation without Correct Relays

Based on punctured channel codes, the IRC scheme presented in Subsection 4.4.2 may increase the number of correct relays in E_2 when at least one relay is able to decode the source message correctly. However, when E_3 occurs, i.e., all relays have decoding errors, the punctured bit may not be correctly generated. In this case, still exchanging punctured bits leads to

error propagation in the IRC phase and thus is not able to improve the system performance. To this end, other types of information other than punctured bits should be exchanged, e.g., the receive signals at the relays. Motivated by a SIMO system using signal combining strategies to exploit receive diversity as depicted in Subsection 2.6.1, an IRC scheme based on receive signal exchange is applied in E_3 [WXW+12]. Depending on the amount of exchanged received signals, signal combining is performed on different subcarriers at the relays, leading to two cooperation approaches as distinguished in the sequel.

Full Cooperation

In case of full cooperation for receive signal exchange, the whole received OFDM symbols at the relays are shared with each other in the VAA, leading to an overhead of $\Phi_{\mathrm{IRC}} = KL$ complex symbols to be exchanged when E_3 occurs. By applying MRC at each relay, the combined signal on subcarrier ℓ at relay R_k is written as

$$r_{\mathrm{full},k,\ell} = \sum_{j=1}^{K} h^*_{\mathrm{AR},j,\ell} y_{\mathrm{AR},j,\ell} \tag{4.9}$$

assuming that the signal $y_{\mathrm{AR},j,\ell}$, $\forall j, j \neq k$ from relay R_j is perfectly received at R_k. This is based on the fact that the relays are located close to each other within the VAA and the IR channels are only subject to a Guassian noise disturbance n_{IRC} with high receive SNR. Furthermore, it is noted that the local CSI at each relay has also to be exchanged within the VAA used for MRC, which is considered later on. Due to the large amount of overhead, full cooperation yields a tremendous decrease of system throughput but is still investigated to serve as a benchmark.

Partial Cooperation

In order to reduce the cooperation overhead, only part of the receive signals are shared between the relays in the partial cooperation approach. To this end, the part of receive signals to be exchanged should be selected properly. In [Yue00, KKS04] a generalized selection combining (GSC) strategy was investigated that combines either the receive signals or the LLRs from some of the communication links in a SIMO system. This combining strategy can be applied at the distributed relays with decreased amount of exchanged information compared to full cooperation. For illustration of this partial cooperation approach, a subcarrier wise relay index κ_ℓ is firstly defined as

$$\kappa_\ell = \arg\max_k \{|h_{\mathrm{AR},k,\ell}|^2\} \,, \tag{4.10}$$

where $|h_{\mathrm{AR},k,\ell}|^2$ is proportional to the instantaneous $\mathrm{SNR}_{\mathrm{AR},k,\ell}$ on subcarrier ℓ at R_k. Furthermore, the vector corresponding to the highest subcarrier wise SNR of the AR link among the relays is defined as

$$\hat{\mathbf{h}}_{\mathrm{AR}} = [|h_{\mathrm{AR},\kappa_1,1}|^2, |h_{\mathrm{AR},\kappa_2,2}|^2, ..., |h_{\mathrm{AR},\kappa_L,L}|^2] \tag{4.11}$$

based on the subcarrier wise selected relay (4.10). Subsequently, $\hat{\mathbf{h}}_{\mathrm{AR}}$ is sorted in decreasing order, yielding the sorted vector $\hat{\mathbf{h}}_{\mathrm{AR,s}}$, where $\hat{h}_{\mathrm{AR,s},\ell} > \hat{h}_{\mathrm{AR,s},\ell+1}$, $\forall \ell$, $\ell \neq L$. For partial cooperation, only the subcarriers with respect to the first $\lceil \lambda L \rceil$ terms in $\hat{\mathbf{h}}_{\mathrm{AR,s}}$ are selected for receive signal exchange, where λ denotes a proportion factor in the range $0 < \lambda \leq 1$. Note that for the selected subcarriers, only one relay with index κ_ℓ transmits its corresponding receive signals. Therefore, the overhead is reduced to $\Phi_{\mathrm{IRC}} = \lceil \lambda L \rceil$. The combined signal at relay R_k on a selected subcarrier reads

$$r_{\mathrm{partial},k,\ell} = h^*_{\mathrm{AR},k,\ell} y_{\mathrm{AR},k,\ell} + h^*_{\mathrm{AR},\kappa_\ell,\ell} y_{\mathrm{AR},\kappa_\ell,\ell} \tag{4.12}$$

assuming perfect exchange for the signal $y_{\kappa_\ell,\ell}$, whereas no signal combining takes place on the non-selected subcarriers. The combining strategy (4.12) guarantees that the subcarrier wise signal with the highest $\mathrm{SNR}_{\mathrm{AR},\ell}$ is always involved. Note that the selected relay R_{κ_ℓ} gets no exchanged receive signal on subcarrier ℓ since only one relay exchanges its receive signal for each subcarrier.

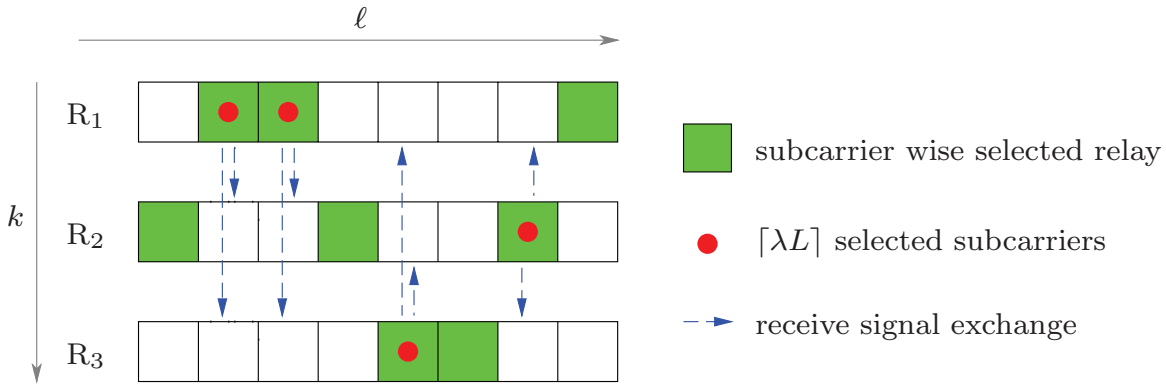

Figure 4.6: An example of partial cooperation for receive signal exchange in E_3 based on subcarrier wise relay selection with $K = 3$, $L = 8$, $\lambda = 1/2$. The hatched subcarriers correspond to the selected relays. The 4 subcarriers with dot are further selected.

Fig. 4.6 illustrates the partial cooperation approach for receive signal exchange with $K = 3$ relays, $L = 8$ subcarriers and proportional factor $\lambda = 1/2$ as an example. The subcarriers 2 and 3 at R_1 have the highest $\mathrm{SNR}_{\mathrm{AR},\ell}$ and thus the corresponding receive signals on these two subcarriers

are exchanged to R_2 and R_3. Similarly, R_2 exchanges its receive signal on subcarrier 7 and the receive signal on subcarrier 5 is exchanged at R_3. No receive signal exchange takes place on the other half amount of subcarriers 1, 4, 6 and 8 due to $\lambda = 1/2$.

Exchange of CSI

In order to apply the full and partial cooperation approaches, the relays need to share the CSI of the AR links for both subcarrier wise relay selection and signal combining. This requires extra overhead and should be considered adequately. Suppose that each relay knows its own CSI of the AR link perfectly, which consists of N_{H} complex symbols in time domain, exchanging the CSI among all relays leads to an overhead of $\Phi_{\mathrm{CH}} = KN_{\mathrm{H}}$. Furthermore, it is assumed that all channels are block fading and stay invariant for N_{inv} OFDM symbols, during which the channel coefficients need to be exchanged only once. Therefore, the data rate is decreased by a factor

$$\rho = \frac{N_{\mathrm{inv}}\Phi_{\mathrm{IRC}}}{N_{\mathrm{inv}}\Phi_{\mathrm{IRC}} + \Phi_{\mathrm{CH}}} \tag{4.13}$$

for IRC in E_3. Clearly, this effect becomes negligible with growing N_{inv}. Note that when the energy consumption for baseband processing is considered, extra FFT operations are required to obtain the channel coefficients in frequency domain used for the presented combining strategies. This aspect is important in practical system designs as discussed in [WXW+11, WXW+12], but is not included in this work.

Quantization of Receive Signals

Considering a time-discrete system, the continuous-valued receive signals to be exchanged need to be quantized before transmission in the IRC phase. To this end, two quantization strategies can be applied, namely, bit quantization (BQ) and symbol quantization (SQ), with both block diagrams at relay R_i that exchanges its receive signal to R_j shown in Fig. 4.7. In case of BQ in Fig. 4.7(a), the real part and imaginary part of the receive signal $y_{\mathrm{AR},i,\ell}$ to be exchanged are quantized separately by a linear quantizer $\mathcal{Q}$ with Q quantization levels [Pro00] causing the quantization noise n_{Q}. Subsequently, the quantized bits are serially aligned and modulated by M_{IRC}-QAM for exchange in the IR channel. The signal $y_{\mathrm{AR},i,\ell}$ is reconstructed by de-quantization after reception at R_j. Note that the receive signal $y_{\mathrm{AR},i,\ell}$ is firstly de-rotated by a ZF equalizer, yielding the signal to be quantized as

$$\tilde{y}_{\mathrm{AR},i,\ell} = \frac{y_{\mathrm{AR},i,\ell}}{h_{\mathrm{AR},i,\ell}} = x_{\mathrm{A},\ell} + \frac{n_{\mathrm{R},i,\ell}}{h_{\mathrm{AR},i,\ell}} \,. \tag{4.14}$$

By implementing the ZF equalizer before quantization, the quantization noise n_{Q} will not be amplified by equalizing the signal after de-quantization at R_j. This leads to performance advantages compared to the case without ZF equalization, as shown by the numerical results later on.

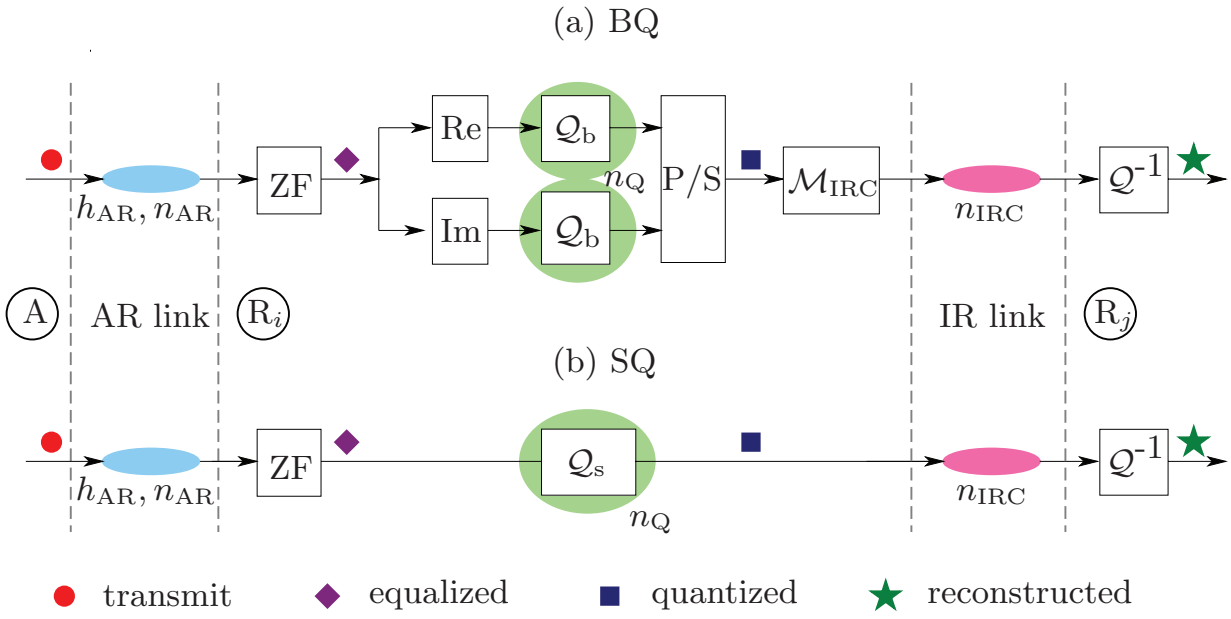

Figure 4.7: Block diagram for receive signal exchange in E_3 with quantization, (a) for BQ and (b) for SQ. The receive signal at R_i is quantized and exchanged to R_j via the IR channel.

Assuming 16-QAM transmission in the AR link and $Q = 3$ bit quantization for both real and imaginary parts of the receive signals to be exchanged, one exemplary transmit symbol, the corresponding equalized symbol, quantized symbol and reconstructed symbol are marked respectively on the constellation plane, as shown in Fig. 4.8(a) for BQ. It is noted that even one bit error during the IR transmission, e.g., $001 \rightarrow 011$ for the real part may lead to catastrophic imprecision when de-quantizing the receive signal at R_j. To mitigate this impact, SQ can be applied that directly quantizes the equalized signal in symbol level at relay R_i, with the block diagram shown in Fig. 4.7(b). The quantized symbol is exchanged in the IRC phase and reconstructed at R_j by de-quantization $\mathcal{Q}^{-1}$ after reception and detection. As an example, 64-QAM is employed for SQ, the constellation plane in Fig. 4.8(b) indicates that SQ achieves more robustness against quantization noise n_{Q} compared to BQ since a neighboring symbol error will not influence the precision of the de-quantized symbol much. However, BQ corresponds to a more practical scenario since the continuous-valued receive signals have to be firstly quantized by ADC in digital communication systems.

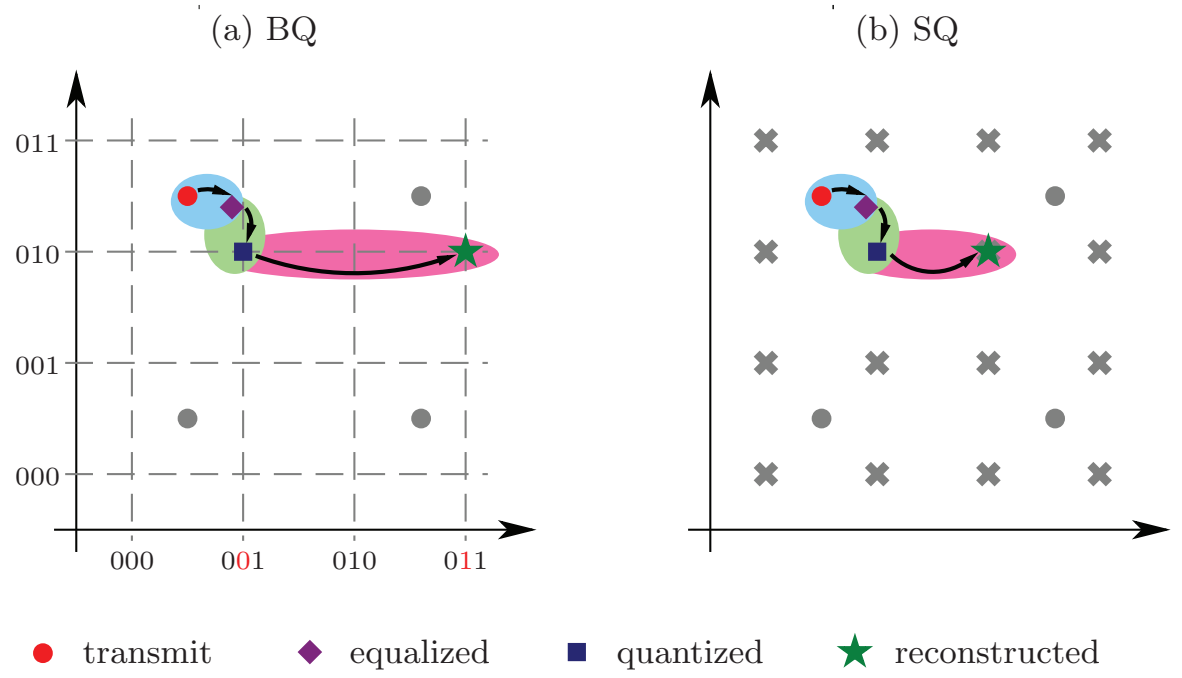

Figure 4.8: Constellation illustration for impact of quantizing the continuous-valued receive signals, (a) for BQ and (b) for SQ.

4.4.4 Throughput Analysis

Compared to the benchmark system in Fig. 4.1 without IRC, IRC consumes extra physical resources, namely, energy and time. For a given SNR, the transmit power $\mathcal{P}_{\mathrm{R}}$ at the relays for the RB transmission is related to the distance d_{RB}. Similarly, the transmit power $\mathcal{P}_{\mathrm{IRC}}$ for IRC within the VAA is related to the distance d_{IRC} between the relays. Since the relays are assumed to be close to each other in this chapter, i.e., $d_{\mathrm{IRC}} \ll d_{\mathrm{RB}}$, the following relation holds

$$\frac{\mathcal{P}_{\mathrm{IRC}}}{\mathcal{P}_{\mathrm{R}}} \propto \left(\frac{d_{\mathrm{IRC}}}{d_{\mathrm{RB}}}\right)^{\alpha} \ll 1 \tag{4.15}$$

due to the path-loss effect. To this end, the transmit power $\mathcal{P}_{\mathrm{IRC}}$ for IRC can be reasonably neglected compared to $\mathcal{P}_{\mathrm{R}}$. Besides transmit power, IRC requires extra baseband and RF circuit power, which are considered adequately in [WXW+11, WXW+12] based on the energy model proposed in [XP12]. This enables system performance evaluation with respect to the total energy consumption, which gives insights into practical system designs with hardware implementation. These aspects are not discussed in this work.

As depicted in Subsection 4.4.1, a dedicated time slot is assigned to IRC, as shown in Fig. 4.2 for the transmission time line. Denoting T_{s} as one symbol duration in single-carrier transmission for IRC, the required time

duration when the punctured bits are exchanged in E_2 is given by

$$T_{\mathrm{pun}} = \left\lceil \frac{N_{\mathrm{IRC}}}{M_{\mathrm{IRC}}} \right\rceil T_{\mathrm{s}} \, . \tag{4.16}$$

On the other hand, the time duration for exchanging the receive signals as well as the channel coefficients when applying BQ for both real and imaginary parts of the continuous-valued signal in E_3 is calculated as

$$T_{\mathrm{rec}} = \left\lceil \frac{2Q\Phi_{\mathrm{IRC}}}{\rho M_{\mathrm{IRC}}} \right\rceil T_{\mathrm{s}} \, . \tag{4.17}$$

Alternatively, considering exchange of continuous-valued receive signals or SQ, this time duration amounts to

$$T_{\mathrm{rec}} = \left\lceil \frac{\Phi_{\mathrm{IRC}}}{\rho} \right\rceil T_{\mathrm{s}} \, . \tag{4.18}$$

Since the presented IRC scheme is adaptive, the total time required for IRC T_{IRC} depends on different events. Note that after exchanging the receive signals among the relays for signal combining and re-decoding when E_3 occurs, the CRC bits are exchanged again, yielding 3 sub-events defined as

$$\mathrm{E}_4 = \mathrm{E}_3 \cap (\mathrm{E}_3 \to \mathrm{E}_1) \tag{4.19a}$$

$$\mathrm{E}_5 = \mathrm{E}_3 \cap (\mathrm{E}_3 \to \mathrm{E}_2) \tag{4.19b}$$

$$\mathrm{E}_6 = \mathrm{E}_3 \cap (\mathrm{E}_3 \to \mathrm{E}_3) \ , \tag{4.19c}$$

where $\mathrm{E}_3 \to \mathrm{E}_i$ represents the event that E_3 turns to E_i by re-decoding based on the exchanged receive signals. It is emphasized that if $\mathrm{E}_3 \to \mathrm{E}_2$ occurs, i.e., at least one but not all relays are correct after receive signal exchange, the punctured bits are further exchanged. On the other hand, $\mathrm{E}_3 \to \mathrm{E}_3$ indicates that all relays are still erroneous after exchanging the receive signals. In this case, one possibility could be switching to AF to avoid error propagation [DZ09a, DZ09b]. However, as a simple approach, DF is still used here with K relays transmitting to B using D-OSTBC. To sum up, depending on the different events, T_{IRC} is given by

$$T_{\mathrm{IRC}} = \begin{cases} KT_{\mathrm{s}} & \text{if } \mathrm{E}_1 \\ (2K - |\mathcal{D}|)\, T_{\mathrm{s}} + T_{\mathrm{pun}} & \text{if } \mathrm{E}_2 \\ 2KT_{\mathrm{s}} + T_{\mathrm{rec}} & \text{if } \mathrm{E}_4,\, \mathrm{E}_6 \\ (3K - |\mathcal{D}''|)\, T_{\mathrm{s}} + T_{\mathrm{rec}} + T_{\mathrm{pun}} & \text{if } \mathrm{E}_5 \, . \end{cases} \tag{4.20}$$

Here $\mathcal{D}''$ represents the set containing all correct relays after the receive signal exchange. Moreover, each relay requires one individual symbol duration T_{s}

to broadcast its CRC bit, resulting in KT_s to determine the set $\mathcal{D}$ in the VAA. In contrast, only the erroneous relays have to update and send their decoding status after re-decoding. T_rec is involved in $\mathrm{E}_3 = \mathrm{E}_4 \cup \mathrm{E}_5 \cup \mathrm{E}_6$. T_pun shows up in E_5 besides in E_2 since the punctured bits are also exchanged in this case.

In order to achieve a fair comparison between the scheme without IRC and the IRC scheme presented in this chapter, the throughput of the overall system is analyzed that takes into account the extra time consumption T_IRC. Since T_IRC depends on different events, the averaged throughput of the overall system η considering IRC is calculated by

$$\eta = \sum_{\substack{i=1 \\ i \neq 3}}^{6} \Pr\{\mathrm{E}_i\} \frac{L \log_2 M \, R_\mathrm{C}}{2T_\mathrm{OFDM} + T_{\mathrm{IRC},i}} \left(1 - \mathrm{FER}_\mathrm{B}\right) \ , \tag{4.21}$$

where $\Pr\{\mathrm{E}_i\}$ and $T_{\mathrm{IRC},i}$ denote the event probability and the time duration for IRC in case that E_i occurs, respectively. Furthermore, the FER at the destination is denoted as FER_B. Both $\Pr\{\mathrm{E}_i\}$ and FER_B can be achieved by simulations. The throughput η defined in (4.21) represents the number of correct information bits received at B per unit time such that it captures the impact of the extended time duration T_IRC in case of IRC.

4.5 Performance Evaluation

In this section, numerical results are shown for one-way distributed relaying networks using adaptive IRC presented in Subsection 4.4.2 and Subsection 4.4.3. The performance of IRC is visualized by investigating either the probability that an erroneous relay is correctly re-decoded after IRC or comparing the probabilities for occurrence of different number of correct relays before and after IRC. Furthermore, the FER at the destination B is compared for IRC with various parametrization. These scenarios are re-considered by resorting to the throughput analysis in Subsection 4.4.4 that takes into account the extra time consumed by IRC.

Parameter Settings

A distributed relaying network with $K = 4$ relays is considered. The constituted VAA joins the direct line between the source and the destination with $d_\mathrm{AR} = d_\mathrm{RB} = 0.5$ and $d_\mathrm{AB} = 1$. The relay channels for all AR and RB links are assumed to be Rayleigh block fading with $N_\mathrm{H} = 5$ equal power channel taps and the path-loss exponent is set to $\alpha = 4$. Furthermore, the channel coefficients stay invariant during $N_\mathrm{inv} = 12$ OFDM symbols.

As in the previous chapter, power allocation is also not considered here. Therefore, the available power is normalized at each transmitting node and is equally assigned to the subcarriers. The source power $\mathcal{P}_{\mathrm{A}}$ is equal to the power $\mathcal{P}_{\mathrm{R}}$ at the VAA, where $\mathcal{P}_{\mathrm{R}}$ is equally allocated to the active relays participating in the D-OSTBC transmission to the destination. The SNR is defined as $\mathrm{SNR} = \mathrm{SNR}_{\mathrm{AR}} = \mathrm{SNR}_{\mathrm{RB}} = 1/(\sigma_n^2 d^\alpha)$ with $d \in \{d_{\mathrm{AR}}, d_{\mathrm{RB}}\}$. One OFDM symbol occupies $L = 256$ subcarriers with 16-QAM modulation. On the other hand, the IR links within the VAA are only subject to AWGN disturbance with a high receive SNR, e.g., $\mathrm{SNR}_{\mathrm{IRC}} = 30\,\mathrm{dB}$ due to closely located relays and 256-QAM is used for IRC. For practical preference, the BQ approach is adopted when exchanging the receive signals in E_3 with the quantization level set to $Q = 4$ and ZF equalizer before quantization.

For punctured bit exchange in IRC, RCPC codes are applied if not otherwise stated. The mother code rate is set to $R_{\mathrm{C,mom}} = 1/3$ and the generator polynomials are $[13, 15, 11]_8$. This code is used to encode $N_b = 512$ information bits at the source, leading to a codeword length of $N = 1536$. After puncturing out $N_{\mathrm{pun}} = 512$ bits, the effective code rate and codeword length are $R_{\mathrm{C}} = 0.5$ and $N_c = 1024$, respectively. Therefore, each OFDM symbol is encoded individually, as $N_c = L \log_2 M$ holds. The BCJR algorithm is used for decoding. Denoting K_{act} the active number of relays transmitting to B, the VAA employs an OSTBC of rate $R_{\mathrm{OSTBC}} = 3/4$ [TSC98] when $K_{\mathrm{act}} = 3$ or $K_{\mathrm{act}} = 4$. When $K_{\mathrm{act}} = 2$, the Alamouti code [Ala98] is used with $R_{\mathrm{OSTBC}} = 1$. The relay simply unicasts to the destination when $K_{\mathrm{act}} = 1$. Employing rate matching as discussed in Subsection 4.3.2, the channel code rate for the RB link transmission is adjusted to $R_{\mathrm{C,RB}} = 2/3$ by RCPC codes in case of using the OSTBC of rate $R_{\mathrm{OSTBC}} = 3/4$.

Impact of Punctured Bit Exchange

In order to investigate the performance of exchanging different number of punctured bits N_{IRC} in E_2, the event E_3 is ignored in this part, i.e., no receive signal is exchanged but all relays participate in the D-OSTBC transmission to the destination. Firstly, the probability P_{w2r} that an erroneous relay is correctly re-decoded with the help of the N_{IRC} punctured bits received in the IRC phase is shown in Fig. 4.9. Obviously, P_{w2r} increases as $\mathrm{SNR}_{\mathrm{IRC}}$ grows due to less distorted punctured bits during IRC. On the other hand, exchanging more punctured bits leads to improved re-decoding quality, e.g., when all $N_{\mathrm{pun}} = N_{\mathrm{IRC}} = 512$ punctured bits are exchanged, the erroneous relay can always be corrected during the whole $\mathrm{SNR}_{\mathrm{IRC}}$ region under investigation. However, higher number of N_{IRC} yields larger overhead, which degrades the overall system throughput. This performance trade-off is to be visualized in the numerical results later on.

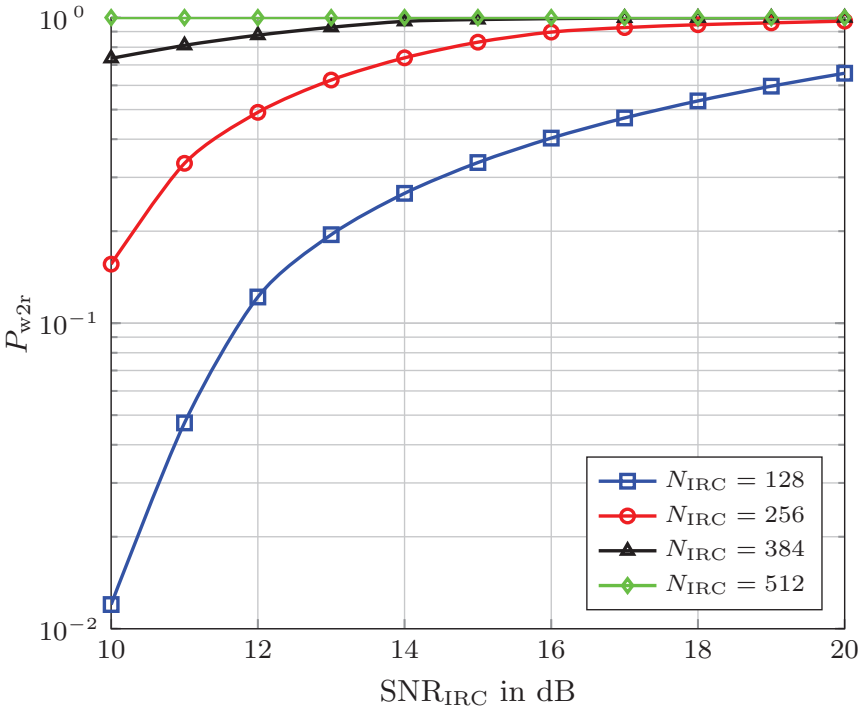

Figure 4.9: Probability that an erroneous relay becomes correct after re-decoding when different number of punctured bits N_{IRC} are exchanged in E_2 depending on $\mathrm{SNR}_{\mathrm{IRC}}$.

The event probabilities for different number of correct relays, i.e., $|\mathcal{D}|$ before re-decoding and $|\mathcal{D}'|$ after re-decoding are shown in Fig. 4.10. In this case, only exchanging punctured bits in E_2 is considered with either $N_{\mathrm{IRC}} = 128$ or $N_{\mathrm{IRC}} = 512$ as examples. It can be observed in Fig. 4.10(a) before re-decoding or for the case without IRC, that event E_1 ($|\mathcal{D}| = 4$) occurs more likely at the high SNR region and vice versa for E_3 ($|\mathcal{D}| = 0$). Event E_2 is the superposition of $|\mathcal{D}| \in \{1, 2, 3\}$, which takes place more frequently at the medium SNR region. When re-decoding is performed at the erroneous relays in case of IRC, the number of correct relays may increase. For example, the probabilities for $|\mathcal{D}'| = 1$ and $|\mathcal{D}'| = 2$ slide leftwards and decrease tremendously whereas the probability increases for $|\mathcal{D}'| = 4$ over the whole SNR range by comparing Fig. 4.10(a) and Fig. 4.10(b) with $N_{\mathrm{IRC}} = 128$ exchanged punctured bits. It is noted that the probability that all relays fail to decode the source message correctly remains unchanged since this event (E_3) is ignored here. Moreover, when all punctured bits are exchanged, i.e., $N_{\mathrm{IRC}} = 512$, the curves for 1, 2 and 3 correct relays after re-decoding totally vanish, as shown in Fig. 4.10(c). This indicates that when enough punctured bits are exchanged in the current system setup, all relays will be error-free after re-decoding if at least one relay is able to decode the source message correctly.

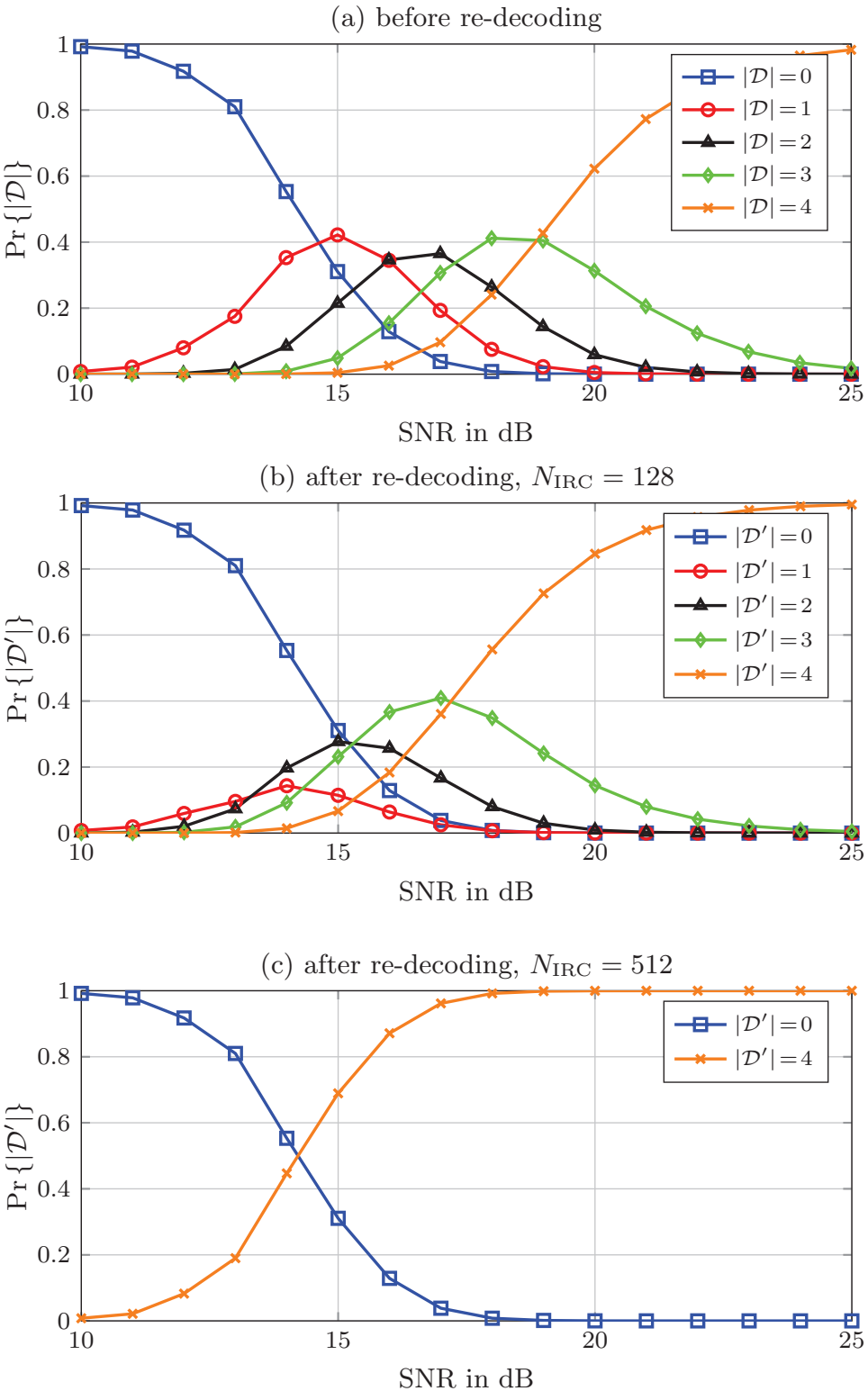

Figure 4.10: Event probabilities for different number of correct relays, (a) for $|\mathcal{D}|$ before re-decoding or no IRC, (b) and (c) for $|\mathcal{D}'|$ after re-decoding with $N_{\mathrm{IRC}} = 128$ and $N_{\mathrm{IRC}} = 512$ exchanged punctured bits in E_2, respectively.

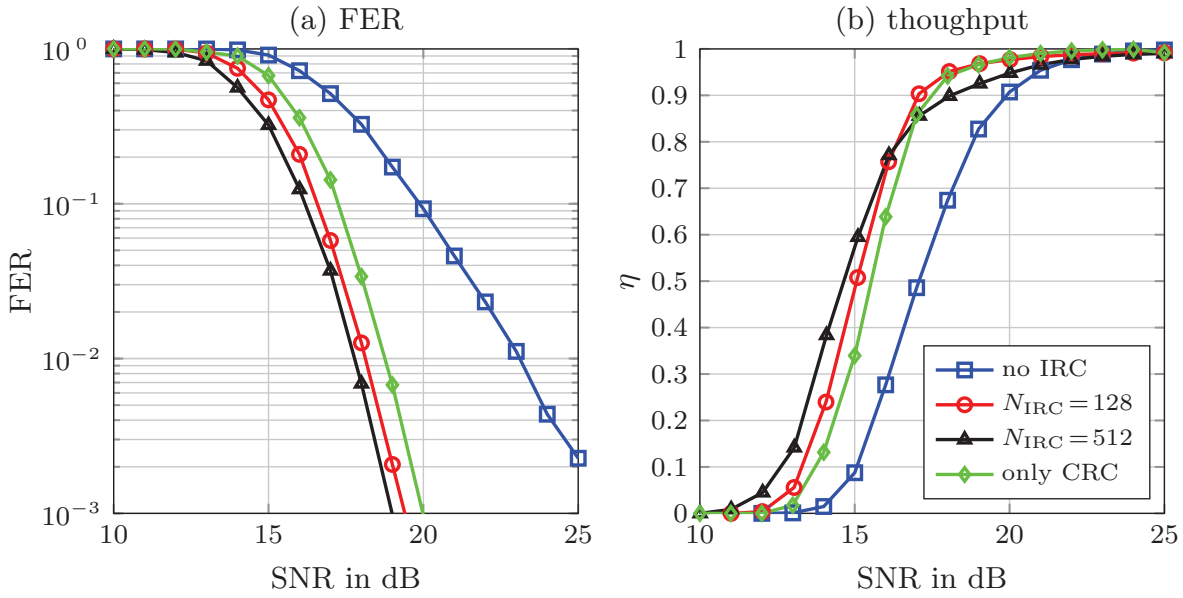

Figure 4.11: Performance of IRC only considering punctured bit exchange with $N_{\mathrm{IRC}} = 128$ or $N_{\mathrm{IRC}} = 512$ in E_2, (a) for FER at B and (b) for system throughput. The case that only the CRC bits are exchanged is presented as a reference.

The FER at B and the overall system throughput are presented in Fig. 4.11 only considering punctured bit exchange with $N_{\mathrm{IRC}} = 128$ or $N_{\mathrm{IRC}} = 512$ in E_2. As a reference similar to [LW03], the case that only the CRC bits are exchanged ($N_{\mathrm{IRC}} = 0$) is also shown, where the relays with correct decoding results transmit to B using D-OSTBC without other types of information exchange within the VAA. As can be observed in Fig. 4.11(a), the IRC scheme achieves tremendous diversity gain compared to the case without IRC. Furthermore, exchanging more punctured bits leads to improved FER performance in the sense of a horizontal SNR shift. When only the CRC bits are exchanged, the diversity gain is preserved but suffers from an SNR loss to the IRC scheme with punctured bit exchange. When resorting to the throughput analysis, the IRC scheme is still much superior to the case without IRC. However, larger amount of punctured bit exchange leads to performance degradation with growing SNR, although it's still superior in the low SNR region. This is because better re-decoding quality is dominant when the AR link is weak whereas less punctured bits are sufficient in the high SNR region which yield reduced exchange overhead for IRC. Additionally, IRC with $N_{\mathrm{IRC}} = 128$ outperforms the case with only CRC exchange over the whole SNR range, confirming the benefit of the proposed IRC scheme.

The throughput performance shown above is achieved by adopting fixed amount of exchanged punctured bits in E_2 irrespective of the re-decoding

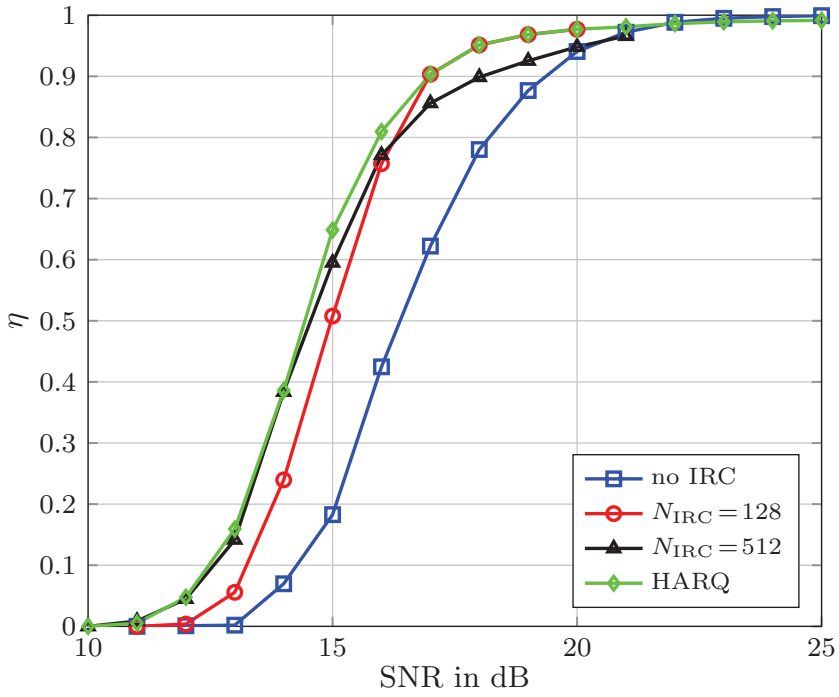

Figure 4.12: System throughput for IRC only considering punctured bit exchange in E_2 using HARQ.

status at the erroneous relays. As indicated in Fig. 4.11(b), larger N_{IRC} is required in the low SNR region and vice versa. To combine both characteristics, the HARQ scheme [Che06] can be applied that enables adaptive transmission of the punctured bits within the VAA. By choosing a step size, e.g., $\Delta N_{\mathrm{IRC}} = 128$ bits, the selected correct relay R_κ sends each time ΔN_{IRC} bits whereas the erroneous relay performs re-decoding with the help of all previously received punctured bits and subsequently broadcasts its re-decoding status in the VAA. R_κ stops the re-transmission process when having either received the ACK from all erroneous relays or sent out all N_{pun} available punctured bits. Applying this HARQ scheme for punctured bit exchange, the system throughput is shown in Fig. 4.12, which takes into account the adaptive amount of exchanged punctured bits and the CRC exchange after each re-transmission. It can be observed in the figure that HARQ is beneficial over the whole SNR range compared to the cases with fixed N_{IRC} since it searches automatically the optimal amount of required punctured bits leading to correct re-decoding.

As an alternative for channel coding, LDPC codes are considered instead of convolutional codes for the distributed relaying network with IRC. In order to facilitate punctured bit exchange in E_2, a mother code of rate $R_{\mathrm{C,mom}} = 1/3$ is used at the source to encode the information word with the parity-check matrix generated by the PEG algorithm [HEA05] and

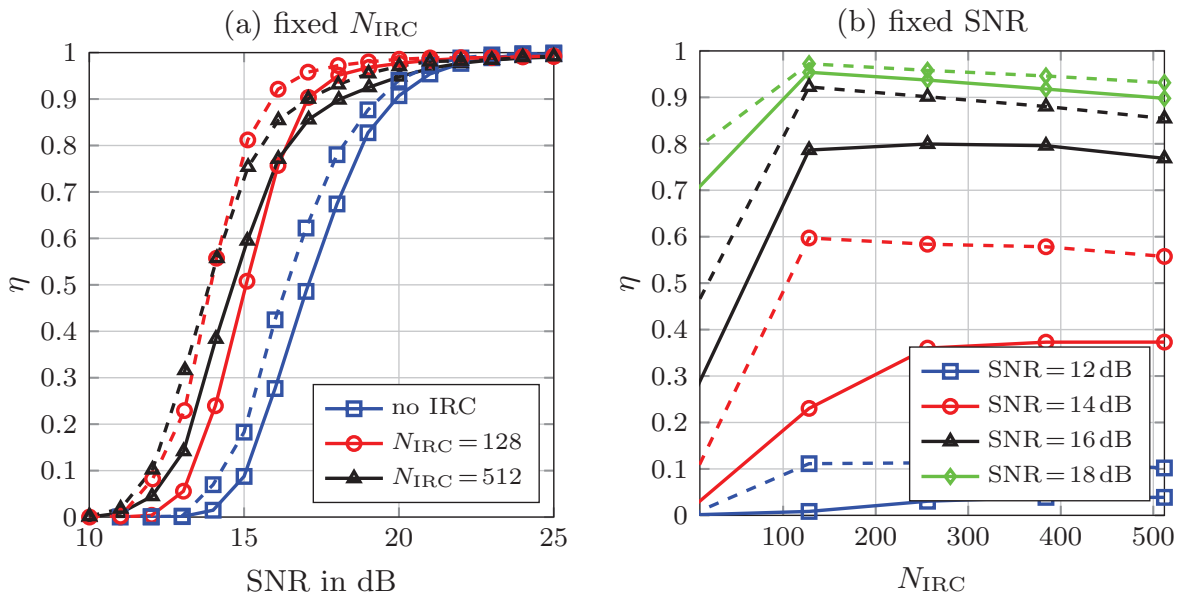

Figure 4.13: System throughput for IRC only considering punctured bit exchange in E_2 using convolutional codes (-) or LDPC codes (- -), (a) depending on SNR with fixed N_{IRC} and (b) depending on N_{IRC} with fixed SNR.

optimized degree distribution achieved from [Urb01]. Afterwards, $N_{\mathrm{pun}} = 512$ code bits are randomly chosen and punctured out to result in the code for transmission with effective code rate $R_{\mathrm{C}} = 0.5$. Note that optimal design of rate-compatible punctured LDPC codes can be found in [HKM04, HKKM06], which specifies deliberately the locations of the punctured bits to yield improved performance than random specification. This aspect is beyond the scope of this work and thus not considered here. The throughput performance using convolutional codes in Fig. 4.11(b) is re-evaluated using LDPC codes and shown in Fig. 4.13(a). As can be observed in the figure, LDPC codes lead to higher throughput in general as a stronger code family. More importantly, the cross point between $N_{\mathrm{IRC}} = 128$ and $N_{\mathrm{IRC}} = 512$ comes earlier in case of applying LDPC codes because for a fixed number of N_{IRC}, smaller SNR is required to support correct re-decoding by a stronger channel code. The throughput performance is shown in Fig. 4.13(b) with different number of exchanged punctured bits N_{IRC} at fixed SNR values. The superiority of LDPC codes is again observed here in contrast to convolutional codes. Obviously, less punctured bits are required with growing SNR as the optimal value of N_{IRC} leading to the highest throughput decreases correspondingly. Furthermore, this optimal value is smaller for LDPC codes at fixed SNRs, e.g., the optimal value is $N_{\mathrm{IRC}} = 128$ for LDPC codes while it is $N_{\mathrm{IRC}} = 512$ for convolutional codes at SNR = 14dB.

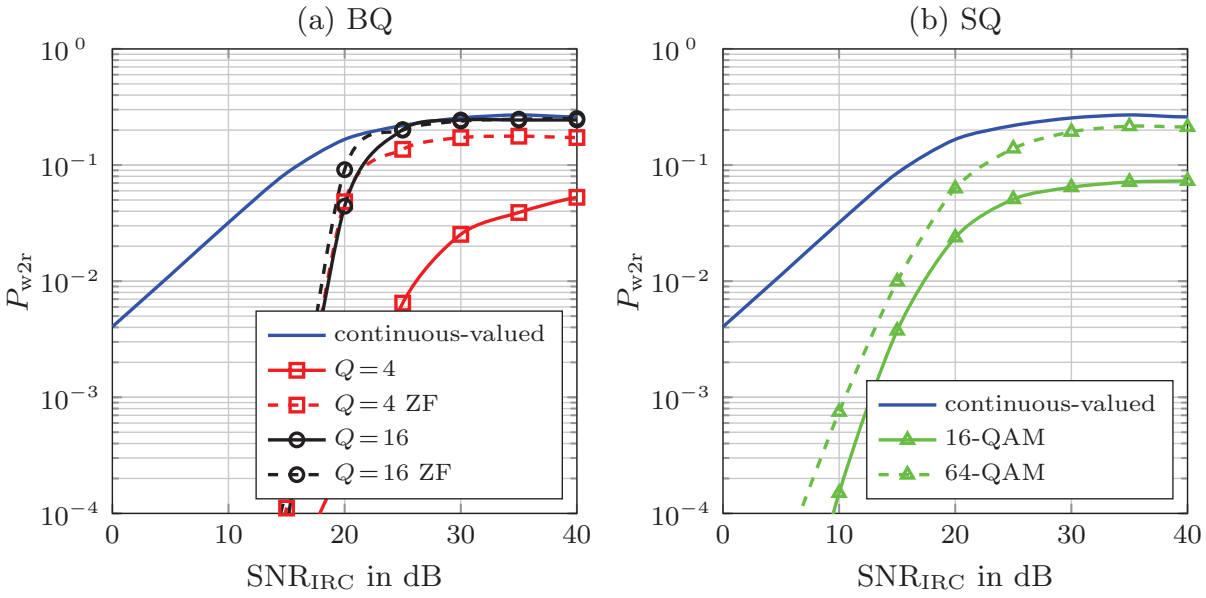

Figure 4.14: Probability that an erroneous relay becomes correct after re-decoding when receive signals are exchanged in E_3 with (a) BQ and (b) SQ depending on $\mathrm{SNR}_{\mathrm{IRC}}$.

Impact of Receive Signal Exchange

In this part, the performance of exchanging receive signals at the VAA in E_3 is evaluated for both the full and partial cooperation approaches. In case of E_2 and E_5, all $N_{\mathrm{pun}} = 512$ punctured bits are exchanged as an example. Firstly, the probability P_{w2r} that an erroneous relay is correctly re-decoded after signal combining is shown in Fig. 4.14 with respect to $\mathrm{SNR}_{\mathrm{IRC}}$, where transmitting continuous-valued receive signals without quantization achieves the best performance. When BQ is employed with $Q = 16$ bits to quantize the real part and imaginary part of each complex symbol, both schemes with and without the ZF equalizer approach the continuous-valued transmission at high $\mathrm{SNR}_{\mathrm{IRC}}$ because of small quantization noise n_{Q}. The scheme without ZF equalization before quantization leads to significantly degraded performance when $Q = 4$ due to the amplification of n_{Q} by de-rotation. However, de-rotating the signal by ZF before quantization avoids this problem and approaches the continuous-valued transmission with only a slightly degraded performance. Noticeably, using $Q = 4$ and $M_{\mathrm{IRC}} = 256$ in case of BQ achieves the same overhead as continuous-valued transmission, as one continuous-valued signal results in one digitally modulated symbol. However, using quantization leads to a more realistic scenario in view of implementation. Furthermore, Fig. 4.14(a) shows that continuous-valued transmission achieves much better performance with decreasing $\mathrm{SNR}_{\mathrm{IRC}}$ since one bit

error during the IR transmission for BQ may result in completely corrupted signal after de-quantization. The performance at lower $\mathrm{SNR}_{\mathrm{IRC}}$ can be improved by applying SQ as shown in Fig. 4.14(b). Therein, continuous-valued transmission still achieves superior performance. However, SQ with 64-QAM not only approaches this performance upper-bound but also outperforms BQ in less robust IR channel conditions. Additionally, it is observed that the re-decoding quality is degraded severely when the quantization alphabet is reduced to 16-QAM due to less quantization accuracy.

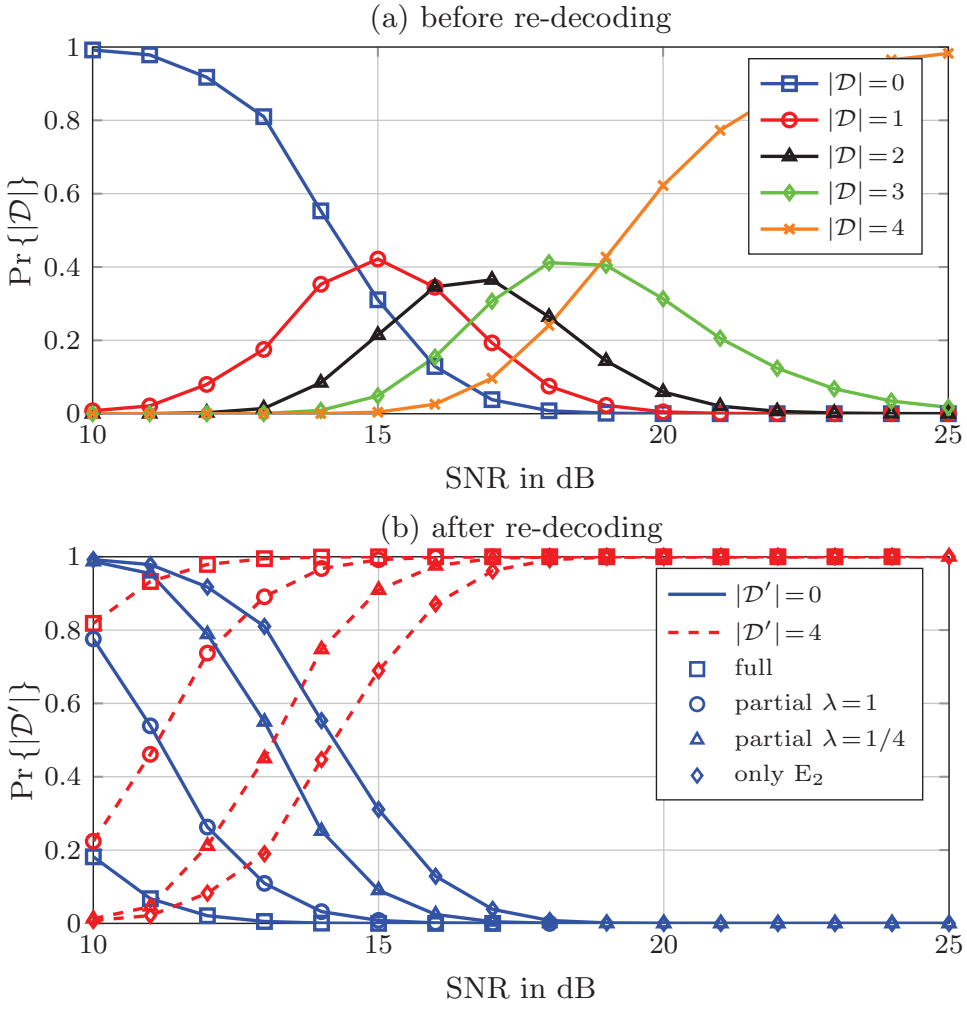

Figure 4.15: Event probabilities for different number of correct relays, (a) for $|\mathcal{D}|$ before re-decoding or no IRC, and (b) for $|\mathcal{D}'|$ after re-decoding with both full and partial cooperation approaches for receive signal exchange in E_3.

The event probabilities for different number of correct relays before and after re-decoding are drawn in Fig. 4.15 considering receive signal exchange in E_3. The case that only exchanging punctured bits in E_2 is also presented as a reference. By re-decoding after signal combining based on receive signal

exchange, the probability that all relays are still erroneous after IRC gets smaller, as shown in Fig. 4.15(b). It can be also observed that exchanging larger amount of receive signals leads to improved re-decoding quality, as partial cooperation with $\lambda = 1$ is superior to that with $\lambda = 1/4$ whereas full cooperation gains over partial cooperation. However, a fair comparison between these cases is achieved by the throughput analysis taking into account the exchange overhead in the sequel.

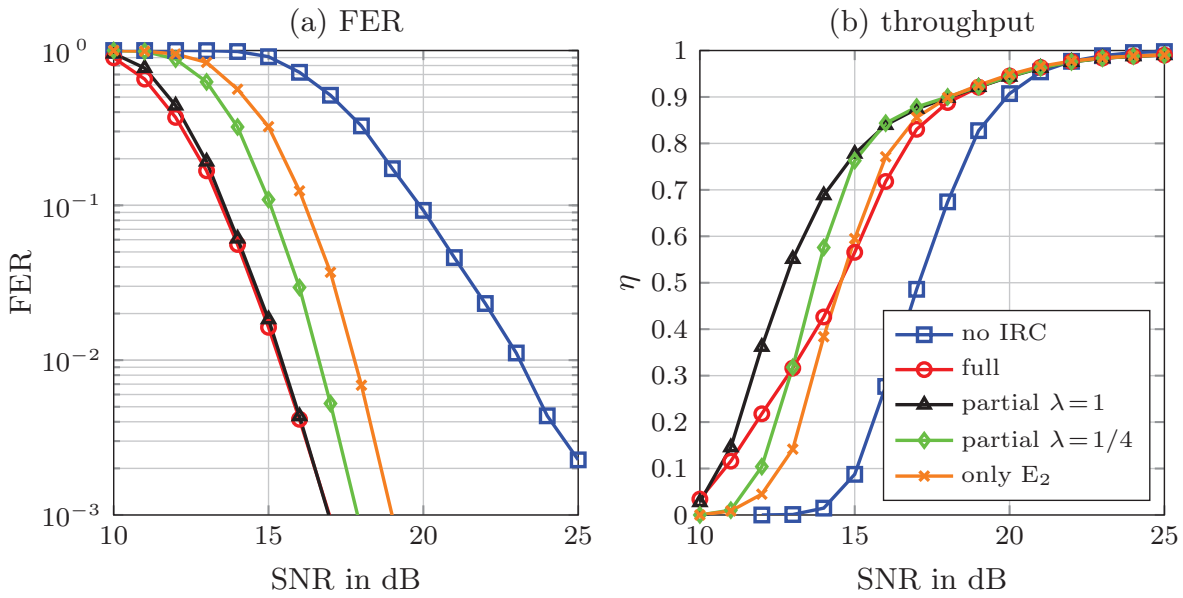

Figure 4.16: Performance of IRC considering receive signal exchange in E_3 with both full and partial cooperation approaches, (a) for FER at B and (b) for system throughput.

The FER and throughput performance are evaluated in Fig. 4.16 when the receive signals are exchanged in E_3 with both full and partial cooperation approaches. Apparently, larger amount of exchanged receive signals lead to improved FER performance ignoring the exchange overhead for IRC, as shown in Fig. 4.16(a). It is worth to note that partial cooperation with $\lambda = 1$ already approaches full cooperation but the required overhead is reduced significantly. This aspect is incorporated in performance evaluation by the throughput analysis. As can be observed in Fig. 4.16(b), exchanging receive signals when all relays are erroneous in E_3 improves the throughput in general compared to the case of IRC only with punctured bit exchange in E_2, especially in the low SNR region. However, due to the large amount of overhead, using full cooperation becomes even slightly worse than ignoring E_3 as the SNR increases, although it outperforms partial cooperation with $\lambda = 1/4$ at low SNR. The partial cooperation approach with $\lambda = 1$ achieve the most superior throughput performance in this system setup.

4.6 Chapter Summary

This chapter is concentrated on one-way distributed relaying networks, in which the source communicates with the destination supported by multiple single-antenna relays. By clustering these relays into a virtual antenna array (VAA), MIMO technologies in a MIMO relay scenario can be applied at both the receiver side and transmitter side of the VAA. To this end, information exchange between the relays termed inter-relay cooperation (IRC) is required, as enabled by employing a dedicated time slot between the AR and RB transmissions. In Section 4.2, the basic system model is described first. Subsequently, possible MIMO diversity schemes operating in a distributed manner are explicated in Section 4.3, which depend on the allowed level of cooperation within the VAA. Afterwards, specific adaptive IRC schemes using a dedicated time slot are proposed in Section 4.4 based on punctured channel codes and receive signal exchange according to the decoding status of the relays in the VAA [WXW+11, WXW+12, WLW+16a]. The superior performance of the proposed IRC approach with appropriate parametrization is verified in Section 4.5, where a fair comparison is achieved by resorting to a throughput analysis that incorporates the IRC overhead.

Chapter 5

Two-Way SISO Relaying

5.1 Overview

For cooperative communications with relays supporting transmission from the source to the destination, the effective path-loss between the terminals can be reduced, thus yielding enhanced system performance and coverage extension. However, the spectral efficiency is limited due to the half-duplex constraint at the relay. To combat this drawback, one-way relaying communications are extended to a two-way sense, where both terminals are treated as sources that intend to exchange information with each other via relays by exploiting the broadcast nature of wireless links and the principle of network coding. To accomplish this bi-directional communication with increased spectral efficiency, each source first transmits its message to the relay separately in two phases. The relay then estimates and broadcasts a network coded message back to the sources in a third phase, resulting in three phases in total. The number of required phases can be reduced to two to fully compensate the halved spectral efficiency for one-way relaying. In this case, two sources transmit to the relay simultaneously and the relay broadcasts a joint message estimated from the superimposed receive signal. Due to the highest spectral efficiency, this two-phase scheme is mainly considered requiring efficient detection and decoding schemes at the relay to estimate the network coded message. The main contribution is to analyze these schemes based on mutual information and enhance the performance by allowing more design flexibilities in coded OFDM systems. Moreover, simultaneous transmission from both sources to the relay poses synchronization challenges that have to be handled properly in practical system designs. These aspects are investigated in this chapter with one relay node.

The basis system setup for two-way relaying networks is demonstrated in Section 5.2. General descriptions for the various relaying schemes with four phases, three phases and two phases are given as well. Focusing on the two-phase scheme, different detection and decoding schemes to estimate the network coded message at the relay are presented in Section 5.3 with detailed illustration and analysis based on mutual information. In Section 5.4, it is shown that the performance of the schemes presented in the previous section is strongly dependent on the channel ratio of both links from the sources to the relay. Therefore, an optimal phase control strategy requiring CSI at the transmitter side is developed to yield the best phase difference for these schemes, respectively [WWD13a, WLW+16b]. Meanwhile, the CSI overhead can be reduced significantly by linear approximation of the channel phase. Subsequently, the asynchrony caused by carrier frequency offset mismatch in the simultaneous transmission from both sources to the relay is investigated and corresponding approaches are introduced to mitigate the resulting impairments in Section 5.5 [WLW+14, WLW+16b]. In addition, the two-way relaying network is extended employing a multiple-antenna relay in Section 5.6, which facilitates the application of MIMO technologies exploiting multiplexing gain due to increased spatial degrees of freedom [WWD13b, WWD14b, WLW+16b]. In the final analysis, Section 5.7 summarizes the contributions and main results of this chapter.

5.2 Basics of Two-Way Relaying Communications

In the context of two-way relaying communications, relaying schemes requiring different number of transmission phases can be applied. In this section, the basic concepts of this aspect are demonstrated to show the general mechanism of these schemes, namely, the four-phase, three-phase and two-phase schemes. Special interests are attached to the two-phase scheme due to its highest spectral efficiency, where the principle of analog network coding and digital network is distinguished.

5.2.1 Four-Phase Scheme

In two-way relaying communications employing the four-phase scheme as a straightforward approach without network coding, the transmissions are carried out in orthogonal time slots, as shown in Fig. 5.1 [FBW06]. Specifically, the message from source A is delivered to source B via relay R in two successive time slots due to the half-duplex constraint. Subsequently,

source B sends its message to source A in the same manner, resulting in four transmission phases in total. It is noted that such a two-way relaying scheme essentially corresponds to two independent one-way relaying processes, and thus the one-way relaying techniques introduced in Chapter 2 can be applied in this context. Furthermore, the direct link between the two sources can be utilized in the 1st phase and the 3rd phase of the transmission scheme.

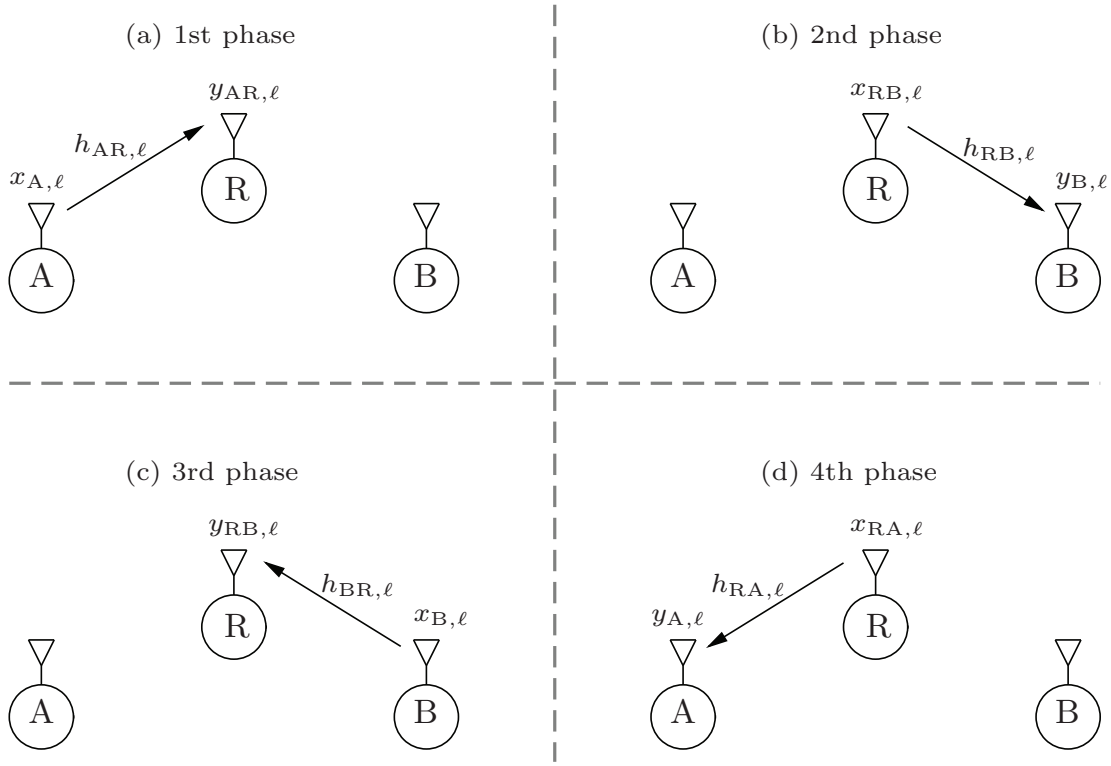

Figure 5.1: A two-way relaying communication system employing the four-phase scheme. The bi-directional data exchange is accomplished in four successive time slots shown in (a)-(d).

$$y_{\mathrm{AR},\ell} = h_{\mathrm{AR},\ell} x_{\mathrm{A},\ell} + n_{\mathrm{AR},\ell} \tag{5.1}$$

$$y_{\mathrm{B},\ell} = h_{\mathrm{RB},\ell} x_{\mathrm{RB},\ell} + n_{\mathrm{B},\ell} \tag{5.2}$$

$$y_{\mathrm{BR},\ell} = h_{\mathrm{BR},\ell} x_{\mathrm{B},\ell} + n_{\mathrm{BR},\ell} \tag{5.3}$$

$$y_{\mathrm{A},\ell} = h_{\mathrm{RA},\ell} x_{\mathrm{RA},\ell} + n_{\mathrm{A},\ell} \tag{5.4}$$

The system equations for the four orthogonal transmissions are presented in (5.1)-(5.4). Similar to that in the previous chapters, coded OFDM is assumed for all transmissions to combat multi-path fading while the description is focused on the ℓth subcarrier in the frequency domain. To distinguish the signals at the relay in different time slots, e.g., $y_{\mathrm{AR},\ell}$ and $y_{\mathrm{BR},\ell}$ are denoted

as the receive signals from source A in the 1st phase and from source B in the 3rd phase, respectively. Moreover, the channel coefficients, e.g., $h_{\mathrm{AR},\ell}$ and $h_{\mathrm{RA},\ell}$ describe the channels from source A to relay R and from relay R to source A in the frequency domain, respectively. In this work, the channels are assumed to be not reciprocal, i.e., $h_{\mathrm{AR},\ell} \neq h_{\mathrm{RA},\ell}$ holds in general.

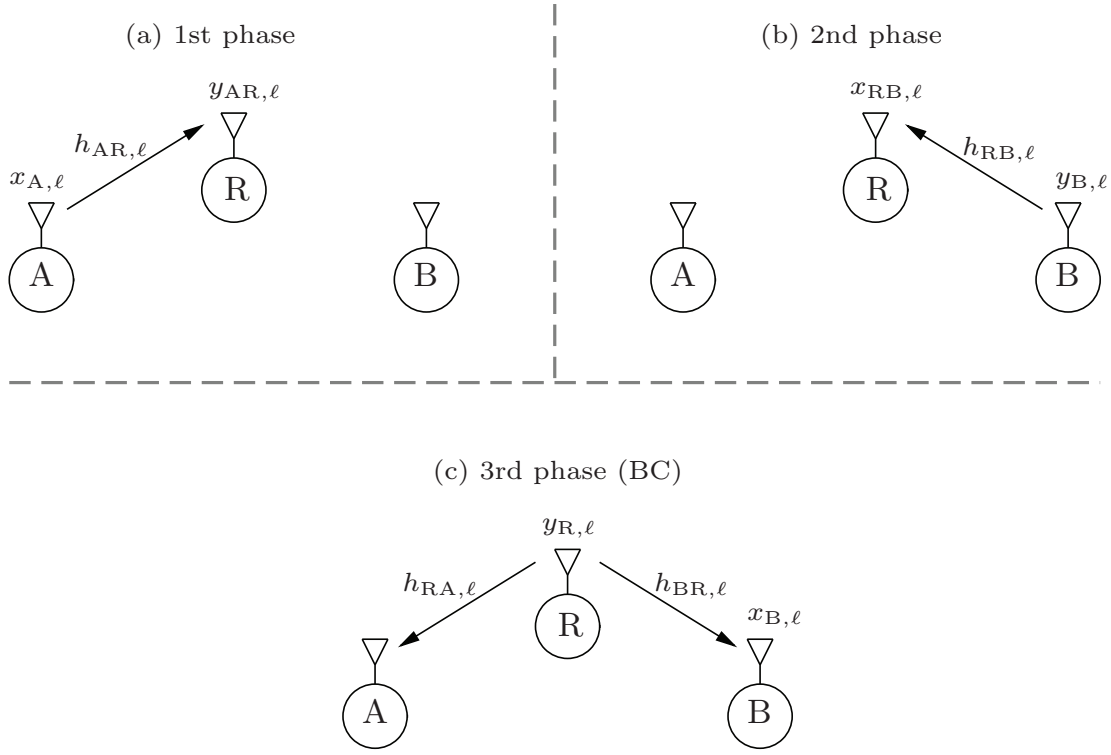

Figure 5.2: A two-way relaying communication system employing the three-phase scheme. After successive transmissions from source A and B to relay R shown in (a) and (b), relay R performs network coding to the estimated source messages and broadcasts the network-coded signal back to the sources shown in (c).

5.2.2 Three-Phase Scheme

Due to the half-duplex constraint, the spectral efficiency of two-way relaying employing the four-phase scheme as well as one-way relaying is halved compared to direct transmission without relay. To compensate this performance loss, a three-phase scheme shown in Fig. 5.2 can be applied [FBW06]. In this two-way relaying scheme, relay R estimates the source messages from the receive signals in the first two phases successively. Since these two transmissions take place in orthogonal time slots, the direct link between source A and B can also be considered. Afterwards, a network coded signal is generated containing information of both source messages, which is

broadcast back to the sources in the 3rd phase termed the broadcast (BC) phase. Based on the fact that both sources are aware of their own messages transmitted in the previous time slots, network decoding is performed at each source to retrieve the desired message from the counterpart.

$$y_{\mathrm{AR},\ell} = h_{\mathrm{AR},\ell} x_{\mathrm{A},\ell} + n_{\mathrm{AR},\ell} \tag{5.5}$$

$$y_{\mathrm{BR},\ell} = h_{\mathrm{BR},\ell} x_{\mathrm{B},\ell} + n_{\mathrm{BR},\ell} \tag{5.6}$$

$$y_{\mathrm{A},\ell} = h_{\mathrm{RA},\ell} x_{\mathrm{R},\ell} + n_{\mathrm{A},\ell} \tag{5.7a}$$

$$y_{\mathrm{B},\ell} = h_{\mathrm{RB},\ell} x_{\mathrm{R},\ell} + n_{\mathrm{B},\ell} \tag{5.7b}$$

The system equations on the ℓth subcarrier are presented in (5.5) and (5.6) for the successive transmissions to relay R and in (5.7) for the BC transmission. Therein, $x_{\mathrm{R},\ell}$ denotes the network coded signal at relay R that contains information from both source messages. After the BC phase, source A, e.g., utilizes the receive signal $y_{\mathrm{A},\ell}$ as well as its own message $x_{\mathrm{A},\ell}$ to estimate its desired message $x_{\mathrm{B},\ell}$ from source B. Such a network decoding process is performed at source B similarly.

5.2.3 Two-Phase Scheme with Physical-Layer Network Coding

In order to further increase the spectral efficiency, the required number of time slots for two-way relaying communications can be reduced to two applying physical-layer network coding (PLNC) [PY06, PY07, WNPS10, ZLL06]. In such a two-phase relaying scheme depicted in Fig 5.3, two sources A and B transmit to relay R simultaneously in the multiple-access (MA) phase. In the sequel, relay R estimates a network coded signal directly from the receive signal, which is then broadcast to the sources in the BC phase. Similar to that in the three-phase scheme, network decoding is performed at both sources to estimate the desired signal from each other.

Since the bi-directional message exchange is accomplished in two time slots, the loss of spectral efficiency due to the half-duplex constraint for relaying communications can be completely compensated. Therefore, we concentrate on the two-phase scheme applying PLNC in this work. In the sequel, the parameters relevant to this system setup are defined and explained. It is assumed that the binary information words $\mathbf{b}_{\mathrm{A}}$ and $\mathbf{b}_{\mathrm{B}}$ at both sources are of the same length N_b. These two information words are encoded by the same linear channel code Γ with code rate $R_{\mathrm{C}} = N_b/N_c$ into binary source codewords $\mathbf{c}_{\mathrm{A}} = \Gamma(\mathbf{b}_{\mathrm{A}})$ and $\mathbf{c}_{\mathrm{B}} = \Gamma(\mathbf{b}_{\mathrm{B}})$ of length N_c. Afterwards, both source codewords are mapped to the OFDM symbol vectors $\mathbf{x}_{\mathrm{A}} = \mathcal{M}(\mathbf{c}_{\mathrm{A}})$

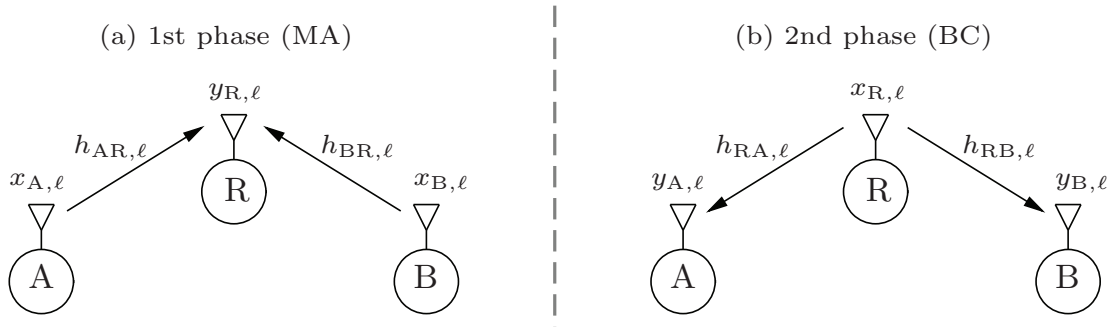

Figure 5.3: A two-way relaying communication system employing the two-phase scheme. In the MA phase, both sources A and B transmit to relay R simultaneously as shown in (a). Relay R estimates a network coded signal from the superimposed receive signal and broadcasts it back to the sources in the BC phase shown in (b).

and $\mathbf{x}_{\mathrm{B}} = \mathcal{M}(\mathbf{c}_{\mathrm{B}})$. These symbol vectors at the sources are transmitted to relay R simultaneously in the MA phase, yielding the receive signal on the ℓth subcarrier at relay R as

$$y_{\mathrm{R},\ell} = h_{\mathrm{AR},\ell} x_{\mathrm{A},\ell} + h_{\mathrm{BR},\ell} x_{\mathrm{B},\ell} + n_{\mathrm{R},\ell} \; . \tag{5.8}$$

As illustrated above, $h_{\mathrm{AR},\ell}$ and $h_{\mathrm{BR},\ell}$ represent the channel coefficients from the sources to the relay on the ℓth subcarrier in the frequency domain.

Upon reception at the relay of the superimposed signal vector $\mathbf{y}_{\mathrm{R}} = [y_{\mathrm{R},1} \; y_{\mathrm{R},2} \; \cdots \; y_{\mathrm{R},L}]^T$, network coding is performed that maps $\mathbf{y}_{\mathrm{R}}$ to the network coded signal $\mathbf{x}_{\mathrm{R}} = \mathcal{C}(\mathbf{y}_{\mathrm{R}})$. Depending on different network coding strategies, the function $\mathcal{C}(\cdot)$ generates $\mathbf{x}_{\mathrm{R}}$ that is broadcast to both sources in the BC phase as

$$y_{\mathrm{A},\ell} = h_{\mathrm{RA},\ell} x_{\mathrm{R},\ell} + n_{\mathrm{A},\ell} \tag{5.9a}$$

$$y_{\mathrm{B},\ell} = h_{\mathrm{RB},\ell} x_{\mathrm{R},\ell} + n_{\mathrm{B},\ell} \tag{5.9b}$$

for the signal on the ℓth subcarrier. In the final analysis, each source performs network decoding with the help of its own information transmitted in the MA phase to estimate the desired message from its counterpart. For example, source A estimates the information word $\hat{\mathbf{b}}_{\mathrm{B}} = \mathcal{C}^{-1}(\mathbf{y}_{\mathrm{A}}, \mathbf{b}_{\mathrm{A}})$ from $\mathbf{y}_{\mathrm{A}} = [y_{\mathrm{A},1} \; y_{\mathrm{A},2} \; \cdots \; y_{\mathrm{A},L}]^T$ using $\mathbf{b}_{\mathrm{A}}$. Here, $\mathcal{C}^{-1}(\cdot)$ denotes the network decoding function corresponding to $\mathcal{C}(\cdot)$.

Analog Network Coding

The principle of analog network coding (ANC) is initially considered in [KGK07], where the receive signal at relay R is linearly amplified similarly as

the AF strategy for one-way relaying communications. Corresponding to AF-CP in Subsection 3.3.1 [WW11], varying amplification factor β_ℓ can be chosen to amplify the subcarrier wise receive signal as $x_{\mathrm{R},\ell} = \mathcal{C}(y_{\mathrm{R},\ell}) = \beta_\ell y_{\mathrm{R},\ell}$, where β_ℓ is defined as

$$\beta_\ell = \sqrt{\frac{1}{|h_{\mathrm{AR},\ell}|^2 + |h_{\mathrm{BR},\ell}|^2 + \sigma_n^2}} \tag{5.10}$$

to achieve constant power over all subcarriers. In contrast, a universal amplification factor β results in the same gain for all subcarriers. Similar to that defined for AF-CG in Subsection 3.3.2 [WW11], β in the context of ANC for PLNC is given as

$$\beta = \sqrt{\frac{1}{||\mathbf{h}_{\mathrm{AR}}||^2/L + ||\mathbf{h}_{\mathrm{BR}}||^2/L + \sigma_n^2}} \,. \tag{5.11}$$

Accordingly, the transmit signal vector at relay R can be calculated as

$$\mathbf{x}_{\mathrm{R}} = \mathcal{C}(\mathbf{y}_{\mathrm{R}}) = \beta \mathbf{y}_{\mathrm{R}} \tag{5.12}$$

employing the universal β, which leads to lower computational efforts compared to the carrier wise calculation using β_ℓ.

For elaboration of network decoding, the operation at source A after the BC phase is taken as an example with AF-CP at relay R. Substituting $x_{\mathrm{R},\ell} = \beta_\ell y_{\mathrm{R},\ell}$ into (5.9a) with some simple equation reformulations, the ℓth receive signal at source A yields

$$\begin{aligned} y_{\mathrm{A},\ell} &= h_{\mathrm{RA},\ell}\beta_\ell(h_{\mathrm{AR},\ell}x_{\mathrm{A},\ell} + h_{\mathrm{BR},\ell}x_{\mathrm{B},\ell} + n_{\mathrm{R},\ell}) + n_{\mathrm{A},\ell} \\ &= \underbrace{h_{\mathrm{RA},\ell}\beta_\ell h_{\mathrm{BR},\ell}x_{\mathrm{B},\ell}}_{\text{desired signal}} + \underbrace{h_{\mathrm{RA},\ell}\beta_\ell h_{\mathrm{AR},\ell}x_{\mathrm{A},\ell}}_{\text{self-interference}} + \underbrace{h_{\mathrm{RA},\ell}\beta_\ell n_{\mathrm{R},\ell} + n_{\mathrm{A},\ell}}_{\text{equivalent noise}} \,. \end{aligned} \tag{5.13}$$

Since source A knows its transmitted message in the MA phase, the signal contribution from $x_{\mathrm{A},\ell}$ in the equation above is treated as self-interference and thus can be subtracted from the receive signal $y_{\mathrm{A},\ell}$. Afterwards, a common decoding is applied to the remaining interference-free signal containing $x_{\mathrm{B},\ell}$ with the subcarrier wise SNR defined as

$$\mathrm{SNR}_\ell = \frac{|h_{\mathrm{RA},\ell}\beta_\ell h_{\mathrm{BR},\ell}|^2}{(|h_{\mathrm{RA},\ell}\beta_\ell|^2 + 1)\sigma_n^2} \,. \tag{5.14}$$

Digital Network Coding

The disadvantage of ANC is on one hand the amplification of noise at the relay. On the other hand, the receive signal at each source in the BC phase

is a linear superposition of desired signal and interference as shown in (5.13). In other words, the desired signal only bears part of the receive signal power, resulting in severe power inefficiency. To conquer these drawbacks, digital network coding (DNC) can be applied at the relay that maps the receive signal vector $\mathbf{y}_\mathrm{R}$ to the network coded signal vector $\mathbf{x}_\mathrm{R}$ with finite alphabet.

One of the key issues for DNC is the design of the network coding function $\mathcal{C}(\cdot)$. Since each receive sequence $\mathbf{y}_\mathrm{R}$ corresponds to one or several transmit message pairs $(\mathbf{x}_\mathrm{A}, \mathbf{x}_\mathrm{B})$, the mapping rule $\mathbf{x}_\mathrm{R} = \mathcal{C}(\mathbf{y}_\mathrm{R})$ can be equivalently interpreted as $\mathbf{x}_\mathrm{R} = \mathcal{C}(\mathbf{x}_\mathrm{A}, \mathbf{x}_\mathrm{B})$. In order to achieve a successful network decoding at the sources, any arbitrary $\mathcal{C}(\cdot)$ has to fulfill the following requirement [KAPT09b]

$$\mathcal{C}(\mathbf{x}_\mathrm{A}, \mathbf{x}_\mathrm{B}) \neq \mathcal{C}(\mathbf{x}'_\mathrm{A}, \mathbf{x}_\mathrm{B}) \quad \text{for any } \mathbf{x}_\mathrm{A} \neq \mathbf{x}'_\mathrm{A} \tag{5.15a}$$

$$\mathcal{C}(\mathbf{x}_\mathrm{A}, \mathbf{x}_\mathrm{B}) \neq \mathcal{C}(\mathbf{x}_\mathrm{A}, \mathbf{x}'_\mathrm{B}) \quad \text{for any } \mathbf{x}_\mathrm{B} \neq \mathbf{x}'_\mathrm{B}\,, \tag{5.15b}$$

which refers to the general exclusive law. For example, any two different transmit signal vectors $\mathbf{x}_\mathrm{A}$ and $\mathbf{x}'_\mathrm{A}$ at source A, i.e., $\mathbf{x}_\mathrm{A} \neq \mathbf{x}'_\mathrm{A}$, should lead to different network coded outputs when source B transmits the same $\mathbf{x}_\mathrm{B}$. Otherwise, source B is not able to perform network decoding successfully after the BC phase since it can not distinguish whether $\mathbf{x}_\mathrm{A}$ or $\mathbf{x}'_\mathrm{A}$ was transmitted by source A.

In this work, the bit-level XOR operation is employed as a special case fulfilling the general exclusive law in (5.15) due to its simplicity [LJS06]. To this end, denoting $\mathbf{c}_\mathrm{R}$ as the relay codeword, the mapping rule can be defined in bit-level as

$$\mathbf{c}_\mathrm{R} = \mathcal{C}(\mathbf{c}_\mathrm{A}, \mathbf{c}_\mathrm{B}) = \mathbf{c}_\mathrm{A} \oplus \mathbf{c}_\mathrm{B}\,. \tag{5.16}$$

Since the same linear channel code is employed at both sources in the MA phase, $\mathbf{c}_\mathrm{R}$ is still a valid codeword in the same codebook. Subsequently, $\mathbf{x}_\mathrm{R} = \mathcal{M}(\mathbf{c}_\mathrm{R})$ is generated and broadcast to the sources in the BC phase. For network decoding, source A, e.g., first estimates the relay codeword $\hat{\mathbf{c}}_{\mathrm{R,A}}$, which is XORed with the self-interference term $\mathbf{c}_\mathrm{A}$ to estimate the desired message $\hat{\mathbf{c}}_\mathrm{B} = \hat{\mathbf{c}}_{\mathrm{R,A}} \oplus \mathbf{c}_\mathrm{A}$ from the counterpart. The estimate $\hat{\mathbf{c}}_\mathrm{A} = \hat{\mathbf{c}}_{\mathrm{R,B}} \oplus \mathbf{c}_\mathrm{B}$ is achieved similarly at source B.

The bottleneck of the DNC-based approach for PLNC is the decoding errors at relay R when estimating the relay codeword $\mathbf{c}_\mathrm{R}$ from the receive signal. These errors will propagate to the sources in the BC phase and thus jeopardize the overall end-to-end performance significantly. Therefore, it is crucial to focus on the MA phase, where different PLNC schemes are developed at the relay to estimate $\mathbf{c}_\mathrm{R}$. These schemes are reviewed and compared in the upcoming section, with the emphasis on mutual information

analysis. Note that network coded based capacity of the MA channel is studied theoretically in [KS09, ULL17b]. However, they are not discussed here as the main focus of this work is on developing practical PLNC schemes.

5.3 APP-based Schemes

In this section, several PLNC schemes are presented that estimate the relay codeword $\mathbf{c}_\mathrm{R}$ from the receive signal $\mathbf{y}_\mathrm{R}$ at the relay [Wüb10, WL10, WWD13a]. For this purpose, the relay may either estimate the source messages explicitly followed by network coding, or directly estimate the relay message. Furthermore, these schemes are all based on the APPs obtained from $\mathbf{y}_\mathrm{R}$, which are firstly introduced in the following subsection.

5.3.1 Definitions

In order to simplify the description for APPs at the relay with deterministic channel realizations in the MA phase, some basic relations between the occurring signals and their corresponding probabilities on the ℓth subcarrier are elaborated. Furthermore, the subcarrier index ℓ is omitted in the sequel for the sake of simplicity unless otherwise stated.

Since sources A and B transmit simultaneously to relay R in the MA phase, the receive signal y_R defined in (5.8) is determined by both source messages $x_\mathrm{A} = \mathcal{M}(c_\mathrm{A})$ and $x_\mathrm{B} = \mathcal{M}(c_\mathrm{B})$. Assuming M-QAM modulation with $m = \log_2 M$, this leads to M^2 different noise-free receive signals s_AB at relay R as

$$s_\mathrm{AB} = h_\mathrm{AR} x_\mathrm{A} + h_\mathrm{BR} x_\mathrm{B} \,. \tag{5.17}$$

Letting $\mathcal{S}_\mathrm{AB}(i)$ be a hypothesis defined by the code bit tuples $c_\mathrm{A} = [c_{\mathrm{A},1}\ c_{\mathrm{A},2}\ \cdots\ c_{\mathrm{A},m}]$ and $c_\mathrm{B} = [c_{\mathrm{B},1}\ c_{\mathrm{B},2}\ \cdots\ c_{\mathrm{B},m}]$, the set $\mathcal{S}_\mathrm{AB}$ contains all the M^2 hypotheses with index $0 \leq i \leq M^2 - 1$. As a short hand notation, $c_\mathrm{AB} = [c_\mathrm{A}\ c_\mathrm{B}]$ is denoted as the combined code bit tuple and the corresponding polynomial description with indeterminate D is given as

$$\begin{aligned} c_\mathrm{AB} &= [c_{\mathrm{A},1}\ c_{\mathrm{A},2}\ \cdots\ c_{\mathrm{A},m}\ c_{\mathrm{B},1}\ c_{\mathrm{B},2}\ \cdots\ c_{\mathrm{B},m}] \\ &\triangleq c_{\mathrm{A},1} + c_{\mathrm{A},2} D + \cdots + c_{\mathrm{A},m} D^{m-1} \\ &\quad + c_{\mathrm{B},1} D^m + c_{\mathrm{B},2} D^{m+1} + \cdots + c_{\mathrm{B},m} D^{2m-1} \,. \end{aligned} \tag{5.18}$$

Therefore, c_AB belongs to a GF $\mathcal{C}_\mathrm{AB} = \mathbb{F}_{M^2}$ with $c_\mathrm{AB} = \mathcal{C}_\mathrm{AB}(i)$, or equivalently $s_\mathrm{AB} = \mathcal{S}_\mathrm{AB}(i)$, representing the ith event in $\mathbb{F}_{M^2}$. Additionally, for further derivations, the element wise bit-level XOR combination of c_A and c_B is denoted as

$$c_{\mathrm{A}\oplus\mathrm{B}} = c_\mathrm{A} \oplus c_\mathrm{B} = [c_{\mathrm{A},1} \oplus c_{\mathrm{B},1}\ c_{\mathrm{A},2} \oplus c_{\mathrm{B},2}\ \cdots\ c_{\mathrm{A},m} \oplus c_{\mathrm{B},m}] \,. \tag{5.19}$$

Based on the above definitions as well as the instantaneous channel coefficients h_{AR} and h_{BR}, the relations between the code bit tuple $(c_{\mathrm{A}}, c_{\mathrm{B}})$, the transmit signal tuple $(x_{\mathrm{A}}, x_{\mathrm{B}})$ and the noise-free receive signal s_{AB} at relay R for BPSK and QPSK modulation are shown in Tab. 5.1 and Tab. 5.2 as examples, respectively.

i	c_{A}	c_{B}	$c_{\mathrm{A}\oplus\mathrm{B}}$	c_{AB}	x_{A}	x_{B}	s_{AB}
0	0	0	0	0	1	1	$h_{\mathrm{AR}} + h_{\mathrm{BR}}$
1	1	0	1	1	-1	1	$-h_{\mathrm{AR}} + h_{\mathrm{BR}}$
2	0	1	1	D	1	-1	$h_{\mathrm{AR}} - h_{\mathrm{BR}}$
3	1	1	0	$1+D$	-1	-1	$-h_{\mathrm{AR}} - h_{\mathrm{BR}}$

Table 5.1: Mapping rules of the code bit tuple $(c_{\mathrm{A}}, c_{\mathrm{B}})$, the transmit signal tuple $(x_{\mathrm{A}}, x_{\mathrm{B}})$ and the noise-free receive signal s_{AB} at relay R for BPSK modulation with $i = 0, 1, \cdots, 3$.

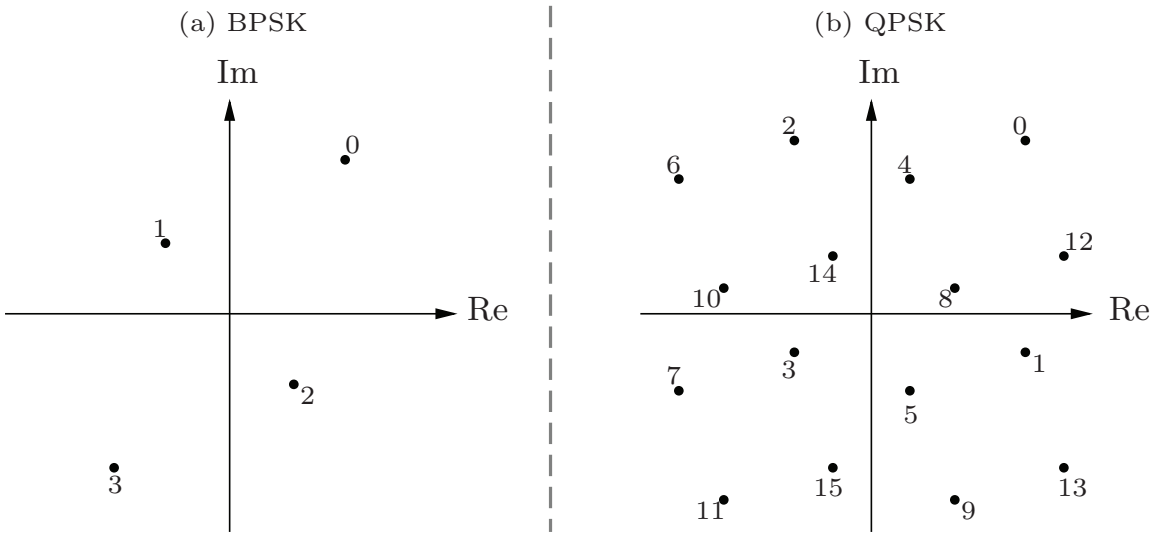

Figure 5.4: Graphical illustration for the constellation set of the noise-free receive signal at relay R on the ℓth subcarrier in multi-path fading channels. (a) for BPSK with $h_{\mathrm{AR}} = 0.8 + 0.6j$, $h_{\mathrm{BR}} = 0.3 + j$, $i = 0, 1, \cdots, 3$ and (b) for QPSK with $h_{\mathrm{AR}} = j$, $h_{\mathrm{BR}} = -0.2 + 0.5j$, $i = 0, 1, \cdots, 15$.

In order to visualize the superimposed signal constellation set, graphical examples of s_{AB} are presented in Fig. 5.4 and Fig. 5.5 on the ℓth subcarrier for given channel realizations. As can be observed, BPSK and QPSK

i	c_{A}	c_{B}	$c_{\mathrm{A}\oplus\mathrm{B}}$	c_{AB}	x_{A}	x_{B}	s_{AB}
0	00	00	00	0	1	1	$h_{\mathrm{AR}} + h_{\mathrm{BR}}$
1	10	00	10	1	j	1	$jh_{\mathrm{AR}} + h_{\mathrm{BR}}$
2	01	00	01	D	-1	1	$-h_{\mathrm{AR}} + h_{\mathrm{BR}}$
3	11	00	11	$1+D$	$-j$	1	$-jh_{\mathrm{AR}} + h_{\mathrm{BR}}$
4	00	10	10	D^2	1	j	$h_{\mathrm{AR}} + jh_{\mathrm{BR}}$
5	10	10	00	$1+D^2$	j	j	$jh_{\mathrm{AR}} - jh_{\mathrm{BR}}$
6	01	10	11	$D+D^2$	-1	j	$-h_{\mathrm{AR}} + jh_{\mathrm{BR}}$
7	11	10	01	$1+D+D^2$	$-j$	j	$-jh_{\mathrm{AR}} + jh_{\mathrm{BR}}$
8	00	01	01	D^3	1	-1	$h_{\mathrm{AR}} - h_{\mathrm{BR}}$
9	10	01	11	$1+D^3$	j	-1	$jh_{\mathrm{AR}} - h_{\mathrm{BR}}$
10	01	01	00	$D+D^3$	-1	-1	$-h_{\mathrm{AR}} - h_{\mathrm{BR}}$
11	11	01	10	$1+D+D^3$	$-j$	-1	$-jh_{\mathrm{AR}} - h_{\mathrm{BR}}$
12	00	11	11	D^2+D^3	1	$-j$	$h_{\mathrm{AR}} - jh_{\mathrm{BR}}$
13	10	11	01	$1+D^2+D^3$	j	$-j$	$jh_{\mathrm{AR}} - jh_{\mathrm{BR}}$
14	01	11	10	$D+D^2+D^3$	-1	$-j$	$-h_{\mathrm{AR}} - jh_{\mathrm{BR}}$
15	11	11	00	$1+D+D^2+D^3$	$-j$	$-j$	$-jh_{\mathrm{AR}} - jh_{\mathrm{BR}}$

Table 5.2: Mapping rules of the code bit tuple $(c_{\mathrm{A}}, c_{\mathrm{B}})$, the transmit signal tuple $(x_{\mathrm{A}}, x_{\mathrm{B}})$ and the noise-free receive signal s_{AB} at relay R for QPSK modulation with $i = 0, 1, \cdots, 15$.

lead to 4 and 16 hypotheses, which correspond to Tab. 5.1 and Tab. 5.2, respectively. Note that these hypotheses are well separated in Fig. 5.4. However, in certain channel conditions, some hypotheses can be completely superimposed. For example, when $h_{\mathrm{AR}} = h_{\mathrm{BR}} = 1$, both transmit symbol tuples $(x_{\mathrm{A}}, x_{\mathrm{B}}) = (1, -1)$ and $(x_{\mathrm{A}}, x_{\mathrm{B}}) = (-1, 1)$ lead to the same hypothesis $s_{\mathrm{AB}} = 0$ for BPSK, resulting in only 3 spatially separated hypotheses in the complex plane. When applying QSPK at both sources, 16 different transmit symbol tuples $(x_{\mathrm{A}}, x_{\mathrm{B}})$ lead to only 9 separated hypotheses, which can be observed in Fig. 5.5.

For APP calculations, the probability density of y_{R} conditioned on the

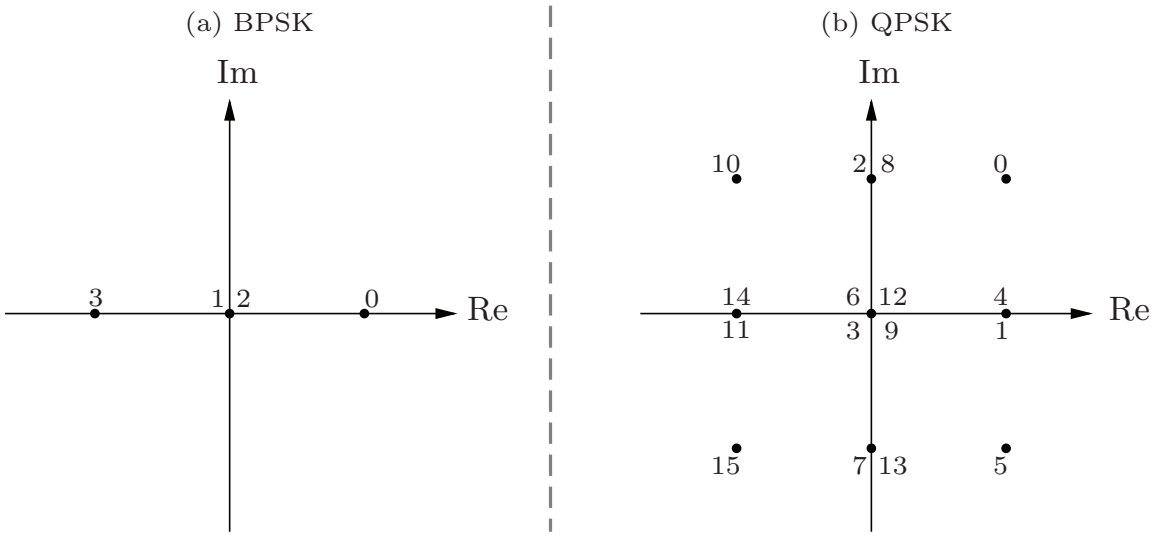

Figure 5.5: Graphical illustration for the constellation set of the noise-free receive signal at relay R with $h_{\mathrm{AR}} = h_{\mathrm{BR}} = 1$. (a) for BPSK with $i = 0, 1, \cdots, 3$ and (b) for QPSK with $i = 0, 1, \cdots, 15$.

code bit combination $c_{\mathrm{AB}} \in \mathcal{C}_{\mathrm{AB}}$ with deterministic channel realizations is deduced from AWGN channels as [Kam11]

$$\begin{aligned} & p\{y_{\mathrm{R}}|c_{\mathrm{AB}} = \mathcal{C}_{\mathrm{AB}}(i)\} \\ = \; & p\{y_{\mathrm{R}}|s_{\mathrm{AB}} = \mathcal{S}_{\mathrm{AB}}(i)\} \\ = \; & \frac{1}{\pi\sigma_n^2} \exp\left\{-\frac{|y_{\mathrm{R}} - \mathcal{S}_{\mathrm{AB}}(i)|^2}{\sigma_n^2}\right\} . \end{aligned} \tag{5.20}$$

Applying Bayes' rule, the APP P_i that $c_{\mathrm{AB}} = \mathcal{C}_{\mathrm{AB}}(i)$ was transmitted given the receive signal y_{R} yields

$$\begin{aligned} P_i &= \Pr\{c_{\mathrm{AB}} = \mathcal{C}_{\mathrm{AB}}(i)|y_{\mathrm{R}}\} \\ &= p\{y_{\mathrm{R}}|c_{\mathrm{AB}} = \mathcal{C}_{\mathrm{AB}}(i)\} \frac{\Pr\{c_{\mathrm{AB}} = \mathcal{C}_{\mathrm{AB}}(i)\}}{\Pr\{y_{\mathrm{R}}\}} \\ &= p\{y_{\mathrm{R}}|c_{\mathrm{AB}} = \mathcal{C}_{\mathrm{AB}}(i)\}\alpha . \end{aligned} \tag{5.21}$$

Additionally, it is assumed that the occurrence of all transmit symbols are equally probable. Therefore, the a-priori probabilities for $c_{\mathrm{AB}} = \mathcal{C}_{\mathrm{AB}}(i)$ are given by

$$\Pr\{c_{\mathrm{AB}} = \mathcal{C}_{\mathrm{AB}}(i)\} = \frac{1}{M^2} . \tag{5.22}$$

Correspondingly, the constant α can be calculated using the completeness

condition $\sum_i P_i = 1$ to normalize the probabilities P_i as

$$\alpha = \frac{\Pr\{c_{\mathrm{AB}} = \mathcal{C}_{\mathrm{AB}}(i)\}}{\Pr\{y_{\mathrm{R}}\}} = \frac{1}{M^2 \Pr\{y_{\mathrm{R}}\}} \,. \tag{5.23}$$

The APPs determine the probabilities of different transmit code bit combinations c_{AB} based on the receive signal y_{R}. These APPs can be used to calculate the LLRs for the individual code bits c_{A} and c_{B}, or the XORed code bit $c_{\mathrm{A}\oplus\mathrm{B}}$ directly. In the sequel, the LLRs of different code bits are obtained from the APPs to facilitate several PLNC detection and decoding schemes at the relay, which are termed APP-based schemes to be elaborated in detail.

5.3.2 Separated Channel Decoding

In order to generate the network coded signal at relay R, the individual source messages can be estimated first, essentially corresponding to a traditional MA transmission [CT91]. To this end, separated channel decoding (SCD) can be applied that targets at decoding the estimates $\hat{\mathbf{c}}_{\mathrm{A}}$ and $\hat{\mathbf{c}}_{\mathrm{B}}$ explicitly from $\mathbf{y}_{\mathrm{R}}$. Subsequently, the relay codeword is achieved by $\mathbf{c}_{\mathrm{R}} = \hat{\mathbf{c}}_{\mathrm{A}} \oplus \hat{\mathbf{c}}_{\mathrm{B}}$.

Focusing on the ℓth subcarrier with the corresponding APPs defined in (5.21), the probability that $c_{\mathrm{A},\nu} = \xi$ is transmitted given the receive signal y_{R} can be calculated as

$$\Pr\{c_{\mathrm{A},\nu} = \xi | y_{\mathrm{R}}\} = \sum_{i \in \Omega^{\xi}_{\mathrm{A},\nu}} P_i \tag{5.24}$$

with $\nu = 1, 2, \cdots, m$ and $\xi = \{0, 1\}$. Furthermore, $\Omega^{\xi}_{\mathrm{A},\nu}$ denotes the set of indices with the code bit $c_{\mathrm{A},\nu}$ equal to ξ according to Tab. 5.1 and Tab. 5.2. For example, the set $\Omega^{0}_{\mathrm{A},1} = \{0, 2\}$ collects all events i with $c_{\mathrm{A},1} = 0$ for BPSK. When QPSK is taken into account, $\Omega^{0}_{\mathrm{A},1} = \{0, 2, 4, 6, 8, 10, 12, 14\}$ is specified. Correspondingly, the LLR $L_{\mathrm{A},\nu}$ for the code bit $c_{\mathrm{A},\nu}$ can be formulated as

$$L_{\mathrm{A},\nu} = \ln\left(\frac{\Pr\{c_{\mathrm{A},\nu} = 0 | y_{\mathrm{R}}\}}{\Pr\{c_{\mathrm{A},\nu} = 1 | y_{\mathrm{R}}\}}\right) \,, \tag{5.25}$$

which is collected in the LLR vector $\mathbf{L}_{\mathrm{A}}$ for the whole codeword and fed to a soft-input channel decoder. After binary decoding, the estimate $\hat{\mathbf{c}}_{\mathrm{A}}$ of the source codeword from source A is obtained. Similarly, the LLR calculation and channel decoding are performed with respect to the codeword from source B, resulting in the estimate $\hat{\mathbf{c}}_{\mathrm{B}}$. Subsequently, network coding is performed to generate the relay codeword $\mathbf{c}_{\mathrm{R}} = \hat{\mathbf{c}}_{\mathrm{A}} \oplus \hat{\mathbf{c}}_{\mathrm{B}}$. The corresponding block diagram at relay R for such a SCD scheme is shown in Fig. 5.6.

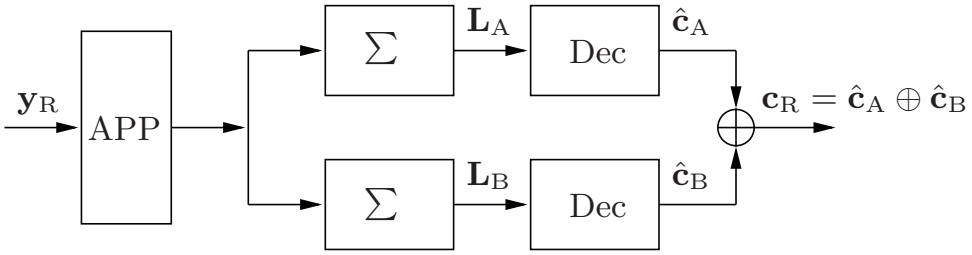

Figure 5.6: Block diagram at relay R for SCD. The individual source messages $\mathbf{c}_\mathrm{A}$ and $\mathbf{c}_\mathrm{B}$ are estimated by binary channel decoding using $\mathbf{L}_\mathrm{A}$ and $\mathbf{L}_\mathrm{B}$, respectively. Network coding $\mathbf{c}_\mathrm{R} = \hat{\mathbf{c}}_\mathrm{A} \oplus \hat{\mathbf{c}}_\mathrm{B}$ is then performed.

Graphical Illustration

To illustrate the LLR calculation in (5.25) using the sets $\Omega^{\xi}_{\mathrm{A},\nu}$ and $\Omega^{\xi}_{\mathrm{B},\nu}$, graphical examples are presented in Fig. 5.7 for BPSK with the same channel condition as that in Fig. 5.4(a). Therein, the event sets $\Omega^{0}_{\mathrm{A},1} = \{0, 2\}$ and $\Omega^{1}_{\mathrm{A},1} = \{1, 3\}$ are used for the calculation of $L_{\mathrm{A},1}$ as

$$L_{\mathrm{A},1} = \ln\left(\frac{P_0 + P_2}{P_1 + P_3}\right) , \tag{5.26}$$

which are in accordance with the solid lines and the dashed lines in the figure, respectively. Similarly, $L_{\mathrm{B},1}$ is calculated utilizing the sets $\Omega^{0}_{\mathrm{B},1} = \{0, 1\}$ and $\Omega^{1}_{\mathrm{B},1} = \{2, 3\}$ by

$$L_{\mathrm{B},1} = \ln\left(\frac{P_0 + P_1}{P_2 + P_3}\right) . \tag{5.27}$$

Considering QPSK with the same channel condition as that in Fig. 5.4(b), the graphical illustration for the above LLR calculations is focused on the first code bit in one modulated symbol, i.e., $c_{\mathrm{A},1}$ and $c_{\mathrm{B},1}$, as shown in Fig. 5.8. Specifically, the LLR $L_{\mathrm{A},1}$ is calculated using $\Omega^{0}_{\mathrm{A},1} = \{0, 2, 4, 6, 8, 10, 12, 14\}$ and $\Omega^{1}_{\mathrm{A},1} = \{1, 3, 4, 5, 6, 11, 13, 15\}$, whereas the sets $\Omega^{0}_{\mathrm{B},1} = \{0, 1, 2, 3, 8, 9, 10, 11\}$ and $\Omega^{1}_{\mathrm{B},1} = \{4, 5, 6, 7, 12, 13, 14, 15\}$ correspond to the calculation for $L_{\mathrm{B},1}$. This leads to the LLR formulations for QPSK as

$$L_{\mathrm{A},1} = \ln\left(\frac{P_0 + P_2 + P_4 + P_6 + P_8 + P_{10} + P_{12} + P_{14}}{P_1 + P_3 + P_5 + P_7 + P_9 + P_{11} + P_{13} + P_{15}}\right) \tag{5.28}$$

$$L_{\mathrm{B},1} = \ln\left(\frac{P_0 + P_1 + P_2 + P_3 + P_8 + P_9 + P_{10} + P_{11}}{P_4 + P_5 + P_6 + P_7 + P_{12} + P_{13} + P_{14} + P_{15}}\right) . \tag{5.29}$$

It is noted in Fig. 5.8 for QPSK, that SCD leads to relatively larger |LLR| for $c_{\mathrm{A},1}$ as the sets $\Omega^{0}_{\mathrm{A},1}$ and $\Omega^{1}_{\mathrm{A},1}$ are spatially well separated for the given

channel realization. In contrast, $\Omega^0_{\mathrm{B},1}$ and $\Omega^1_{\mathrm{B},1}$ are not enough distinguished, resulting in smaller |LLR|. A closer look at the |LLR| distributions taking into account the fading channel characteristic is presented later on.

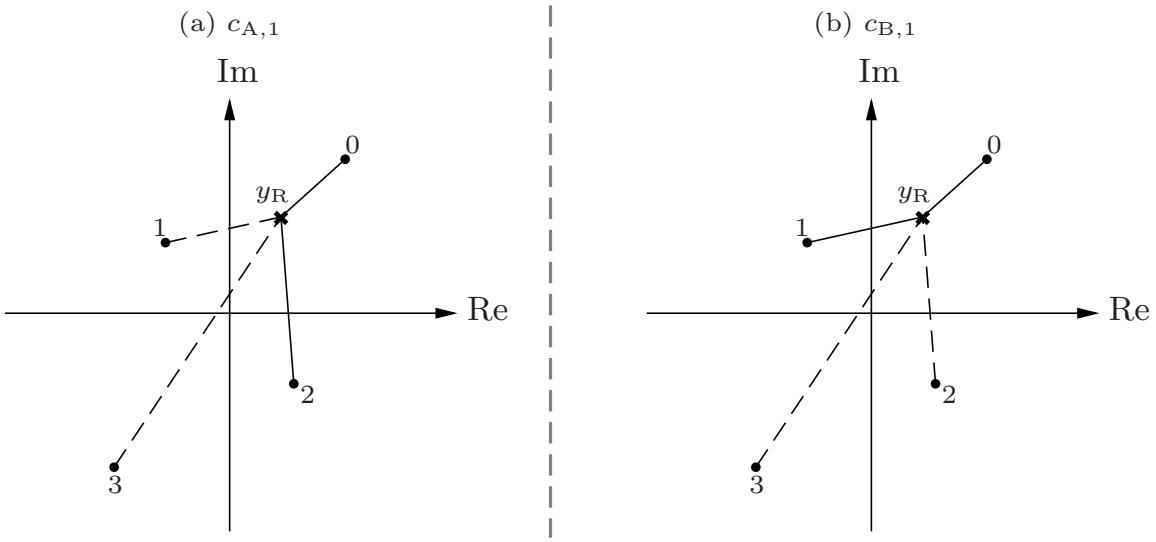

Figure 5.7: Graphical illustration of the LLR calculation for SCD with BPSK. The receive signal y_{R} is marked by 'x'. Solid lines and dashed lines correspond to entries s_{AB} with code bit equal to 0 and 1, respectively. (a) for code bit $c_{\mathrm{A},1}$ and (b) for code bit $c_{\mathrm{B},1}$, $i = 0, 1, \cdots, 3$.

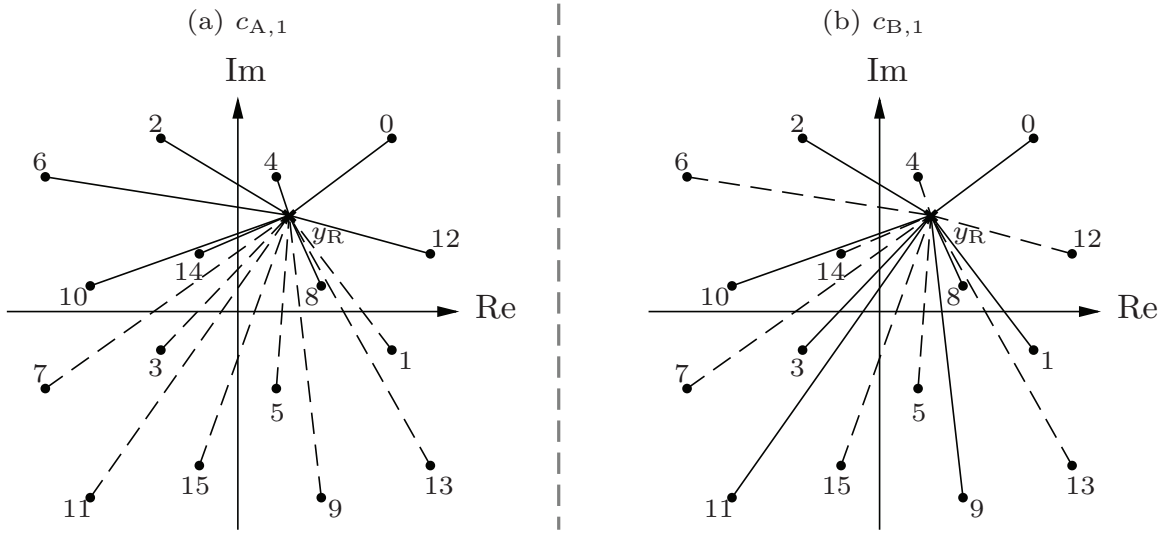

Figure 5.8: Graphical illustration of the LLR calculation for SCD with QPSK. The receive signal y_{R} is marked by 'x'. Solid lines and dashed lines correspond to entries s_{AB} with code bit equal to 0 and 1, respectively. (a) for code bit $c_{\mathrm{A},1}$ and (b) for code bit $c_{\mathrm{B},1}$, $i = 0, 1, \cdots, 15$.

Parallel SCD vs. Successive SCD

The SCD scheme presented above decodes the source messages $\mathbf{c}_\mathrm{A}$ and $\mathbf{c}_\mathrm{B}$ in parallel and thus is termed P-SCD. Alternatively, the decoding results from the stronger link in the MA channel can be subtracted from the receive signal and a common decoding for the other codeword with respect to this interference reduced signal is performed. Such a successive SCD scheme is termed S-SCD [WL10, Len16]. For example, assuming that the AR link has a higher SNR compared to the BR link without loss of generality, $\hat{\mathbf{c}}_\mathrm{A}$ is firstly decoded using the LLR vector $\mathbf{L}_\mathrm{A}$. Subsequently, the signal contribution from $\mathbf{x}_\mathrm{A}$ is subtracted from $\mathbf{y}_\mathrm{R}$, after which $\hat{\mathbf{c}}_\mathrm{B}$ is estimated in a single-user (SU) scenario.

Mutual Information

In order to investigate the performance upper-bound of the SCD scheme, a MI based analysis is applied. To this end, the MI $I_{\mathrm{S,A}}$ between the individual bit wise signal c_A and the receive signal y_R for separated decoding of the source message from A is determined as [Pfl11]

$$\begin{aligned} I_{\mathrm{S,A}} &= I\left(c_\mathrm{A}; y_\mathrm{R}\right) \\ &= \sum_{c_\mathrm{A}=\xi} \int_{-\infty}^{\infty} \Pr\left\{c_\mathrm{A}=\xi, y_\mathrm{R}\right\} \log_2 \frac{\Pr\left\{c_\mathrm{A}=\xi, y_\mathrm{R}\right\}}{\Pr\left\{c_\mathrm{A}=\xi\right\} \Pr\left\{y_\mathrm{R}\right\}} \mathrm{d}y_\mathrm{R} \\ &= \frac{1}{M^2} \sum_{c_\mathrm{A}=\xi} \int_{-\infty}^{\infty} \sum_{i \in \Omega_\mathrm{A}^\xi} p\left\{y_\mathrm{R} | c_\mathrm{AB} = \mathcal{C}_\mathrm{AB}(i)\right\} \\ &\quad \cdot \log_2 \frac{\sum_{i \in \Omega_\mathrm{A}^\xi} p\left\{y_\mathrm{R} | c_\mathrm{AB} = \mathcal{C}_\mathrm{AB}(i)\right\}}{\Pr\left\{c_\mathrm{A}=\xi\right\} \sum_{\forall i} p\left\{y_\mathrm{R} | c_\mathrm{AB} = \mathcal{C}_\mathrm{AB}(i)\right\}} \mathrm{d}y_\mathrm{R} \end{aligned} \tag{5.30}$$

with $\Pr\left\{c_\mathrm{A}=\xi\right\} = 1/2$ and the probability density of y_R defined in (5.20). Here, both indices ℓ and ν are omitted for ease of representation. For the above MI calculation, the signal from source B is treated as non-Gaussian interference with finite alphabet due to deterministic channel coefficients. It is noted that there is no closed-form solution for the integral in (5.30) and therefore this has to be solved numerically. Similarly, the MI $I_{\mathrm{S,B}}$ between c_B and y_R can be obtained.

Since the MI in (5.30) is a subcarrier wise definition relating to deterministic channel coefficients, its ergodic behavior in fading channels has to be averaged over sufficient channel realizations. On the other hand, it is assumed that each OFDM symbol is independently encoded. Therefore, the performance of P-SCD to estimate the network coded signal for one OFDM

symbol is constrained by [WWD13a]

$$I_{\mathrm{S}}^{\mathrm{P}} = \min\left\{ \frac{1}{L}\sum_{\ell} I_{\mathrm{S,A},\ell}, \frac{1}{L}\sum_{\ell} I_{\mathrm{S,B},\ell} \right\} . \tag{5.31}$$

Here, the minimum MI from parallely decoding the two individual source messages is dominant since both codewords $\mathbf{c}_{\mathrm{A}}$ and $\mathbf{c}_{\mathrm{B}}$ have to be estimated correctly in order to obtain an error-free network coded message. Contrarily, the performance upper-bound for S-SCD is given by the MI [WWD13a]

$$I_{\mathrm{S}}^{\mathrm{S}} = \min\left\{ \max\left\{ \frac{1}{L}\sum_{\ell} I_{\mathrm{S,A},\ell}, \frac{1}{L}\sum_{\ell} I_{\mathrm{S,B},\ell} \right\}, \frac{1}{L}\sum_{\ell} I_{\mathrm{SU},\ell} \right\} , \tag{5.32}$$

where I_{SU} denotes the subcarrier wise MI for the SU scenario with a lower SNR in the MA phase. Assuming again that the AR link is stronger, the MI between c_{A} and y_{R} taking the signal contribution from B as non-Gaussian interference with finite alphabet corresponds to decoding the source message from A correctly. Subsequently, I_{SU} representing the MI of the BR link regarding to the interference reduced signal relates to a successful successive decoding of the source message from B and can be calculated as

$$I_{\mathrm{SU}} = I\left(c_{\mathrm{B}}; y_{\mathrm{R}} | x_{\mathrm{A}} = 0\right) . \tag{5.33}$$

Similar to P-SCD, the minimum of these two terms is taken, leading to the MI with respect to the network coded message for S-SCD.

5.3.3 Joint Channel Decoding and Physical-Layer Network Coding

For two-way relaying communications with PLNC, the relay aims to generate a network coded message from the receive signal rather than the individual source messages. To this end, it is not necessary that relay R has to estimate $\mathbf{c}_{\mathrm{A}}$ and $\mathbf{c}_{\mathrm{B}}$ explicitly as performed by SCD presented in the previous subsection. Optionally, the relay codeword $\mathbf{c}_{\mathrm{R}} = \mathbf{c}_{\mathrm{A}\oplus\mathrm{B}}$ can be directly estimated from $\mathbf{y}_{\mathrm{R}}$ without the knowledge of the individual source messages $\mathbf{c}_{\mathrm{A}}$ and $\mathbf{c}_{\mathrm{B}}$. Since channel decoding and network coding is performed concurrently, this scheme is termed joint channel decoding and physical-layer network coding (JCNC) [ZH08, ZL09].

Recall that the same linear channel code is employed at both sources. Therefore, the modulo-2 sum $\mathbf{c}_{\mathrm{A}\oplus\mathrm{B}} = \mathbf{c}_{\mathrm{A}} \oplus \mathbf{c}_{\mathrm{B}}$ is also a valid codeword of this code. To this end, the APPs for each XORed code bit $c_{\mathrm{A}\oplus\mathrm{B}} = 0$ and

$c_{\mathrm{A}\oplus\mathrm{B}} = 1$ can be computed as

$$\Pr\{c_{\mathrm{A}\oplus\mathrm{B},\nu} = \xi | y_{\mathrm{R}}\} = \sum_{i \in \Psi_\nu^\xi} P_i \tag{5.34}$$

using the APPs P_i defined in (5.21). Here, Ψ_ν^ξ denotes the set containing all indices with the XORed code bit $c_{\mathrm{A}\oplus\mathrm{B},\nu} = c_{\mathrm{A},\nu} \oplus c_{\mathrm{B},\nu}$ equal to $\xi \in \{0, 1\}$. For the BPSK example, the set $\Psi_1^0 = \{0, 3\}$ indicates all events i with $c_{\mathrm{A}\oplus\mathrm{B},\nu} = 0$ as shown in Tab. 5.1. Correspondingly, the LLR for each XORed code bit is given by

$$L_{\mathrm{A}\oplus\mathrm{B},\nu} = \ln\left(\frac{\Pr\{c_{\mathrm{A}\oplus\mathrm{B},\nu} = 0 | y_{\mathrm{R}}\}}{\Pr\{c_{\mathrm{A}\oplus\mathrm{B},\nu} = 1 | y_{\mathrm{R}}\}}\right) , \tag{5.35}$$

which is sent to a binary channel decoder that produces the relay codeword $\mathbf{c}_{\mathrm{R}} = \hat{\mathbf{c}}_{\mathrm{A}\oplus\mathrm{B}}$ directly. In contrast to SCD with two decoding chains, the JCNC scheme requires channel decoding only once per MA channel, and therefore the computational complexity is reduced. The corresponding block diagram at relay R for JCNC is shown in Fig. 5.9.

Figure 5.9: Block diagram at relay R for JCNC. The relay codeword $\mathbf{c}_{\mathrm{R}} = \hat{\mathbf{c}}_{\mathrm{A}\oplus\mathrm{B}}$ is directly estimated by a binary channel decoder using $\mathbf{L}_{\mathrm{A}\oplus\mathrm{B}}$.

Graphical Illustration

The LLR calculation in (5.35) based on the set Ψ_ν^ξ is illustrated graphically in Fig. 5.10 for both BPSK and QPSK modulation according to the occurrence of the XORed code bit $c_{\mathrm{A}\oplus\mathrm{B},\nu}$ in Tab. 5.1 and Tab. 5.2, respectively. Specifically, the LLR $L_{\mathrm{A}\oplus\mathrm{B},1}$ is calculated using the event sets $\Psi_1^0 = \{0, 3\}$ and $\Psi_1^1 = \{1, 2\}$ for BPSK by

$$L_{\mathrm{A}\oplus\mathrm{B},1} = \ln\left(\frac{P_0 + P_3}{P_1 + P_2}\right) . \tag{5.36}$$

Note that the calculation above is only different from (5.26) and (5.27) for SCD in summation of the APPs. Similarly for QPSK, the sets $\Psi_1^0 = \{0, 2, 5, 7, 8, 10, 13, 15\}$ and $\Psi_1^1 = \{1, 3, 4, 6, 9, 11, 12, 14\}$ are used to calculate the LLR of the first bit in the code bit tuple as

$$L_{\mathrm{A}\oplus\mathrm{B},1} = \ln\left(\frac{P_0 + P_2 + P_5 + P_7 + P_8 + P_{10} + P_{13} + P_{15}}{P_1 + P_3 + P_4 + P_6 + P_9 + P_{11} + P_{12} + P_{14}}\right) . \tag{5.37}$$

It is noted that for the channel realization used in Fig. 5.4(b), JCNC leads to relatively smaller LLRs for $c_{\mathrm{A}\oplus\mathrm{B}}$ compared to SCD since the sets Ψ_1^0 and Ψ_1^1 are not well spatially separated. This will be elaborated in the sequel by considering the density distribution of the LLRs.

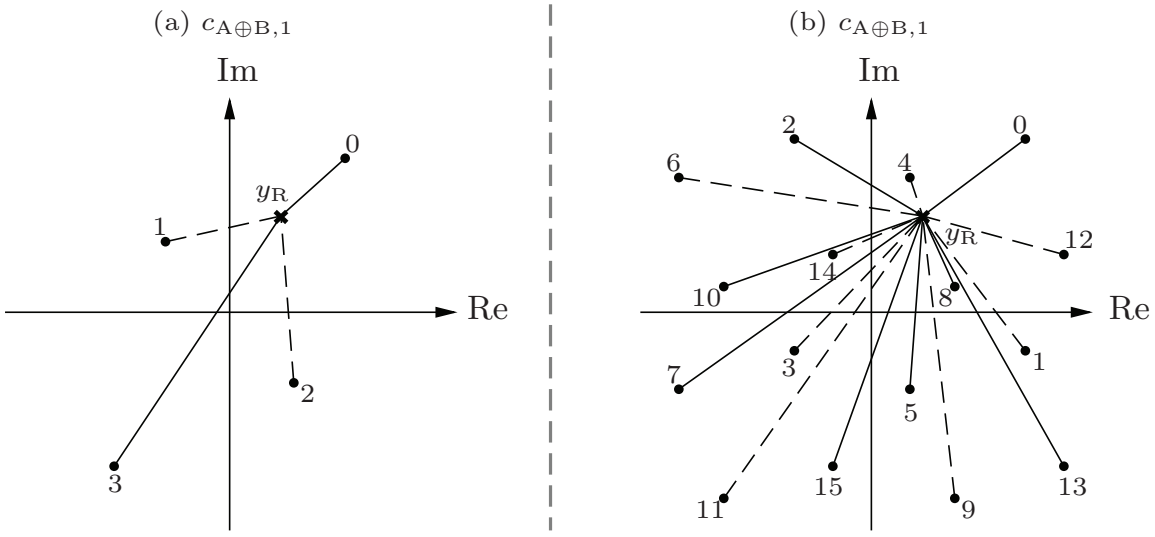

Figure 5.10: Graphical illustration of the LLR calculation for JCNC. The receive signal y_{R} is marked by 'x'. Solid lines and dashed lines correspond to entries s_{AB} with first bit in the XORed code bit tuple $c_{\mathrm{A}\oplus\mathrm{B},1}$ equal to 0 and 1, respectively. (a) for BPSK with $i = 0, 1, \cdots, 3$ and (b) for QPSK with $i = 0, 1, \cdots, 15$.

Mutual Information

The performance upper-bound of the JCNC scheme is determined by the MI between the XORed signal $c_{\mathrm{A}\oplus\mathrm{B}}$ and the receive signal y_{R} given by [Pfl11]

$$\begin{aligned} I_{\mathrm{J}} &= I\left(c_{\mathrm{A}\oplus\mathrm{B}}; y_{\mathrm{R}}\right) \\ &= \sum_{c_{\mathrm{A}\oplus\mathrm{B}}=\xi} \int_{-\infty}^{\infty} \Pr\left\{c_{\mathrm{A}\oplus\mathrm{B}} = \xi, y_{\mathrm{R}}\right\} \log_2 \frac{\Pr\left\{c_{\mathrm{A}\oplus\mathrm{B}} = \xi, y_{\mathrm{R}}\right\}}{\Pr\left\{c_{\mathrm{A}\oplus\mathrm{B}} = \xi\right\} \Pr\left\{y_{\mathrm{R}}\right\}} \mathrm{d}y_{\mathrm{R}} \\ &= \frac{1}{M^2} \sum_{c_{\mathrm{A}\oplus\mathrm{B}}=\xi} \int_{-\infty}^{\infty} \sum_{i\in\Psi^{\xi}} p\left\{y_{\mathrm{R}} | c_{\mathrm{AB}} = \mathcal{C}_{\mathrm{AB}}(i)\right\} \\ &\quad \cdot \log_2 \frac{\sum_{i\in\Psi^{\xi}} p\left\{y_{\mathrm{R}} | c_{\mathrm{AB}} = \mathcal{C}_{\mathrm{AB}}(i)\right\}}{\Pr\left\{c_{\mathrm{A}\oplus\mathrm{B}} = \xi\right\} \sum_{\forall i} p\left\{y_{\mathrm{R}} | c_{\mathrm{AB}} = \mathcal{C}_{\mathrm{AB}}(i)\right\}} \mathrm{d}y_{\mathrm{R}} \end{aligned} \tag{5.38}$$

with $\Pr\left\{c_{\mathrm{A}\oplus\mathrm{B}} = \xi\right\} = 1/2$. It is emphasized that (5.38) can be interpreted as the MI of transmitting the network coded signal $c_{\mathrm{A}\oplus\mathrm{B}}$ to the relay via

a virtual channel. For example, this implies that $c_{\mathrm{A}\oplus\mathrm{B}} = 0$ is mapped to the noise-free receive signal $s_{\mathrm{AB}} = \pm(h_{\mathrm{AR}} + h_{\mathrm{BR}})$ and $c_{\mathrm{A}\oplus\mathrm{B}} = 1$ is mapped to $s_{\mathrm{AB}} = \pm(h_{\mathrm{AR}} - h_{\mathrm{BR}})$ for BPSK. Consequently, the MI regarding each OFDM transmission involving one codeword is obtained by averaging the subcarrier wise $I_{\mathrm{J},\ell}$ in (5.38) over all subcarriers as $\frac{1}{L}\sum_{\ell} I_{\mathrm{J},\ell}$.

LLR Distribution

The LLRs defined in (5.25) and (5.35) using the APPs are delivered to the channel decoding module for SCD and JCNC, respectively. Since the LLRs with larger amplitude offer higher reliability and thus benefit more from channel decoding, the LLR distribution of the individual code bit c_{A} for P-SCD and the XORed code bit $c_{\mathrm{A}\oplus\mathrm{B}}$ for JCNC are investigated. In this context, the cumulative distribution function (CDF) of the LLR amplitude |LLR| at the relay is shown in Fig. 5.11 for different channel conditions with SNR = 5 dB. Furthermore, QPSK modulation is adopted at both sources A and B as an example.

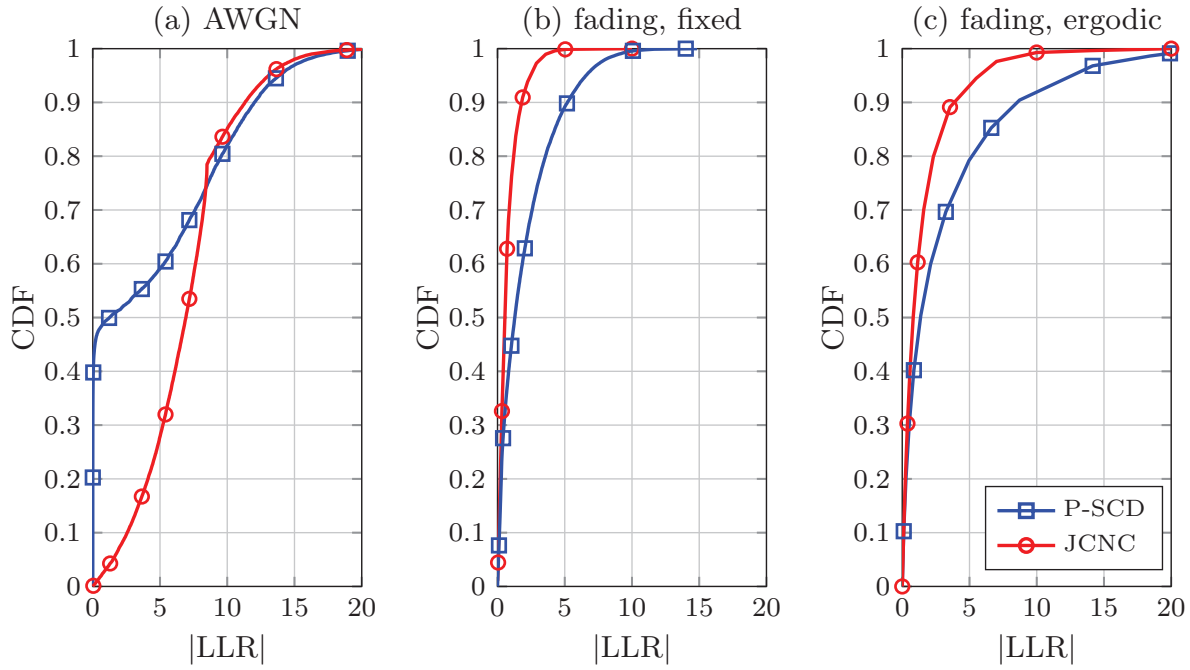

Figure 5.11: CDF of LLR amplitudes before channel decoding for P-SCD and JCNC in (a) AWGN channels, (b) multi-path fading channels on the ℓth subcarrier with fixed channel realization $h_{\mathrm{AR},\ell} = j$ and $h_{\mathrm{BR},\ell} = -0.2 + 0.5j$, and (c) multi-path fading channels averaged over the subcarriers and different channel realizations, SNR = 5 dB and QPSK modulation.

Firstly, AWGN channels are considered with the constellation set of the noise-free receive signal $\mathcal{S}_{\mathrm{AB}}$ shown in Fig. 5.5(b). In this case, it can be observed in Fig. 5.11(a), that approximately half of the LLRs for P-SCD approach 0. This is due to the fact that some constellation points in $\mathcal{S}_{\mathrm{AB}}$ are completely superimposed in case of no channel noise and therefore cannot be distinguished by SCD at all due to this ambiguity. These superimposed points have been visualized in Fig. 5.5(b). For example, the events $i = 3, 6, 9, 12$ all result in $s_{\mathrm{AB}} = 0$, which degrades the performance of SCD significantly. However, these hypotheses correspond to the same XORed code bit tuple $c_{\mathrm{A}\oplus\mathrm{B}} = [1\ 1]$, all of which belong to the sets Ψ_1^1 and Ψ_2^1. Therefore, JCNC is immune to this ambiguity and produces LLRs with larger amplitude compared to SCD, as shown in Fig. 5.11(a).

Considering multi-path fading channels employing OFDM, the LLR distribution concerning one subcarrier is investigated with the fixed channel realization used in Fig. 5.4(b). In this case, the channel coefficients lead to distributed noise-free constellation points s_{AB} at the relay. SCD benefits from this spatial separation and thus larger LLRs are produced compared to JCNC, which can be observed in Fig. 5.11(b). The CDF distribution of the LLRs over all subcarriers and different channel realizations is shown in Fig. 5.11(c). In this scenario, SCD still achieves larger LLR amplitudes compared to JCNC since channel coding is more beneficial with different constellation maps over the subcarriers.

5.3.4 Generalized Joint Channel Decoding and Physical-Layer Network Coding

The separated decoding of both source codewords $\mathbf{c}_{\mathrm{A}}$ and $\mathbf{c}_{\mathrm{B}}$ by SCD and the joint decoding of the XORed codeword $\mathbf{c}_{\mathrm{A}\oplus\mathrm{B}}$ from the receive signal $\mathbf{y}_{\mathrm{R}}$ operate in the binary bit-level. Alternatively, the decoding process at relay R can be performed in the non-binary field $\mathbb{F}_{M^2}$. To this end, the M^2-ary code bit combination $\mathbf{c}_{\mathrm{AB}}$ is estimated from $\mathbf{y}_{\mathrm{R}}$. Subsequently, the estimate $\hat{\mathbf{c}}_{\mathrm{AB}}$ is mapped to the relay codeword $\mathbf{c}_{\mathrm{R}}$ by PLNC. Compared to SCD and JCNC, this scheme takes into account the channel codes from both sources and thus is able to fully exploit the available information contained in the superimposed receive signal at the relay, which is termed generalized joint channel decoding and physical-layer network coding (G-JCNC) [WL10, Wüb10]. The corresponding block diagram for G-JCNC is shown in Fig. 5.12, which shows that $\mathbf{c}_{\mathrm{AB}}$ is directly estimated by the decoder. Note that since the decoding is performed in the non-binary field $\mathbb{F}_{M^2}$ instead of in the binary field for SCD and JCNC, higher decoding complexity is expected for G-JCNC.

Figure 5.12: Block diagram at relay R for G-JCNC. After a non-binary channel decoding over $\mathbb{F}_{M^2}$, the estimate $\hat{\mathbf{c}}_\mathrm{AB}$ is mapped to the corresponding network coded message $\mathbf{c}_\mathrm{R}$ for PLNC.

In the sequel, the validity of the G-JCNC scheme with the joint decoding operated in the non-binary field is examined, which requires to observe the code structure of $\mathbf{c}_\mathrm{AB}$ applied in the MA phase. Note that for G-JCNC, the encoding process is assumed to be slightly different in contrast to that defined in Subsection 5.2.3, as is visualized in Fig. 5.13. Here, instead of modulating m successive code bits as previously assumed for SCD and JCNC, m identical encoders are applied to the information bit streams $\mathbf{b}_{\mathrm{A},1}, \mathbf{b}_{\mathrm{A},2}, \cdots, \mathbf{b}_{\mathrm{A},m}$ for G-JCNC, where $\mathbf{b}_\mathrm{A}$ is essentially divided into sub-sequences $\mathbf{b}_{\mathrm{A},\nu}$ with $\nu = 1, 2, \cdots, m$. Correspondingly, the encoding process at source A yields $\mathbf{c}_{\mathrm{A},\nu} = [c_{\mathrm{A},\nu,1}\ c_{\mathrm{A},\nu,2}\ \cdots\ c_{\mathrm{A},\nu,L}] = \Gamma(\mathbf{b}_{\mathrm{A},\nu})$. As a result, the code bits $c_{\mathrm{A},\nu,\ell}$ with $\nu = 1, 2, \cdots, m$ involved in one modulated symbol $x_{\mathrm{A},\ell}$ have identical connections in the code structure of the applied channel code Γ. Furthermore, the encoding process at source B is performed likewise.

For linear channel codes, each code bit basically consists of the modulo-2 sum of some information bits. For example, the code bit $c_{\mathrm{A},\nu,\ell}$ in the codeword $\mathbf{c}_\mathrm{A}$ is achieved by the sum of uth and wth information bits in $\mathbf{b}_\mathrm{A}$, i.e.,

$$c_{\mathrm{A},\nu,\ell} = b_{\mathrm{A},\nu,u} \oplus b_{\mathrm{A},\nu,w}\ . \tag{5.39}$$

Assuming both sources employ the same channel code, the ℓth element in the code bit polynomial can be written as

$$\begin{aligned}
c_{\mathrm{AB},\ell} &= [c_{\mathrm{A},1,\ell}\ c_{\mathrm{A},2,\ell}\ \cdots\ c_{\mathrm{A},m,\ell}\ c_{\mathrm{B},1,\ell}\ c_{\mathrm{B},2,\ell}\ \cdots\ c_{\mathrm{B},m,\ell}] \\
&= [b_{\mathrm{A},1,u} \oplus b_{\mathrm{A},1,w}\ b_{\mathrm{A},2,u} \oplus b_{\mathrm{A},2,w}\ \cdots\ b_{\mathrm{A},m,u} \oplus b_{\mathrm{A},m,w} \\
&\quad\ b_{\mathrm{B},1,u} \oplus b_{\mathrm{B},1,w}\ b_{\mathrm{B},2,u} \oplus b_{\mathrm{B},2,w}\ \cdots\ b_{\mathrm{B},m,u} \oplus b_{\mathrm{B},m,w}] \\
&= (b_{\mathrm{A},1,u} + b_{\mathrm{A},2,u}D + \cdots + b_{\mathrm{A},m,u}D^{m-1} \\
&\quad + b_{\mathrm{B},1,u}D^m + b_{\mathrm{B},2,u}D^{m+1} + \cdots + b_{\mathrm{B},m,u}D^{2m-1}) \\
&\quad \oplus (b_{\mathrm{A},1,w} + b_{\mathrm{A},2,w}D + \cdots + b_{\mathrm{A},m,w}D^{m-1} \\
&\quad + b_{\mathrm{B},1,w}D^m + b_{\mathrm{B},2,w}D^{m+1} + \cdots + b_{\mathrm{B},m,w}D^{2m-1}) \\
&= b_{\mathrm{AB},u} \oplus b_{\mathrm{AB},w}\ ,
\end{aligned} \tag{5.40}$$

which indicates that the code bit polynomial $c_{\mathrm{AB},\ell}$ can be interpreted as the modulo-2 sum in $\mathbb{F}_{M^2}$ of the information bit polynomials $b_{\mathrm{AB},u}$ and $b_{\mathrm{AB},w}$

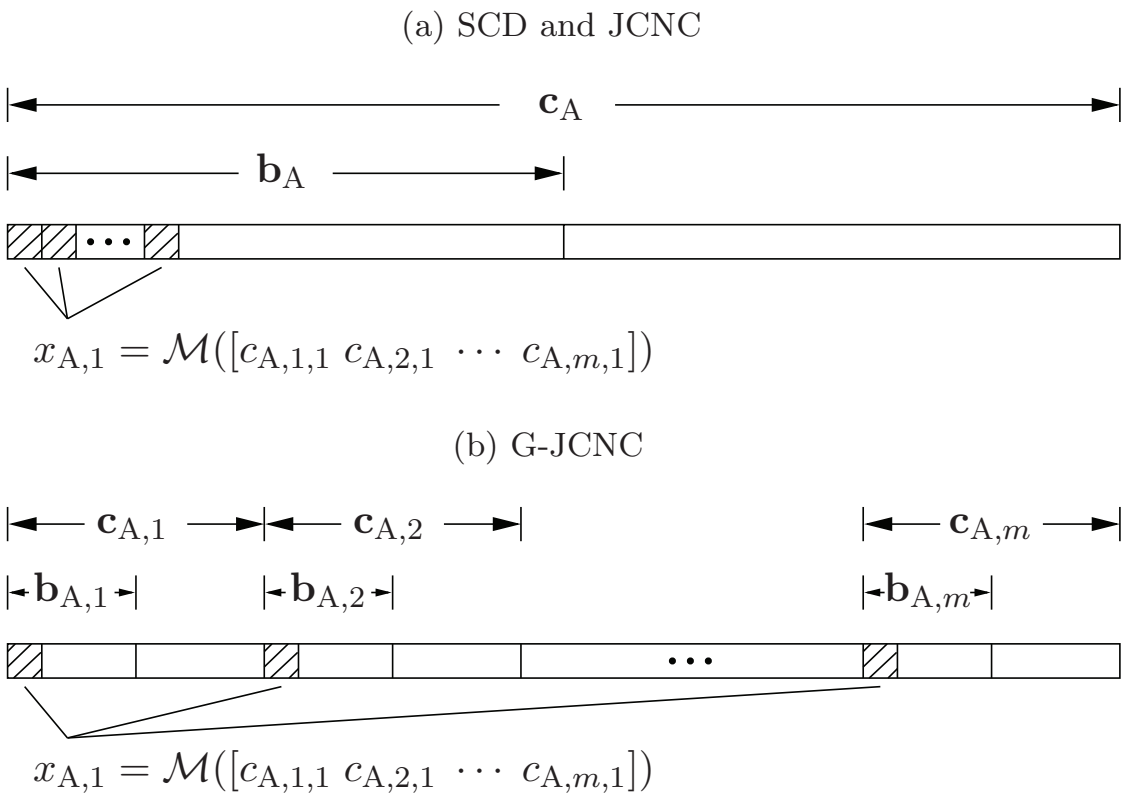

Figure 5.13: Coding structure at source A as an example for SCD and JCNC in (a) and for G-JCNC in (b).

defined as

$$b_{\mathrm{AB},u} = [b_{\mathrm{A},1,u}\ b_{\mathrm{A},2,u}\ \cdots\ b_{\mathrm{A},m,u}\ b_{\mathrm{B},1,u}\ b_{\mathrm{B},2,u}\ \cdots\ b_{\mathrm{B},m,u}] \tag{5.41a}$$

$$b_{\mathrm{AB},w} = [b_{\mathrm{A},1,w}\ b_{\mathrm{A},2,w}\ \cdots\ b_{\mathrm{A},m,w}\ b_{\mathrm{B},1,w}\ b_{\mathrm{B},2,w}\ \cdots\ b_{\mathrm{B},m,w}]\ . \tag{5.41b}$$

Similarly, a code bit equal to the modulo-2 sum of more than 2 information bits can be calculated by nesting the above operation, which still belongs to $\mathbb{F}_{M^2}$. Correspondingly, non-binary decoding is performed at the relay with respect to the combined codeword $\mathbf{c}_\mathrm{AB}$.

For G-JCNC, LDPC codes are considered in this thesis [WL10, Wüb10]. Similar works are found in [ZL09] for repeat accumulate codes and in [TC10a, TC10b] for convolutional codes. To decode the LDPC code, a modified sum-product algorithm (SPA) at the relay is employed based on the investigations in [KFL01, DM98]. Specifically, instead of the LLRs, the APPs are directly fed to the non-binary channel decoder in $\mathbb{F}_{M^2}$ and updated iteratively within the modified SPA. To this end, the APP vector $\mathbf{p} = [P_0\ P_1\ \cdots\ P_{M^2-1}]$ with $P_i = \Pr\{c_\mathrm{AB} = \mathcal{C}_\mathrm{AB}(i)|y_\mathrm{R}\}$ defined in (5.21) is generated from the decoding process. Consequently, the updated APPs $\mathbf{p}$ are mapped to the binary code bit $c_{\mathrm{R},\ell}$ in the relay codeword by PLNC. As

an example, the mapping rules are given by

$$c_{\mathrm{R},\ell} = \hat{c}_{\mathrm{A}\oplus\mathrm{B},\ell} = \begin{cases} 0 & \text{if } \arg\max\limits_{i} P_i = \{0,3\} \\ 1 & \text{if } \arg\max\limits_{i} P_i = \{1,2\} \end{cases} \tag{5.42}$$

and

$$c_{\mathrm{R},\ell} = \hat{c}_{\mathrm{A}\oplus\mathrm{B},\ell} = \begin{cases} 00 & \text{if } \arg\max\limits_{i} P_i = \{0,5,10,15\} \\ 10 & \text{if } \arg\max\limits_{i} P_i = \{1,4,11,14\} \\ 01 & \text{if } \arg\max\limits_{i} P_i = \{2,7,8,13\} \\ 11 & \text{if } \arg\max\limits_{i} P_i = \{3,6,9,12\} \end{cases} \tag{5.43}$$

for BPSK and QPSK, which are in accordance with the definitions in Tab. 5.1 and Tab. 5.2, respectively. For instance, if P_0 is the largest among the 4 updated APPs from the non-binary decoder in G-JCNC, the corresponding XORed code bit is decided to be 0 in case of BPSK.

Mutual Information

For performance evaluation of the G-JCNC scheme, the MI between s_{AB} relating to the transmit signal tuple $(x_{\mathrm{A}}, x_{\mathrm{B}})$ by (5.17) and the receive signal y_{R} at the relay is calculated as [Pfl11]

$$\begin{aligned} I'_{\mathrm{G}} &= I\left(s_{\mathrm{AB}}; y_{\mathrm{R}}\right) = I\left(c_{\mathrm{AB}}; y_{\mathrm{R}}\right) \\ &= \sum_{\forall i} \int_{-\infty}^{\infty} \Pr\left\{c_{\mathrm{AB}} = \mathcal{C}_{\mathrm{AB}}(i), y_{\mathrm{R}}\right\} \\ &\quad \cdot \log_2 \frac{\Pr\left\{c_{\mathrm{AB}} = \mathcal{C}_{\mathrm{AB}}(i), y_{\mathrm{R}}\right\}}{\Pr\left\{c_{\mathrm{AB}} = \mathcal{C}_{\mathrm{AB}}(i)\right\} \Pr\left\{y_{\mathrm{R}}\right\}} \mathrm{d}y_{\mathrm{R}} \\ &= \frac{1}{M^2} \sum_{\forall i} \int_{-\infty}^{\infty} p\left\{y_{\mathrm{R}} | c_{\mathrm{AB}} = \mathcal{C}_{\mathrm{AB}}(i)\right\} \\ &\quad \cdot \log_2 \frac{M^2 p\left\{y_{\mathrm{R}} | c_{\mathrm{AB}} = \mathcal{C}_{\mathrm{AB}}(i)\right\}}{\sum_{\forall i} p\left\{y_{\mathrm{R}} | c_{\mathrm{AB}} = \mathcal{C}_{\mathrm{AB}}(i)\right\}} \mathrm{d}y_{\mathrm{R}} \,. \end{aligned} \tag{5.44}$$

It is noted that I'_{G} essentially corresponds to the sum-rate in the MA phase. In order to achieve a fair comparison with the SCD and JCNC schemes, the code rate at the sources has to be smaller than $I_{\mathrm{G}} = I'_{\mathrm{G}}/2$ to recover the individual source messages correctly at the relay assuming a symmetric MA channel, i.e., when the relay is located in the middle of both sources. Furthermore, I_{G} has to be averaged over all subcarriers in one OFDM symbol as $\frac{1}{L}\sum_{\ell} I_{\mathrm{G},\ell}$ for practical concerns.

5.3.5 Performance Evaluation

In this subsection, the performance of the above mentioned APP-based PLNC detection and decoding schemes is presented and compared with respect to MI and FER at the relay, both of which are supposed to be for the relay message. A symmetric network topology is employed with both sources and the relay on a line. The distances of both the AR link and the BR link are set to $d_{\mathrm{AR}} = d_{\mathrm{BR}} = 1$. In general, multi-path fading channels are assumed with $N_{\mathrm{H}} = 5$ equal power taps. AWGN channels are also considered in the MI analysis for comparison.

Mutual Information

The MI regarding to P-SCD, S-SCD, JCNC and G-JCNC are compared for BPSK and QPSK, as shown in Fig. 5.14 and Fig. 5.15, respectively. The four-phase and three-phase schemes are also presented as references [FBW06]. Therein, each phase of both schemes is essentially an end-to-end transmission and thus the corresponding MI can be computed by using I_{SU} in (5.33) for the single-user scenario. Specifically, due to higher number of required time slots, the normalized MI per bit amounts to $\frac{1}{2}I_{\mathrm{SU}}$ for the four-phase scheme and $\frac{2}{3}I_{\mathrm{SU}}$ for the three-phase scheme. This is because 2 OFDM symbols are exchanged using 4 time slots in the former case whereas this is accomplished using 3 time slots in the latter case.

Focusing on the two-phase scheme, it can be observed that SCD achieves only half of the maximum MI due to the ambiguity of some transmit signal tuples in AWGN channels. For example, considering BPSK at both sources, $(x_{\mathrm{A}}, x_{\mathrm{B}}) = (+1, -1)$ and $(x_{\mathrm{A}}, x_{\mathrm{B}}) = (-1, +1)$ lead to the same noise-free receive signal $y_{\mathrm{R}} = 0$ at the relay and thus can not be distinguished by SCD at all. However, since these two signal tuples result in the same XOR-based network coded signal, the maximum MI can still be achieved by JCNC, which actually benefits from this signal ambiguity. Additionally, the MI for G-JCNC with BPSK saturates at $\frac{3}{4}$ since 4 transmit symbol tuples $(x_{\mathrm{A}}, x_{\mathrm{B}})$ lead to 3 noise-free constellation points s_{AB}. Similarly, the maximum achievable MI for G-JCNC with QPSK amounts to $\frac{3}{2}$ due to the fact that the real part and imaginary part of a QPSK signal are independent and thus equal to two parallel BPSK transmissions.

For multi-path fading channels, the ergodic MI is achieved by averaging over sufficient channel realizations. In this case, all APP-based schemes under investigation approach the maximum achievable MI for both BPSK and QPSK, although the schemes behave quite differently at low and medium SNRs. Note that unlike in AWGN channels, the channel gains for the AR link and the BR link are generally different for each channel realization in fading

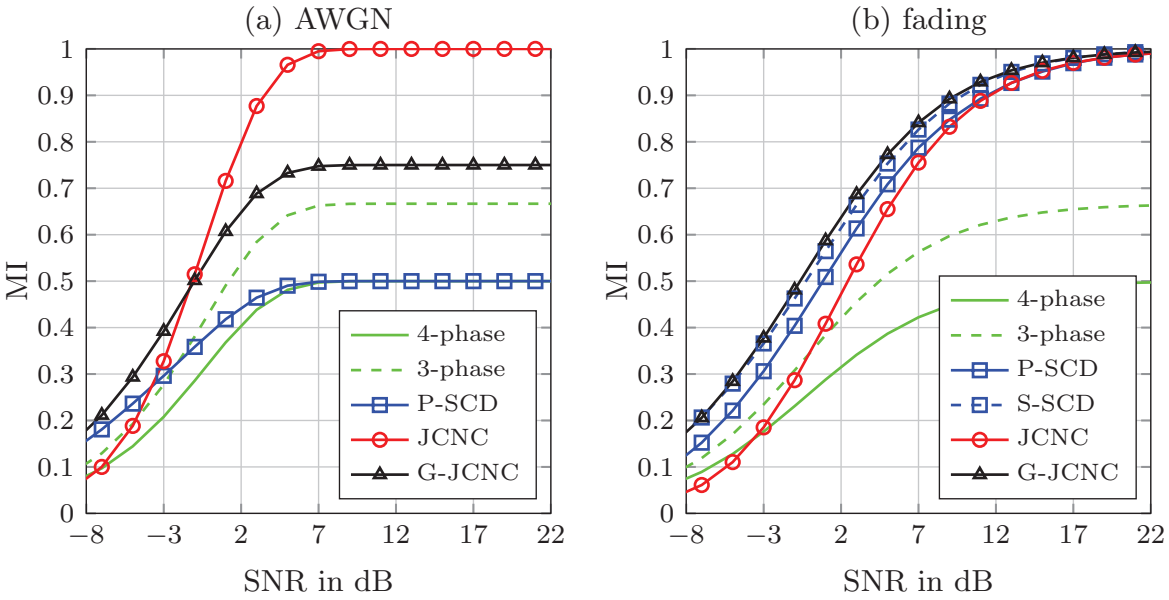

Figure 5.14: MI for SCD, JCNC and G-JCNC in the two-phase two-way relaying scheme. The four-phase and three-phase schemes are also present as references. BPSK is adopted for all scenarios, (a) for AWGN channels and (b) for multi-path fading channels using OFDM.

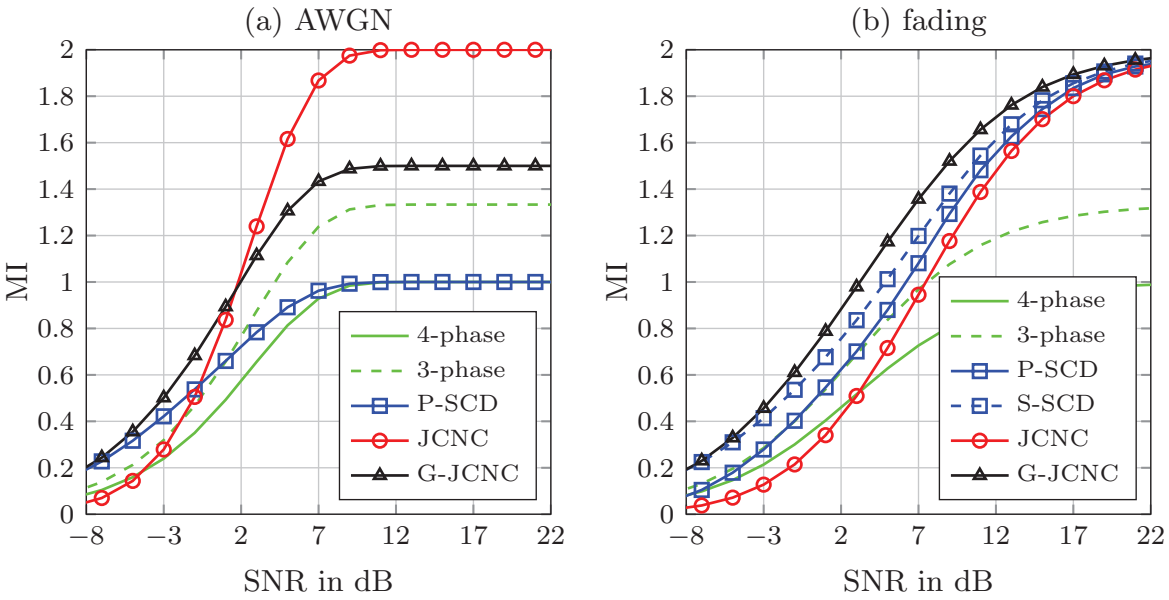

Figure 5.15: MI for SCD, JCNC and G-JCNC in the two-phase two-way relaying scheme. The four-phase and three-phase schemes are also present as references. QPSK is adopted for all scenarios, (a) for AWGN channels and (b) for multi-path fading channels using OFDM.

channels. Therefore, S-SCD is distinguished from P-SCD, which achieves superior performance. Furthermore, G-JCNC outperforms all other schemes over the whole SNR region. This is attributed to the fact that the randomness of the channel coefficients h_{AR} and h_{BR} helps to avoid the ambiguity of transmitting certain symbol tuples, e.g., $(x_{\mathrm{A}}, x_{\mathrm{B}}) = (+1, -1)$ and $(x_{\mathrm{A}}, x_{\mathrm{B}}) = (-1, +1)$ for BPSK. However, JCNC is not able to take this advantage due to more separated constellation points for LLR calculations, thus yielding smaller LLR amplitudes compared to SCD, as shown in Fig. 5.11.

Frame Error Rate

The FER performance of the relay codeword, denoted as $\mathrm{FER}_{\mathrm{R}}$, for the APP-based PLNC detection and decoding schemes is shown in Fig. 5.16. As different behaviors among the schemes are observed for MI at varying SNR ranges, the FER is also presented for different code rates with QPSK as an example. When an LDPC code of medium rate $R_{\mathrm{C}} = 0.5$ is applied, P-SCD outperforms JCNC by approximately 1 dB. This is due to the fact that P-SCD produces for the individual code bits LLRs with larger amplitude contrary to JCNC for the XORed code bits, which has been demonstrated by the LLR distribution in Fig. 5.11(c). Therefore, P-SCD is able to exploit the frequency selectivity from multi-path fading by channel coding more efficiently compared to JCNC. Additionally, S-SCD improves the performance by approximately 2 dB in contrast to P-SCD but is still 1 dB worse than G-JCNC. For a high code rate $R_{\mathrm{C}} = 0.875$, JCNC approaches P-SCD with only a slight performance degradation whereas the improvement by S-SCD compared to P-SCD is also decreased. Furthermore, G-JCNC achieves tremendous performance gain over all other schemes in both cases with different code rates. These observations are in accordance with those for MI presented in Fig. 5.15(b).

5.4 Phase Control Strategy

It has been shown in Subsection 5.3.5 that the MI saturates at half of the maximal achievable value for P-SCD in AWGN channels due to the ambiguity of transmitting certain symbol tuples $(x_{\mathrm{A}}, x_{\mathrm{B}})$. However, such ambiguity can be beneficial for JCNC since the superimposed constellation points lead to the same network coded message. These observations indicate that the APP-based PLNC detection and decoding schemes are sensitive to the channel conditions, e.g., the phase information [ULL17a]. In other words, each scheme favors different channel conditions, which can be adjusted by an optimal phase control strategy to be introduced in the sequel [WWD13a].

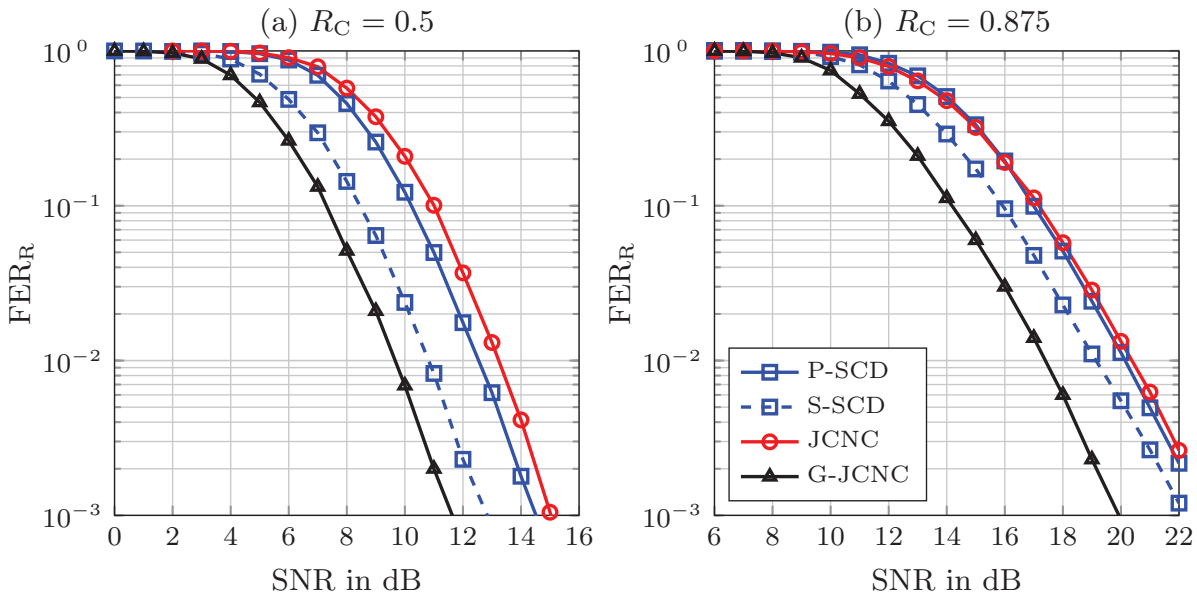

Figure 5.16: FER performance for the XORed codeword at the relay in multi-path fading channels with QPSK. The applied LDPC code has a medium rate $R_C = 0.5$ in (a) and a high rate $R_C = 0.875$ in (b).

5.4.1 Mutual Information with Optimal Phase Control

Motivated by [HCH+09] a phase difference can be generated, which re-orders the constellation points of the superimposed signal by pre-rotating the transmit signal at, e.g., source B with $e^{j\Delta\phi}$ before transmission. Taking AWGN channels as an example, the corresponding noise-free receive signal at relay R reads $x_A + e^{j\Delta\phi}x_B$. When multi-path fading channels are considered, the analysis is still focused on the ℓth subcarrier. In this case, source B requires the phase difference between h_{AR} and h_{BR} in order to generate a constant phase difference $\Delta\phi$. To this end, a phase pre-rotation with

$$\theta = \Delta\phi + \angle h_{AR} - \angle h_{BR} \tag{5.45}$$

is employed at source B, resulting in the receive signal at relay R as

$$y_R = h_{AR}x_A + h_{BR}e^{j\theta}x_B + n_R \, . \tag{5.46}$$

The term $h_{BR}e^{j\theta}$ can be interpreted as an equivalent channel coefficient for the BR link such that the MI calculation in (5.30), (5.38) and (5.44) can be easily adapted accordingly. Note that a 'blind' rotation of $\theta = \Delta\phi$ doesn't help since the phase information in fading channels is equally distributed. Therefore, the starting point is irrelevant and no potential performance improvement can be achieved. In Fig. 5.17, the dependency of MI on the

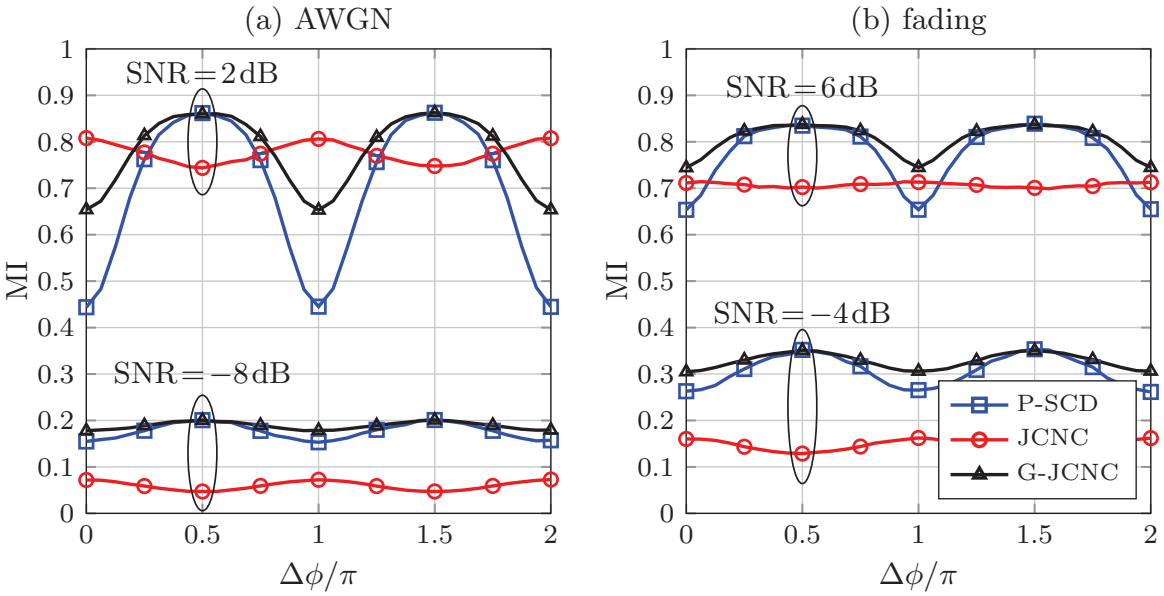

Figure 5.17: Impact of the phase difference $\Delta\phi$ on MI for P-SCD, JCNC and G-JCNC in both high SNR and low SNR regions with BPSK. (a) for AWGN channels and (b) for multi-path fading channels.

phase difference $\Delta\phi$ obtained by phase control in (5.46) for different APP-based schemes is presented with BPSK in AWGN channels and multi-path fading channels. It can be observed that the MI for P-SCD[1] and G-JCNC are highly related to $\Delta\phi$ and achieves the maximum with, e.g., $\Delta\phi = \frac{\pi}{2}$, which essentially generates a QPSK signal in the complex plane. On the other hand, the maximum MI for JCNC is obtained with, e.g., $\Delta\phi = 0$. As illustrated before, this is because JCNC benefits from the ambiguity at $s_{\mathrm{AB}} = 0$ in AWGN channels. In contrast, since the constellation points are naturally separated in space in fading channels, JCNC is less sensitive to $\Delta\phi$ with the maximum MI still achieved at $\Delta\phi = 0$.

The performance presented above is evaluated for QPSK and shown in Fig. 5.18. In this case, the optimal phase rotation for P-SCD and G-JCNC is $\Delta\phi = \frac{\pi}{4}$ in AWGN channels and $\Delta\phi = \frac{\pi}{8}$ in fading channels, as these angles lead to the most spatially distributed constellation points. However, less improvement can be achieved compared to BPSK. This is due to the fact that a phase rotation $\Delta\phi = \frac{\pi}{2}$ for BPSK makes full use of the other dimension in the complex plane, whereas the phase rotation for QPSK only tries to distribute the two dimensional superimposed constellation set as much as possible. Furthermore, the MI for JCNC is improved tremendously

[1]The optimal phase shown in Tab. 5.3 is equivalent for both P-SCD and S-SCD since decoding for the stronger link in P-SCD dominates the performance of S-SCD.

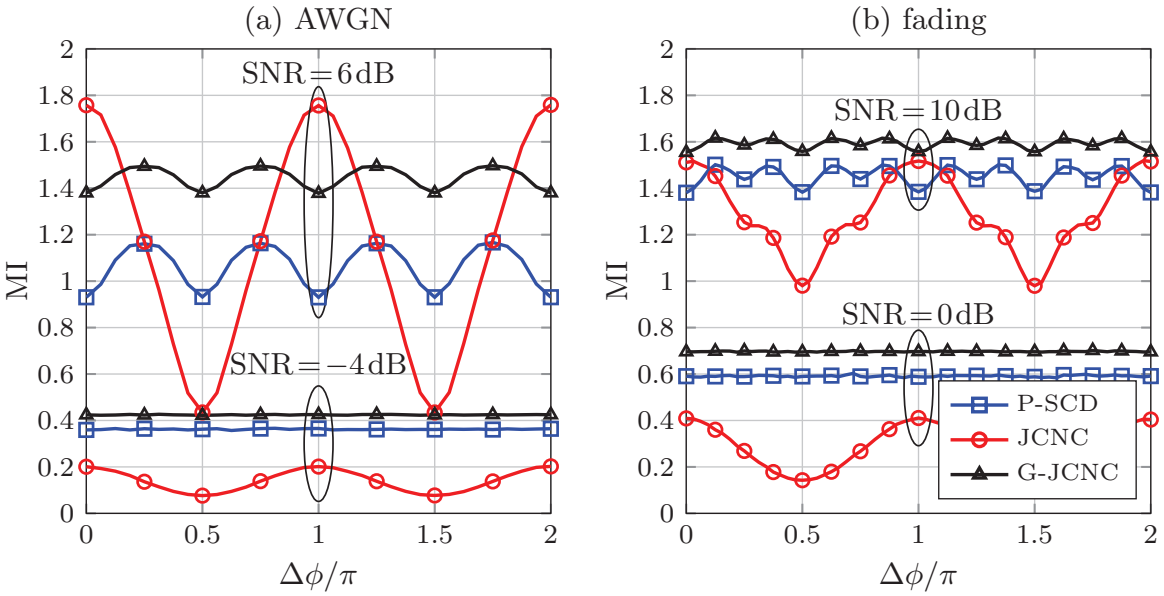

Figure 5.18: Impact of the phase difference $\Delta\phi$ on MI for P-SCD, JCNC and G-JCNC in both high SNR and low SNR regions with QPSK. (a) for AWGN channels and (b) for multi-path fading channels.

by phase control that achieves $\Delta\phi = 0$, especially in the high SNR region. This corresponds to the observations in [KAPT09b], which shows that some incoherent channel conditions can be catastrophic when directly mapping the receive signal to the XOR-based network coded message with QPSK, whereas the impact on BPSK is less dramatic.

modulation	channel	P-SCD	JCNC	G-JCNC
BPSK	AWGN	$\frac{\pi}{2}$	0	$\frac{\pi}{2}$
	fading	$\frac{\pi}{2}$	0	$\frac{\pi}{2}$
QPSK	AWGN	$\frac{\pi}{4}$	0	$\frac{\pi}{4}$
	fading	$\frac{\pi}{8}$	0	$\frac{\pi}{8}$

Table 5.3: Exemplary optimal phase $\Delta\phi$ leading to the maximum MI for P-SCD, JCNC and G-JCNC. Both AWGN channels and fading channels are considered with BPSK and QPSK, respectively.

Finally, the optimal phase $\Delta\phi$ that achieves the maximum MI for different APP-based schemes in both AWGN channels and fading channels with BPSK and QPSK is summarized in Tab. 5.3 for direct comparison.

5.4.2 Linear Approximation of Channel Phase

In order to perform the phase control strategy depicted in (5.46), the instantaneous CSI, i.e., the phase information of the channel coefficients h_{AR} and h_{BR} estimated at the relay has to be fed back to the sources before data transmission. Practically, this results in extra overhead. In this context, a phase approximation strategy is applied that reduces the overhead significantly while the corresponding performance degradation is tolerable.

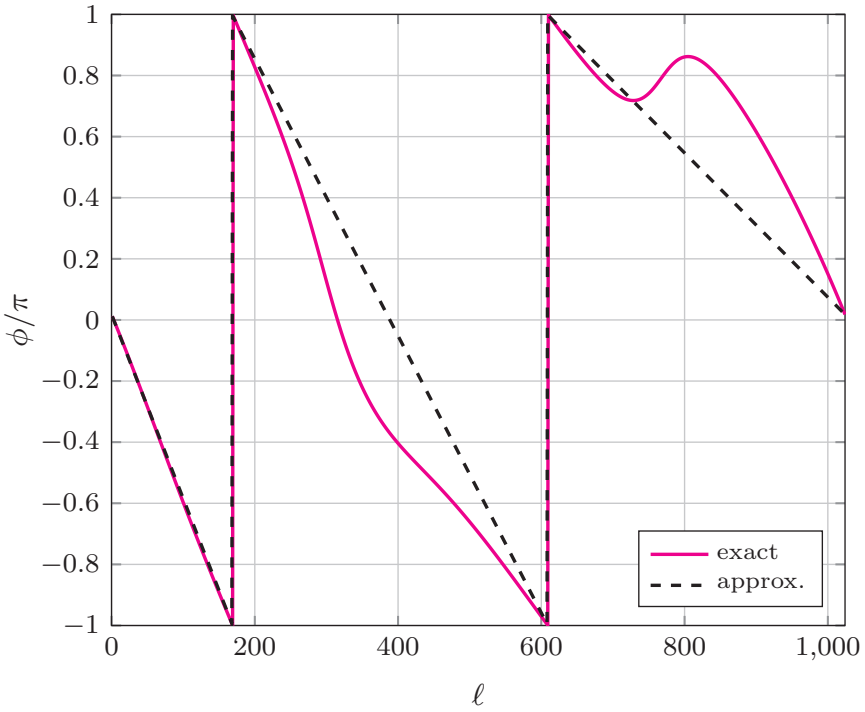

Figure 5.19: Exact and approximate phase information $\phi(\ell)$ of the channel response with $N_{\mathrm{H}} = 5$ channel taps and $L = 1024$ subcarriers. Linear approximation is employed based on the boundary value $\phi(1) = \phi(L)$ and the positions of the extreme values $\pm\pi$.

In Fig. (5.19) a phase example is shown with $N_{\mathrm{H}} = 5$ channel taps and $L = 1024$ subcarriers. Here, $\phi(\ell)$ represents the angle of the channel coefficient on the ℓth subcarrier in OFDM systems. Since ϕ fluctuates continuously, the phase information over all subcarriers can be linearly approximated using only the boundary value $\phi(1) = \phi(L)$ and the positions of the extreme values $\phi(\ell) = \pm\pi$. The approximated phase is also presented in Fig. (5.19).

Based on such a linear phase approximation strategy, the relay only needs to feed the boundary value and the indices of the extreme values per channel realization back to the sources to perform phase control. To observe the performance loss caused by the approximated phase information, the MI

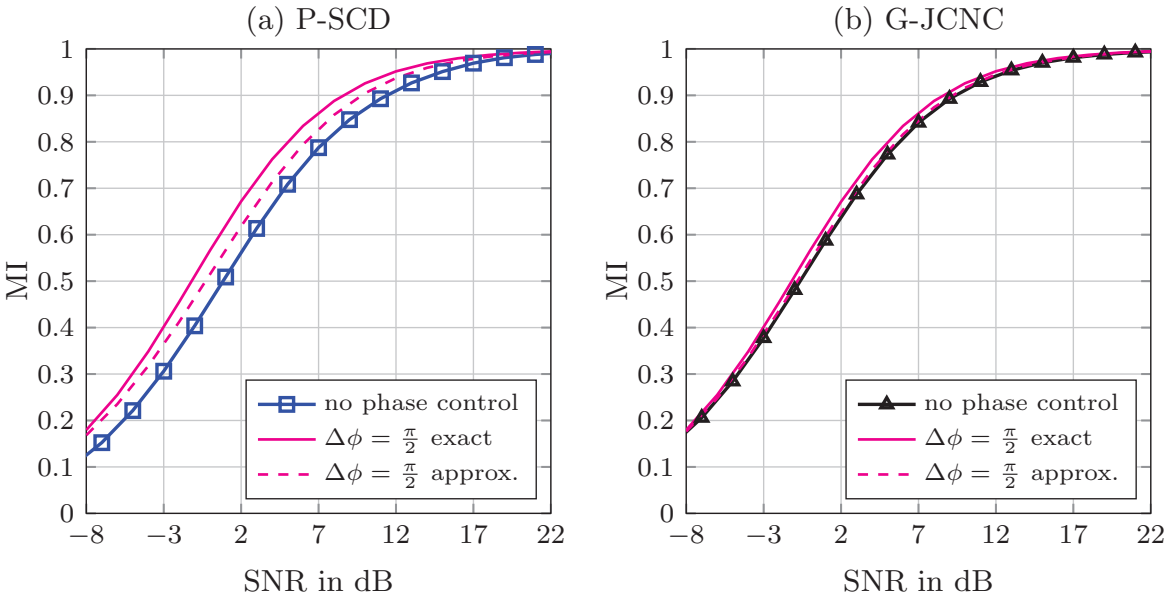

Figure 5.20: MI over multi-path fading channels with $N_{\mathrm{H}} = 5$ taps using BPSK and the optimal phase difference $\Delta\phi = \frac{\pi}{2}$ for P-SCD in (a) and G-JCNC in (b). The MI with both exact and approximate phase information is compared to the case without phase control.

for P-SCD and G-JCNC with one best phase difference $\Delta\phi = \frac{\pi}{2}$ is shown in Fig. 5.20 for multi-path fading channels with BPSK. In this case, the approximated phase leads to only 1 dB loss for P-SCD and 0.5 dB loss for G-JCNC at MI equal to 0.5, indicating that G-JCNC is more robust against P-SCD with imprecise phase information. However, the feedback overhead is reduced to a large extent compared to feeding the exact phase information back to the sources. Additionally, in contrast to the case without phase control, the phase pre-rotation still leads to performance improvement even when the approximated phase is used, especially for P-SCD. This confirms the practicability of the proposed phase control strategy.

Throughput with Capacity-Approaching Codes

In order to verify the accessibility of the MI improved by the proposed phase control strategy for the APP-based schemes, the capacity-approaching LDPC codes applied in the DVB-S2 standard [DVB09] are adopted at both sources over a wide range of code rates, namely, $R_{\mathrm{C}} = \{\frac{1}{4}, \frac{1}{3}, \frac{1}{2}, \frac{3}{5}, \frac{2}{3}, \frac{3}{4}, \frac{4}{5}, \frac{5}{6}, \frac{8}{9}, \frac{9}{10}\}$. The short frame structure is employed with a codeword length of $N_c = 16200$. Preserving the parameter settings for OFDM transmissions, channel encoding is applied among multiple OFDM symbols with different channel realizations correspondingly to exploit the frequency selectivity more adequately.

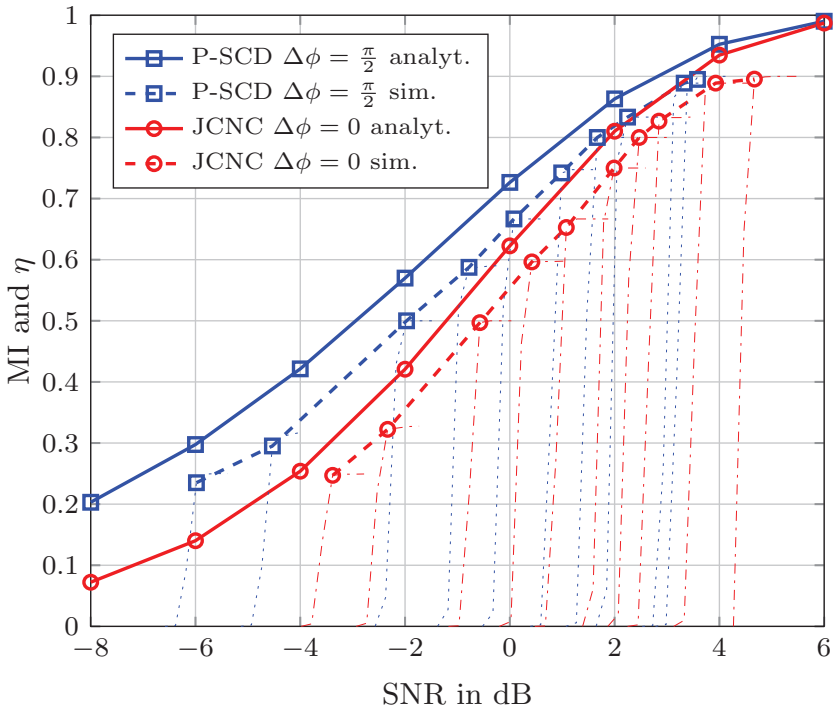

Figure 5.21: Throughput and MI for P-SCD (· · ·) and JCNC (- · -) with BPSK and optimal phase control in AWGN channels.

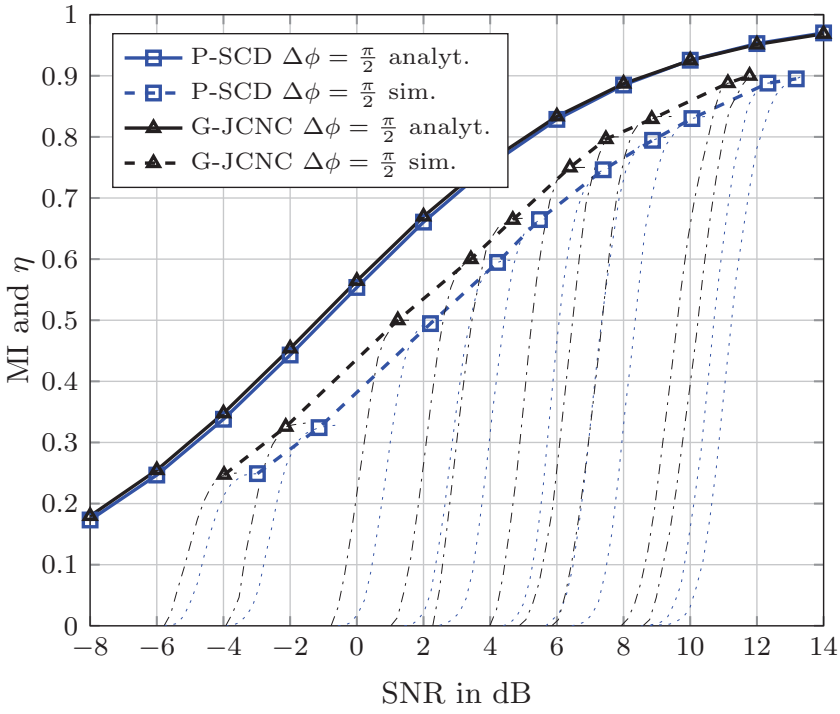

Figure 5.22: Throughput and MI for P-SCD (· · ·) and JCNC (- · -) with BPSK and phase control using approximate phase information in multi-path fading channels with $N_{\mathrm{H}} = 5$ taps.

In Fig. 5.21 the simulated throughput η with respect to the MA phase compared with the corresponding analytical MI for P-SCD and JCNC is presented in AWGN channels with BPSK ($m = 1$). The optimal phase rotation is applied, i.e., $\Delta\phi = \frac{\pi}{2}$ for P-SCD and $\Delta\phi = 0$ for JCNC according to Tab. 5.3. Here, the normalized throughput η is defined as

$$\eta = m \cdot R_{\mathrm{C}} \cdot (1 - \mathrm{FER}_{\mathrm{R}}) \; . \tag{5.47}$$

As a numerical approach, the minimum required SNR threshold γ leading to $\mathrm{FER}_{\mathrm{R}} = 10^{-3}$ is achieved by simulations with various code rates. These points $(\gamma, 0.999R_{\mathrm{C}})$ are then connected by dashed lines (- -) to compare with the analytical MI. As can be observed in the figure, P-SCD outperforms JCNC with optimal phase control, which corresponds the characteristic shown in Fig. 5.17(a). Due to the application of capacity-approaching LDPC codes, the analytical MI is approached by the simulated throughput with approximately 1 dB loss.

Considering multi-path fading channels using OFDM, P-SCD and G-JCNC with optimal phase control $\Delta\phi = \frac{\pi}{2}$ corresponding to Tab. 5.3 for BPSK are compared in Fig. 5.22. For practical concerns, the linearly approximated phase information is used. As can be observed, the analytical MI for P-SCD and G-JCNC are almost identical with exact optimal phase control, which is in accordance with the observation from Fig. 5.17(a). Comparing the throughput obtained from simulations, G-JCNC outperforms P-SCD because G-JCNC is more robust against imprecise phase information, as concluded from Fig. 5.20. In addition, the performance loss of the simulated throughput to the analytical MI grows to approximately 3 dB for P-SCD and 2 dB for G-JCNC, respectively. Besides the impreciseness caused by linear estimation of the channel phase, this may be attributed to the lack of frequency selectivity provided by OFDM such that the coding gain is still not fully exploited.

5.5 Carrier Frequency Offset Mismatch

In Section 5.3 different APP-based PLNC detection and decoding schemes haven been presented at the relay to estimate the relay message. Therein, perfect signal synchronization is assumed such that the system equation (5.8) in the MA phase holds. However, in practical systems, signal asynchrony exists jeopardizing the performance of the APP-based schemes. Basically, two types of asynchronicity are crucial for PLNC described as follows.

- **Time asynchrony**: since both sources transmit to the relay simultaneously in the MA phase, the receive sequence from both sources

may be misaligned in time if not received exactly at the same time instant. Such a time asynchrony can be mitigated when jointly considered within the channel decoder [WFL09], e.g., for convolutional codes [YL15], LDPC codes [WZY13] and cyclic block codes [WHN15]. In case of OFDM transmissions, it has been demonstrated in [LWLZ12], that the time misalignment can be incorporated into the channel in frequency domain and equalized therein if the delay ΔT plus the channel response in time domain is within the CP, i.e., $\Delta T + \tau_{\max} < T_{\mathrm{CP}}$.

- **Frequency asynchrony**: practically, the carrier frequency difference between the local oscillators at the transmitter and the receiver due to hardware imprecision causes carrier frequency offset (CFO). For end-to-end transmissions, the CFO can be completely compensated assuming perfect CFO estimation. However, the MA phase in two-way relaying communications results in two CFOs between the signals from both sources to the relay. These two CFOs, if not matched, cannot be totally compensated even though both of them are perfectly estimated. Such a CFO mismatch has to be coped with properly to mitigate the resulting performance degradation. This aspect is studied for different APP-based schemes in [WLW+14] and discussed in the sequel.

5.5.1 System Formulation for CFO

For CFO-related analysis, one OFDM symbol is considered instead of the subcarrier wise description in (5.8) to formulate the MA transmission. To this end, the $L \times 1$ receive signal vector $\mathbf{y}_{\mathrm{R}}$ in frequency domain is given by

$$\mathbf{y}_{\mathrm{R}} = \mathbf{H}_{\mathrm{AR}}\mathbf{x}_{\mathrm{A}} + \mathbf{H}_{\mathrm{BR}}\mathbf{x}_{\mathrm{B}} + \mathbf{n}_{\mathrm{R}} \tag{5.48}$$

when the CFOs in both links are absent. Here, $\mathbf{H}_{\mathrm{AR}}$ and $\mathbf{H}_{\mathrm{BR}}$ denote the $L \times L$ main diagonal channel matrices in frequency domain, where each entry of both matrices represents a subcarrier wise channel coefficient $h_{\mathrm{AR},\ell}$ or $h_{\mathrm{BR},\ell}$. In Fig. 5.23, graphical patterns of both channel gain matrices are presented with $L = 16$ subcarriers and no CFO influence. As can be observed, the matrices are diagonal, which indicates that the subcarriers are independent with each other, and thus can be considered individually.

With the presence of CFOs, the channels in the MA phase are distorted. Complying with the CFO model depicted in [KHF09, SJ09], the system equation in matrix representation is re-formulated as

$$\begin{aligned} \mathbf{y}_{\mathrm{R}} =& \mathbf{E}_{\mathrm{A}}\mathbf{H}_{\mathrm{AR}}\mathbf{x}_{\mathrm{A}} + \mathbf{E}_{\mathrm{B}}\mathbf{H}_{\mathrm{BR}}\mathbf{x}_{\mathrm{B}} + \mathbf{n}_{\mathrm{R}} && \text{(5.49a)} \\ =& \underbrace{\mathbf{\Lambda}_{\mathrm{A}}\mathbf{x}_{\mathrm{A}} + \mathbf{\Lambda}_{\mathrm{B}}\mathbf{x}_{\mathrm{B}}}_{\text{desired signal}} + \underbrace{\overline{\mathbf{\Lambda}}_{\mathrm{A}}\mathbf{x}_{\mathrm{A}} + \overline{\mathbf{\Lambda}}_{\mathrm{B}}\mathbf{x}_{\mathrm{B}}}_{\text{ICI}} + \mathbf{n}_{\mathrm{R}} && \text{(5.49b)} \end{aligned}$$

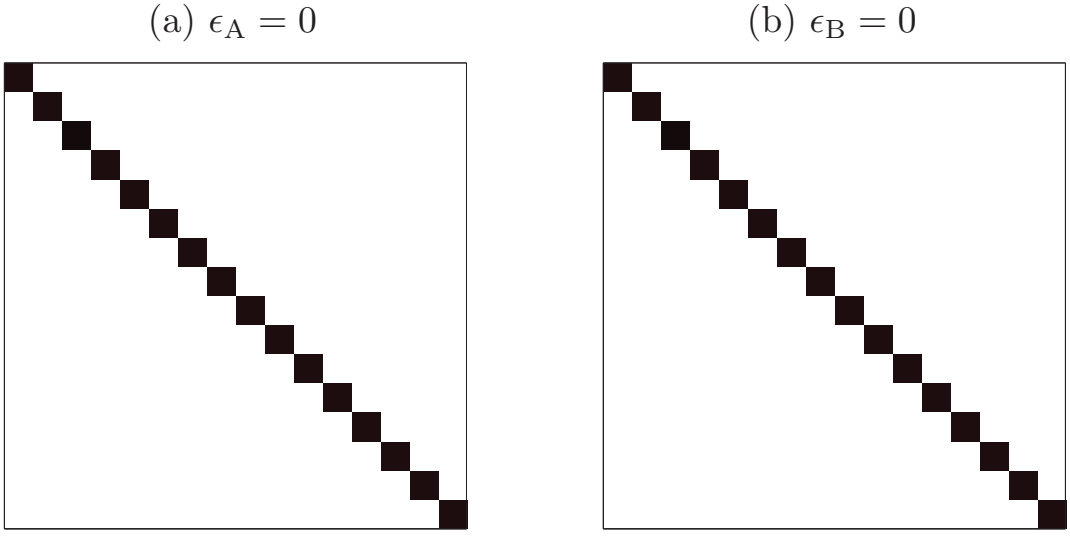

Figure 5.23: Graphical patterns of both channel gain matrices in the MA phase without CFO. (a) for the AR link with $\epsilon_{\mathrm{A}} = 0$ and (b) for the BR link with $\epsilon_{\mathrm{B}} = 0$.

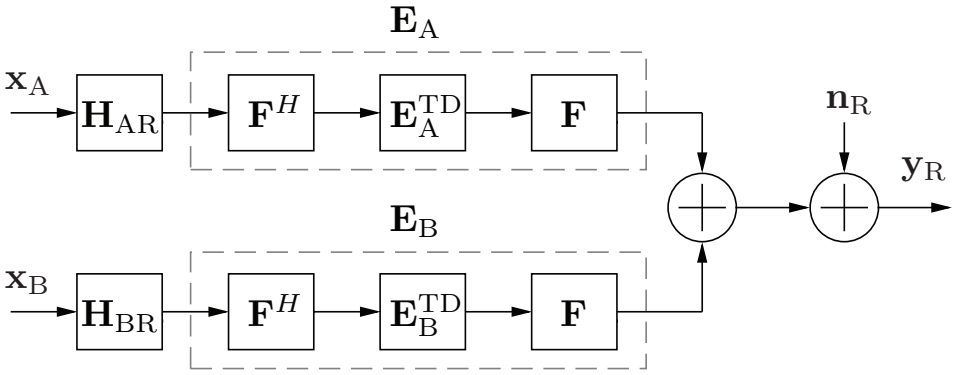

Figure 5.24: Block diagram of the MA phase corresponding to (5.49a), which includes the impact of CFO on one whole OFDM symbol vector.

with the corresponding system block diagram shown in Fig. 5.24. Therein, the CFO between each source, e.g., source A, and relay R is covered by $\mathbf{E}_{\mathrm{A}} = \mathbf{F}\mathbf{E}_{\mathrm{A}}^{\mathrm{TD}}\mathbf{F}^H$ with dimension $L \times L$. The $L \times L$ DFT matrix is denoted by $\mathbf{F}$, which is unitary with $\mathbf{F}\mathbf{F}^H$ equal to the identity matrix $\mathbf{I}$. The $L \times L$ CFO distortion matrix $\mathbf{E}_{\mathrm{A}}^{\mathrm{TD}}$ is diagonal and defined in time domain (TD) as

$$\mathbf{E}_{\mathrm{A}}^{\mathrm{TD}} = \mathrm{dg}\left\{\begin{bmatrix} 1 & \mathrm{e}^{\frac{j2\pi\epsilon_{\mathrm{A}}}{L}} & \cdots & \mathrm{e}^{\frac{j2\pi\epsilon_{\mathrm{A}}(L-1)}{L}} \end{bmatrix}\right\} . \tag{5.50}$$

Here, ϵ_{A} denotes the CFO from the AR link normalized to subcarrier spacing, which is assumed to be perfectly known at the relay. The operator $\mathrm{dg}\{\cdot\}$

transforms a vector into a diagonal matrix. Without CFO, i.e., $\epsilon_{\mathrm{A}} = 0$, $\mathbf{E}_{\mathrm{A}}$ is reduced to an identity matrix, indicating that the orthogonality of the channel matrix $\mathbf{H}_{\mathrm{AR}}$ is preserved. However, this orthogonality is destroyed by the non-diagonal matrix $\mathbf{E}_{\mathrm{A}}$ if $\epsilon_{\mathrm{A}} \neq 0$. In this case, the equivalent channel matrix $\mathbf{E}_{\mathrm{A}}\mathbf{H}_{\mathrm{AR}} = \mathbf{\Lambda}_{\mathrm{A}} + \overline{\mathbf{\Lambda}}_{\mathrm{A}}$ is composed of the main diagonal matrix $\mathbf{\Lambda}_{\mathrm{A}}$ corresponding to the desired signal and the non-diagonal interference matrix $\overline{\mathbf{\Lambda}}_{\mathrm{A}}$ resulting in inter-carrier interference (ICI) as shown in (5.49b). Furthermore, the CFO influence to the BR link can be deduced similarly.

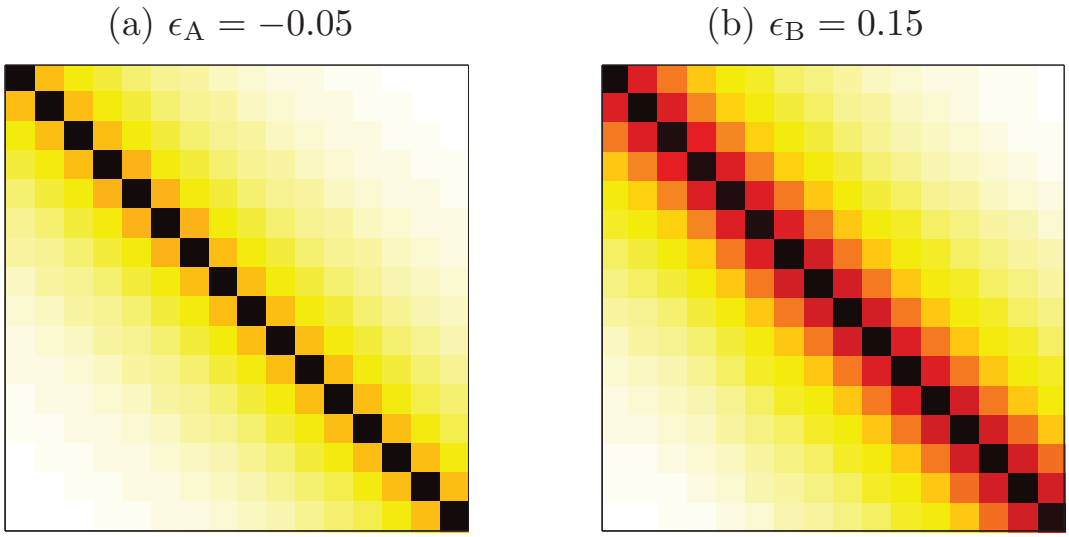

Figure 5.25: Graphical patterns of both equivalent channel gain matrices in the MA phase before CFO compensation. (a) for the AR link with $\epsilon_{\mathrm{A}} = -0.05$ and (b) for the BR link with $\epsilon_{\mathrm{B}} = 0.15$.

To visualize the impact of CFOs, an example is shown in Fig. 5.25 for the graphical patterns of both equivalent channel gain matrices with $\epsilon_{\mathrm{A}} = -0.05$, $\epsilon_{\mathrm{B}} = 0.15$ and $L = 16$ subcarriers. Obviously, ϵ_{B} results in more ICI compared to ϵ_{A}. Both ICIs will be superimposed at the relay and jeopardize the performance of the APP-based PLNC schemes. Thus, the ICI has to be dealt with properly, as discussed in the upcoming subsections.

5.5.2 Carrier Frequency Offset Compensation

A direct approach is to compensate the CFOs in time domain after signal reception at the relay. However, unlike complete CFO compensation in end-to-end transmissions, nulling both CFOs at the relay for the MA transmission in (5.49) is impossible if $\epsilon_{\mathrm{A}} \neq \epsilon_{\mathrm{B}}$. In this case, complete compensation of one CFO, e.g., ϵ_{A} for the AR link, results in $\epsilon'_{\mathrm{A}} = 0$ and $\epsilon'_{\mathrm{B}} = \epsilon_{\mathrm{B}} - \epsilon_{\mathrm{A}} \neq 0$, where ϵ'_{A} and ϵ'_{B} denote the remaining CFOs after compensation.

Alternatively, an average CFO compensation strategy by $-\frac{\epsilon_\mathrm{A}+\epsilon_\mathrm{B}}{2}$ presented in [LWLZ12] can be applied before the APP-based schemes. Such average compensation yields both remaining CFOs as

$$\epsilon'_\mathrm{A} = \epsilon_\mathrm{A} - \frac{\epsilon_\mathrm{A}+\epsilon_\mathrm{B}}{2} = \frac{\epsilon_\mathrm{A}-\epsilon_\mathrm{B}}{2} \tag{5.51a}$$

$$\epsilon'_\mathrm{B} = \epsilon_\mathrm{B} - \frac{\epsilon_\mathrm{A}+\epsilon_\mathrm{B}}{2} = \frac{\epsilon_\mathrm{B}-\epsilon_\mathrm{A}}{2}\ . \tag{5.51b}$$

Applying the average CFO compensation strategy, the performance degradation due to CFO mismatch can still be significant when the initial relative CFO $|\epsilon_\mathrm{A}-\epsilon_\mathrm{B}|$ is large. Besides, the individual CFOs are assumed to be perfected estimated. To this end, a more sophisticated scheme based on the space-alternating generalized expectation-maximization (SAGE) algorithm [FH94] has been presented in [XXX12] that jointly estimates and compensates the CFOs in an iterative manner by fixing one group of parameter and updating the other. Generalization for multi-user (more than 2) CFO compensation using the SAGE algorithm was presented in [LK07]. Furthermore, a joint multi-layer detection and CFO compensation algorithm was presented in [KHF09] for asynchronous multi-user MIMO systems[2]. These aspects yield more robustness against severe CFO mismatch but also result in high computational complexity. For ease of practical implementation, only complete compensation of one CFO and average compensation are discussed whereas the SAGE algorithm is beyond the scope of this work.

In order to compare the two aforementioned CFO compensation strategies, the graphical example in Fig. 5.25 is re-considered subject to complete compensation and average compensation in Fig. 5.26 and Fig. 5.27, respectively. When complete CFO compensation of ϵ_A is adopted, which leads to $\epsilon'_\mathrm{A}=0$ and $\epsilon'_\mathrm{B}=0.2$, the ICI from the AR link totally disappears in Fig. 5.26(a) but it increases tremendously in Fig. 5.26(b). It can be thus inferred that complete compensation of one CFO may amplify the influence of its counterpart dramatically. For average CFO compensation with $\epsilon'_\mathrm{A}=-0.1$ and $\epsilon'_\mathrm{B}=0.1$, a compromise is achieved between the two CFOs, which suppresses the larger CFO while not amplifying the smaller CFO too much, as shown in Fig. 5.27.

It is noted that both ICI components $\overline{\mathbf{\Lambda}}_\mathrm{A}$ and $\overline{\mathbf{\Lambda}}_\mathrm{B}$ in (5.49b) contribute to impairment that degrades the performance of the APP-based schemes. Therefore, the total ICI power $\mathcal{P}_\mathrm{ICI}$ is calculated numerically by averaging over multi-path fading channels with respect to the relative CFO $|\epsilon_\mathrm{A}-\epsilon_\mathrm{B}|$

[2]When the relay is equipped with multiple antennas, the MA phase corresponds to a multi-user MIMO scenario. However, the CFO mismatch is only considered in the SISO relaying case. Extension to MIMO relaying is straightforward when CFO compensation is performed separately from multi-layer detection.

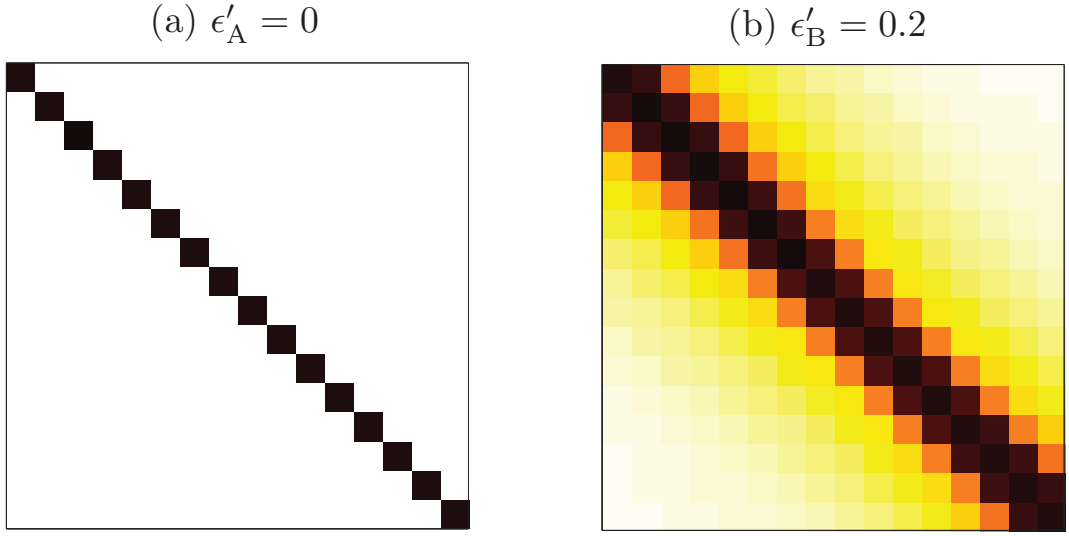

Figure 5.26: Graphical patterns of both equivalent channel gain matrices in the MA phase after complete CFO compensation of ϵ_{A}. (a) for the AR link with $\epsilon'_{\mathrm{A}} = 0$ and (b) for the BR link with $\epsilon'_{\mathrm{B}} = 0.2$.

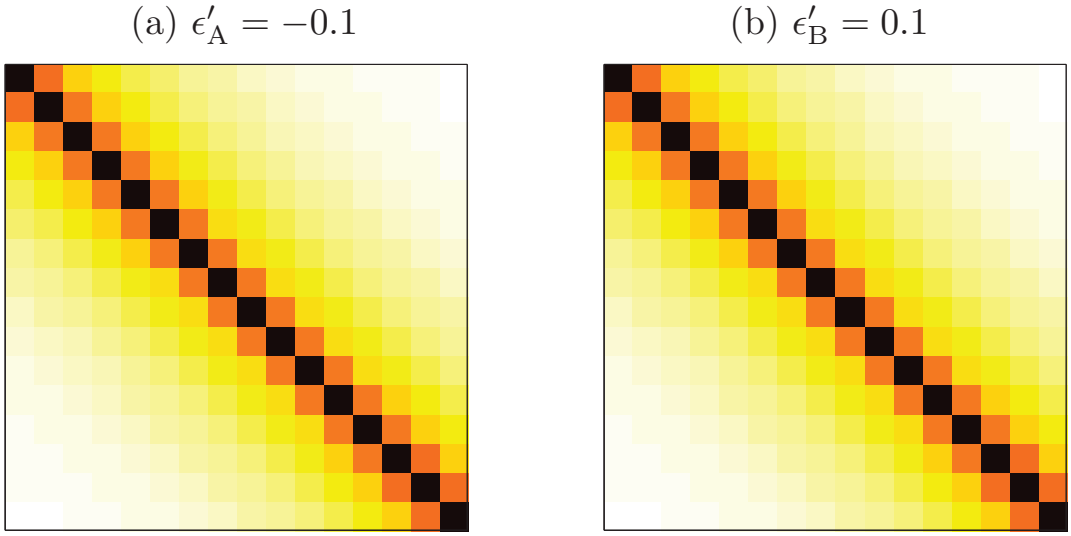

Figure 5.27: Graphical patterns of both equivalent channel gain matrices in the MA phase after average CFO compensation. (a) for the AR link with $\epsilon'_{\mathrm{A}} = -0.1$ and (b) for the BR link with $\epsilon'_{\mathrm{B}} = 0.1$.

for both CFO compensation strategies. As shown in Fig. 5.28, the average compensation leads to less amount of total ICI in contrast to the complete compensation of one CFO, especially for increasing relative CFO. In the sequel, the average CFO compensation strategy is adopted before initial detection due to less total ICI unless otherwise stated.

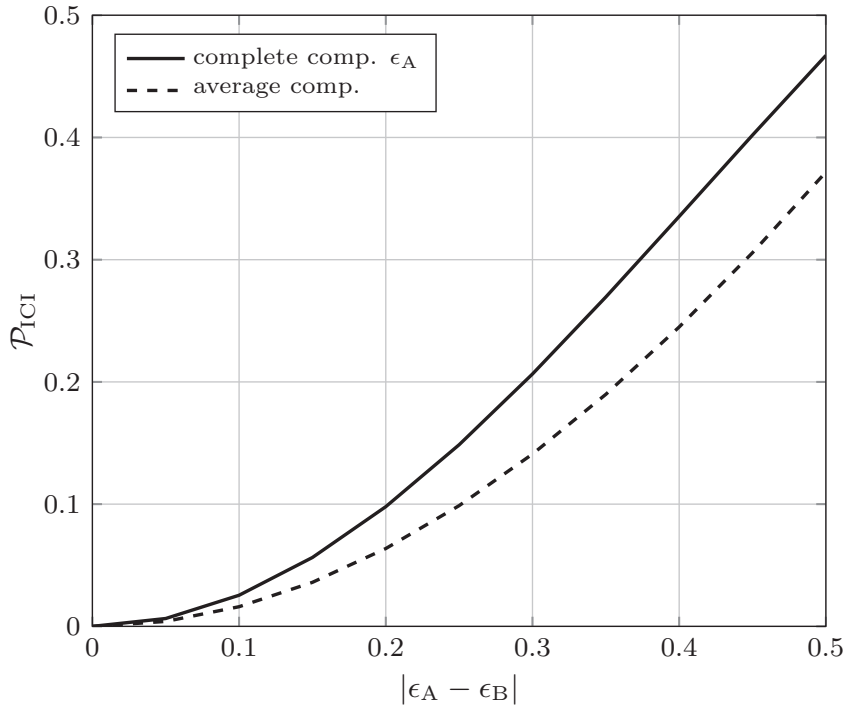

Figure 5.28: Total ICI power $\mathcal{P}_{\mathrm{ICI}}$ versus relative CFO $|\epsilon_{\mathrm{A}} - \epsilon_{\mathrm{B}}|$ after both complete CFO compensation of ϵ_{A} and average CFO compensation.

5.5.3 Inter-Carrier Interference Cancellation

After CFO compensation in the time domain, ICI cancellation (ICIC) in the frequency domain is performed to further mitigate the remaining impairment caused by CFO mismatch. Basically, the ICI components shown in (5.49b) are reconstructed using the estimated individual messages and subtracted from the receive signal. Subsequently, the decoding is performed again with respect to the ICI reduced signal. Note that since JCNC only produces the relay codeword $\mathbf{c}_{\mathrm{R}}$ without explicit estimation of $\mathbf{c}_{\mathrm{A}}$ and $\mathbf{c}_{\mathrm{B}}$, ICIC is not applicable for this scheme. On the other hand, the individual source messages are also estimated for SCD and G-JCNC besides $\mathbf{c}_{\mathrm{R}}$, which can be used to perform ICIC.

ICIC for P-SCD and G-JCNC

Considering P-SCD and G-JCNC, both of which estimate the individual source messages simultaneously, the ICIC process can be represented as

$$\tilde{\mathbf{y}}_{\mathrm{R}} = \mathbf{y}_{\mathrm{R}} - \overline{\mathbf{\Lambda}}_{\mathrm{A}}\hat{\mathbf{x}}_{\mathrm{A}} - \overline{\mathbf{\Lambda}}_{\mathrm{B}}\hat{\mathbf{x}}_{\mathrm{B}} \tag{5.52a}$$

$$\begin{aligned} &= \mathbf{\Lambda}_{\mathrm{A}}\mathbf{x}_{\mathrm{A}} + \mathbf{\Lambda}_{\mathrm{B}}\mathbf{x}_{\mathrm{B}} + \mathbf{n}_{\mathrm{R}} \\ &\quad + \overline{\mathbf{\Lambda}}_{\mathrm{A}}(\mathbf{x}_{\mathrm{A}} - \hat{\mathbf{x}}_{\mathrm{A}}) + \overline{\mathbf{\Lambda}}_{\mathrm{B}}(\mathbf{x}_{\mathrm{B}} - \hat{\mathbf{x}}_{\mathrm{B}}) \,, \end{aligned} \tag{5.52b}$$

where $\hat{\mathbf{x}}_\mathrm{A}$ and $\hat{\mathbf{x}}_\mathrm{B}$ denote the estimates of the source symbol vectors at the relay. $\tilde{\mathbf{y}}_\mathrm{R}$ denotes the interference-reduced signal. For ease of representation, let (5.49) denote here the system equation after the initial average CFO compensation. Inserting (5.49b) into (5.52a), it can be observed that the ICI reduced signal contains the ICI-free signal without CFO mismatch and the remaining ICI, which correspond to the first line and the second line of (5.52b), respectively. Note that this ICIC process can be performed iteratively to further improve the performance, as shown in Fig. 5.29 for the block diagram of P-SCD and G-JCNC with CFO compensation and ICIC. As the iteration number increases, less amount of remaining ICI leads to reduced impairment.

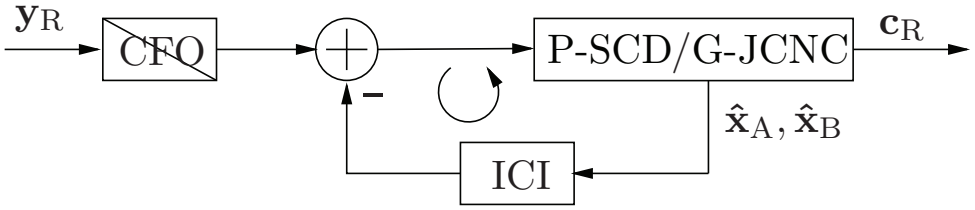

Figure 5.29: Bock diagram for P-SCD and G-JCNC with CFO compensation and iterative ICIC at the relay.

ICIC for S-SCD

For S-SCD with CFO compensation and ICIC, a modified S-SCD scheme is developed with the block diagram presented in Fig. 5.30. After the initial average CFO compensation, the codeword from the stronger link, e.g., $\hat{\mathbf{c}}_\mathrm{A}$, is estimated. Subsequently, the ICI as well as the desired signal regarding $\hat{\mathbf{x}}_\mathrm{A}$ is subtracted from the receive signal as

$$\tilde{\mathbf{y}}_\mathrm{R} = \mathbf{y}_\mathrm{R} - (\mathbf{\Lambda}_\mathrm{A} + \overline{\mathbf{\Lambda}}_\mathrm{A})\hat{\mathbf{x}}_\mathrm{A} \tag{5.53a}$$

$$\begin{aligned} &= (\mathbf{\Lambda}_\mathrm{B} + \overline{\mathbf{\Lambda}}_\mathrm{B})\mathbf{x}_\mathrm{B} + \mathbf{n}_\mathrm{R} \\ &\quad + (\mathbf{\Lambda}_\mathrm{A} + \overline{\mathbf{\Lambda}}_\mathrm{A})(\mathbf{x}_\mathrm{A} - \hat{\mathbf{x}}_\mathrm{A}) \, . \end{aligned} \tag{5.53b}$$

Assuming correct decoding of the source message from A, i.e., $\hat{\mathbf{x}}_\mathrm{A} = \mathbf{x}_\mathrm{A}$, both the signal and the ICI component contributed from $\mathbf{x}_\mathrm{A}$ are completely removed, indicating that the second line of (5.53b) is equal to 0. Since the resulting interference reduced signal contains only the signal contribution from $\mathbf{x}_\mathrm{B}$, the corresponding CFO leading to the ICI term $\overline{\mathbf{\Lambda}}_\mathrm{B}$ can be completely compensated as in an end-to-end transmission. Afterwards, $\hat{\mathbf{c}}_\mathrm{B}$ is estimated from the ICI-free signal as in a SU scenario. Such an ICIC process

in combination with successive decoding also can be performed iteratively for further performance improvement.

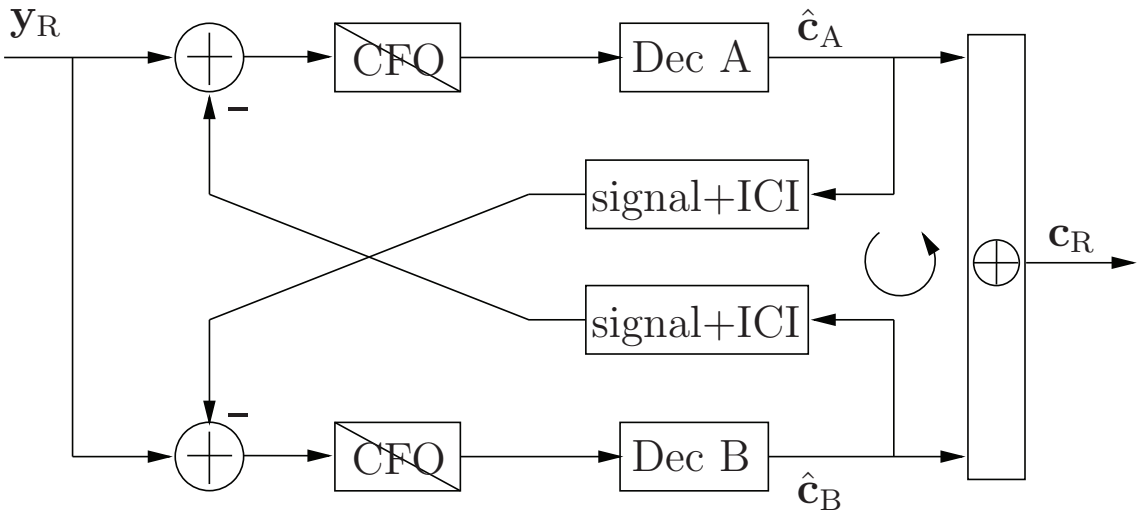

Figure 5.30: Block diagram for S-SCD with CFO compensation and iterative ICIC in combination with successive decoding at the relay.

It is noted that when jointly considering SCD and ICIC, employing the S-SCD scheme is more reasonable compared to P-SCD because the signal cancellation for both ICI and successive decoding makes use of the estimated individual message. Therefore, both ICI and the desired signal $(\mathbf{\Lambda}_\mathrm{A}+\overline{\mathbf{\Lambda}}_\mathrm{A})\hat{\mathbf{x}}_\mathrm{A}$ in (5.53a) can be subtracted from the receive signal simultaneously in the modified S-SCD scheme. On the other hand, as shown in (5.52a) for P-SCD, only the ICI term $\overline{\mathbf{\Lambda}}_\mathrm{A}\hat{\mathbf{x}}_\mathrm{A}$ is subtracted, leaving $\mathbf{\Lambda}_\mathrm{A}\hat{\mathbf{x}}_\mathrm{A}$ still as 'interference' for re-decoding. However, since P-SCD with iterative ICIC is similar to iterative parallel interference cancellation for multi-user detection [LaL96], its performance is still evaluated later on.

Hard vs. Soft Interference Cancellation

As shown in Fig. 5.29 and Fig. 5.30, the interference is reconstructed using the hard decided code bits, e.g., $\hat{\mathbf{c}}_\mathrm{A}$, at the relay with $\hat{\mathbf{x}}_\mathrm{A} = \mathcal{M}(\hat{\mathbf{c}}_\mathrm{A})$ and subtracted from the receive signal. However, when decoding errors occur, the interference will be estimated erroneously, which leads to error propagation that jeopardizes the decoding performance after such a hard interference cancellation (hIC).

In order to mitigate the performance degradation caused by hIC, reliability information is utilized to estimate $\hat{\mathbf{x}}_\mathrm{A}$ and $\hat{\mathbf{x}}_\mathrm{B}$ for the calculation in (5.52) and (5.53), which is termed soft interference cancellation (sIC) [WJ99]. For the sake of illustration, BPSK modulation is assumed with straightforward

extension to higher modulation alphabets. The estimated source symbol, e.g., $\hat{x}_{\mathrm{A},\ell}$, on the ℓth subcarrier is given by the soft bit as [WJ99]

$$\hat{x}_{\mathrm{A}} = \tanh\left(\frac{L_{\mathrm{A}}}{2}\right) \tag{5.54}$$

with the subscript ℓ omitted for ease of notation. Here, L_{A} represents the LLR after soft-input soft-output channel decoding for SCD. When G-JCNC is applied, the APPs are directly updated in a non-binary channel decoder. To this end, according to Tab. 5.1, the estimated source symbols are determined by [WLW+14]

$$\hat{x}_{\mathrm{A}} = (P_0 + P_2) \cdot 1 + (P_1 + P_3) \cdot (-1) \tag{5.55a}$$

$$\hat{x}_{\mathrm{B}} = (P_0 + P_1) \cdot 1 + (P_2 + P_3) \cdot (-1) \tag{5.55b}$$

with the APPs P_i defined in (5.21). The soft source symbol estimate, e.g., $\hat{x}_{\mathrm{A}} \in (-1, 1)$ in (5.54) and (5.55) approaches ± 1 when the corresponding code bit c_{A} is correctly decoded with high probability, which is equivalent to hIC. Otherwise, it approaches 0, which implies nearly no interference cancellation regarding this subcarrier wise signal. Thus, the impact of error propagation is mitigated significantly by applying sIC.

Performance Evaluation

The performance of the APP-based PLNC detection and decoding schemes is evaluated subject to CFO mismatch. Average CFO compensation before the initial detection is employed due to less amount of total ICI compared to complete compensation of one CFO, as shown in Fig. 5.28. For interference cancellation, sIC is applied because of its robustness against hIC [WJ99]. Furthermore, QPSK and LDPC code with rate $\mathrm{R_C} = 0.5$ are employed.

The FER performance at the relay denoted as $\mathrm{FER_R}$ of the XORed packet $\mathbf{c}_{\mathrm{R}}$ for P-SCD is shown in Fig. 5.31. For relative CFOs $|\epsilon_{\mathrm{A}} - \epsilon_{\mathrm{B}}| = 0.4$ and $|\epsilon_{\mathrm{A}} - \epsilon_{\mathrm{B}}| = 0.2$, the corresponding CFOs after average compensation yield ± 0.2 and ± 0.1, respectively. As can be observed in the figure, the CFO mismatch results in tremendous performance degradation without ICIC. However, ICIC improves the performance significantly. For a larger relative CFO, i.e., $|\epsilon_{\mathrm{A}} - \epsilon_{\mathrm{B}}| = 0.4$, further gain can be achieved with increasing number of iterations, which converges at the fourth iteration and amounts to, e.g., only 2 dB loss compared to the case without CFO at $\mathrm{FER_R} = 10^{-2}$. The performance improvement provided by further iterations is limited for a smaller relative CFO. Specifically, ICIC with only 1 iteration already approaches the ideal case with no CFO within 0.5 dB loss when $|\epsilon_{\mathrm{A}} - \epsilon_{\mathrm{B}}| = 0.2$, indicating that performing ICIC once is sufficient in this case.

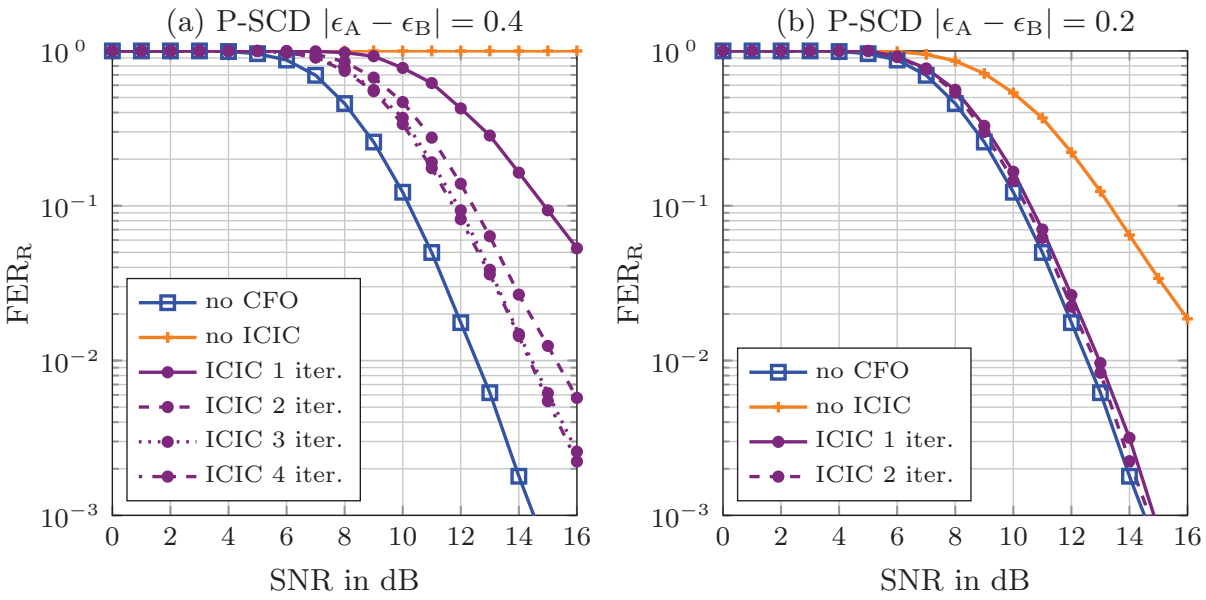

Figure 5.31: FER of the relay codeword for P-SCD with relative CFO $|\epsilon_A - \epsilon_B| = 0.4$ in (a) and $|\epsilon_A - \epsilon_B| = 0.2$ in (b). Average CFO compensation and sIC for ICIC are applied.

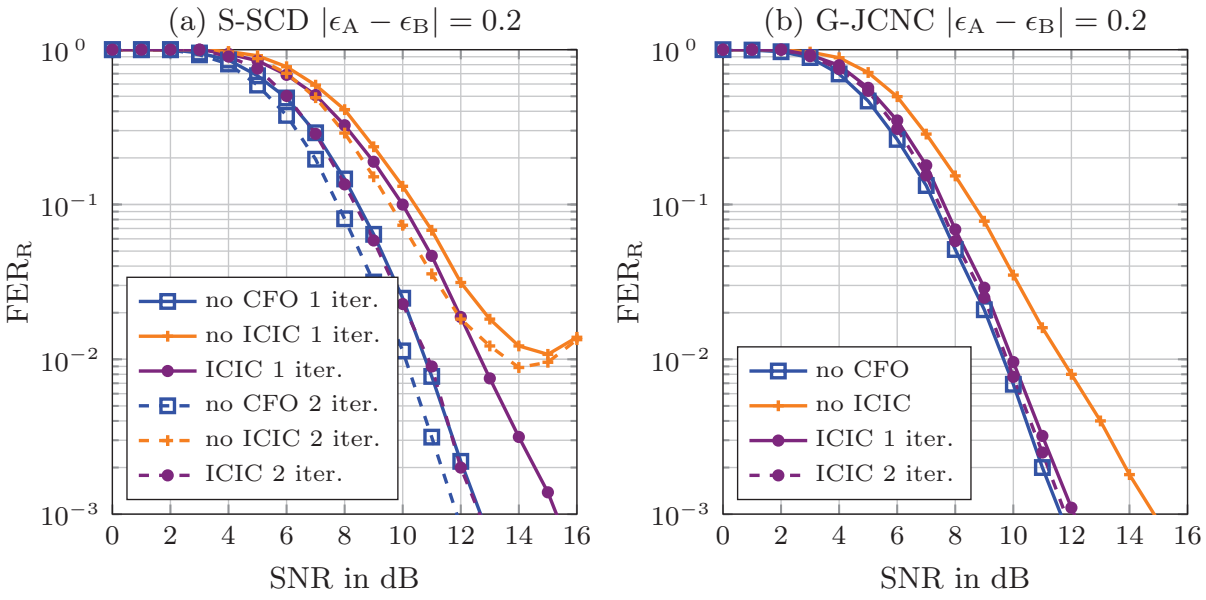

Figure 5.32: FER of the relay codeword for S-SCD in (a) and G-JCNC in (b) with relative CFO $|\epsilon_A - \epsilon_B| = 0.2$. Average CFO compensation and sIC for ICIC as well as successive decoding are applied.

The FER performance for modified S-SCD and G-JCNC is shown in Fig. 5.32 with relative CFO $|\epsilon_A - \epsilon_B| = 0.2$. Note that the iterations herein are referred to both ICIC and successive decoding for S-SCD. It can

be observed that ICIC for the modified S-SCD scheme also improves the performance dramatically, which approaches the ideal case without CFO within 1dB loss after the second iteration. On the other hand, G-JCNC exhibits the most robust performance against CFO mismatch in comparison to P-SCD and modified S-SCD without ICIC, which shows less than 2dB loss to the ideal case without CFO at $\mathrm{FER_R} = 10^{-2}$. Moreover, similar to that for P-SCD, ICIC with 1 iteration leads to significantly improved performance by approaching the ideal case with a slight dB loss for G-JCNC. Therefore, further iteration only contributes negligible gain in this case, as shown in Fig. 5.32(b).

5.6 Extenstion to MIMO Relaying

In the previously defined system setup for SISO relaying, the transmit signals from both sources are superimposed at the single-antenna relay. Therefore, it is not possible to spatially separate the two signals due to lack of degrees of freedom and only APP-based detection from the superimposed receive signal is feasible. To loose this constraint, multiple antennas are allowed at the relay, which essentially forms a multi-user multi-layer transmission in the MA phase. As a result, besides the APP-based schemes, common MIMO detection techniques of low complexity can be applied to obtain the individually estimated source messages, which are then network coded for BC transmission. Such a MIMO relay based PLNC strategy is examined in this section with the help of MI analysis [WWD13b, WWD14b].

5.6.1 System Model

In this section, the two-phase two-way relaying scheme is extended to the case that the relay is equipped with multiple antennas. The system model is shown in Fig. 5.33, where both sources transmit to the K-antenna relay simultaneously in the MA phase. Similar to (5.8) for SISO relaying, the corresponding receive signal $y_{\mathrm{R},k,\ell}$ in the MIMO case on the ℓth subcarrier at the kth antenna at relay R yields

$$y_{\mathrm{R},k,\ell} = h_{\mathrm{AR},k,\ell} x_{\mathrm{A},\ell} + h_{\mathrm{BR},k,\ell} x_{\mathrm{B},\ell} + n_{\mathrm{R},k,\ell} \tag{5.56}$$

with $k = 1, 2, \cdots, K$ denoting the antenna index. Collecting the receive signal on the ℓth subcarrier at each antenna into a $K \times 1$ vector $\mathbf{y}'_{\mathrm{R},\ell} = [y_{\mathrm{R},1,\ell}\ y_{\mathrm{R},2,\ell}\ \cdots\ y_{\mathrm{R},K,\ell}]^T$, results in the MIMO system equation on the ℓth subcarrier given by

$$\mathbf{y}'_{\mathrm{R},\ell} = \mathbf{H}'_\ell \mathbf{x}'_\ell + \mathbf{n}'_{\mathrm{R},\ell}\ . \tag{5.57}$$

Note that the superscript, prime $'$, e.g., in $\mathbf{y}'_{\mathrm{R},\ell}$ is used to distinguish with the vector $\mathbf{y}_{\mathrm{R}}$ defined in Subsection 5.2.3 over the L subcarriers in one OFDM symbol. Moreover, $\mathbf{x}'_\ell = [x_{\mathrm{A},\ell}\ x_{\mathrm{B},\ell}]^T$ denotes the 2×1 transmit symbol vector. By further denoting $\mathbf{h}'_{k,\ell} = [h_{\mathrm{AR},k,\ell}\ h_{\mathrm{BR},k,\ell}]^T$ as the 2×1 channel vector in the MA phase at the kth antenna, the $K \times 2$ MIMO channel matrix from both sources to the relay is stacked as $\mathbf{H}'_\ell = [\mathbf{h}'_{1,\ell}\ \mathbf{h}'_{2,\ell}\ \cdots\ \mathbf{h}'_{K,\ell}]^T$. The above definitions refer to the ℓth subcarrier. In order to represent the complete receive signals at the relay for $\ell = 1, 2, \cdots, L$, the receive signal matrix $\mathbf{Y}_{\mathrm{R}} = [\mathbf{y}'_{\mathrm{R},1}\ \mathbf{y}'_{\mathrm{R},2}\ \cdots\ \mathbf{y}'_{\mathrm{R},L}]^T$ of dimension $L \times K$ is defined additionally that collects and stacks the L receive signal vectors $\mathbf{y}'_{\mathrm{R},\ell}$ over the subcarriers.

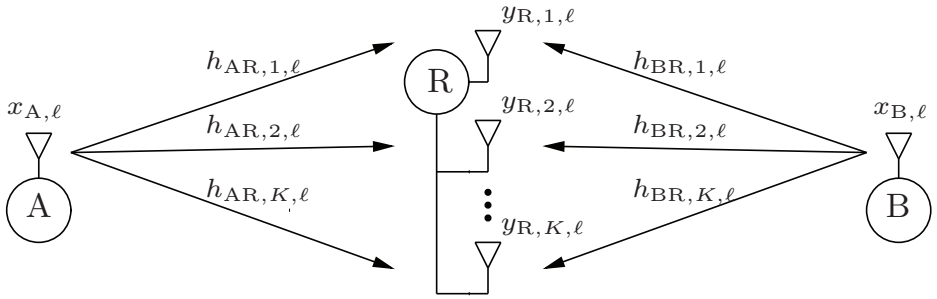

(a) MA phase

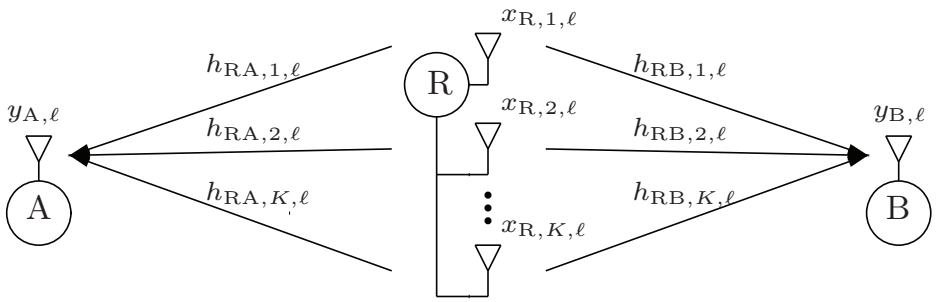

(b) BC phase

Figure 5.33: System model of a two-phase two-way relaying system. Both sources transmit to the relay simultaneously in the MA phase (a) while the relay transmits using space-time codes in the BC phase (b). The relay is equipped with $K > 1$ antennas.

Upon receiving the superimposed signal, the relay performs an estimation of the XORed codeword $\mathbf{c}_{\mathrm{R}} = \hat{\mathbf{c}}_{\mathrm{A}\oplus\mathrm{B}}$ based on $\mathbf{Y}_{\mathrm{R}}$, which is then mapped to the symbol vector $\mathbf{x}_{\mathrm{R}} = \mathcal{M}(\mathbf{c}_{\mathrm{R}})$ for broadcasting in the BC phase. In case of multiple antennas at the relay, diversity-exploiting schemes can be applied at the transmitter side, e.g., OSTBC, as reviewed in Subsection 2.6.2. Denoting the ℓth space-time coded signal at the kth antenna as $x_{\mathrm{R},k,\ell}$, the

transmission in the BC phase is shown in Fig. 5.33(b). The corresponding system equation is given by

$$y_{\mathrm{A},\ell} = \sum_{k=1}^{K} h_{\mathrm{RA},k,\ell} x_{\mathrm{R},k,\ell} + n_{\mathrm{A},\ell} \tag{5.58a}$$

$$y_{\mathrm{B},\ell} = \sum_{k=1}^{K} h_{\mathrm{RB},k,\ell} x_{\mathrm{R},k,\ell} + n_{\mathrm{B},\ell} \ . \tag{5.58b}$$

Similar to that in Chapter 4, the application of OSTBC for the BC transmission is assumed in this section. Ignoring the data rate loss due to orthogonal code designs, the equivalent system equation from relay R to both sources A and B can be written as [TJC98]

$$y_{\mathrm{A},\ell} = \sqrt{\frac{1}{K} \sum_{k=1}^{K} |h_{\mathrm{RA},k,\ell}|^2} x_{\mathrm{R},\ell} + n_{\mathrm{A},\ell} \tag{5.59a}$$

$$y_{\mathrm{B},\ell} = \sqrt{\frac{1}{K} \sum_{k=1}^{K} |h_{\mathrm{RB},k,\ell}|^2} x_{\mathrm{R},\ell} + n_{\mathrm{B},\ell} \tag{5.59b}$$

in contrast to (5.9) for the SISO relaying case. Afterwards, OSTBC detection and network decoding are performed successively to estimate the desired message at each source.

In the sequel, the impact of introducing multiple antennas at the relay is studied. Specifically, the APP-based PLNC detection and decoding schemes in Section 5.3 are adapted to the multiple-antenna relay scenario. Furthermore, since the MA phase corresponds to a multi-user MIMO system, common MIMO detection techniques can be applied at the relay, which are investigated and compared with the APP-based schemes.

5.6.2 Impact on APP-based Schemes

When the relay is equipped with multiple antennas, each antenna receives an independent superimposed signal about the source symbol vector $\mathbf{x}'$ [3]. Therefore, the superimposed signal constellation $\mathcal{S}_{\mathrm{AB},k}$ at the kth antenna is determined by the corresponding channel vector $\mathbf{h}'$ and is different as well as uncorrelated at each antenna. To this end, the probability density for $\mathbf{y}'$ at the relay conditioned on transmitting the code bit combination

[3] The subcarrier index ℓ is omitted as in the previous parts for ease of notation unless otherwise stated.

$c_{\mathrm{AB}} = \mathcal{C}_{\mathrm{AB}}(i)$ at the sources can be calculated as [Kam11]

$$p\{\mathbf{y}'_{\mathrm{R}}|c_{\mathrm{AB}} = \mathcal{C}_{\mathrm{AB}}(i)\} = \prod_{k=1}^{K} p\{y_{\mathrm{R},k}|c_{\mathrm{AB}} = \mathcal{C}_{\mathrm{AB}}(i)\} \tag{5.60a}$$

$$= \frac{1}{(\pi\sigma_n^2)^K} \exp\left\{-\frac{||\mathbf{y}'_{\mathrm{R}} - \mathbf{H}'\mathcal{X}(i)||^2}{\sigma_n^2}\right\} . \tag{5.60b}$$

Each probability density $p\{y_{\mathrm{R},k}|c_{\mathrm{AB}} = \mathcal{C}_{\mathrm{AB}}(i)\}$ forming the product in (5.60a) is given by (5.20) for SISO relaying with $\mathcal{S}_{\mathrm{AB},k}$ depending on the kth MA channel. Alternatively, an equivalent illustration for $p\{\mathbf{y}'_{\mathrm{R}}|c_{\mathrm{AB}} = \mathcal{C}_{\mathrm{AB}}(i)\}$ is shown in (5.60b). Therein, $\mathcal{X}$ denotes the set containing all M^2 transmit symbol vector $\mathbf{x}'$, with $\mathcal{X}(i) = \mathcal{M}\{\mathcal{C}_{\mathrm{AB}}(i)\}$ representing the ith element in $\mathcal{X}_{\mathrm{AB}}(i)$ given that the code bit combination $c_{\mathrm{AB}} = \mathcal{C}_{\mathrm{AB}}(i)$ is transmitted, $i = 0, 1, \cdots, M^2 - 1$.

Similar to (5.21) for SISO relaying, the APP P_i with multiple antennas at the relay can be extended to

$$\begin{aligned} P_i &= \Pr\{c_{\mathrm{AB}} = \mathcal{C}_{\mathrm{AB}}(i)|\mathbf{y}'_{\mathrm{R}}\} \\ &= p\{\mathbf{y}'_{\mathrm{R}}|c_{\mathrm{AB}} = \mathcal{C}_{\mathrm{AB}}(i)\}\frac{\Pr\{c_{\mathrm{AB}} = \mathcal{C}_{\mathrm{AB}}(i)\}}{\Pr\{\mathbf{y}'_{\mathrm{R}}\}} \\ &= p\{\mathbf{y}'_{\mathrm{R}}|c_{\mathrm{AB}} = \mathcal{C}_{\mathrm{AB}}(i)\}\alpha , \end{aligned} \tag{5.61}$$

where the constant α is denoted as

$$\alpha = \frac{\Pr\{c_{\mathrm{AB}} = \mathcal{C}_{\mathrm{AB}}(i)\}}{\Pr\{\mathbf{y}'_{\mathrm{R}}\}} = \frac{1}{M^2\Pr\{\mathbf{y}'_{\mathrm{R}}\}} \tag{5.62}$$

using the completeness condition $\sum_i Pi = 1$ to normalize P_i.

Correspondingly, the LLR calculation (5.25) for SCD and (5.35) for JCNC can be easily adapted to MIMO relaying with the APPs P_i defined above. Considering G-JCNC, these APPs are directly updated iteratively in the non-binary channel decoder to estimate $\mathbf{c}_{\mathrm{AB}}$ followed by PLNC mapping. In other words, introducing multiple antennas at the relay only influences the APP calculations whereas the decoding schemes remain unchanged. With respect to MI presented in (5.30), (5.38) and (5.44) for SCD, JCNC and G-JCNC, respectively, are calculated by integration over $\mathbf{y}'_{\mathrm{R}}$ instead of y_{R}. In accordance, the probability density $p\{y_{\mathrm{R}}|c_{\mathrm{AB}} = \mathcal{C}_{\mathrm{AB}}(i)\}$ defined in (5.20) is replaced by $p\{\mathbf{y}'_{\mathrm{R}}|c_{\mathrm{AB}} = \mathcal{C}_{\mathrm{AB}}(i)\}$ defined in (5.60).

5.6.3 Common Multi-User MIMO Detection Schemes

The APP-based PLNC detection and decoding schemes can be applied to two-way relaying systems with an arbitrary number of antennas K at the relay.

However, when equipping with multiple antennas, i.e., $K > 1$, the MA phase corresponds to a $2 \times K$ multi-user MIMO channel that allows the application of various MIMO techniques. In the sequel, several common multi-layer MIMO detection schemes are applied to the two-way relaying networks using the two-phase scheme, which estimate $\mathbf{c}_\mathrm{A}$ and $\mathbf{c}_\mathrm{B}$ explicitly from the receive signal matrix $\mathbf{Y}_\mathrm{R}$. Subsequently, network coding is applied to generate the relay codeword $\mathbf{c}_\mathrm{R} = \hat{\mathbf{c}}_\mathrm{A} \oplus \hat{\mathbf{c}}_\mathrm{B}$ for broadcasting. Note that the MIMO detection techniques are implemented independently to PLNC in the work, i.e., no APP-based PLNC schemes are followed in succession. Alternative schemes with joint consideration of MIMO detection and PLNC are referred to [ZL10, CKL12, ZNL$^+$12]. Although common MIMO detection schemes also fall into the category 'separated decoding' presented in Subsection 5.3.2 since both source messages are individually estimated at the relay, the term 'SCD' still indicates the APP-based scheme exclusively.

Linear Equalization

For linear equalization (LE), the receive signal vector $\mathbf{y}'_\mathrm{R}$ is filtered by a $2 \times K$ matrix $\mathbf{G}$, resulting in the 2×1 filtered signal vector $\tilde{\mathbf{x}}'_\mathrm{R} = [\tilde{x}_\mathrm{A}\ \tilde{x}_\mathrm{B}]^T = \mathbf{G}\mathbf{y}'_\mathrm{R}$ that contains the estimated messages for x_A and x_B in each layer, respectively. The filtering matrix $\mathbf{G}$ for linear detectors employing either the zero-forcing (ZF) or minimum mean square error (MMSE) criterion is given as

$$\mathbf{G} = \begin{cases} \mathbf{H}'^{+} = \left(\mathbf{H}'^{H}\mathbf{H}'\right)^{-1}\mathbf{H}' & \text{ZF} \\ \underline{\mathbf{H}}'^{+} = \left(\underline{\mathbf{H}}'^{H}\underline{\mathbf{H}}'\right)^{-1}\underline{\mathbf{H}}' & \text{MMSE}\,. \end{cases} \tag{5.63}$$

Here, the operator $(\cdot)^+$ denotes the pseudo inverse of a matrix. Note that MMSE corresponds to ZF for the extended system [Küh06], which has an extended channel matrix $\underline{\mathbf{H}}'$ of dimension $(K+2) \times 2$ defined as

$$\underline{\mathbf{H}}' = \begin{bmatrix} \mathbf{H}' \\ \sigma_n \mathbf{I}_2 \end{bmatrix}\,. \tag{5.64}$$

On the other hand, the receive signal vector has also to be extended for MMSE to adapt to the dimension as

$$\underline{\mathbf{y}}'_\mathrm{R} = \begin{bmatrix} \mathbf{y}'_\mathrm{R} \\ \mathbf{0}_{2\times 1} \end{bmatrix}\,. \tag{5.65}$$

Furthermore, the corresponding estimation errors of different layers are determined by the diagonal elements of the error covariance matrix $\mathbf{\Phi}$, which

is given by

$$\mathbf{\Phi} = \begin{cases} \sigma_n^2 \left(\mathbf{H}'^H \mathbf{H}'\right)^{-1} & \text{ZF} \\ \sigma_n^2 \left(\underline{\mathbf{H}}'^H \underline{\mathbf{H}}'\right)^{-1} & \text{MMSE} . \end{cases} \tag{5.66}$$

Applying the filtering matrix to the receive signal vector, the filtered signal vector yields $\tilde{\mathbf{x}}'_{\mathrm{R}} = \mathbf{H}'^{+}\mathbf{y}'_{\mathrm{R}}$ for ZF or $\tilde{\mathbf{x}}'_{\mathrm{R}} = \underline{\mathbf{H}}'^{+}\underline{\mathbf{y}}'_{\mathrm{R}}$ for MMSE. When ZF is performed, the cross-layer interference is removed completely. However, the Gaussian noise is also amplified significantly. For MMSE a compromise is achieved between the interference and the amplified noise. Subsequently, the filtered vector $\tilde{\mathbf{x}}'_{\mathrm{R}}$ is demodulated using the equivalent channel coefficient and noise variance vectors

$$\mathbf{h}'_{\mathrm{eq}} = \begin{cases} \mathbf{1}_{2\times 1} & \text{ZF} \\ \mathrm{dg}\left\{\mathbf{G}\mathbf{H}'\right\} & \text{MMSE} \end{cases} \tag{5.67a}$$

$$\boldsymbol{\sigma}^2_{n,\mathrm{eq}} = \begin{cases} \begin{bmatrix} \|\mathbf{g}_1\|^2 \\ \|\mathbf{g}_2\|^2 \end{bmatrix} \sigma_n^2 & \text{ZF} \\ \begin{bmatrix} \|\mathbf{g}_1\|^2 \\ \|\mathbf{g}_2\|^2 \end{bmatrix} \sigma_n^2 + \begin{bmatrix} |\varepsilon_1|^2 \\ |\varepsilon_2|^2 \end{bmatrix} & \text{MMSE} , \end{cases} \tag{5.67b}$$

with $\mathbf{g}_1$ and $\mathbf{g}_2$ denoting the 1st and the 2nd rows of $\mathbf{G}$, respectively. Furthermore, the non-diagonal terms of $\mathbf{G}\mathbf{H}'$ are represented by ε_1 and ε_1 in both layers. The operator $\mathrm{dg}(\cdot)$ collects the diagonal terms of a matrix to form a column vector. Finally, channel decoding is performed with respect to the output of the demodulator for both layers to estimate the source codewords $\mathbf{c}_{\mathrm{A}}$ and $\mathbf{c}_{\mathrm{B}}$. This further leads to the relay codeword $\mathbf{c}_{\mathrm{R}} = \hat{\mathbf{c}}_{\mathrm{A}} \oplus \hat{\mathbf{c}}_{\mathrm{B}}$ for broadcasting.

Successive Interference Cancellation

The linear estimation schemes detect different layers in parallel. Alternatively, the layers can be detected successively, where the cross-layer interference resulting from the layer already detected in the layer to be detected is reconstructed and eliminated. Such a non-linear detection technique is termed successive interference cancellation (SIC). Here, the SIC based on QR decomposition (QRD) of the channel matrix is emphasized as an example.

The $2 \times K$ MIMO channel in the MA phase can be decomposed into $\mathbf{H}' = \mathbf{Q}\mathbf{R}$, where $\mathbf{Q}$ denotes a $K \times 2$ matrix with orthonormal columns and $\mathbf{R}$ denotes a 2×2 upper triangular matrix under the ZF criterion. In case of MMSE, QRD is applied to the extended channel matrix (5.64) as $\underline{\mathbf{H}}' = \underline{\mathbf{Q}}\underline{\mathbf{R}}$. Employing $\mathbf{Q}^H$ and $\underline{\mathbf{Q}}^H$ as the filtering matrix for ZF and

MMSE, respectively, yields the filter output given by [WBKK03, Wüb06]

$$\tilde{\mathbf{x}}'_{\mathrm{R}} = \begin{cases} \mathbf{R}\mathbf{x}' + \mathbf{Q}^H\mathbf{n} & \text{ZF} \\ \underline{\mathbf{R}}\mathbf{x}' - \sigma_n\mathbf{Q}_2^H\mathbf{x}' + \mathbf{Q}_1^H\mathbf{n} & \text{MMSE} \end{cases}, \tag{5.68}$$

where $\underline{\mathbf{Q}}$ is partitioned into a $K \times 2$ matrix $\mathbf{Q}_1$ and a 2×2 lower triangular matrix $\mathbf{Q}_2$. Note that the statistical property of the equivalent noise is changed for MMSE since the columns of $\mathbf{Q}_1$ are not orthonormal. Due to the upper triangular structure of $\mathbf{R}$ and $\underline{\mathbf{R}}$, the 2nd layer is detected first, whose impact is subtracted when detecting the 1st layer subsequently. In this case, the equivalent channel coefficient and noise variance vectors are given as

$$\mathbf{h}_{\mathrm{eq}} = \begin{cases} \mathrm{dg}\{\mathbf{R}\} & \text{ZF} \\ \mathrm{dg}\{\underline{\mathbf{R}}\} - \mathrm{dg}\left\{\sigma_n\mathbf{Q}_2^H\right\} & \text{MMSE} \end{cases} \tag{5.69a}$$

$$\boldsymbol{\sigma}^2_{n,\mathrm{eq}} = \begin{cases} \mathbf{1}_{2\times 1}\sigma_n^2 & \text{ZF} \\ \begin{bmatrix} \|\mathbf{q}_1\|^2 \\ \|\mathbf{q}_2\|^2 + |\varepsilon_3|^2 \end{bmatrix}\sigma_n^2 & \text{MMSE} \end{cases}. \tag{5.69b}$$

Here, $\mathbf{q}_1$ and $\mathbf{q}_2$ represent the 1st and 2nd rows of $\mathbf{Q}_1^H$, respectively. ε_3 denotes the lower triangular term of $\mathbf{Q}_2^H$. After demodulation, channel coding with respect to the individual source messages is performed followed by network coding.

Since erroneous decisions of the detected layer will propagate to the next layer to be detected, the performance of SIC can be improved by first detecting the layer with higher reliability. Note that for OFDM systems with channel coding applied to each OFDM symbol, the same detection order is required on all subcarriers. For such an ordered SIC (OSIC) detection scheme, the ordering criterion based on SINR optimization from [WK06] is adopted for performance evaluation later on. In this context, the layer that has the smaller averaged estimation error $\overline{\Phi}_\jmath$ over all subcarriers in one OFDM symbol is detected first. Here, $\overline{\Phi}_\jmath$ is defined as

$$\overline{\Phi}_\jmath = \frac{1}{L}\sum_{\ell=1}^{L}[\boldsymbol{\Phi}_\ell]_{\jmath,\jmath} \tag{5.70}$$

with $\boldsymbol{\Phi}_\ell$ denoting the error covariance matrix on the ℓth subcarrier defined in (5.66). The operator $[\cdot]_{\jmath,\jmath}$ indicates the $\jmath$th diagonal element of a squared matrix with $\jmath = 1, 2$.

Regarding to the MI calculation for PLNC in the MA phase using MIMO detection schemes, the minimum MI of the two detected layers dominates the PLNC performance since both source messages have to be decoded correctly in order to generate an error-free network coded message. When the ZF criterion is considered, each detected layer corresponds to a SU transmission with the cross-layer interference completely nulled and thus the MI C_{SU} can be adapted for each layer using the equivalent channel coefficient and noise variance vectors $\mathbf{h}_{\mathrm{eq}}$ and $\boldsymbol{\sigma}^2_{n,\mathrm{eq}}$. Considering MMSE, the detected signals in both layers still contain remaining cross-layer interference, which can be treated as Gaussian noise and therefore incorporated in the equivalent noise variance for MI calculation, as discussed in [OWF10] for more details.

5.6.4 Performance Evaluation

In this subsection, the impact of introducing multiple antennas at the relay is visualized by simulation results with respect to mutual information and frame error rate. Since the characteristics of the APP-based schemes behave differently over the code rate region as presented in Section 5.3 for SISO relaying, the performance is also evaluated considering both a medium code rate $R_{\mathrm{C}} = 0.5$ and a high code rate $R_{\mathrm{C}} = 0.875$ herein for MIMO relaying when simulating the frame error rate.

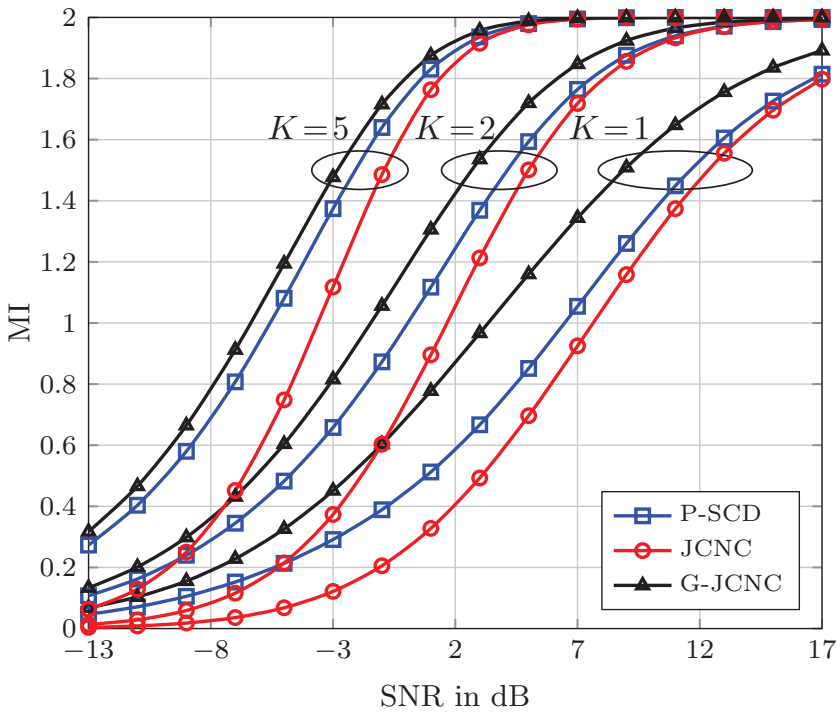

Figure 5.34: MI for the APP-based schemes over multi-path fading channels using OFDM with QPSK. The relay is equipped with different number of antennas, namely, $K = 1, 2, 5$.

Mutual Information

The MI for the APP-based PLNC detection and decoding schemes with different number of antennas at the relay, namely, $K = 1, 2, 5$, are shown in Fig. 5.34 for QPSK. Obviously, more receive antennas at the relay lead to higher MI. Irrespective of K, it can be observed that P-SCD outperforms JCNC whereas G-JCNC achieves the most superior performance over the whole code rate region. Furthermore, JCNC approaches P-SCD with higher code rates. Of special interest is that with growing K, P-SCD approaches G-JCNC, e.g., the loss of MI for P-SCD to G-JCNC is reduced from 4 dB for $K = 1$ to 1 dB for $K = 5$ at the MI equal to 1. This implies that P-SCD may be more attractive with multiple antennas at the relay in implementation aspects due to lower computational complexity compared to G-JCNC.

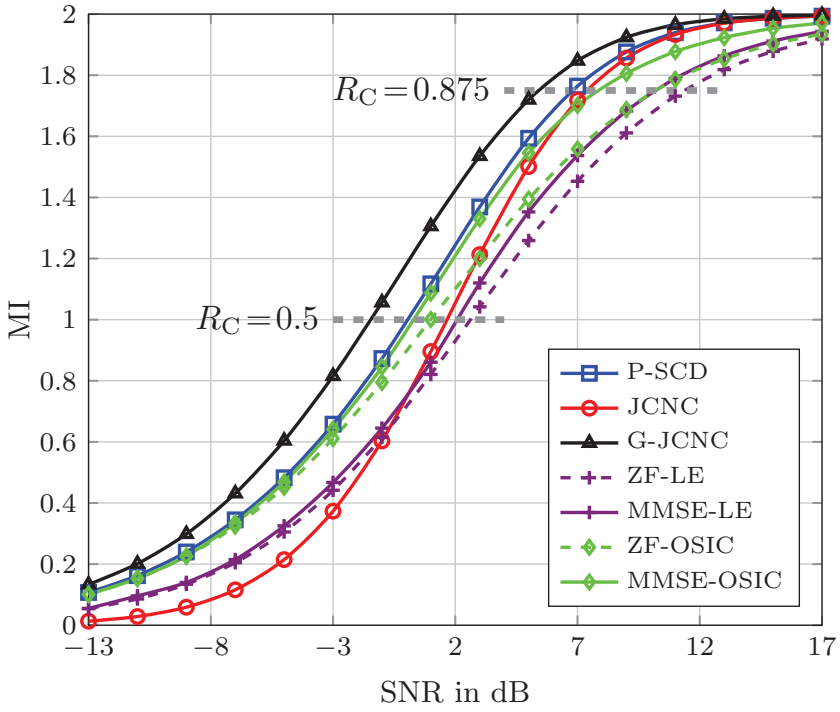

Figure 5.35: MI for the APP-based schemes and common multi-layer MIMO detection schemes over multi-path fading channels using OFDM with QPSK and $K = 2$ antennas at the relay.

In Fig. 5.35 the APP-based schemes are compared with different MIMO detection schemes with respect to MI for $K = 2$ antennas at the relay. Note that the ordering criterion (5.70) is employed for the QRD-based SIC MIMO detector. Obviously, MMSE outperforms ZF and SIC outperforms LE in general. It is well known and shown in the figure, that the MMSE-based OSIC achieves significant performance gains in contrast to LE in both the medium and high code rate regions. Furthermore, the MMSE-based SIC

performs close to P-SCD in the low and medium code rate regions, but no APP calculations based on the superimposed receive signal at the relay are required. These observations in the context of PLNC for two-way relaying coincide with those in classical MIMO systems presented, e.g., in [OWF10].

Frame Error Rate

The FER performance of the XORed codeword at the relay is presented in Fig. 5.36 for different multi-layer MIMO detection schemes with $K = 2$. As shown in the figure, the MMSE-based OSIC scheme outperforms other schemes dramatically, which is in accordance with the observation for MI in Fig. 5.35. Therefore, it is employed for comparison with the APP-based schemes subsequently.

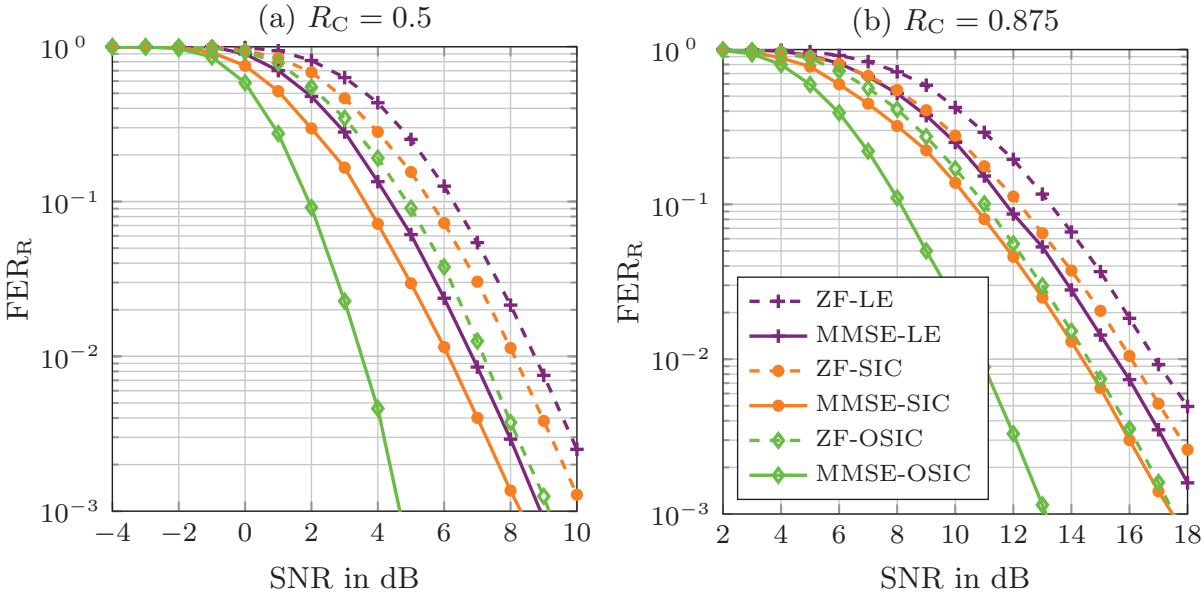

Figure 5.36: FER performance of the XORed codeword at the relay for common multi-layer MIMO detection schemes with $K = 2$ antennas. The code rate is $R_C = 0.5$ in (a) and $R_C = 0.875$ in (b).

In Fig. 5.37, the FER performance of the APP-based schemes is compared to the MMSE-based OSIC with the relay equipping with $K = 2$ antennas. In contrast to Fig. 5.16, the performance loss of P-SCD to G-JCNC is getting smaller with increasing number of antennas at the relay, which corresponds to the observation for MI in Fig. 5.34. Furthermore, the MMSE-based OSIC approaches P-SCD for the medium code rate $R_C = 0.5$ according to Fig. 5.35. On the other hand, the performance degrades significantly with higher code rates, e.g., $R_C = 0.875$, which indicates that the code rate results in dramatic influence on the system performance for different schemes.

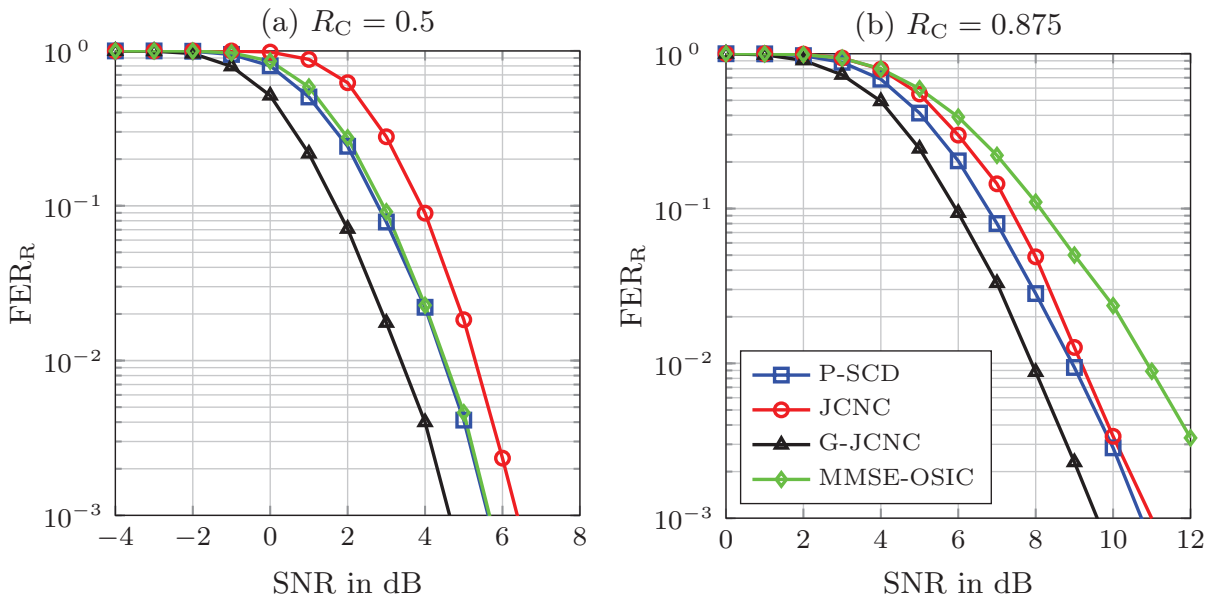

Figure 5.37: FER performance of the XORed codeword at the relay for the APP-based schemes and MMSE-OSIC with $K = 2$ antennas. The code rate is $R_C = 0.5$ in (a) and $R_C = 0.875$ in (b).

5.7 Chapter Summary

In order to compensate the halved spectral efficiency in one-way relaying networks, two-way relaying communications are considered with the focus on the two-phase scheme using physical-layer network coding (PLNC). In this case, two sources exchange messages with each other by first transmitting simultaneously to the relay in the multiple-access (MA) phase. Upon receiving the superimposed signal, a XOR-based network coded message is estimated, which is further broadcast back to the sources in the broadcast (BC) phase. After examining the basics of such a two-way relaying system with one single-antenna relay in Section 5.2, several APP-based detection and decoding schemes are presented in Section 5.3 with the emphasis on a mutual information analysis for these schemes in coded OFDM systems [WWD13a, WLW+16b]. It is shown that in multi-path fading channels using OFDM transmission, separated channel decoding (SCD) that first decodes the individual source messages outperforms joint channel decoding and physical-layer network coding (JCNC) that directly estimates the network coded message. Furthermore, generalized JCNC (G-JCNC) that decodes the joint message in non-binary GF achieves the best performance, although consuming higher computational complexity. In Section 5.4, an optimal phase control strategy is proposed by phase pre-rotation according to the phase difference of both uplinks in the MA transmission

as the APP-based PLNC schemes are in favor of varying channel ratio [WWD13a, WLW+16b]. Moreover, reduction of the required overhead by providing CSI at the transmitter side is also investigated. Due to the distributed nature of the two sources, carrier frequency offset (CFO) mismatch arises in the MA phase and jeopardizes the performance at the relay. To mitigate the resulting impairments in the sense of inter-carrier interference (ICI) in the frequency domain, CFO compensation and ICI cancellation schemes are developed in Section 5.5 and simulation results show the effectiveness of these schemes [WLW+14, WLW+16b]. Lastly, the two-way SISO relaying scenario is extended by employing a MIMO relay in Section 5.6. Therein, multiple antennas at the relay facilitate the application of MIMO techniques due to enhanced spatial degrees of freedom. To this end, multi-layer detection schemes in MIMO systems, e.g., successive interference cancellation (SIC), can be used to estimate both source messages separately [WWD13b, WWD14b, WLW+16b]. The relay codeword is then calculated by XOR operation and broadcast by, e.g., OSTBC. Performance evaluation indicates that using common MIMO schemes accounting for low complexity approaches the APP-base schemes in some specific cases.

Chapter 6

Two-Way Distributed Relaying

6.1 Overview

Similar to the extension from one-way SISO relaying in Chapter 3 to one-way distributed relaying in Chapter 4, distributed relays are also allowed in this chapter as an extension from the two-way relaying communication with a single relay in Chapter 5. Due to the increased number of available relay applying PLNC, the possibility that at least one relay estimating the network coded message correctly is higher. By letting only relays with error-free decoding results of the XORed packet transmit to the sources in the BC phase, error propagation can be avoided effectively. Moreover, the characteristic that different relays are able to decode one source message correctly can be exploited in designing the distributed relaying scheme adaptively. The corresponding signaling overhead needs also to be considered adequately in performance evaluation. Taking these aspects into account, novel adaptive BC transmission approaches are studied in this chapter in the context of distributed two-way relaying networks.

The basic system model as well as transmission principles are described first in Section 6.2, where two sources exchange information via multiple relays in two phases. Subsequently, a traditional adaptive BC transmission scheme is presented in Section 6.3 by allowing only relays with correctly decoded XORed message to participate in the BC transmission. To fully exploit the property of the APP-based PLNC schemes in case of distributed two-way relaying, the event that a relay only perfectly estimates one individual source message is specified, which motivates a modified adaptive BC transmission

scheme as depicted in Section 6.4 [WWD14a, WLW+16b]. An efficient signaling strategy is also presented for practical implementation of the proposed adaptive scheme. In view of performance analysis, a semi-analytical derivation of the outage probability for the end-to-end system is conducted. These outage results as well as error rate and throughput performance from link-level simulation are given in Section 6.5. In Section 6.6, the content and main conclusions of this chapter is summarized in the final course.

6.2 System Model

The two-phase two-way distributed relaying system model is shown in Fig. 6.1, where both sources and $K > 1$ relays are equipped with a single antenna. In the MA phase, sources A and B transmit to relay R_k, $k = 1, 2, \cdots, K$, simultaneously, resulting in the superimposed receive signal on the ℓth subcarrier at R_k as

$$y_{\mathrm{R},k,\ell} = h_{\mathrm{AR},k,\ell} x_{\mathrm{A},\ell} + h_{\mathrm{BR},k,\ell} x_{\mathrm{B},\ell} + n_{\mathrm{R},k,\ell} \, . \tag{6.1}$$

This is essentially identical to (5.57) in Section 5.6 for MIMO two-way relaying, but k is intended for the relay indexing instead of antenna indexing. Upon receiving $\mathbf{y}_{\mathrm{R},k}$, each relay R_k estimates the network coded message $\mathbf{c}_{\mathrm{R},k}$ individually. Note that since the relays are unaware of the receive signal from each other, the schemes in Section 5.6 facilitated from the MIMO-relaying configuration are not implementable. To this end, each relay together with the source pair forms the MA transmission in the single-antenna scenario, where the APP-based PLNC schemes presented in Section 5.3 can be applied accordingly. Assuming that all relays are able to decode the XORed codeword correctly, i.e., $\mathbf{c}_{\mathrm{R},k} = \mathbf{c}_{\mathrm{A}} \oplus \mathbf{c}_{\mathrm{B}}$, the spatial diversity exploiting schemes can be employed in the BC phase. For example, distributed Alamouti is used when $K = 2$ [ZB11]. Besides, relay selection is studied in [LLV10]. Here, typically as applied in Chapter 4, the relays employ D-OSTBC with R_k transmitting its spatial component in the OSTBC matrix. This yields the ℓth receive signal at source u, $u \in [\mathrm{A}, \mathrm{B}]$

$$y_{u,\ell} = \sum_{k=1}^{K} h_{\mathrm{R}u,k,\ell} x_{\mathrm{R},k,\ell} + n_{u,\ell} \tag{6.2}$$

and the corresponding equivalent system equation ignoring the data rate loss from OSTBC design

$$y_{u,\ell} = \sqrt{\frac{1}{K} \sum_{k=1}^{K} |h_{\mathrm{R}u,k,\ell}|^2} x_{\mathrm{R},\ell} + n_{u,\ell} \, . \tag{6.3}$$

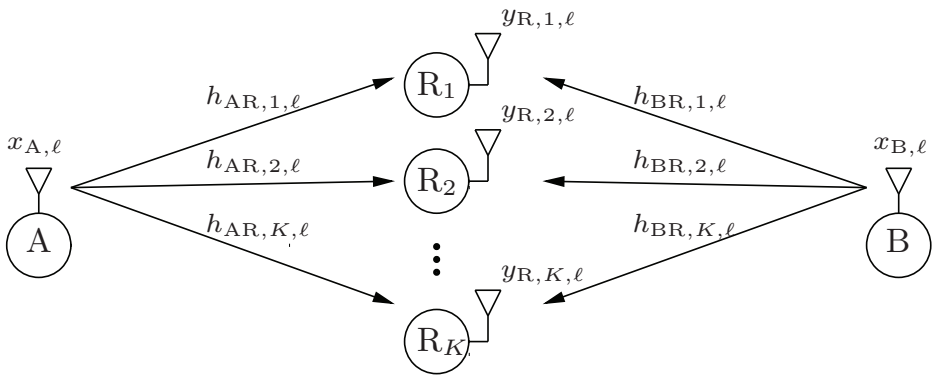

(a) MA phase

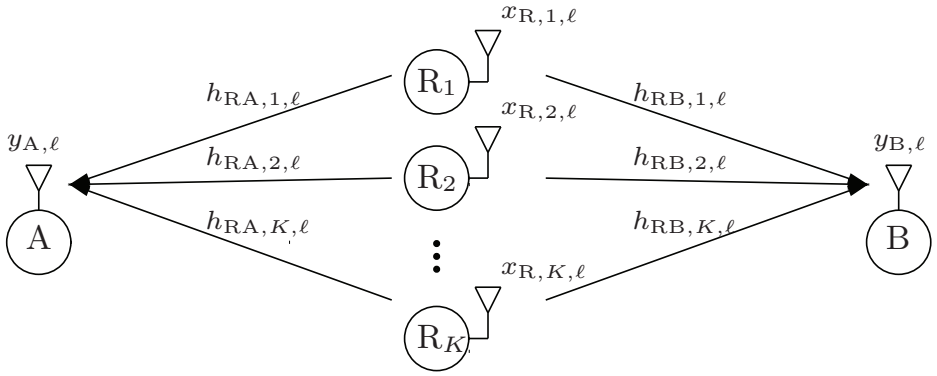

(b) BC phase

Figure 6.1: System model of a two-phase two-way relaying system with K distributed single-antenna relays. Both sources transmit to the relays simultaneously in the MA phase (a), while the relays transmit using distributed space-time codes in the BC phase (b).

After reception in the BC phase, space-time linear detection is performed at each source with respect to the applied D-OSTBC before estimating the relay codeword. Consequently, the desired message from the counterpart is determined by network decoding.

6.3 Traditional Adaptive Broadcast Transmission

Based on [ZB11], a traditional adaptive BC transmission scheme using D-OSTBC is presented in this section [WWD14a]. The core role is to let only relays that estimate the network coded message correctly transmit in the BC phase. After the scheme description, an outage analysis is given to analytically evaluate the performance of the adaptive scheme.

6.3.1 Scheme Description

As indicated in Chapter 4, the key issue to mitigate error propagation in DF-based distributed relaying networks is that relays with correct decoding results forward the source message while failing relays keep silent. Therefore, the relays should be aware of the decoding status and adapt D-OSTBC transmission in the BC phase correspondingly. To this end, the application of the same CRC code with perfect error detection functionality and negligible overhead is assumed at both sources.

In the traditional adaptive BC transmission scheme, each relay R_k can determine its decoding status about the network coded message using the employed CRC code since the XORed combination of two arbitrary codewords is still a valid codeword in the codebook assuming linear channel codes. Note that this is a straightforward extension from one-way relaying [LW03] to two-way relaying. Specifically, only relays decoding the network coded message correctly, i.e., $\mathbf{c}_{\mathrm{R},k} = \mathbf{c}_{\mathrm{A}} \oplus \mathbf{c}_{\mathrm{B}}$, participate in the BC transmission using, e.g., D-OSTBC. Denoting $\mathcal{D}_{\mathrm{R}}$ the decoding set that contains the error-free relays in the MA phase with respect to the XORed message, the traditional adaptive BC transmission scheme is summarized as follows.

- If $\mathcal{D}_{\mathrm{R}} \neq \emptyset$, $\mathrm{R}_k \in \mathcal{D}_{\mathrm{R}}$ transmit to the source nodes. Accordingly, the BC transmission in (6.2) is adapted to

$$y_{u,\ell} = \sum_{\mathrm{R}_k \in \mathcal{D}_{\mathrm{R}}} h_{\mathrm{R}u,k,\ell} x_{\mathrm{R},k,\ell} + n_{u,\ell} \ , \tag{6.4}$$

  which implies that the involved relays $\mathrm{R}_k \in \mathcal{D}_{\mathrm{R}}$ send their corresponding layers in the employed OSTBC matrix. For example, a two-way relaying network with $K = 3$ relays is considered in Fig. 6.2(a), where R_1 and R_2 decode the network coded message correctly. Therefore, these two relays transmit in the BC phase using $\mathbf{T}_{\mathrm{A}\oplus\mathrm{B}}$ with respect to the XORed message while R_3 is silent.

  After receiving in the BC phase, each source performs D-OSTBC detection and estimates the relay message. Subsequently, network decoding is applied to retrieve the desired message.

- If no relay is able to decode correctly, i.e., $\mathcal{D}_{\mathrm{R}} = \emptyset$, a MA outage occurs resulting in an end-to-end outage, as shown in Fig. 6.2(b).

6.3.2 Outage Analysis

In this subsection, the general outage analysis in [LW03] for one-way relaying is extended to the two-way context. With the help of the total probability law,

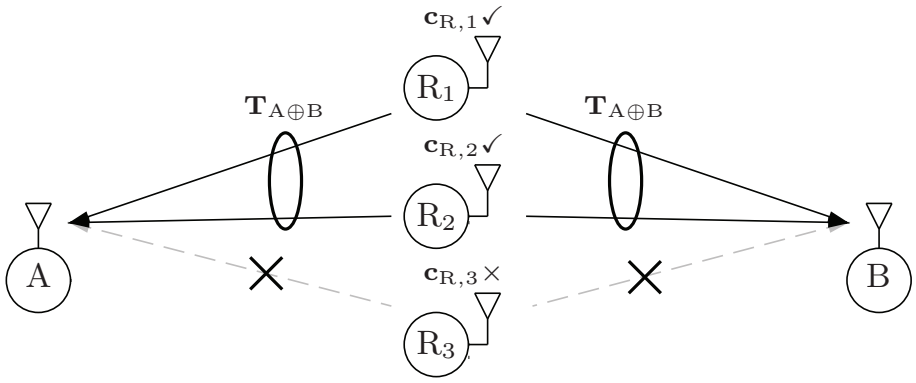

(a) Two relays decode the XORed message correctly

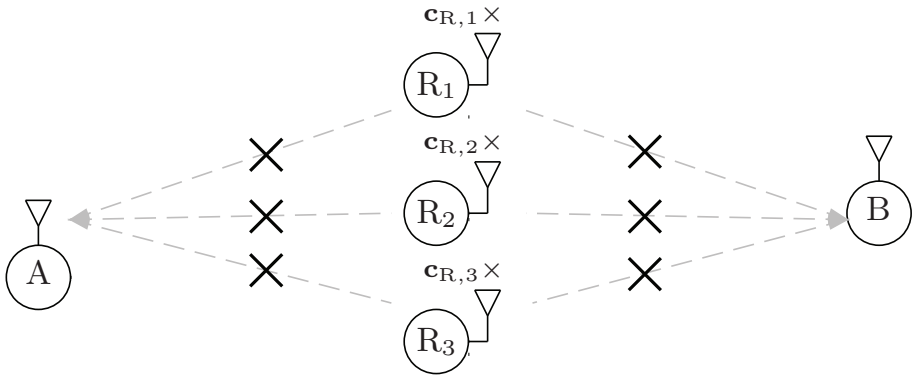

(b) All relays fail to decode the XORed message

Figure 6.2: Two examples for graphical illustration of the traditional adaptive BC transmission scheme with $K = 3$ relays. Gray dashed lines represent links without information transmission.

the end-to-end outage probability P_{out} of the distributed two-way relaying system is given by

$$P_{\mathrm{out}} = \sum_{\mathcal{D}_{\mathrm{R}}} \Pr\{\mathcal{D}_{\mathrm{R}}\} \left(1 - \prod_{u=\{\mathrm{A},\mathrm{B}\}} \Big(1 - \Pr\{R > I_u | \mathcal{D}_{\mathrm{R}}\} \Big) \right), \tag{6.5}$$

where $\Pr\{\mathcal{D}_{\mathrm{R}}\}$ represents the probability that a certain decoding set $\mathcal{D}_{\mathrm{R}}$ occurs. Furthermore, $\Pr\{R > I_u | \mathcal{D}_{\mathrm{R}}\}$ denotes the probability that source u is in outage as the target rate R in the BC phase is greater than the corresponding mutual information I_u between the active relays and source u. Assuming the application of D-OSTBC without rate loss due to orthogonal code design, I_u can be formulated as [LW03]

$$I_u = \frac{1}{L} \sum_{\ell=1}^{L} \log_2 \left(1 + \frac{\mathrm{SNR}}{|\mathcal{D}_{\mathrm{R}}|} \sum_{\mathrm{R}_k \in \mathcal{D}_{\mathrm{R}}} |h_{\mathrm{R}u,k,\ell}|^2 \right) \tag{6.6}$$

using the equivalent system equation (6.3) for OSTBC. Note that this expression is an average over the subcarriers in one coded OFDM symbol, whereas the corresponding derivations in [LW03] are respective of flat fading channels without OFDM. Furthermore, the transmit power at the relay cluster is normalized among the $|\mathcal{D}_{\mathrm{R}}|$ active relays involved in the BC transmission. In contrast to one-way relaying, the two-way relaying system is in outage, when at least one source fails to decode the relay message as indicated by the product in (6.5). When $\mathcal{D}_{\mathrm{R}} = \emptyset$ occurs, the system is in outage with probability 1 since no relay transmits if they all fail to decode, or equivalently, the outage probability in this case is given by

$$\Pr\{\mathcal{D}_{\mathrm{R}} = \emptyset\}\Pr\{R > I_u | \mathcal{D}_{\mathrm{R}} = \emptyset\} = \Pr\{\mathcal{D}_{\mathrm{R}} = \emptyset\} \, . \tag{6.7}$$

Outage Analysis in Symmetric Networks

In this subsection, a special case is examined for outage analysis of the traditional adaptive BC transmission scheme, where all channels in the two-way relaying system have identical normalized variance, i.e., $\sigma^2_{h_{u\mathrm{R},k}} = \sigma^2_{h_{\mathrm{R}u,k}} = 1$. Geographically, all relays are assumed to be located at the same position but still the involved channels are uncorrelated. In such a symmetric condition, the outage behavior at all relays is statistically equivalent. Correspondingly, the system end-to-end outage probability can be expressed as

$$\begin{aligned} P_{\mathrm{out}} = & \sum_{\kappa=0}^{K} \binom{K}{\kappa} \overbrace{(1-p_{\mathrm{R}})^{\kappa} p_{\mathrm{R}}^{K-\kappa}}^{W_\kappa} \\ & \times \left(1 - \left(1 - \Pr\left\{ R > I_{\mathrm{A}} \middle| |\mathcal{D}_{\mathrm{R}}| = \kappa \right\} \right)^2 \right) . \end{aligned} \tag{6.8}$$

In the above equation, p_{R} represents the outage probability at one relay with respect to the network coded message. Additionally, the kernel W_κ denotes the probability that a specific combination of κ relays decode the network coded message correctly with $\binom{K}{\kappa}$ possibilities in total, $\kappa = 0, \cdots, K$. The calculation in (6.8) sums up the outage probability in the BC phase when κ relays are error-free with respect to the network coded message over $0 \leq \kappa \leq K$. Note that p_{R} is derived in [JK10] based on the capacity region of the MA channel [CT91], which corresponds to SCD. In this work, practical APP-based PLNC schemes presented in Section 5.3 are considered, where p_{R} is achieved by link-level simulations. Therefore, the outage analysis in this chapter relies on a semi-analytical method.

6.4 Modified Adaptive Broadcast Transmission

In case of all relays failing to decode the XORed message correctly, it could happen that only one source message is correctly decoded at a relay. This event is ignored in the traditional adaptive BC transmission scheme presented in the previous section, however can be incorporated in designing two-way distributed relaying strategies by letting the relay broadcast the individual error-free message, resulting in a modified adaptive BC scheme depicted in this section [WWD14a]. Furthermore, outage analysis and signaling overhead for the adaptive BC transmission scheme are examined as well.

6.4.1 Scheme Description

In the traditional scheme, the system is in outage when all relays fail to decode the network coded message. However, it might happen that some relays only decode one source message correctly while the network coded message is erroneous when SCD or G-JCNC is applied for PLNC decoding[1]. This case is ignored in the traditional scheme, indicating that some relays discard useful information that may support the BC transmission when $\mathcal{D}_{\mathrm{R}} = \emptyset$ occurs.

In order to improve the end-to-end outage performance, the traditional adaptive scheme is extended by incorporating this case as well. To this end, the relays that only decode $\mathbf{c}_{\mathrm{A}}$ correctly are collected in the decoding set $\mathcal{D}_{\mathrm{R}}^{\mathrm{A}}$. Note that the relays belonging to $\mathcal{D}_{\mathrm{R}}^{\mathrm{A}}$ must not be in $\mathcal{D}_{\mathrm{R}}$. The decoding set $\mathcal{D}_{\mathrm{R}}^{\mathrm{B}}$ is defined similarly. The modified adaptive BC transmission scheme is defined as follows.

- If $\mathcal{D}_{\mathrm{R}} \neq \emptyset$, the relays $\mathrm{R}_k \in \mathcal{D}_{\mathrm{R}}$ transmit the relay message using D-OSTBC as in the traditional scheme.
- If $\mathcal{D}_{\mathrm{R}} = \emptyset$, $\mathcal{D}_{\mathrm{R}}^{\mathrm{A}} \neq \emptyset$ or $\mathcal{D}_{\mathrm{R}}^{\mathrm{B}} \neq \emptyset$, the relays $\mathrm{R}_i \in \mathcal{D}_{\mathrm{R}}^{\mathrm{A}}$ and $\mathrm{R}_j \in \mathcal{D}_{\mathrm{R}}^{\mathrm{B}}$ transmit $\mathbf{x}_{\mathrm{R},i}^{\mathrm{A}}$ and $\mathbf{x}_{\mathrm{R},j}^{\mathrm{B}}$ using their respective D-OSTBCs to the sources simultaneously in the BC phase. Here, $\mathbf{x}_{\mathrm{R},i}^{\mathrm{A}}$ and $\mathbf{x}_{\mathrm{R},j}^{\mathrm{B}}$ denote the correctly decoded individual source messages from A and B after D-OSTBC encoding, respectively. Therefore, the ℓ-th receive signal at source u is formulated as

$$y_{u,\ell} = \sum_{\mathrm{R}_i \in \mathcal{D}_{\mathrm{R}}^{\mathrm{A}}} h_{\mathrm{R}u,i,\ell} x_{\mathrm{R},i,\ell}^{\mathrm{A}} + \sum_{\mathrm{R}_j \in \mathcal{D}_{\mathrm{R}}^{\mathrm{B}}} h_{\mathrm{R}u,j,\ell} x_{\mathrm{R},j,\ell}^{\mathrm{B}} + n_{u,\ell} \,. \tag{6.9}$$

[1]Note that both SCD and G-JCNC estimate not only the relay message $\mathbf{c}_{\mathrm{R}}$ but also the individual source messages $\mathbf{c}_{\mathrm{A}}$ and $\mathbf{c}_{\mathrm{B}}$. However, JCNC is not applicable because only the XORed message is estimated without explicit recovery of the individual messages.

In Fig.6.3(a), an example with $K = 3$ relays is shown to illustrate this case. As can be observed in the figure, R_1 and R_2 only decode the source message from A correctly and thus transmit it using D-OSTBC $\mathbf{T}_\mathrm{A}$ with respect to $\mathbf{c}_\mathrm{A}$ in the BC phase. On the other hand, $\mathbf{c}_\mathrm{B}$ is correctly decoded at R_3, which is modulated to $\mathbf{x}_{\mathrm{R},3}^{\mathrm{B}}$ and broadcast simultaneously with the space-time coded $\mathbf{x}_{\mathrm{R},1}^{\mathrm{A}}$ and $\mathbf{x}_{\mathrm{R},2}^{\mathrm{A}}$.

Upon receiving in the BC phase, each source u subtracts the self-interference term with respect to $\mathbf{x}_\mathrm{R}^u$ in (6.9) and performs D-OSTBC detection to estimate the message from the counterpart.

- Otherwise, the system is in outage.

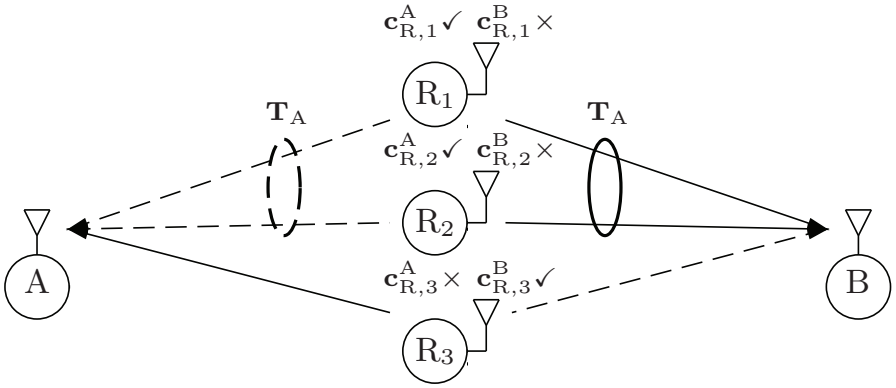

(a) Two relays decode $\mathbf{c}_\mathrm{A}$ correctly, one relay decodes $\mathbf{c}_\mathrm{B}$ correctly

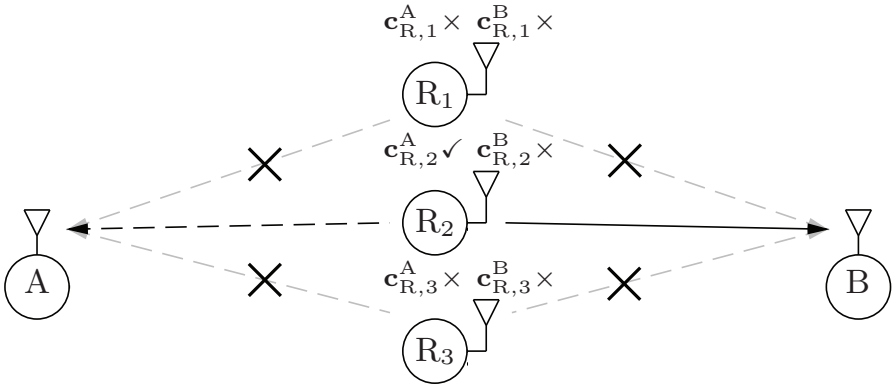

(b) One relay decodes $\mathbf{c}_\mathrm{A}$ correctly, no relay decodes $\mathbf{c}_\mathrm{B}$ correctly

Figure 6.3: Two examples for graphical illustration of the modified adaptive BC transmission scheme with $K = 3$ relays. Black dashed lines represent self-interference links whereas gray dashed lines represent links without information transmission.

Note that simultaneously broadcasting $\mathbf{c}_{\mathrm{A}\oplus\mathrm{B}}$ and $\mathbf{c}_u$ when $\mathcal{D}_\mathrm{R} \neq \emptyset$ and $\mathcal{D}_\mathrm{R}^u \neq \emptyset$ is problematic due to superposition of different messages. Thus, the

individual message is only transmitted when $\mathcal{D}_\mathrm{R} = \emptyset$ in the modified adaptive BC scheme. Moreover, in case of $\mathcal{D}_\mathrm{R} = \emptyset$, one empty set from $\mathcal{D}_\mathrm{R}^u$, e.g., $\mathcal{D}_\mathrm{R}^\mathrm{A} = \emptyset$, leads to no information about $\mathbf{c}_\mathrm{A}$ received at source B, also resulting in an end-to-end outage since a successful transmission is only achieved if both source messages are exchanged correctly. An example is shown in Fig.6.3(b), where only R_2 decodes the individual source message $\mathbf{c}_\mathrm{A}$ from A correctly, which is further forwarded in the BC phase. However, no relay succeeds in decoding $\mathbf{c}_\mathrm{B}$. Correspondingly, source A gets no desired message and thus the system is in outage. As a result, the system performance is improved when both $\mathcal{D}_\mathrm{R}^\mathrm{A}$ and $\mathcal{D}_\mathrm{R}^\mathrm{B}$ are not empty sets.

6.4.2 Outage Analysis

Recall that in the traditional adaptive scheme, the system is in outage if $\mathcal{D}_\mathrm{R} = \emptyset$ happens, i.e., no relay is able to decode the relay message correctly. In contrast, the modified adaptive scheme exploits the decoding results of the individual source messages at the relays for SCD and G-JCNC. Thus, relays decoding $\mathbf{c}_\mathrm{R}$ erroneously but one individual source message $\mathbf{c}_u$ correctly can assist the end-to-end transmission to improve the overall system performance. In this context, the end-to-end outage probability in (6.5) for the traditional scheme only has to be rewritten by adapting the outage in case of $\mathcal{D}_\mathrm{R} = \emptyset$ (first term in the summation with $k = 0$) to yield that for the modified scheme, which is given by

$$P_\mathrm{out} = \sum_{\mathcal{D}_\mathrm{R}/\emptyset} \Pr\{\mathcal{D}_\mathrm{R}\} \left(1 - \prod_{u=\{\mathrm{A},\mathrm{B}\}} \Big(1 - \Pr\{R > I_u | \mathcal{D}_\mathrm{R}\}\Big)\right) \tag{6.10a}$$

$$+ \sum_{(\mathcal{D}_\mathrm{R}^\mathrm{A}, \mathcal{D}_\mathrm{R}^\mathrm{B}) | \mathcal{D}_\mathrm{R} = \emptyset} \Pr\{(\mathcal{D}_\mathrm{R}^\mathrm{A}, \mathcal{D}_\mathrm{R}^\mathrm{B})\} \times \left(1 - \prod_{u=\{\mathrm{A},\mathrm{B}\}} \Big(1 - \Pr\{R > I_u^* | (\mathcal{D}_\mathrm{R}^\mathrm{A}, \mathcal{D}_\mathrm{R}^\mathrm{B})\}\Big)\right) \tag{6.10b}$$

using the total probability law. Therein, it can be implied by the summation in (6.10b), that the event $\mathcal{D}_\mathrm{R} = \emptyset$ is divided into sub-events with different combinations of relays $(\mathcal{D}_\mathrm{R}^\mathrm{A}, \mathcal{D}_\mathrm{R}^\mathrm{B})$ decoding one source message correctly. Correspondingly, the following relation holds

$$\Pr\{\mathcal{D}_\mathrm{R} = \emptyset\} = \sum_{(\mathcal{D}_\mathrm{R}^\mathrm{A}, \mathcal{D}_\mathrm{R}^\mathrm{B}) | \mathcal{D}_\mathrm{R} = \emptyset} \Pr\{(\mathcal{D}_\mathrm{R}^\mathrm{A}, \mathcal{D}_\mathrm{R}^\mathrm{B})\} \,. \tag{6.11}$$

Furthermore, the mutual information I_u^* in (6.10b) between the $|\mathcal{D}_\mathrm{R}^u|$ relays with correctly decoded individual message $\mathbf{c}_\mathrm{R}^u$ and the targeted end node for

one coded OFDM symbol is defined as

$$I_u^* = \frac{1}{L}\sum_{\ell=1}^{L}\log_2\left(1+\frac{\mathrm{SNR}}{|\mathcal{D}_{\mathrm{R}}^{\mathrm{A}}|+|\mathcal{D}_{\mathrm{R}}^{\mathrm{B}}|}\sum_{\mathrm{R}_k\in\mathcal{D}_{\mathrm{R}}^{u}}|h_{\mathrm{R}u,k,\ell}|^2\right). \tag{6.12}$$

Note that when $\mathcal{D}_{\mathrm{R}}$ is empty, a total number of $|\mathcal{D}_{\mathrm{R}}^{\mathrm{A}}|+|\mathcal{D}_{\mathrm{R}}^{\mathrm{B}}|$ relays are active and participate in the D-OSTBC transmission. Thus, the normalization factor $|\mathcal{D}_{\mathrm{R}}^{\mathrm{A}}|+|\mathcal{D}_{\mathrm{R}}^{\mathrm{B}}|$ in (6.12) guarantees that the transmit power at the relay cluster is normalized among the active relays in this case. Additionally, the outage probability in (6.10b) when $\mathcal{D}_{\mathrm{R}}=\emptyset$ occurs for the modified scheme is smaller than $\Pr\{\mathcal{D}_{\mathrm{R}}=\emptyset\}$ in (6.7) for the traditional scheme, indicating the superior performance of the modified scheme.

Outage Analysis in Symmetric Networks

Similar to the traditional scheme demonstrated in the previous section, the special case of symmetric link characteristics is considered for the modified adaptive scheme. The outage behavior remains unchanged when at least one relay decodes the relay message correctly, which has been derived as shown in (6.8) when $1\le\kappa\le K$. Thus, the first term, i.e., (6.10a) can be rewritten in the same form as (6.8) except that κ starts with 1. The second term, i.e., (6.10b) can be reformulated as

$$\begin{aligned}P^* =& \sum_{q=0}^{K}\sum_{r=0}^{q}\binom{K}{r}\binom{K-r}{q-r}W_{r,q-r}^*\\ &\times\left(1-\prod_{u=\{\mathrm{A},\mathrm{B}\}}\left(1-\Pr\left\{R>I_u^*\middle|(|\mathcal{D}_{\mathrm{R}}^{\mathrm{A}}|=r,|\mathcal{D}_{\mathrm{R}}^{\mathrm{B}}|=q-r)\right\}\right)\right)\end{aligned} \tag{6.13}$$

to distinguish the cases with different number of relays decoding one source message correctly. Specifically, the kernel $W_{r,q-r}^*$ denotes the probability of one possible combination of q relays that yield the decoding results fulfilling $|\mathcal{D}_{\mathrm{R}}^{\mathrm{A}}|=r$, $|\mathcal{D}_{\mathrm{R}}^{\mathrm{B}}|=q-r$ and $|\mathcal{D}_{\mathrm{R}}|=0$ with $\binom{K}{r}\binom{K-r}{q-r}$ possibilities in total. Here $q=|\mathcal{D}_{\mathrm{R}}^{\mathrm{A}}|+|\mathcal{D}_{\mathrm{R}}^{\mathrm{B}}|$ represents the total number of relays with one correctly estimated source message. Now, a MA outage occurs if either $r=0$ or $q-r=0$ since only one source message is recovered correctly within the relay cluster leading to an end-to-end outage. In contrast, both source messages are transmitted in the BC phase when $2\le q\le K$ and $1\le r\le q-1$. As a result, both sources have the chance to recover the desired message from the counterpart.

In order to deduce $W_{r,q-r}^*$, $p_{\mathrm{R}}^{\mathrm{A}}$ and $p_{\mathrm{R}}^{\mathrm{B}}$ denoting the outage probabilities at one relay regarding the individual messages are again achieved by simulations

for SCD and G-JCNC. Actually, $W^*_{r,q-r}$ is independent on r in symmetric networks because the outage characteristic of the r relays decoding $\mathbf{c}_\mathrm{A}$ correctly and $q-r$ relays decoding $\mathbf{c}_\mathrm{B}$ correctly are essentially identical. Therefore, taking the overall $2K$ individual decoding results among K relays into account, the expression of $W^*_{r,q-r}$ for different APP-based schemes is given by

$$W^*_{r,q-r} = \begin{cases} (1-p_\mathrm{R}^\mathrm{A})^q (p_\mathrm{R}^\mathrm{A})^{2K-q} & \text{P-SCD} \\ (p_\mathrm{R}^\mathrm{B}-p_\mathrm{R}^\mathrm{A})^q (p_\mathrm{R}^\mathrm{A})^{K-q} & \text{S-SCD} \\ (p_\mathrm{R}-p_\mathrm{R}^\mathrm{A})^q (2p_\mathrm{R}^\mathrm{A}-p_\mathrm{R})^{K-q} & \text{G-JCNC} \end{cases} \tag{6.14}$$

and illustrated as follows.

- For P-SCD, p_R^A and p_R^B are statistically equal among all relays in a symmetric network and independent from each other. Note that the following relation holds

$$p_\mathrm{R} = 1-(1-p_\mathrm{R}^\mathrm{A})(1-p_\mathrm{R}^\mathrm{B}) = 1-(1-p_\mathrm{R}^\mathrm{A})^2 \tag{6.15}$$

  since the network coded message is erroneous if at least one individual source message is falsely decoded. The kernel $W^*_{r,q-r}$ corresponds to q times correct decoding and $2K-q$ times erroneous decoding with respect to the individual messages, amounting to $2K$ individual decoding results in total.

- For S-SCD, let p_R^A denote the outage probability of decoding the message from the stronger link. p_R^B then represents the outage probability of the SU decoding with respect to the interference reduced signal. Note that the performance of the successive decoding is dependent on the initial decoding, indicating that both sources messages will be erroneous if the initial decoding fails. In other words, both decoding processes are highly correlated with each other. Therefore, $p_\mathrm{R} = p_\mathrm{R}^\mathrm{B} > p_\mathrm{R}^\mathrm{A}$ holds with the difference $p_\mathrm{R}^\mathrm{B} - p_\mathrm{R}^\mathrm{A}$ representing the probability that the successive decoding fails even though the initial decoding succeeds. To this end, the probabilities that a relay only decodes one source message from the initial decoding correctly and fails to decode both sources messages yield $(p_\mathrm{R}^\mathrm{B} - p_\mathrm{R}^\mathrm{A})$ and p_R^A, respectively, which can be used to formulate the representation of $W^*_{r,q-r}$.

- For G-JCNC, p_R^A and p_R^B are statistically equal but strongly dependent with each other since both source messages are jointly considered and estimated in the decoder. Furthermore, let $\mathcal{A}$ and $\mathcal{B}$ denote the events that a relay fails to decode $\mathbf{c}_\mathrm{A}$ and $\mathbf{c}_\mathrm{B}$, respectively. By some simple

probability manipulations, the probability $\Pr\{\overline{\mathcal{A}}\mathcal{B}\} = \Pr\{\mathcal{A}\overline{\mathcal{B}}\}$ that only one source message is correctly decoded in a symmetric network can be formulated as [DS11]

$$\begin{aligned}\Pr\{\overline{\mathcal{A}}\mathcal{B}\} &= \Pr\{\mathcal{B}|\overline{\mathcal{A}}\}\Pr\{\overline{\mathcal{A}}\} \\ &= (1 - \Pr\{\overline{\mathcal{B}}|\overline{\mathcal{A}}\})\Pr\{\overline{\mathcal{A}}\} \\ &= \Pr\{\overline{\mathcal{A}}\} - \Pr\{\overline{\mathcal{A}}\overline{\mathcal{B}}\} \\ &= p_{\mathrm{R}} - p_{\mathrm{R}}^{\mathrm{A}} \,.\end{aligned} \tag{6.16}$$

Here, $\Pr\{\overline{\mathcal{A}}\overline{\mathcal{B}}\} = 1 - p_{\mathrm{R}}$ and $\Pr\{\overline{\mathcal{A}}\} = 1 - p_{\mathrm{R}}^{\mathrm{A}}$ represent the probabilities that the relay succeeds to decode both source messages and the individual source message from A, respectively. Correspondingly, the probability that both source messages are erroneously decoded is derived using the completeness condition as

$$\Pr\{\mathcal{A}\mathcal{B}\} = 1 - \Pr\{\overline{\mathcal{A}}\mathcal{B}\} - \Pr\{\mathcal{A}\overline{\mathcal{B}}\} - \Pr\{\overline{\mathcal{A}}\overline{\mathcal{B}}\} = 2p_{\mathrm{R}}^{\mathrm{A}} - p_{\mathrm{R}} \,. \tag{6.17}$$

Consequently, the kernel $W_{r,q-r}^{*}$ can be represented easily with q relays decoding one source message correctly.

6.4.3 Signaling Overhead - CRC over the Air

In practical systems, all relays perform APP-based PLNC detection and decoding individually. By applying the same CRC code at both sources, each relay is aware of its own local decoding status about the relay message. As indicated before, regarding to SCD and G-JCNC, individual source messages can also be estimated, which is exploited in the modified adaptive scheme. Subsequently, the relays transmit adaptively using D-OSTBC in the BC phase, requiring extra signaling overhead as discussed in the sequel.

In the traditional adaptive scheme, each relay $\mathrm{R}_k \in \mathcal{D}_{\mathrm{R}}$ is actually not interested in the decoding status of the other relays but only transmits its own layer of the applied D-OSTBC, whereas the relays not in $\mathcal{D}_{\mathrm{R}}$ keep silent. In this manner, no extra signaling overhead is induced. It is noticed that these silent relays can switch into reception mode and therefore also overhear the signal transmitted by $\mathrm{R}_k \in \mathcal{D}_{\mathrm{R}}$. Based on this fact, in the modified adaptive scheme, if there are messages received within a dedicated time duration denoted as idle time T_{I}, each silent relay recognizes that at least one relay has decoded the relay message correctly. On the other hand, if the relay does not recognize any transmission during T_{I}, it knows that no relay is capable of correctly estimating $\mathbf{c}_{\mathrm{R}}$. In this case, the relay forwards the individual message $\mathbf{x}_{\mathrm{A}}$ or $\mathbf{x}_{\mathrm{B}}$ using its own layer with respect to the applied

D-OSTBC if it is in the decoding set $\mathcal{D}_{\mathrm{R}}^{\mathrm{A}}$ or $\mathcal{D}_{\mathrm{R}}^{\mathrm{B}}$, respectively. Otherwise, the system is in outage.

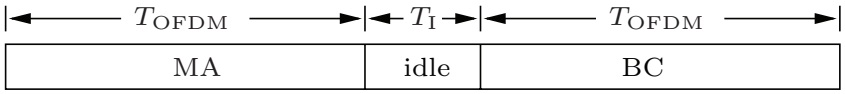

Figure 6.4: Time line of the modified adaptive BC transmission scheme in case of $\mathcal{D}_{\mathrm{R}} = \emptyset$. An idle time T_{I} is dedicated to adapt the transmission with one correctly decoded source message at the relays.

By such an implicit CRC exchange between the relays termed *CRC over the air*, no extra signaling overhead is required other than T_{I}. Recall that T_{OFDM} denotes the time duration to transmit one data frame, the overall time consumption to finish one end-to-end transmission yields $2T_{\mathrm{OFDM}} + T_{\mathrm{I}}$ for the modified adaptive scheme when $\mathcal{D}_{\mathrm{R}} = \emptyset$ occurs, as shown in Fig. 6.4.

6.5 Performance Evaluation

In this section, the performance of both the traditional scheme and the modified scheme with adaptive BC transmission are evaluated and compared. The APP-based PLNC schemes yield different characteristics respective of the adaptive transmission strategy, therefore, the performance for P-SCD, S-SCD and G-JCNC are investigated. Note that since JCNC only estimates the network coded message other than the individual source messages, it is not applicable in the modified adaptive scheme. Furthermore, JCNC is inferior to other APP-based schemes at each relay, as shown in Fig. 5.16. To this end, JCNC is not considered in the sequel for performance evaluations in distributed two-way relaying systems.

Outage Probability

With respect to outage probability analysis, a symmetric network is considered as a special case in Subsection 6.3.2 and 6.4.2, where the same channel gain is assumed for all links. In this part, the outage performance is evaluated with the employed parameters set as follows. The distance between every pair of source and relay nodes is normalized to 1, i.e., $d_{\mathrm{AR}} = d_{\mathrm{BR}} = 1$. The channels are assumed to be multi-path Rayleigh fading with $N_{\mathrm{H}} = 5$ equal power taps. As previously, OFDM with QPSK modulation and $L = 1024$ subcarriers is applied. An LDPC code of rate $R_{\mathrm{C}} = 0.5$ is employed for each OFDM symbol.

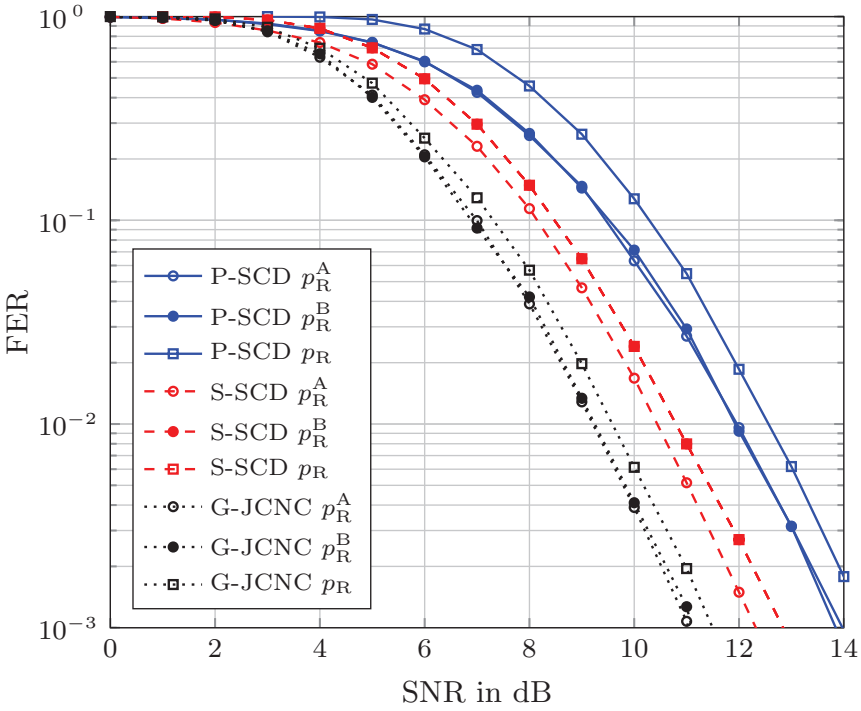

Figure 6.5: FER performance of the XORed codeword and the individual codewords at one relay in the middle between both sources for P-SCD, S-SCD and G-JCNC.

Since the MA outage is determined by different APP-based schemes employing practical decoders, the outage analysis is semi-analytical, where the outage probabilities p_R, p_R^A and p_R^B are achieved by simulating the FER for P-SCD, S-SCD and G-JCNC, respectively, as shown in Fig. 6.5. Note that P_R for the APP-based schemes are identical to FER_R shown in Fig. 5.16(a). It can be observed in Fig. 6.5 that the outage probabilities of both individual codewords p_R^A and p_R^B are identical for P-SCD and G-JCNC. The corresponding outage probability p_R is degraded since decoding errors for one individual source message lead to an outage of the network coded message. On the other hand, the outage probability of the stronger link p_R^A outperforms that of the weaker link p_R^B for S-SCD, while the performance of the network coded message is determined by the latter one. These observations confirm the elaboration in Subsection 6.4.2 that $p_R = p_R^B > p_R^A$.

In Fig. 6.6, the outage probabilities derived in Subsection 6.3.2 and 6.4.2 for the traditional scheme and the modified scheme in a symmetric network are shown. It can be observed that the modified scheme leads to reduced outage probability, especially for P-SCD due to independent decoding of both source messages. However, the improvement is almost negligible for S-SCD and G-JCNC when $K = 4$. This is attributed to the fact that for S-SCD p_R^B depends on p_R^A whereas p_R^A and p_R^B are highly correlated with each

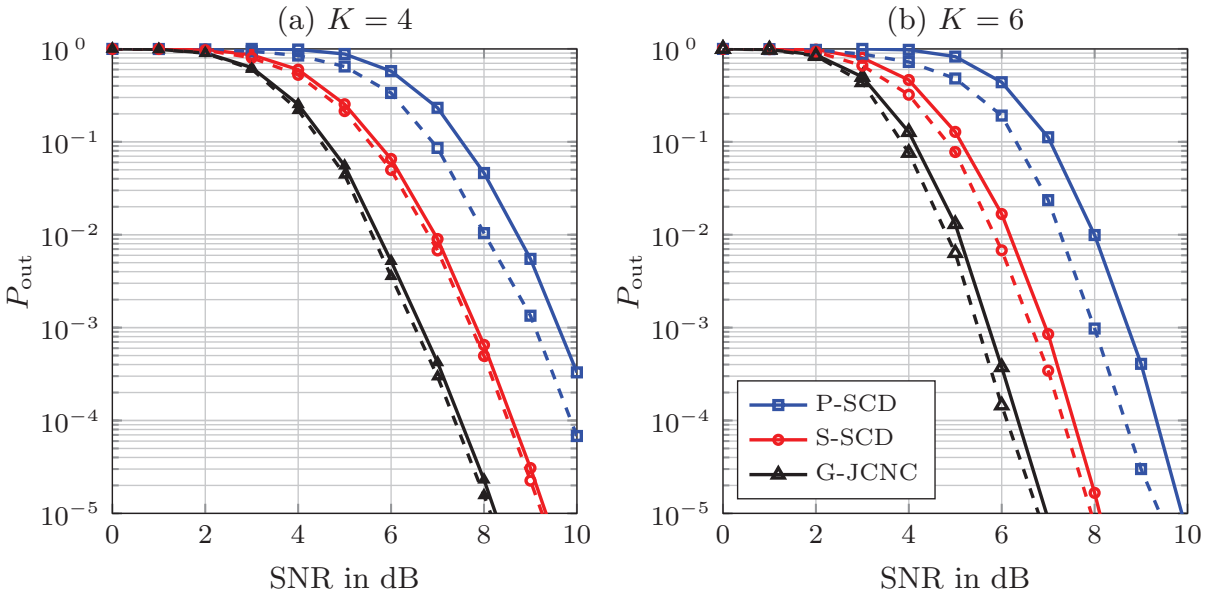

Figure 6.6: Outage probability P_{out} for both traditional scheme (-) and modified scheme (- -) using P-SCD, S-SCD and G-JCNC at each relay. A symmetric network is considered with equal statistics for all links. The targeted rate in the BC phase is set to $R = 0.5$. (a) for $K = 4$ relays and (b) for $K = 6$ relays.

other for G-JCNC. Therefore, it rarely occurs that one relay decodes only one source message correctly, especially in a strongly symmetric network with all links being statistically equal. The improvement grows and becomes more remarkable when $K = 6$ since the event that both $\mathcal{D}_{\text{R}}^{\text{A}}$ and $\mathcal{D}_{\text{R}}^{\text{B}}$ are not empty occurs more frequently with increasing number of relays, which basically provides larger diversity gain.

The improvement of the outage performance is visualized in Fig. 6.7 with increasing number of relays for a fixed SNR = 7dB. Obviously, growing K reduces the outage probability for all schemes. Crucially, the performance gain by using the modified scheme over the traditional scheme is enlarged with more relays.

In order to ascertain the reason of greater performance improvement with increasing number of relays, the event probabilities that different number of relays $|\mathcal{D}_{\text{R}}|$ decode the XORed message correctly as well as that both $\mathcal{D}_{\text{R}}^{\text{A}}$ and $\mathcal{D}_{\text{R}}^{\text{B}}$ are not empty set are numerically calculated from the link-level simulations. P-SCD is assumed as an example with $K = 2$ or $K = 3$ distributed relays. As can be observed in Fig. 6.8, the probabilities that $|\mathcal{D}_{\text{R}}| = 0$ relays and $|\mathcal{D}_{\text{R}}| = K$ relays succeed to decode the network coded message change from 1 to 0 and from 0 to 1 with growing SNR, respectively. Also shown in the figure is that the event probability for both $\mathcal{D}_{\text{R}}^{\text{A}}$ and

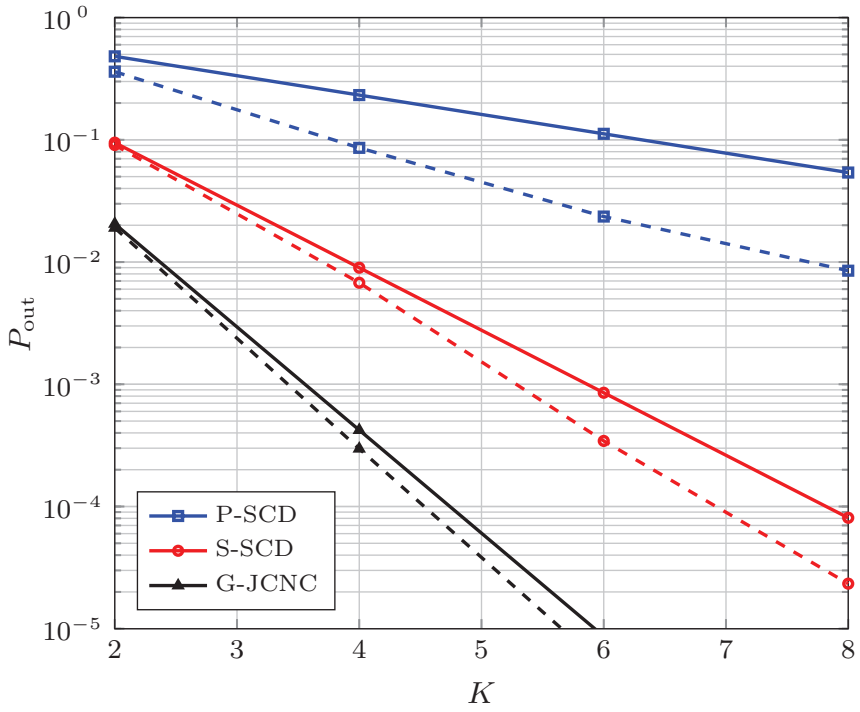

Figure 6.7: Outage probability P_{out} for both traditional scheme (-) and modified scheme (- -) using P-SCD, S-SCD and G-JCNC at each relay with SNR = 7dB and different number of relays. A symmetric network is considered with equal statistics for all links. The targeted rate in the BC phase is set to $R = 0.5$.

$\mathcal{D}_{\text{R}}^{\text{B}}$ being no empty set grows larger with more relays. Since the gain of the modified scheme stems from this event, more frequent occurrence of it contributes to enhanced performance improvement of the modified scheme, as observed in Fig. 6.6 and Fig. 6.7 for larger K.

Frame Error Rate & Throughput

For link-level simulations of the end-to-end system, similar parametrization as in the MA phase described previously is applied in the BC phase. Note that the performance improvement of the modified scheme over the traditional scheme is caused by the event that some relays decode $\mathbf{c}_{\text{A}}$ correctly and some relays decode $\mathbf{c}_{\text{B}}$ correctly. Apparently, this event occurs more frequently in asymmetric networks, where the two source-relay links are weighted differently from each other. To this end, a linear topology of the relay nodes is considered, as shown in Fig. 6.9. In this network, the K relays are equally distributed on a line $\text{R}_1 - \text{R}_K$ with d_{R} denoting the distance between R_1 and R_K. Therefore, the distance between two neighboring relays amounts to $d_{\text{R}}/(K-1)$. Furthermore, the angle of the two lines connecting the sources $\text{A} - \text{B}$ and the relays $\text{R}_1 - \text{R}_K$ respectively is denoted as θ_{R}, yielding the

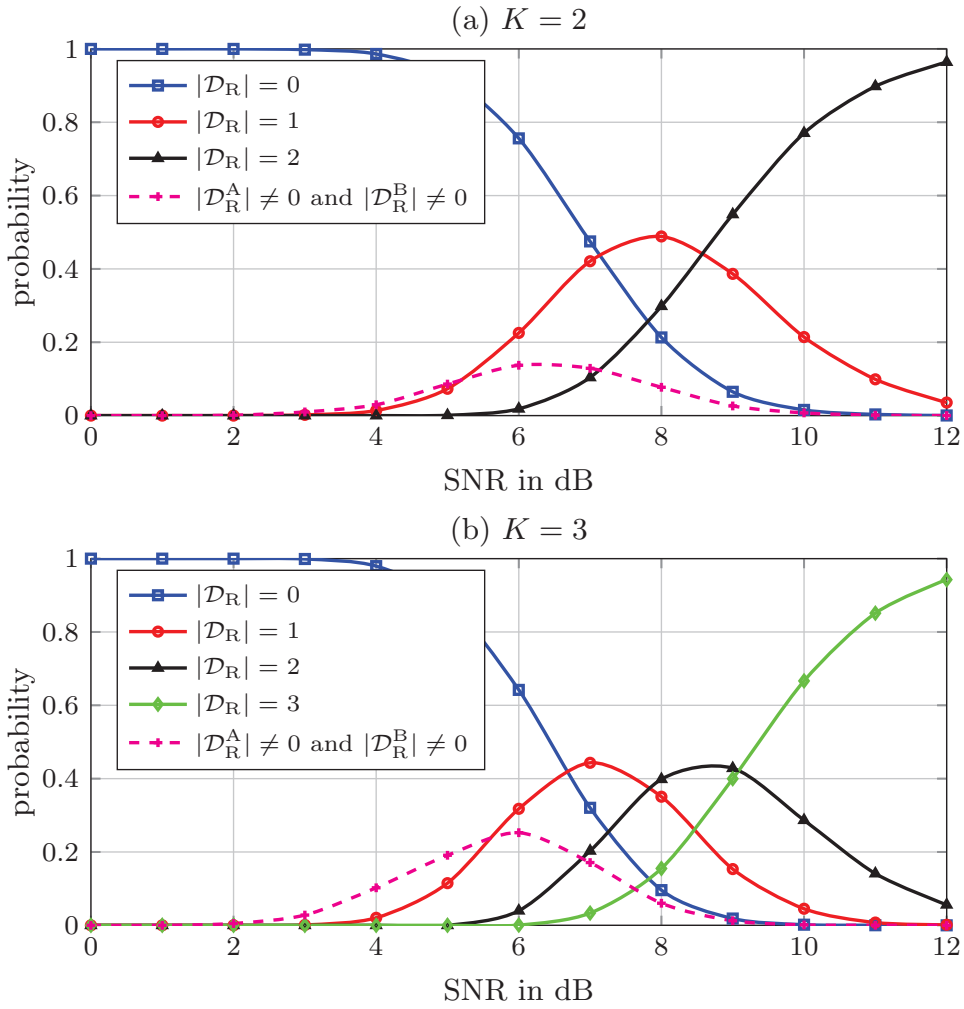

Figure 6.8: Event probabilities for different number of relays $|\mathcal{D}_\mathrm{R}|$ with error-free XORed message and for that both $\mathcal{D}_\mathrm{R}^\mathrm{A}$ and $\mathcal{D}_\mathrm{R}^\mathrm{B}$ are not empty considering P-SCD, (a) for $K = 2$ relays and (b) for $K = 3$ relays.

minimum and maximum distances as

$$d_\mathrm{min} = \sqrt{1 - d_\mathrm{R} \cos\theta_\mathrm{R} + \frac{d_\mathrm{R}^2}{4}} \tag{6.18a}$$

$$d_\mathrm{max} = \sqrt{1 + d_\mathrm{R} \cos\theta_\mathrm{R} + \frac{d_\mathrm{R}^2}{4}} \tag{6.18b}$$

between a source and a relay. For example, d_min corresponds to the link between source A and relay R_1 and d_max corresponds to the link between source A and relay R_K. Furthermore, small θ_R leads to highly asymmetric topology, in which the modified scheme is expected to benefit more. Note that $d_\mathrm{R} = 0$ results in the symmetric network, where all links of the same gain are assumed to be uncorrelated with each other. Additionally, the path-loss factor is set to $\alpha = 4$.

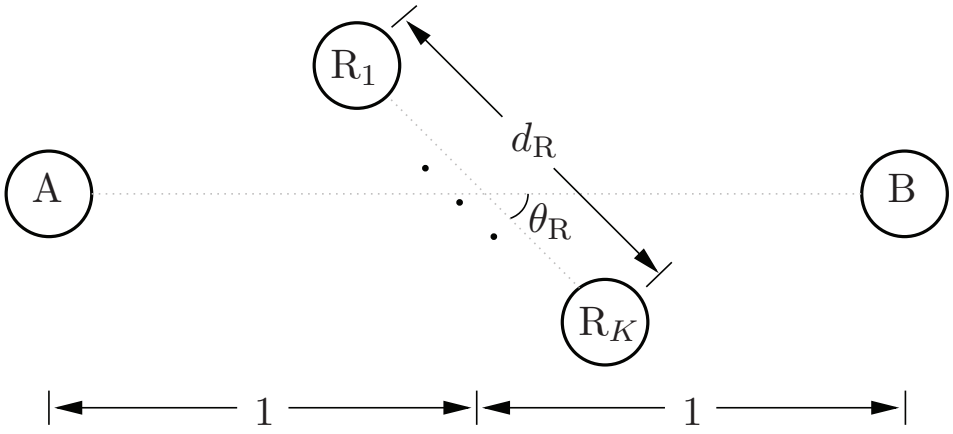

Figure 6.9: A two-way relaying network with K linearly positioned relays. Equal distance is assumed between neighboring relays. The two lines connecting the sources and the relays respectively form an angle θ_{R}.

In the sequel, $K = 4$ relays are assumed with rate matching for the adaptive BC transmission scheme, as employed in Chapter 4 to compensate the data rate loss cause by OSTBC. Specifically, when 2 relays are active, Alamouti code [Ala98] is applied. When 3 or 4 relays are active, the OSTBC of rate $R_{\mathrm{OSTBC}} = 3/4$ [TSC98] is applied with the channel code rate adapted by puncturing to $R'_{\mathrm{C}} = 2/3$. Therefore, the same data rate is achieved when different number of relays are active for transmission in the BC phase.

Fig. 6.10 shows the FER performance of the end-to-end transmission in a symmetric network with $d_{\mathrm{R}} = 0$ and $d_{\mathrm{R}} = 0.4$, respectively. Note that the latter case corresponds to a more realistic scenario since the relays have to be geographically distributed in practice. It can be observed in the figure, that in case of $d_{\mathrm{R}} = 0.4$, the performance is slightly degraded compared to the case for $d_{\mathrm{R}} = 0$. This is because when $d_{\mathrm{R}} = 0.4$, the distances for all links are greater than 1, thus leading to deteriorated outage probability due to smaller channel gain in contrast to the network with $d_{\mathrm{R}} = 0$. Additionally, it is shown that the modified scheme outperforms the traditional scheme significantly for P-SCD, but offers only minor performance gain over the traditional scheme for S-SCD and G-JCNC in a symmetric network, which complies with the observations in Fig. 6.6 for the outage probability. Furthermore, the normalized system throughput with $T_{\mathrm{I}} = 0$ is shown in Fig. 6.11 for the scenarios considered in Fig. 6.10, where similar characteristics of the APP-based schemes in both network topologies can be observed.

As presented in the previous figures, all the employed metrics, namely, semi-analytical outage probability, FER and normalized throughput, indicate that the performance gain achieved by the modified scheme over the traditional

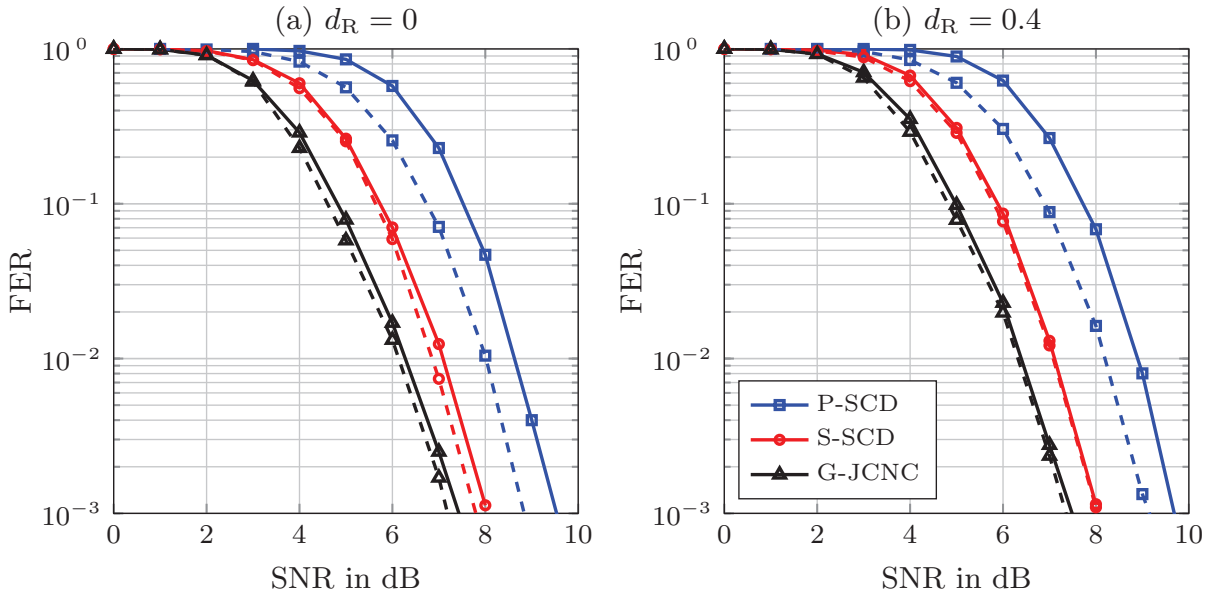

Figure 6.10: FER performance for both traditional scheme (-) and modified scheme (- -) using P-SCD, S-SCD and G-JCNC at each relay. A symmetric network is considered, i.e., $\theta_R = \pi/2$. (a) for $d_R = 0$, i.e., equal statistics for all links, and (b) for $d_R = 0.4$.

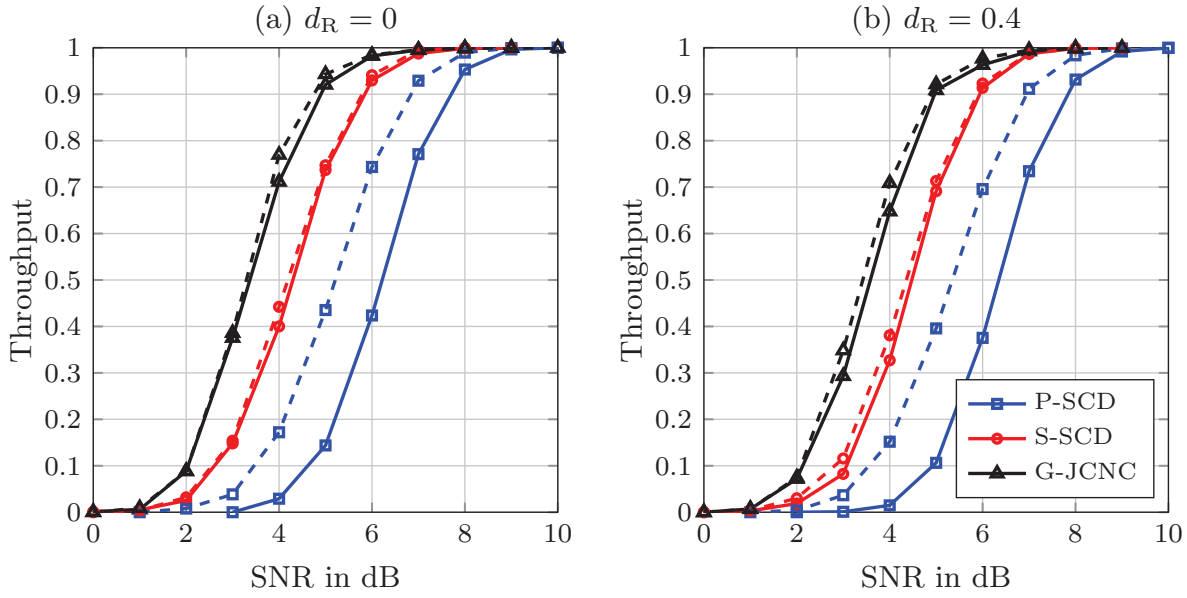

Figure 6.11: Normalized throughput for both traditional scheme (-) and modified scheme (- -) using P-SCD, S-SCD and G-JCNC at each relay. A symmetric network is considered, i.e., $\theta_R = \pi/2$. (a) for $d_R = 0$, i.e., equal statistics for all links, and (b) for $d_R = 0.4$.

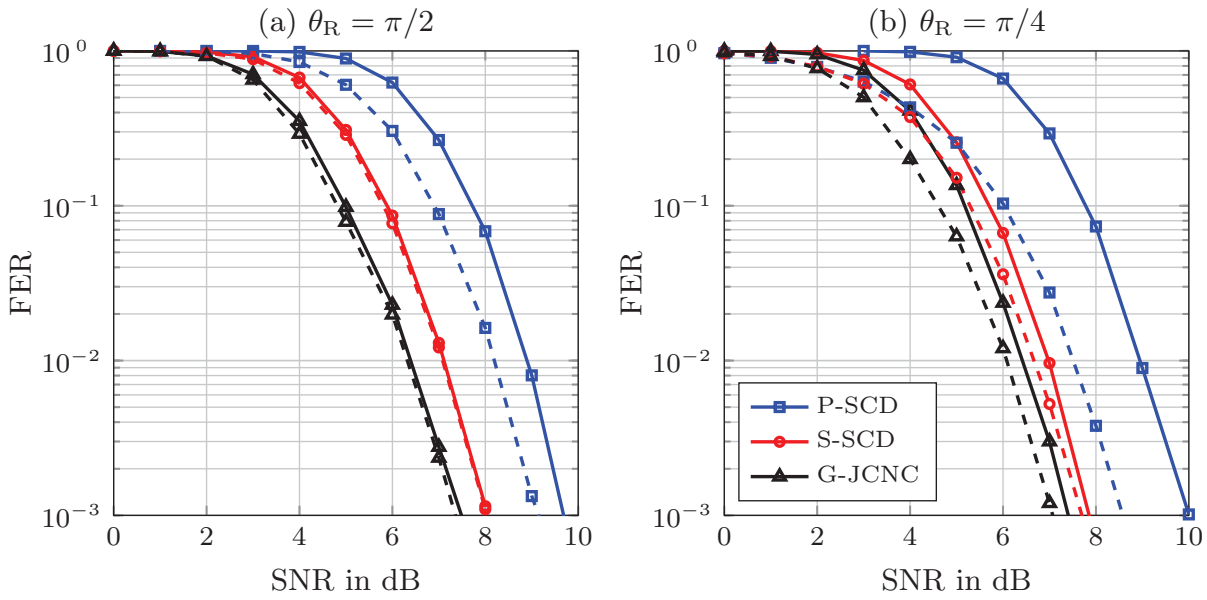

Figure 6.12: FER performance for both traditional scheme (-) and modified scheme (- -) using P-SCD, S-SCD and G-JCNC at each relay. The distance between R_1 and R_4 is set to $d_R = 0.4$. (a) for a symmetric network, i.e., $\theta_R = \pi/2$, and (b) for an asymmetric network with $\theta_R = \pi/4$.

scheme is very limited for S-SCD and G-JCNC in a symmetric network. In order to achieve more remarkable performance improvement, asymmetric networks are considered and compared to the practical symmetric network in Fig. 6.12 and 6.13 for FER and throughput, respectively. Note that Fig. 6.12(a) and 6.13(a) refer to the symmetric network with $d_R = 0.4$, which are identical to Fig. 6.10(b) and 6.11(b), respectively, whereas the asymmetric network with $d_R = 0.4$ and $\theta_R = \pi/4$ is employed in Fig. 6.12(b) and 6.13(b). Therein, significant gain is achieved by the modified scheme over its traditional counterpart, even for S-SCD and G-JCNC. This is because the asymmetric topology leads to increased chances that the relays decode only one source message correctly. Specifically, the relays closer to source u compared to the other source tend to only obtain correct estimation of the individual codeword $\mathbf{c}_u$. As a result, it occurs with higher frequency that both $\mathcal{D}_R^A$ and $\mathcal{D}_R^B$ are not empty set in this case, making the modified scheme more advantageous against the traditional one.

Impact of Idle Time

As indicated in Subsection 6.4.3, the modified scheme requires an idle time T_I to switch the BC transmission mode adaptively, which has to be taken

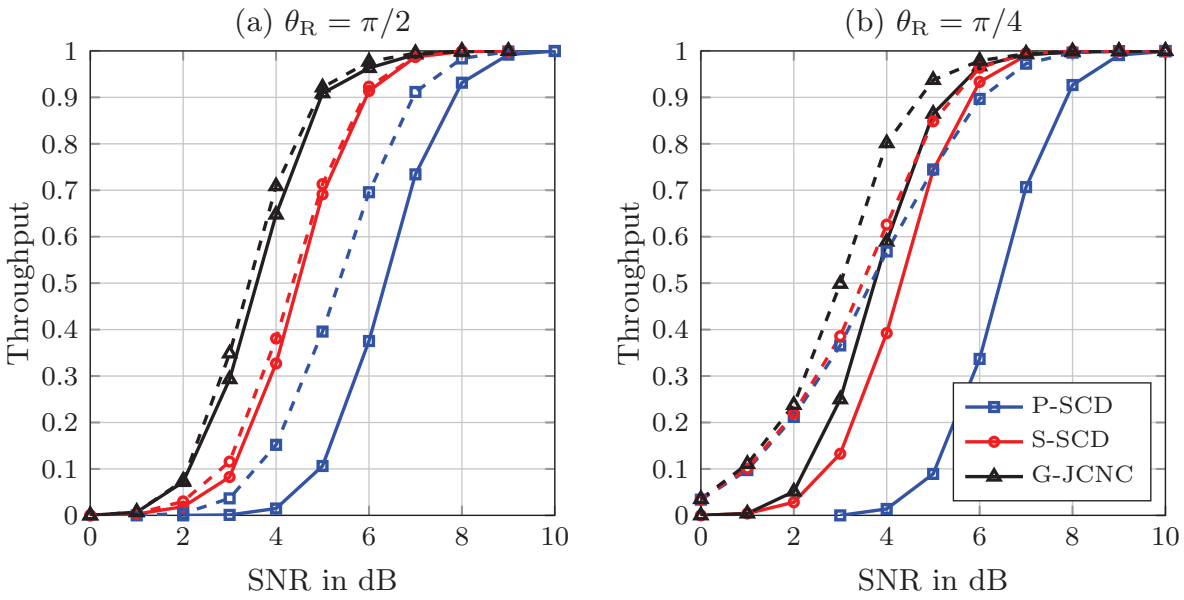

Figure 6.13: Normalized throughput for both traditional scheme (-) and modified scheme (- -) using P-SCD, S-SCD and G-JCNC at each relay. The distance between R_1 and R_4 is set to $d_R = 0.4$. (a) for a symmetric network, i.e., $\theta_R = \pi/2$, and (b) for an asymmetric network with $\theta_R = \pi/4$.

into account for performance evaluation. To this end, the dependency of the normalized throughput on the ratio T_I/T_{OFDM} is shown in Fig. 6.14 for SNR = 4dB. Obviously, longer idle time T_I leads to decreased throughput, e.g., the modified scheme even becomes inferior to the traditional scheme when $T_I/T_{OFDM} > 0.5$ for S-SCD and $T_I/T_{OFDM} > 0.75$ for G-JCNC. Moreover, the performance of the modified scheme decreases more rapidly in Fig. 6.14(b) as the probability of requiring an idle time increases in the asymmetric network compared to the symmetric network. However, the throughput gain compared to the traditional scheme is even more dramatic due to significantly improved FER performance, leading to the conclusion that the modified scheme is much superior to the traditional scheme with reasonable $T_I \ll T_{OFDM}$, especially in asymmetric networks.

6.6 Chapter Summary

In this chapter, distributed two-way relaying communications are considered with multiple single-antenna relays supporting the information exchange between two source nodes. Firstly, the system model is elaborated in Section 6.2 with the basic assumptions of the system setup. After PLNC

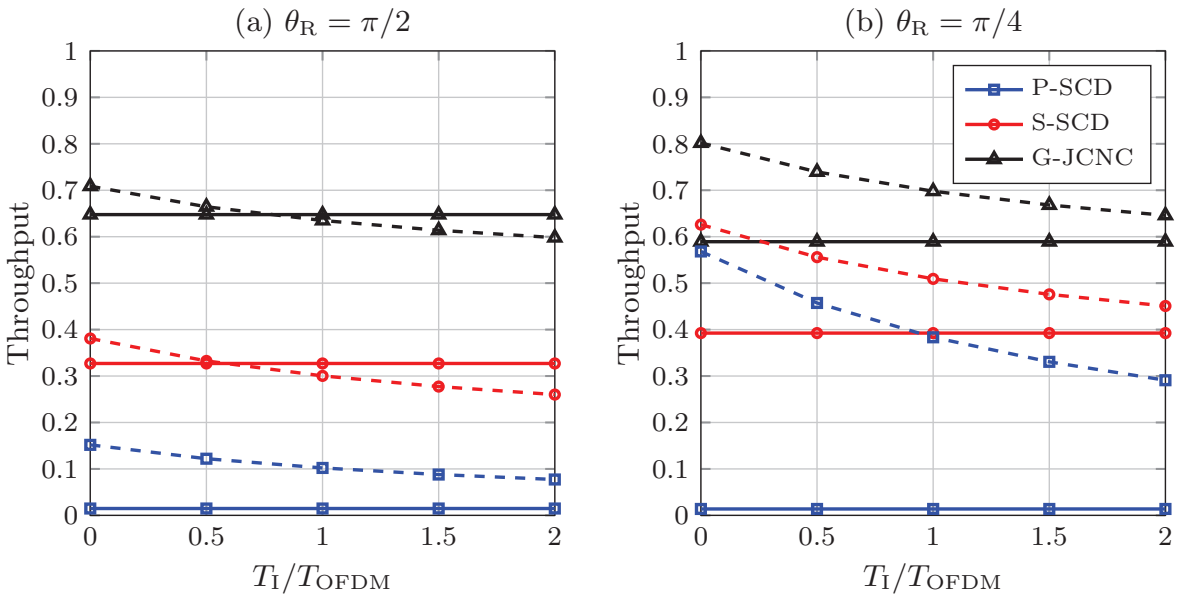

Figure 6.14: Impact of idle time T_I on system throughput for both traditional scheme (-) and modified scheme (- -) using P-SCD, S-SCD and G-JCNC at each relay with SNR = 4dB. The distance between R_1 and R_4 is set to $d_R = 0.4$. (a) for a symmetric network, i.e., $\theta_R = \pi/2$, and (b) for an asymmetric network with $\theta_R = \pi/4$.

detection and decoding at each relay, only relays with correctly estimated network coded message participate in the transmission to the sources in the BC phase in order to avoid error propagation. Such a traditional adaptive BC transmission scheme is presented in Section 6.3. As this scheme neglects the event that different relays may decode only one source message correctly, a modified scheme is studied in Section 6.4 by letting these relays forward the individual message in case of all relays failing to perfectly estimate the XORed packet [WWD14a, WLW+16b]. Therein, a novel signaling approach is also introduced with minor overhead. As demonstrated in Section 6.5, both semi-analytically derived outage probability and numerical error rate as well as throughput performance indicate the superiority of the newly proposed modified adaptive BC transmission scheme over its traditional counterpart.

Chapter 7

Summary

Modern mobile communications require ever increasing data rate with reliable transmission as well as wide area coverage. For this purpose, an attractive approach is the application of relay assisted cooperative communication, where the transmission between the terminals is supported by intermediate relaying nodes enabling cooperations at different levels. However, due to the fact that one node can not transmit and receive at the same time and frequency, practical systems commonly assume half-duplex constraint that halves the spectral efficiency. To overcome this drawback, the one-way relaying communication from the source to the destination is extended to a two-way setup, where both sources intend to exchange information with each other via relays. Based on the concept of network coding and the broadcast nature of the wireless channel, the sources transmit to the relay using the same physical resource, and the relay then estimates and forwards a joint message to the sources. In this way, the spectral efficiency loss is compensated completely. To achieve this goal, sophisticated relaying schemes are presented at the relay to generate a network coded message from the superimposed signal and resulting asynchrony issues are considered carefully to preserve the performance gain by two-way relaying. Moreover, with the presence of multiple relays, novel distributed strategies are developed that allow cooperations between the relays to support the end-to-end transmission in both one-way and two-way scenarios.

In Chapter 2, the fundamentals of digital communication systems to serve the main body of this thesis are reviewed. This includes the baseband transmission model, OFDM, channel coding, digital modulation, spatial diversity schemes in MIMO systems and rudimentary topics for information theory. Chapter 3 deals with one-way SISO relaying, i.e., one single-antenna

relay. Therein, different OFDM-based relaying schemes are presented, which are adapted and modified from the conventional AF and DF relaying schemes due to varying link reliability over the subcarriers in one OFDM symbol [WW11, WLW+16a]. It is shown that when the relay is in the middle of the source and the destination, AF-CP outperforms AF-CG slightly whereas DF is superior to AF in the low SNR region but loses diversity with increasing SNR. The novel DQF scheme with mMRC achieves improved performance to DF by suppressing the subcarriers with less reliability at the destination such that the impact of error propagation is mitigated. Furthermore, the influence of employing stronger channel codes and other network topologies are investigated.

Chapter 4 extends the one-way relaying network in a distributed scenario with multiple single-antenna relays. By clustering these relays into a VAA, distributed MIMO technologies are applied based on IRC that allows message exchange within the VAA. Based on the decoding status of the relays obtained by using a CRC code, punctured bits are exchanged when some but not all relays decode the source message correctly. When no relay is able to achieve correct decoding, part of the receive signals are exchanged. Such an adaptive IRC scheme may increase the number of correctly decoded relays after re-decoding with the help of the exchanged information [WXW+11, WXW+12, WLW+16a]. Letting only the relays with error-free source message transmit to the destination using D-OSTBC, the end-to-end system performance is improved significantly by IRC, with a fair comparison achieved by throughput analysis that embeds the cooperation overhead.

Two-way relaying communications with a single relay are considered in Chapter 5 with the main focus on the two-phase scheme with coded OFDM using PLNC. To estimate the XORed network coded message from the superimposed receive signal at the relay, different APP-based detection and decoding schemes are presented. SCD decodes both source messages individually before network coding whereas JCNC estimates the XORed packet directly. G-JCNC decodes the codeword combination in non-binary GF followed by PLNC mapping. Both MI analysis and link-level simulation results show that SCD outperforms JCNC and G-JCNC achieves the best performance in multi-path fading channels using OFDM [WWD13a, WLW+16b]. The gain of S-SCD over P-SCD is also observed due to interference cancellation. Subsequently, it is indicated that the performance of the APP-based PLNC scheme is strongly dependent on the channel ratio of both source-relay links in the MA phase. To this end, an optimal phase control strategy is proposed that pre-rotates the transmit signal at one source for each transmission yielding an optimal phase difference [WWD13a, WLW+16b]. The overhead for CSI at the transmitter side is reduced significantly by linear

approximation of the channel phase, on the other hand, this only leads to minor performance loss. Another important aspect for two-way relaying with PLNC is the asynchronous MA transmission in practice. Specifically, CFO mismatch due to hardware imprecision when generating carrier frequency is considered. To mitigate the resulting impairments, CFO compensation and iterative ICI cancellation approaches are developed for different APP-based PLNC schemes, which are shown to be very effective even with large relative CFO level [WLW$^+$14, WLW$^+$16b]. At last, a MIMO relay is introduced to support two-way relaying communications. Besides the APP-based schemes, common multi-user multi-layer MIMO detection techniques are applied to first estimate the individual source messages before network coding due to increased spatial degrees of freedom [WWD13b, WWD14b, WLW$^+$16b]. For example, QRD-based MMSE-OSIC scheme approaches P-SCD with minor performance loss at low and medium code rates but no APP calculations based on the superimposed receive signal at the relay are required.

Multiple single-antenna relays are assumed for two-way relaying communications using PLNC in Chapter 6. In this case, each relay applies the APP-based PLNC schemes to estimate the network coded message. In the traditional adaptive BC transmission scheme, only relays with error-free XORed packet participate in the BC transmission using D-OSTBC to avoid error propagation. In case that all relays fails to decode the XORed codeword correctly, the relays with only one correctly decoded source message achieved either from SCD or G-JCNC transmit this individual message in the modified adaptive BC transmission scheme [WWD14a, WLW$^+$16b]. As a result, the sources still have the opportunity to estimate the desired message correctly from the BC phase. Using CRC over the air using an idle time, only minor signaling overhead is required for this modified scheme. The performance gain of the modified scheme over its traditional counterpart is observed by both outage analysis and link-level simulation results, especially in asymmetric networks.

Finally, as an outlook to prospect beyond this thesis, several points still remain open and are left for future work, including

- Fixed network topologies are currently assumed with restrictions, e.g., the relays are supposed to be close to each other to facilitate easier IRC in one-way relaying systems. This should be extended to arbitrary topologies with more flexibility for practical concerns.

- Asynchrony also exists when multiple relays transmit simultaneously, which should be considered in the overall system performance in the distributed relaying scenario.

- Adaptive IRC is presented in one-way distritbuted relaying networks. Extension to two-way relaying is required to determine which information can be exchanged that benefits a more robust BC transmission.
- XOR-based network coding is employed for PLNC in two-way relaying networks. This may be extended to more sophisticated network coding rules based on general exclusive law and jointly designed with channel coding, which is especially a challenging task in distributed relaying networks.

Acronyms

ACK Acknowledgement.
ADC Analog To Digital Converter.
AF Amplify-Forward.
AF-CG Amplify-Forward With Constant Gain.
AF-CP Amplify-Forward With Constant Power.
ANC Analog Network Coding.
APP A-posteriori Probability.
AWGN Additive White Gaussian Noise.

BC Broadcast.
BCJR Bahl, Cocke, Jelinek And Raviv.
BER Bit Error Rate.
BPSK Binary Phase Shift Keying.
BQ Bit Quantization.

CBE Code Bit Error.
CDF Cumulative Distribution Function.
CFO Carrier Frequency Offset.
CP Cyclic Prefix.
CRC Cyclic Redundancy Check.
CSI Channel State Information.

D-OSTBC Distributed Orthogonal Space-Time Block Code.
DEF Decode-Estimate-Forward.
DF Decode-Forward.
DFT Discrete Fourier Transformation.

DNC Digital Network Coding.

DQF Decode-Quantize-Forward.

DT Direct Transmission.

FER Frame Error Rate.

FFT Fast Fourier Transformation.

FIR Finite Impulse Response.

G-JCNC Generalized Joint Channel Decoding And Physical-layer Network Coding.

GF Galois Field.

GI Guard Interval.

GSC Generalized Selective Combining.

HARQ Hybrid Automatic Repeat Request.

HDAF Hybrid Decode-Amplify-Forward.

ICI Inter-Carrier Interference.

ICIC Inter-Carrier Interference Cancellation.

IFFT Inverse Fast Fourier Transformation.

IRC Inter-Relay Cooperation.

ISI Inter-Symbol Interference.

JCNC Joint Channel Decoding And Physical-layer Network Coding.

LDC Linear Dispersion Code.

LDPC Low-Density Parity-Check.

LE Linear Equalization.

LLR Log-Likelihood Ratio.

M-PSK M-ary Phase Shift Keying.

M-QAM M-ary Quadrature Amplitude Modulation.

MA Multiple-Access.

MI Mutual Information.

MIMO Multiple-Input Multiple-Output.

MISO Multiple-Input Single-Output.

MMSE Minimum Mean Square Error.

MRC Maximum Ratio Combining.

NAK Non-Acknowledgement.

OFDM Orthogonal Frequency Division Multiplexing.
OSIC Ordered Successive Interference Cancellation.
OSTBC Orthogonal Space-Time Block Code.

P-SCD Parallel Separated Channel Decoding.
P/S Parallel To Serial.
PEG Progressive Edge Growth.
PLNC Physical-Layer Network Coding.

QF Quantize-Forward.
QOSTBC Quasi Orthogonal Space-Time Block Code.
QPSK Quadrature Phase Shift Keying.
QRD QR Decomposition.

RCPC Rate Compatible Punctured Convolutional.

S-SCD Serial Separated Channel Decoding.
S/P Serial To Parallel.
SAGE Space-Alternating Generalized Expectation-maximization.
SCD Separated Channel Decoding.
SIC Successive Interference Cancellation.
SIMO Single-Input Multiple-Output.
SISO Single-Input Single-Output.
SNR Signal To Noise Ratio.
SPA Sum-Product Algorithm.
SQ Symbol Quantization.
STC Space-Time Code.
STTC Space-Time Trellis Code.
SU Single User.

VAA Virtual Antenna Array.

ZF Zero Forcing.

List of Symbols

Functions and Operators

$\lvert\cdot\rvert$	Absolute value / Cardinality
$\lVert\cdot\rVert$	Vector norm
$[\cdot]_{\jmath,\jmath}$	The $\jmath$th diagonal element of a squared matrix
$\lceil\cdot\rceil$	Rounds to the nearest integer not smaller than input
$\angle$	Angle of
$\mathcal{C}(\cdot)$	Network coding
$\mathcal{C}^{-1}(\cdot)$	Network decoding
$\mathcal{M}(\cdot)$	Mapping
$\mathcal{M}^{-1}(\cdot)$	Demapping
$\mathcal{M}_{\mathrm{IRC}}(\cdot)$	Mapping for IRC
$\mathcal{M}_{\mathrm{IRC}}^{-1}(\cdot)$	Demapping for IRC
$\mathcal{P}_{\mathrm{C}}(\cdot)$	Puncturing
$\mathcal{P}_{\mathrm{C}}^{-1}(\cdot)$	De-puncturing
$\mathcal{Q}_{\mathrm{b}}(\cdot)$	Bit quantization
$\mathcal{Q}_{\mathrm{s}}(\cdot)$	Symbol quantization
$\mathcal{Q}^{-1}(\cdot)$	De-quantization
$\Gamma(\cdot)$	Channel coding
$\Gamma^{-1}(\cdot)$	Channel coding
$\Pi(\cdot)$	Interleaving
$\Pi^{-1}(\cdot)$	De-interleaving
argmax	Argument that maximizes expression
argmin	Argument that minimizes expression
$\mathrm{dg}\{\cdot\}$	Diagonalize a vector(matrix) to a matrix(vector)
$\mathrm{E}\{\cdot\}$	Expectation of

$f(\cdot)$ . . . . . Relay function
$\mathrm{Im}(\cdot)$ . . . . . Imaginary part
$\mathrm{Re}(\cdot)$ . . . . . Real part
$p\{\cdot\}$ . . . . . Density function
$\Pr\{\cdot\}$ . . . . . Probability of
$\tanh(\cdot)$ . . . . Hyperbolic tangent

General and Calligraphic Symbols

$\mathcal{A}_\nu^\xi$ . . . . . Set of symbols with the vth code bit equal to ξ
$\mathcal{C}_{\mathrm{AB}}$ . . . . . Set of all possible code bit combination
$\mathcal{D}$ . . . . . Set of correct relays before IRC
$\mathcal{D}'$ . . . . . Set of correct relays after punctured bits exchange
$\mathcal{D}''$ . . . . . Set of correct relays after receive signal exchange
$\mathcal{D}_{\mathrm{R}}$ . . . . . Set of relays decoding XORed packet correctly
$\mathcal{D}_{\mathrm{R}}^{\mathrm{A}}$ . . . . . Set of relays decoding message from source A correctly
$\mathcal{D}_{\mathrm{R}}^{\mathrm{B}}$ . . . . . Set of relays decoding message from source B correctly
$\mathbb{F}_{M^2}$ . . . . . Non-binary GF in M^2
$\mathcal{P}$ . . . . . Transmit power
$\mathcal{P}_{\mathrm{ICI}}$ . . . . . ICI power
$\mathcal{P}_{\mathrm{IRC}}$ . . . . . Transmit power for IRC
$\mathcal{S}_{\mathrm{AB}}$ . . . . . Set of noise-free superimposed receive signal at relay R
$\mathcal{X}$ . . . . . Set of transmit symbol vectors

Greek Symbols

α . . . . . Path-loss exponent
β . . . . . Amplification factor at relay R for AF
γ . . . . . SNR threshold
$\Delta\phi$ . . . . . Phase difference of both links in MA phase
Δn_{IRC} . . . . Step size in HARQ-based IRC with punctured bits exchange
ϵ . . . . . CFO normalized to subcarrier spacing
η . . . . . Throughput
θ . . . . . Phase rotation at source A for optimal phase control
θ_{R} . . . . . Angle parameter in asymmetric relaying network
κ . . . . . Selected relay in IRC
λ . . . . . Proportional factor in partial cooperation

Λ . . . . . Diagonal matrix of equivalent channel model with CFO

$\overline{\Lambda}$ . . . . . Non-diagonal matrix of equivalent channel model with CFO

ν . . . . . Index of m

ξ . . . . . Variable from 0 and 1

ρ . . . . . Data rate loss factor in IRC

σ_n^2 . . . . . Noise variance

$\tau_{\max}$ . . . . . Maximum channel time delay

Φ_{CH} . . . . . Overhead of CSI exchange in IRC

Φ_{IRC} . . . . . Overhead of message exchange in IRC

$\overline{\Phi}_{\jmath}$ . . . . . Averaged estimation error of the $\jmath$th layer

$\mathbf{\Phi}$ . . . . . Error covariance matrix

Ψ_{ν}^{ξ} . . . . . Set of indices with code bit $c_{\mathrm{A}\oplus\mathrm{B},\nu}$ equal to ξ

$\Omega_{\mathrm{A},\nu}^{\xi}$ . . . . . Set of indices with code bit $c_{\mathrm{A},\nu}$ equal to ξ

Roman Symbols

$\mathbf{A}_{\mathrm{IRC}}$ . . . . . Transfer matrix for IRC

$\mathbf{b}$ . . . . . Information word

$\mathbf{b}_{\mathrm{AB}}$ . . . . . Information word combination

$\hat{\mathbf{b}}$ . . . . . Estimated information word

$\mathbf{c}$ . . . . . Codeword

$\mathbf{c}_{\mathrm{AB}}$ . . . . . Codeword combination

$\mathbf{c}'$ . . . . . Interleaved codeword

$\hat{\mathbf{c}}$ . . . . . Estimated codeword

C . . . . . Channel capacity

C_{G} . . . . . MI for G-JCNC

C_{J} . . . . . MI for JCNC

$C_{\mathrm{S}}^{\mathrm{P}}$ . . . . . MI for P-SCD

$C_{\mathrm{S}}^{\mathrm{S}}$ . . . . . MI for S-SCD

C_{SU} . . . . . MI in a SU scenario

d . . . . . Distance between two nodes

d_{IRC} . . . . . Distance between relays in VAA

d_{R} . . . . . Distance parameter in asymmetric relaying network

D . . . . . Delay element

$\mathbf{E}_{\mathrm{TD}}$ . . . . . CFO distortion matrix in time domain

$\mathbf{F}$	DFT matrix
$\mathbf{G}$	Equalization matrix
$\mathbf{G}_c$	Generator matrix of linear channel codes
$\mathbf{h}$	Channel vector in frequency domain
$\mathbf{H}$	Channel matrix in frequency domain
$\mathbf{H}_c$	Parity-check matrix of linear channel codes
$\mathbf{I}$	Identity matrix
k	Relay / antenna index
K	Number of relays / antennas at relay
K_{act}	Number of active relays
ℓ	subcarrier index
L	Number of subcarriers
$\mathbf{L}$	LLR vector after demapping
L_c	Constraint length for convolution codes
$\mathbf{L}'$	De-interleaved LLR vector
m	Number of bits contained in one symbol
M	Modulation alphabet
M_{IRC}	Modulation alphabet for IRC
$\mathbf{n}$	Gaussian noise vector
n_{Q}	Quantization noise
N	Codeword length of mother code
N_b	Number of information bits
N_c	Number of code bits
N_{H}	Number of multi-path taps
N_{inv}	Number of invariant channel blocks
N_{IRC}	Number of exchanged punctured bits in IRC
N_{pun}	Number of punctured bits using punctured codes
N_{P}	Puncturing period
N_s	Number of involved symbols in STC
N_t	Number of involved time slots in STC
$\mathbf{p}_{\text{IRC}}$	Event probability vector before IRC
p_{R}	Probability of correctly decoding the XORed packet at R
p_{R}^{A}	Probability of correctly decoding source message from A at R
p_{R}^{B}	Probability of correctly decoding source message from B at R

$\mathbf{p}'_{\mathrm{IRC}}$ . . . . . Event probability vector after IRC
P . . . . . APPs
P_{out} . . . . . Outage probability
P_{w2r} . . . . . Probability of correct re-decoding at a relay after IRC
$\mathbf{P}$ . . . . . Matrix to generate redundancy bits
$\mathbf{P}_{\mathrm{C}}$ . . . . . Puncturing pattern matrix
Q . . . . . Number of quantization bits
$\mathbf{Q}$ . . . . . Orthogonal matrix after QRD
$\mathbf{R}$ . . . . . Upper-triangular matrix after QRD
R_{C} . . . . . Code rate
$R_{\mathrm{C,mom}}$ . . . . Mother code rate of punctured code
R_{STBC} . . . . Rate of STBC
$\mathbf{s}_{\mathrm{AB}}$ . . . . . Noise-free superimposed receive signal vector at relay R
$\mathbf{T}$ . . . . . STC matrix
T_{CP} . . . . . Time duration of CP
T_{I} . . . . . Idle time
T_{IRC} . . . . . Time duration of IRC
T_{OFDM} . . . . Time duration of one OFDM frame
T_{pun} . . . . . Time duration for punctured bits exchange
T_{rec} . . . . . Time duration for receive signal exchange
T_{s} . . . . . Symbol duration
u . . . . . Source index
W . . . . . Kernel matrix in outage probability analysis
$\mathbf{x}$ . . . . . Transmit symbol vector
$\mathbf{Y}$ . . . . . Receive signal matrix at a multiple-antenna node
$\mathbf{y}$ . . . . . Receive signal vector

Bibliography

[AJ15] M. R. Avendi and H. Jafarkhani, "Differential Distributed Space-Time Coding with Imperfect Synchronization in Frequency-Selective Channels", *IEEE Transactions on Wireless Communications*, volume 14, no. 4, pp. 1811–1822, Apr. 2015.

[Ala98] S. M. Alamouti, "A Simple Transmit Diversity Technique for Wireless Communications", *IEEE Journal on Selected Areas in Communications*, volume 16, no. 8, pp. 1451–1458, Oct. 1998.

[BCJR74] L. Bahl, J. Cocke, F. Jelinek, and J. Raviv, "Optimal Decoding of Linear Codes for Minimizing Symbol Error Rate", *IEEE Transactions on Information Theory*, volume 20, no. 2, pp. 284–287, Mar. 1974.

[BGT93] C. Berrou, A. Glavieux, and P. Thitimajshima, "Near Shannon Limit Error-Correcting Coding and Decoding: Turbo-Codes (1)", *IEEE International Conference on Communications (ICC'93)*, Geneva, Switzerland, May 1993.

[Bri01] S. ten Brink, "Convergence Behavior of Iteratively Decoded Parallel Concatenated Codes", *IEEE Transactions on Communications*, volume 49, no. 10, pp. 1727–1737, Oct. 2001.

[CFRU01] S.-Y. Chung, G. D. Forney, T. J. Richardson, and R. Urbanke, "On the Design of Low-Density Parity-Check Codes within 0.0045 dB of the Shannon Limit", *IEEE Communications Letters*, volume 5, no. 2, pp. 58–60, Feb. 2001.

[Che06] J.-F. Cheng, "Coding Performance of Hybrid ARQ Schemes", *IEEE Transactions on Communications*, volume 54, no. 6, pp. 1017–1029, Jun. 2006.

[CKL12] H.-H. Chung, S.-H. Kuo, and M.-C. Lin, "A Physical-Layer Network Coding Scheme based on Linear MIMO Detection", *IEEE 75th Vehicular Technology Conference (VTC'12-Spring)*, Yokohama, Japan, May 2012.

[CT91] T. M. Cover and J. A. Thomas, *Elements of Information Theory*, Wiley Series in Telecommunications, 1991.

[DLA02] M. Dohler, E. Lefranc, and H. Aghvami, "Space-Time Block Codes for Virtual Antenna Arrays ", *International Symposium on Personal, Indoor and Mobile Radio Communications (PIMRC'09)*, Lisbon, Portugal, Sept. 2002.

[DM98] M. C. Davey and D. Mackay, "Low Density Parity Check Codes over GF(q)", *IEEE Communications Letters*, volume 2, no. 6, pp. 165–167, Jun. 1998.

[Doh03] M. Dohler, *Virtual Antenna Arrays*, Ph.D. thesis, King's College London, U.K., Nov. 2003.

[DS11] M. H. DeGroot and M. J. Schervish, *Probability and Statistics*, Pearson, 4th edition, 2011.

[DVB09] *Digital Video Broadcasting: Second generation framing structure, channel coding and modulation systems for Broadcasting, Interactive Services, News Gathering and other broadband satellite applications (DVB-S2)*, ETSI EN 302 307, Aug. 2009.

[DZ09a] T. Q. Duong and H.-J. Zepernick, "Hybrid Decode-Amplfiy-Forward Cooperative Communications with Multiple Relays", *IEEE Wireless Communications and Networking Conference (WCNC'09)*, Budapest, Hungary, Apr. 2009.

[DZ09b] T. Q. Duong and H.-J. Zepernick, "On the Performance Gain of Hybrid Decode-Amplfiy-Forward Cooperative Communications", *EURASIP Journal on Wireless Communications and Networking*, volume 2009, no. 12, May 2009.

[Eli55] P. Elias, "Coding for Noisy Channels", *IRE Convention Record*, volume 4, pp. 37–47, 1955.

[FBW06] C. Fragouli, J. Y. Boudec, and J. Widmer, "Network Coding: An Instant Primer", *ACM SIGCOMM Computer Communication Review*, volume 36, no. 1, pp. 63–68, Mar. 2006.

[FH94] J. A. Fessler and A. O. Hero, "Space-Alternating Generalized Expectation-Maximization Algorithm", *IEEE Transactions on Signal Processing*, volume 42, no. 10, pp. 2664–2677, Oct. 1994.

[Gal62] R. G. Gallager, "Low-Density Parity-Check Codes", *IRE Transactions on Information Theory*, volume 8, no. 1, pp. 21–28, Jan. 1962.

[Hag88] J. Hagenauer, "Rate-Compatible Punctured Convolutional Codes (RCPC Codes) and their Applications", *IEEE Transactions on Communications*, volume 36, no. 4, pp. 389–400, Apr. 1988.

[HCH+09] S. Hong, J. Choi, S. U. Hwang, S. Jeon, and J. Seo, "Spatial Diversity Techniques Combined with Rotated Constellation for MIMO-OFDM Systems", *International Symposium on Personal, Indoor and Mobile Radio Communications (PIMRC'09)*, Sydney, Australia, Sept. 2009.

[HEA05] X.-Y. Hu, E. Eleftheriou, and D. M. Arnold, "Regular and Irregular Progressive Edge-Growth Tanner Graphs", *IEEE Transactions on Information Theory*, volume 51, no. 1, pp. 386–398, Jan. 2005.

[HGWC09] Q. Huang, M. Ghogho, J. Wei, and P. Ciblat, "Timing and Frequency Synchronization for OFDM based Cooperative Systems", *IEEE International Conference on Acoustics, Speech and Signal Processing (ICASSP'09)*, Taipei, Taiwan, Apr. 2009.

[HH02] B. Hassibi and B. M. Hochwald, "High-Rate Codes That Are Linear in Space and Time", *IEEE Transactions on Information Theory*, volume 48, no. 7, pp. 1804–1824, Jul. 2002.

[HKKM06] J. Ha, J. Kim, D. Klinc, and S. W. McLaughlin, "Rate-Compatible Punctured Low-Density Parity-Check Codes with Short Block Lengths", *IEEE Transactions on Information Theory*, volume 52, no. 2, pp. 728–738, Feb. 2006.

[HKM04] J. Ha, J. Kim, and S. W. McLaughlin, "Rate-Compatible Puncturing of Low-Density Parity-Check Codes", *IEEE Transactions on Information Theory*, volume 50, no. 11, pp. 2824–2836, Nov. 2004.

[HOP96] J. Hagenauer, E. Offer, and L. Papke, "Iterative Decoding of Binary Block and Convolutional Codes", *IEEE Transactions on Information Theory*, volume 42, no. 2, pp. 429–445, Mar. 1996.

[Jaf01] H. Jafarkhani, "A Quasi-Orthogonal Space-Time Block Code", *IEEE Transactions on Communications*, volume 49, no. 1, pp. 1–4, Jan. 2001.

[JK10] M. Ju and I. Kim, "Relay Selection with Physical-Layer Network Coding", *IEEE Global Communications Conference (GLOBECOM'10)*, Miami, FL, USA, Dec. 2010.

[Kam11] K.-D. Kammeyer, *Nachrichtenübertragung*, Vieweg+Teubner, Reihe Informations-/Kommunikationstechnik, 5th edition, 2011.

[KAPT09a] T. Koike-Akino, P. Popovski, and V. Tarokh, "Denoising Strategy for Convolutionally-Coded Bidirectional Relaying", *IEEE International Conference on Communications (ICC'09)*, , Jun. 2009.

[KAPT09b] T. Koike-Akino, P. Popovski, and V. Tarokh, "Optimized Constellations for Two-Way Wireless Relaying with Physical Network Coding", *IEEE Journal on Selected Areas in Communications*, volume 27, no. 5, pp. 773–787, Jun. 2009.

[KFL01] F. R. Kschischang, B. J. Frey, and H. A. Loeliger, "Factor Graphs and the Sum-Product Algorithm", *IEEE Transactions on Information Theory*, volume 47, no. 2, pp. 498–519, Feb. 2001.

[KGK07] S. Katti, S. Gollakota, and D. Katabi, "Embracing Wireless Interference: Analog Network Coding", *ACM SIGCOMM'07*, Kyoto, Japan, Aug. 2007.

[KHF09] V. Kotzsch, J. Holfeld, and G. Fettweis, "Joint Detection and CFO Compensation in Asynchronous Multi-User MIMO OFDM Systems", *IEEE 69th Vehicular Technology Conference (VTC'09-Spring)*, Barcelona, Spain, Apr. 2009.

[KKS04] S. W. Kim, Y. G. Kim, and M. K. Simon, "Generalized Selection Combining based on the Log-Likelihood Ratio", *IEEE Transactions on Communications*, volume 52, no. 4, pp. 521–524, Apr. 2004.

[KS09] J. Kim and W. E. Stark, "Error Exponent of Exclusive-or Multiple-Access Channels", *IEEE International Symposium on Information Theory (ISIT'09)*, Seoul, South Korea, Jun. 2009.

[Küh06] V. Kühn, *Wireless Communications over MIMO Channels: Applications to CDMA and Multiple Antenna Systems*, John Wiley & Sons, 2006.

[LaL96] M. Latva-aho and J. Lilleberg, "Parallel Interference Cancellation in Multiuser Detection", *IEEE 4th International Symposium on Spread Spectrum Techniques and Applications*, Mainz, Germany, Sept. 1996.

[Len16] F. Lenkeit, *IDMA-based Relaying for Future Mobile Communication Systems*, Ph.D. thesis, Department of Communications Engineering, University of Bremen, Dec. 2016.

[LJS06] P. Larsson, N. Johansson, and K. E. Sunell, "Coded Bi-directional Relaying", *63rd Vehicular Technology Conference (VTC'06-Spring)*, Melbourne, Australia, May 2006.

[LK07] J. Lee and S. Kim, "Time and Frequency Synchronization for OFDMA Uplink System using the SAGE Algorithm", *IEEE Transactions on Wireless Communications*, volume 6, no. 4, pp. 1176–1181, Apr. 2007.

[LLV10] Y. Li, R. H. Y. Louie, and B. Vucetic, "Relay Selection with Network Coding in Two-Way Relay Channels", *IEEE Transactions on Vehicular Technology*, volume 59, no. 9, pp. 4489–4499, Nov. 2010.

[LTW04] J. N. Laneman, D. N. C. Tse, and G. W. Wornell, "Cooperative Diversity in Wireless Networks: Efficient Protocols and Outage Behavior", *IEEE Transactions on Information Theory*, volume 50, no. 12, pp. 3062–3080, Dec. 2004.

[LW00] K. F. Lee and D. B. Williams, "A Space-Time Coded Transmitter Diversity Technique for Frequency Selective Fading Channels", *IEEE Sensor Array and Multichannel Signal Processing Workshop*, Cambridge, MA, USA, Mar. 2000.

[LW03] J. N. Laneman and G. W. Wornell, "Distributed Space-Time-Coded Protocols for Exploiting Cooperative Diversity in Wireless Networks", *IEEE Transactions on Information Theory*, volume 49, no. 10, pp. 2415–2425, Oct. 2003.

[LWLZ12] L. Lu, T. Wang, S. C. Liew, and S. Zhang, "Implementation of Physical-Layer Network Coding", *IEEE International Conference on Communications (ICC'12)*, Ottawa, Canada, Jun. 2012.

[MN96] D. J. C. MacKay and R. M. Neal, "Near Shannon Limit Performance of Low Density Parity Check Codes", *Electronics Letters*, volume 32, no. 18, pp. 1645–1646, Aug. 1996.

[Moo05] T. K. Moon, *Error Correction Coding: Mathematical Methods and Algorithms*, John Wiley & Sons, 2005.

[MP00] S. Mudulodu and A. Paulraj, "A Transmit Diversity Scheme for Frequency Selective Fading Channels", *IEEE Global Communications Conference (GLOBECOM'00)*, San Francisco, CA, USA, Nov. 2000.

[OWF10] E. Ohlmer, U. Wachsmann, and G. Fettweis, "Mutual Information of MIMO Transmission over Correlated Channels with Finite Symbol Alphabet and Link Adaptation", *IEEE Global Communications Conference (GLOBECOM'10)*, Miami, FL, USA, Dec. 2010.

[Pfl11] S. Pfletschinger, "A Practical Physical-Layer Network Coding Scheme for the Uplink of the Two-Way Relay Channel", *45th Asilomar Conference on Signals, Systems and Computers (ASILOMAR'11)*, Monterey, CA, USA, Nov. 2011.

[Pro00] J. G. Proakis, *Digital Communications*, McGraw-Hill, 4th edition, 2000.

[PY06] P. Popovski and H. Yomo, "The Anti-Packets Can Increase the Achievable Throughput of a Wireless Multi-Hop Network", *IEEE International Conference on Communications (ICC'06)*, Istanbul, Turkey, Jun. 2006.

[PY07] P. Popovski and H. Yomo, "Physical Network Coding in Two-Way Wireless Relay Channels", *IEEE International Conference on Communications (ICC'07)*, Glasgow, Scotland, Jun. 2007.

[RU07] T. Richardson and R. Urbanke, *Modern Coding Theory*, Cambridge University Press, preliminary edition, 2007.

[SB05] G. Scutari and S. Barbarossa, "Distributed Space-Time Coding for Regenerative Relay Networks", *IEEE Transactions on Information Theory*, volume 4, no. 5, pp. 2387–2399, Sept. 2005.

[Sha48] C. E. Shannon, "A Mathematical Theory of Communication", *The Bell System Technical Journal*, volume 27, pp. 379–423, Jul. 1948.

[SJ09] M. Schellmann and V. Jungnickel, "Multiple CFOs in OFDM-SDMA Uplink: Interference Analysis and Compensation", *EURASIP Journal on Wireless Communications and Networking*, volume 2009, no. 15, Apr. 2009.

[Ste10] C. Steffens, *Kooperation in OFDM-basierten Relaying-Systemen*, Diploma thesis, Department of Communications Engineering, University of Bremen, Jun. 2010.

[SY08] M. R. Souryal and H. You, "Quantize-and-Forward Relaying with M-ary Phase Shift Keying", *IEEE Wireless Communications and Networking Conference (WCNC'08)*, Las Vegas, NV, USA, Apr. 2008.

[TC10a] D. To and J. Choi, "Convolutional Codes in Two-Way Relay Networks with Physical-Layer Network Coding", *IEEE Transactions on Wireless Communications*, volume 9, no. 9, pp. 2724–2729, Sept. 2010.

[TC10b] D. To and J. Choi, "Reduced-State Decoding in Two-Way Relay Networks with Physical-Layer Network Coding", *IEEE Information Theory Workshop (ITW'10)*, Dublin, Ireland, Sept. 2010.

[TJC98] V. Tarokh, H. Jafarkhani, and A. R. Calderbank, "Space-Time Block Codes from Orthogonal Designs", *IEEE Transactions on Information Theory*, volume 45, no. 5, pp. 1456–1467, Jul. 1998.

[TN07] A. Tajer and A. Nosratinia, "Opportunistic Cooperation via Relay Selection with Minimal Information Exchange", *IEEE International Symposium on Information Theory (ISIT'07)*, Nice, France, Jun. 2007.

[TN08] R. Tannious and A. Nosratinia, "Spectrally-Efficient Relay Selection with Limited Feedback", *IEEE Journal on Selected Areas in Communications*, volume 26, no. 8, pp. 1419–1428, Oct. 2008.

[TNSC99] V. Tarokh, A. Naguib, N. Seshadri, and A. R. Calderbank, "Space-Time Codes for High Data Rate Wireless Communication: Performance Criterion in the Presence of Channel Estimation Errors, Mobility, and Multiple Paths", *IEEE Transactions on Communications*, volume 47, no. 2, pp. 199–207, Feb. 1999.

[TSC98] V. Tarokh, N. Seshadri, and A. R. Calderbank, "Space-Time Codes for High Data Rate Wireless Communication: Performance Criterion and Code Construction", *IEEE Transactions on Information Theory*, volume 44, no. 2, pp. 744–765, Mar. 1998.

[ULL17a] S. S. Ullah, S.-C. Liew, and L. Lu, "Phase Asynchronous Physical-Layer Network Coding: Decoder Design and Experimental Study", *IEEE Transactions on Wireless Communications*, volume 16, no. 4, pp. 2708–2720, Apr. 2017.

[ULL17b] S. S. Ullah, G. Liva, and S.-C. Liew, "Physical-layer Network Coding: A Random Coding Error Exponent Perspective", *http://arxiv.org/abs/1702.01311*, Feb. 2017.

[Urb01] R. Urbanke, 2001, http://ipgdemos.epfl.ch/ldpcopt/.

[Vit67] A. Viterbi, "Error Bounds for Convolutional Codes and an Asymptotically Optimum Decoding Algorithm", *IEEE Transactions on Information Theory*, volume 13, no. 2, pp. 260–269, Apr. 1967.

[WBKK03] D. Wübben, R. Böhnke, V. Kühn, and K. D. Kammeyer, "MMSE Extension of V-BLAST based on Sorted QR Decomposition", *IEEE 58th Vehicular Technology Conference (VTC'03-Fall)*, Orlando, FL, USA, Oct. 2003.

[Wei13] P. Weitkemper, *Signalverarbeitung für die Relay-gestützte Datenübertragung*, Ph.D. thesis, Department of Communications Engineering, University of Bremen, Jun. 2013.

[WFL09] D. Wang, S. Fu, and K. Lu, "Channel Coding Design to Support Asynchronous Physical Layer Network Coding", *IEEE Global Communications Conference (GLOBECOM'09)*, Honolulu, HI, USA, Dec. 2009.

[WHN15] P.-C. Wang, Y.-C. Huang, and K. R. Narayanan, "Asynchronous Physical-Layer Network Coding with Quasi-Cyclic Codes", *IEEE Journal on Selected Areas in Communications*, volume 33, no. 2, pp. 309–322, Feb. 2015.

[WJ99] X. Wang and V. Jungnickel, "Iterative (Turbo) Soft Interference Cancellation and Decoding for Coded CDMA", *IEEE Transactions on Communications*, volume 47, no. 7, pp. 1046–1061, Jul. 1999.

[WK06] D. Wübben and K. D. Kammeyer, "Low Complexity Successive Interference Cancellation for Per-Antenna-Coded MIMO-OFDM Schemes by Applying Parallel-SQRD", *IEEE 63rd Vehicular Technology Conference (VTC'06-Spring)*, Melbourne, Australia, May 2006.

[WL10] D. Wübben and Y. Lang, "Generalized Sum-Product Algorithm for Joint Channel Decoding and Physical-Layer Network Coding in Two-Way Relay Systems", *IEEE Global Communications Conference (GLOBECOM'10)*, Miami, FL, USA, Dec. 2010.

[WLW+14] M. Wu, F. Ludwig, M. Woltering, D. Wübben, A. Dekorsy, and S. Paul, "Analysis and Implementation for Physical-Layer Network Coding with Carrier Frequency Offset", *International ITG Workshop on Smart Antennas (WSA'14)*, Erlangen, Germany, Mar. 2014.

[WLW+16a] M. Wu, F. Ludwig, D. Wübben, A. Dekorsy, K.-D. Kammeyer, and S. Paul, *Communications in Interference-Limited Networks (COIN)*, chapter Physical Layer Cooperation in One-Way Relaying Systems, Springer, Mar. 2016.

[WLW+16b] M. Wu, F. Ludwig, D. Wübben, A. Dekorsy, and S. Paul, *Communications in Interference-Limited Networks (COIN)*, chapter Physical Layer Cooperation in Two-Way Relaying Systems, Springer, Mar. 2016.

[WNPS10] M. P. Wilson, K. Narayanan, H. D. Pfister, and A. Sprintson, "Joint Physical Layer Coding and Network Coding for Bi-Directional Relaying", *IEEE Transactions on Information Theory*, volume 56, no. 11, pp. 5641–5654, Nov. 2010.

[Wu08] M. Wu, *Basics and Optimization of LDPC Codes*, Master project, Department of Communications Engineering, University of Bremen, Nov. 2008.

[Wu09] M. Wu, *Distributed Low-Density Parity-Check Codes in Relay Networks*, Master thesis, Department of Communications Engineering, University of Bremen, Nov. 2009.

[Wüb06] D. Wübben, *Effiziente Detektionsverfahren für Multilayer-MIMO-Systeme*, Ph.D. thesis, Department of Communications Engineering, University of Bremen, Dec. 2006.

[Wüb10] D. Wübben, "Joint Channel Decoding and Physical-Layer Network Coding in Two-Way QPSK Relay Systems by a Generalized Sum-Product Algorithm", *7th International Symposium on Wireless Communication Systems (ISWCS'10)*, York, United Kingdom, Sept. 2010.

[WW11] D. Wübben and M. Wu, "Decode-Quantize-Forward for OFDM-based Relaying Systems", *IEEE 73rd Vehicular Technology Conference (VTC'11-Spring)*, Budapest, Hungary, May 2011.

[WWD11a] M. Wu, D. Wübben, and A. Dekorsy, "BER-based Power Allocation for Amplify-and-Forward and Decode-and-Forward Relaying Systems", *International ITG Workshop on Smart Antennas (WSA'11)*, Aachen, Germany, Feb. 2011.

[WWD11b] M. Wu, D. Wübben, and A. Dekorsy, "BER-based Power Allocation for Decode-and-Forward Relaying with M-QAM Constellations", *7th International Wireless Communications and Mobile Computing Conference (IWCMC'11)*, Istanbul, Turkey, Jul. 2011.

[WWD13a] M. Wu, D. Wübben, and A. Dekorsy, "Mutual Information based Analysis for Physical-Layer Network Coding with Optimal Phase Control", *9th International ITG Conference on Systems, Communications and Coding (SCC'13)*, Munich, Germany, Jan. 2013.

[WWD13b] M. Wu, D. Wübben, and A. Dekorsy, "Physical-Layer Network Coding in Coded OFDM Systems with Multiple-Antenna Relay", *IEEE 77rd Vehicular Technology Conference (VTC'13-Spring)*, Dresden, Germany, Jun. 2013.

[WWD14a] D. Wübben, M. Wu, and A. Dekorsy, "Adaptive Broadcast Transmission in Distributed Two-Way Relaying Networks", *22nd European Signal Processing Conference (EUSIPCO'14)*, Lisbon, Portugal, Sept. 2014.

[WWD14b] D. Wübben, M. Wu, and A. Dekorsy, *Physical-Layer Network Coding with Multiple-Antenna Relays*, chapter in MIMO Processing for 4G and Beyond: Fundamentals and Evolution, CRC Press, Apr. 2014.

[WWK08] P. Weitkemper, D. Wübben, and K.-D. Kammeyer, "Minimum MSE Relaying in Coded Networks", *International ITG Workshop on Smart Antennas (WSA'08)*, Darmstadt, Germany, Feb. 2008.

[WWK09] P. Weitkemper, D. Wübben, and K.-D. Kammeyer, "Minimum MSE Relaying for Arbitrary Signal Constellations in Coded Relay Networks", *IEEE 69th Vehicular Technology Conference (VTC'09-Spring)*, Barcelona, Spain, Apr. 2009.

[WWWK10] M. Wu, P. Weitkemper, D. Wübben, and K.-D. Kammeyer, "Comparison of Distributed LDPC Coding Schemes for Decode-and-Forward Relay Channels", *International ITG Workshop on Smart Antennas (WSA'10)*, Bremen, Germany, Feb. 2010.

[WXW+11] M. Wu, W. Xue, D. Wübben, A. Dekorsy, and S. Paul, "Energy-aware Design of Inter-Relay Cooperation for Distributed Relaying Networks", *8th International Symposium on Wireless Communication Systems (ISWCS'11)*, Aachen, Germany, Nov. 2011.

[WXW+12] M. Wu, W. Xue, D. Wübben, A. Dekorsy, and S. Paul, "An Improved Inter-Relay Cooperation Scheme for Distributed Relaying Networks", *International ITG Workshop on Smart Antennas (WSA'12)*, Dresden, Germany, Mar. 2012.

[WZY13] X. Wu, C. Zhao, and X. You, "Joint LDPC and Physical-Layer Network Coding for Asynchronous Bi-directional Relaying", *IEEE Journal on Selected Areas in Communications*, volume 31, no. 8, pp. 1446–1454, Aug. 2013.

[XP12] W. Xue and S. Paul, "Model for Energy Optimization of Baseband Architectures in Wireless Communications", *International ITG Workshop on Smart Antennas (WSA'12)*, Dresden, Germany, Mar. 2012.

[XXX12] X. Xia, K. Xu, and Y. Xu, "Asynchronous Physical-Layer Network Coding Scheme for Two-Way OFDM Relay", *http://arxiv.org/abs/1204.2692*, Apr. 2012.

[YL15] Q. Yang and S.-C. Liew, "Asynchronous Convolutional-Coded Physical-Layer Network Coding", *IEEE Transactions on Vehicular Technology*, volume 14, no. 3, pp. 1380–1395, Mar. 2015.

[Yue00] L. Yue, "Analysis of Generalized Selection Combining Techniques", *IEEE 51st Vehicular Technology Conference (VTC'00-Spring)*, Tokyo, Japan, May 2000.

[ZB11] K. Zhu and A. G. Burr, "Relay Selection Aided Distributed Space-Time Block Code for Two-Way Relay Channel with Physical-Layer Network Coding", *IEEE 73rd Vehicular Technology Conference (VTC'11-Spring)*, Budapest, Hungary, May. 2011.

[ZH08] A. Zhan and C. He, "Joint Design of Channel Coding and Physical Network Coding for Wireless Network", *International Conference on Neural Networks and Signal Processing*, Zhejiang, China, Jun. 2008.

[ZL09] S. Zhang and S. C. Liew, "Channel Coding and Decoding in a Relay System Operated with Physical-Layer Network Coding", *IEEE*

Journal on Selected Areas in Communications, volume 27, no. 5, pp. 788–796, Oct. 2009.

[ZL10] S. Zhang and S. C. Liew, "Physical-Layer Network Coding with Multiple Antennas", *IEEE Wireless Communications and Networking Conference (WCNC'10)*, Sydney, Australia, Apr. 2010.

[ZLL06] S. Zhang, S. C. Liew, and P. Lam, "Hot Topic: Physical Layer Network Coding", *International Conference on Mobile Computing and Networking (MobiCom)*, Log Angeles, CA, USA, Mar. 2006.

[ZNL+12] S. Zhang, C. Nie, L. Lu, S. Zhang, and G. Qian, "MIMO Physical-Layer Network Coding based on V-BLAST Detection", *International Conference on Wireless Communications and Signal Processing (WCSP'12)*, Huangshan, China, Oct. 2012.

[ZT03] L. Zheng and D. N. C. Tse, "Diversity and Multiplexing: A Fundamental Tradeoff in Multi-antenna Channels", *IEEE Transactions on Information Theory*, volume 49, no. 5, pp. 1073–1096, May 2003.

Index